



SERVIZIO SANITARIO REGIONALE
EMILIA-ROMAGNA
Istituto Ortopedico Rizzoli di Bologna



ICCB 2009



IV International Congress
on Computational Bioengineering

Including the
First European Symposium
on Biomedical Integrative Research

Book of Abstracts

September 16-18, 2009

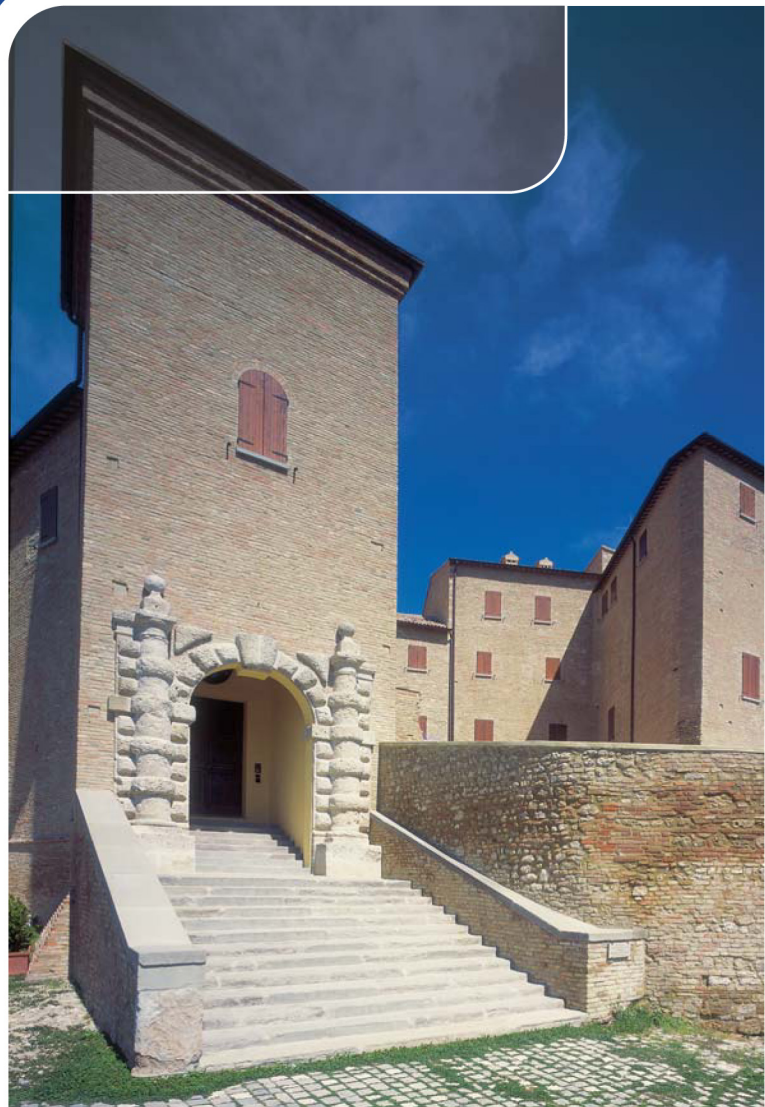
Bertinoro (FC), Italy

Centro Congressi

www.iccb2009.org

Editors:

M. Viceconti, L. Cristofolini, R. Stagni



Scope and Objectives

The use of mathematical modeling and Computer simulation for the study and prediction of biological and biomedical processes is growing, covering all aspects of biology, physiology and pathology from the molecule to the body. Predictive models start to play a key role in clinical medicine, in biology, in pharmacology, in medical technology, in epidemiology.

The objective of this conference is to provide a forum for the discussion and the diffusion of the recent advances in Computational Bioengineering, including the so-called biomedical Integrative Research (Physiome, Virtual Physiological Human, Integrative Biology, etc.) where predictive models describe disparate physiological or pathological sub-processes and are combined to obtain a more systemic understanding.

Coherent with the Team science inspiration of Integrative Research, the conference is intended also as an opportunity for researchers from all over the world to establish collaborations regardless of the geopolitics barriers, detecting areas of cooperation, and promoting the development of partnerships for new research and educational actions in bioengineering.

ICCB Organizing Committee

- Helder Rodrigues, Instituto Superior Técnico, **Lisbon, Portugal**
- Miguel Cerrolaza Un Centrale de Venezuela, **Caracas, Venezuela**
- Jean Louis Coatrieux, University of Rennes, **Rennes, France**
- Manuel Doblaré , University of Zaragoza, **Zaragoza, Spain**
- MarcoViceconti, Istituto Ortopedico Rizzoli, **Bologna, Italy**

Local Organizing Committee

Marco Viceconti, Istituto Ortopedico Rizzoli (Conference co-chairperson)

Luca Cristofolini, DIEM, University of Bologna (Conference co-chairperson)

Rita Stagni, DEIS, University of Bologna (Conference co-chairperson)

Angelo Cappello, DEIS, **University of Bologna**

Alessandro Freddi, DIEM, **University of Bologna**

Fulvia Taddei, **Istituto Ortopedico Rizzoli**

Scientific Committee

- | | |
|--|---|
| 1. <i>Fulvia Taddei, IOR, IT</i> | 16. <i>Taiji Adachi, Kyoto U, JP</i> |
| 2. <i>Luca Cristofolini, U Bologna, IT</i> | 17. <i>Peter Hunter, U Auckland, NZ</i> |
| 3. <i>Rita Stagni, U Bologna, IT</i> | 18. <i>Patrick Prendergast, Trinity College, IE</i> |
| 4. <i>Angelo Cappello, U Bologna, IT</i> | 19. <i>Keita Ito, TU Eindhoven, NL</i> |
| 5. <i>Denis Noble, U Oxford, UK</i> | 20. <i>Stephen Ferguson, MEM Center, CH</i> |
| 6. <i>Yoshihisa Kurachi, U Osaka, Japan</i> | 21. <i>Romuald Bedzinski, TU Wroclaw, PL</i> |
| 7. <i>Randy Thomas, U Evry, France</i> | 22. <i>Gerhard Holzapfel, TU Gratz, AT</i> |
| 8. <i>Ralph Müller, ETH Zurich, CH</i> | 23. <i>Rod Hose, U Sheffield, UK</i> |
| 9. <i>Andrew McCulloch, UCSD, USA</i> | 24. <i>Nicolas Smith, U Oxford, UK</i> |
| 10. <i>Peter Kohl, U Oxford, UK</i> | 25. <i>Rod Smallwood, U Sheffield, UK</i> |
| 11. <i>Stephen Cowin, City U of NY, USA</i> | 26. <i>Chris Jacobs, Columbia U, USA</i> |
| 12. <i>Alejandro Frangi, UPF, Spain</i> | 27. <i>Jeff Weiss, Utah U, USA</i> |
| 13. <i>Dario Farina, Aalborg U, Denmark</i> | 28. <i>Ton van den Bogert, Cleveland Clin, USA</i> |
| 14. <i>James Bresseurm Penn State U, USA</i> | 29. <i>William Taylor, Charitè, DE</i> |
| 15. <i>Roger Kamm, MIT, USA</i> | 30. <i>Wang Chentao, U Shanghai, China</i> |

Wednesday 16th September 2009

09:00 - 09:30 PLENARY LECTURE

P1 Modelling the neural adjustments in muscle fatigue. **Dario Farina** – Centre for Sensory-Motor Interaction (SMI), Department of health science and technology, Aalborg University, Aalborg, Denmark, p.13

09:30 - 10:00 PLENARY LECTURE

P2 Hierarchical Poroelasticity: Movement of interstitial fluid between porosity levels in bones. **Stewen Cowin** – The New York Centre for Biomedical Engineering, City University of New York, New York, USA, p.14

10:30 -11:30 WA#1: Musculoskeletal system -organ

WA11 10:30 -10:45 A MORPHOMETRIC RECONSTRUCTION OF A DISARTICULATED JUVENILE PELVIS. **Peter Watson**, Department of Engineering, University of Hull. p.24

WA12 10:45 -11:00 WHO BENEFITS FROM INTEGRATIVE BIOMEDICAL RESEARCH? THE SOCIO-ECONOMIC ASSESSMENT METHOD OF VPHO **Rainer Thiel**, Empirica Communication and Technology Research, Germany. p.25

WA13 11:00 -11:15 PREDICTING THE FEMORAL NECK RISK OF FRACTURE: TOWARDS A MULTISCALE PROBABILISTIC APPROACH. **Fulvia Taddei**, Laboratorio di Tecnologia Medica, Istituto Ortopedico Rizzoli, Italy. p.26

WA14 11:15 -11:30 FINITE ELEMENT FEMUR GENERATION USING MORPHING AND SPHERICAL PARAMETERIZATION TECHNIQUES. **Najah Hraiech**, ANSYS France, Villeurbanne, France. p.27

10:30 -11:30 WB#1: Data management and modelling tools

WB11 10:30 -10:45 PHYSIOMESPACE: DIGITAL LIBRARY SERVICE FOR BIOMEDICAL DATA. **Debora Testi**, SuperComputingSolutions, Italy. p.29

WB12 10:45 -11:00 PHYSIOMESPACE: EXECUTION SERVICES TO REMOTELY PRE-PROCESS AND PREVIEW BIOMEDICAL DATA. **Gordon Clapworthy**, University of Bedfordshire, UK. p.30

WB13 11:00 -11:15 STRUCTURAL IMAGING OF CORONARY VASCULAR-MYOCARDIAL RELATIONSHIP AND MODEL GENERATION. **Jack Lee**, Computing Laboratory, University of Oxford. p.31

WB14 11:15 -11:30 DESIGN OF A GRID INTERFACE FOR THE HIGHPERFORMING PARALLEL FINITE ELEMENT SOLVER PARFE. **Peter Arbenz**, Computer Science Department, ETH, Zurich, Switzerland. p.32

11:40 -13:10 WA#2: Musculoskeletal system -body

WA21 11:40 -11:55 MUSCLE WRAPPING USING FINITE ELEMENT CONTACT DEFINITIONS. **Philippe Favre**, Orthopaedic Research Laboratory, University of Zürich, Balgrist, Switzerland; Institute for Biomechanics, ETH, Zürich, Switzerland. p.34

WA22 11:55 -12:10 ASSESSMENT OF EFFECTIVE CONNECTIVITY IN TETRAPLEGIC AND HEALTHY SUBJECTS BY USING A NEURAL MASS MODEL. **Melissa Zavaglia**, Department of Electronics, Computer Science, and Systems, University of Bologna, Cesena, Italy. p.35

WA23 12:10 -12:25 3D MODELING OF PATIENT-SPECIFIC MUSCULOSKELETAL SYSTEM USING MRI IMAGES AND THE EOS® SYSTEM. **Jérôme Hauselle**, LBM, Arts et Metiers ParisTech, UMR CNRS 8005, France. p.36

WA24 12:25 -12:40 PREDICTING THE WHOLE MUSCLE ACTIVATION SPECTRUM COHERENT WITH A GIVEN MOTION TASK: A FEASIBILITY STUDY. **Saulo Martelli**, Laboratorio di Tecnologia Medica, Istituto Ortopedico Rizzoli, Bologna, Italy. p.37

WA25 12:40 -12:55 THE INTERACTION BETWEEN MUSCULOSKELETAL LOADING, POSTURAL STABILITY AND MUSCULAR CONTROL. **William R. Taylor**, Julius Wolff Institut, Charité – Universitätsmedizin Berlin, Germany. p.38

WA26 12:55 -13:10 ON MEASURING 3-D IN VIVO KINEMATICS, VISUALIZING, AND MODELLING THE CARPAL BONES OF THE WRIST. **Joseph J. Trey Crisco**, Department of Orthopaedics, Brown University/Lifespan. p.39

11:40 -12:40 WB#2: VPH NoE special session

WB21 11:40 -11:55 VIRTUAL PHYSIOLOGICAL HUMAN: INTEGRATIVE STUDIES. **Rod Smallwood**, University of Sheffield, UK p.41

WB22 11:55 -12:10 VPH NOE WORKPACKAGE 2 -EXEMPLAR PROJECTS. **Randal Thomas**, IBISC, CNRS FRE 3190, Evry F-91000, France. p.42

WB23 12:10 -12:25 IMPLEMENTING A TOOLKIT FOR THE VIRTUAL PHYSIOLOGICAL HUMAN (VPH) COMMUNITY. **Johnathan Cooper**, University of Oxford, UK p.43

14:30 -15:30 WA#3: Musculoskeletal system -tissue

WA31 14:30 -14:45 THE POTENTIAL OF FLAT-PANEL FLUOROSCOPY CT TO QUANTIFY VERTEBRAL TRABECULAR ARCHITECTURE IN VIVO. **Lars Mulder**, Biomedical Engineering, Eindhoven University of Technology, Eindhoven, the Netherlands. p.45

WA32 14:45 -15:00 SIMULATION OF TISSUE DIFFERENTIATION IN SCAFFOLDS FOR BONE TISSUE ENGINEERING. **Clara Sandino**, Institute for Bioengineering of Catalonia, Barcelona, Spain. p.46

WA33 15:00 -15:15 STRAIN MAPPING FOR TIME-LAPSED MICROSTRUCTURAL IMAGING OF BONE FAILURE -A VALIDATION STUDY **David Christen**, Institute for Biomechanics, ETH Zürich, Zürich, Switzerland. p.47

WA34 15:15 -15:30 ASSESSMENT OF BONE STRENGTH IN-VIVO DURING LONG TERM BEDREST AND RECOVERY. **Bert van Rietbergen**, Eindhoven University of Technology, Netherlands.

14:00 -15:30 WB#3: Cellular Modelling

- WB31** 14:00 -14:15 THE EPITHELIOME PROJECT: MULTI-PARADIGM, MULTISCALE MODELLING OF CELLS AND TISSUES. **Rod Smallwood**, Department of Computer Science, University of Sheffield, UK. p.49
- WB32** 14:15 -14:30 AN AGENT-BASED MODEL OF 'ANTISOCIAL' CELLS. **Dawn Walker**, Department of Computer Science, University of Sheffield, Sheffield S3 7HQ, U.K. p.50
- WB33** 14:30 -14:45 MICROFLUIDIC DIELECTRIC SPECTROSCOPY CYTOMETER: MODELLING AND OPTIMIZATION. **Federica Caselli**, Department of Civil Engineering, University of Rome "Tor Vergata", via del Politecnico 1, 00133 Rome, Italy. p.51
- WB34** 14:45 -15:00 CYTOSKELETON REORGANIZATION OF SPREAD CELL ON MICROPATTERNED ISLANDS: A FUNCTIONAL MODEL. **Loosli Yannick**, Orthopedic Research Laboratory, University of Zürich, Balgrist, Switzerland. p.52
- WB35** 15:00 -15:15 FINITE DEFORMATION BASED MODEL OF CYTOSKELETON. **Eligiusz Postek**, University of Sheffield, Department of Computer Science, UK. p.53
- WB36** 15:15 -15:30 DISPERSION EFFECTS OF ACTIVE CONTRACTILE FILAMENTS IN SMOOTH MUSCLE CELLS. **Sae-II Murtada**, Royal Institute of Technology (KTH), Department of Solid Mechanics Osquars Backe 1, SE-100 44 Stockholm, Sweden. p.54

15:30 - 16:00 PLENARY LECTURE

P3 Toward integrated management of cerebral aneurisms. **Alejandro Frangi** – Center for Computational Imaging & Simulation Technologies in Biomedicine (CISTIB), Universitat Pompeu Fabra, Spain, p.15

17:00 -18:30 WA#4: Musculoskeletal system -constituent

- WA41** 17:00 -17:15 SIMULATION OF THE MINERAL HETEROGENEITY OF BONE IN HEALTH AND DISEASE. **Carolin Lukas**, Max Planck Institute of Colloids and Interfaces – Department of Biomaterials, Potsdam, Germany. p.56
- WA42** 17:15 -17:30 ASSESSMENT OF BV/TV DISTRIBUTION IN VERTEBRAE FOR SPECIMEN SPECIFIC AND STATISTICAL MODELLING. **Sarrawat Rehman**, Institute of Medical and Biological Engineering, University of Leeds, U.K. p.57
- WA43** 17:30 -17:45 CONTACT MECHANICS OF A DISCRETE FIBER-REINFORCED CARTILAGE MODEL. **Patrik Christen**, Institute for Surgical Technology and Biomechanics, University of Bern, Bern, Switzerland. p.58
- WA44** 17:45 -18:00 ISOLATION, LOADING AND ESTIMATING THE POROELASTIC PROPERTIES OF A SINGLE OSTeon. **Stephen C. Cowin**, Departments of Mechanical and Biomedical Engineering, City College of New York, New York, USA. p.59
- WA45** 18:00 -18:15 CAN HUMAN TISSUE MINERAL DENSITY BE ASSUMED CONSTANT? **Simone Tassani**, Laboratorio di Tecnologia Medica, Istituti Ortopedici Rizzoli, Bologna, Italy. p.60
- WA46** 18:15 -18:30 OSTeon CLASSIFICATION IN HUMAN FEMUR, TIBIA AND FIBULA SHAFT BY CIRCULARLY POLARIZED LIGHT. **Massimiliano Baleani**, Laboratorio di Tecnologia Medica, Istituti Ortopedici Rizzoli, Bologna, Italy. p.61

17:00 -18:30 WB#4: Cardiovascular system -neurovascular

- WB41** 17:00 -17:15 A MATHEMATICAL CEREBROVASCULAR MODEL INCLUDING THE CIRCLE OF WILLIS AND CORTICAL ANASTOMOSES. **Massimo Giannessi**, Department of Electronics, Computer Science, and Systems, University of Bologna, Italy. p.63
- WB42** 17:15 -17:30 A COMPUTATIONAL MODEL FOR BLOOD FLOW IN PATIENTSPECIFIC CEREBRAL VENOUS TREE. **Harvey Ho**, Bioengineering Institute, University of Auckland, New Zealand. p.64
- WB43** 17:30 -17:45 FAST VIRTUAL STENTING IN CEREBRAL ANEURYSMS: VALIDATION WITH FINITE ELEMENT ANALYSIS. **Eleonora Flore**, Center for Computational Imaging and Simulation Technologies in Biomedicine (CISTIB) – Universitat Pompeu Fabra (UPF), CIBER-BBN. p.65
- WB44** 17:45 -18:00 A NOVEL APPROACH FOR COMPUTATIONAL HAEMODYNAMIC CHARACTERISATION OF CEREBRAL ANEURYSMS. **Alberto Marzo**, Academic Unit of Medical Physics, School of Medicine and Biomedical Sciences, University of Sheffield, Sheffield, UK. p.66
- WB45** 18:00 -18:15 NEW ORIENTATION DISTRIBUTION FUNCTIONS IN THE MICROSHERE-BASED MODELING OF BLOOD VESSELS. **Miguel A. Martínez**, Group of Structural Mechanics and Materials modelling. Aragón Institute of Engineering Research. University of Zaragoza. p.67
- WB46** 18:15 -18:30 COMPUTATIONAL STUDY OF THE EFFECTS OF DRUGS ON GROWTH AND RUPTURE OF INTRACRANIAL ANEURYSMS. **Pankaj Singh**, Academic Unit of Medical Physics, School of Medicine and Biomedical Sciences, University of Sheffield, Sheffield, UK. p.68

Thursday 17th September 2009

09:00 -09:30 PLENARY LECTURE

P5 09:00 – 09:30 Computational Modelling and Simulation in Heart Rhythm Research. **Blanca Rodriguez**, University of Oxford, United Kingdom. p.16

09:30 - 10:00 PLENARY LECTURE

P6 09:30 – 10:00 Integrating Macro with Micro scale transport in the small intestine: a multigrid Lattice-Boltzmann model. **James G. Brasseur**, Department of Mechanical Engineering, Pennsylvania State University, USA, p.17

10:30 -11:30 TA#1: Musculoskeletal system -subject specific

TA11 10:30 -10:45 SUBJECT-SPECIFIC P-FE ANALYSIS OF THE PROXIMAL FEMUR UTILIZING MICROMECHANICS-BASED MATERIAL PROPERTIES. **Zohar Yosibash**, Dept. of Mechanical Engineering, Ben-Gurion Univ., Beer-Sheva 84105, Israel. p.70

TA21 10:45 -11:00 DEVELOPMENT AND VALIDATION OF SPECIMEN-SPECIFIC MICRO-CT BASED FINITE ELEMENT MODELS OF MOUSE TIBIAE. **Antonia Torcasio**, Division of Biomechanics and Engineering Design, K.U.Leuven, Leuven, Belgium. p.71

TA31 11:00 -11:15 CONSTRUCTION OF A COMPLETE DIGITISED JUVENILE FEMUR FOR USE IN MUSCULOSKELETAL AND FINITE ELEMENT MODELS. **David Lunn**, Department of Engineering, University of Hull, UK. p.72

TA41 11:15 -11:30 A VALIDATION OF SUBJECT-SPECIFIC FINITE ELEMENT MODELS OF PROXIMAL FEMUR IN SIDEWAYS FALL CONFIGURATION. **Lorenzo Grassi**, Laboratorio di Tecnologia Medica, Istituto Ortopedico Rizzoli, Bologna, Italy. p.73

10:30 -11:30 TB#1: Modelling human movement

TB11 10:30 -10:45 SENSITIVITY ANALYSIS OF AN ENERGETIC MUSCLE MODEL APPLIED AT WHOLE BODY LEVEL IN RECUMBENT CYCLING. **Maria Cristina Bisi**, DEIS, University of Bologna, Italy. p.75

TB21 10:45 -11:00 QUANTITATIVE EVALUATION OF GAIT ABNORMALITIES IN TYPE 2 DIABETIC PATIENTS. **Marco Knaflitz**, Department of Electronics, Politecnico di Torino, Italy. p.76

TB31 11:00 -11:15 3D JOINTS KINEMATICS WITH FLUOROSCOPY: ALGORITHM OPTIMIZATION. **Luca Tersi**, Department of Electronics, Computer Science and Systems -University of Bologna, Italy. p.77

TB41 11:15 -11:30 AN EMG-DRIVEN MUSCULOSKELETAL MODELING APPROACH TO ESTIMATE ARTICULAR LOADING AT THE KNEE. **Kurt Manal**, Center for Biomedical Engineering Research, University of Delaware, USA. p.78

11:40 -13:10 TA#2: New numerical methods and tools

TA21 11:40 -11:55 MULTISCALE MODELING OF TISSUE PERFUSION USING HOMOGENIZATION OF DUAL POROUS LAYERED MEDIA. **Eduard Rohan**, Department of Mechanics, Faculty of Applied Sciences, University of West Bohemia in Pilsen, Czech Republic. p.80

TA22 11:55 -12:10 CFD SIMULATIONS TO PREDICT THE PERMEABILITY OF BIOLOGICAL AND SYNTHETIC CELLULAR MATERIALS. **Giancarlo Pennati**, Laboratory of Biological Structure Mechanics – LaBS, Dept. of Structural Engineering, Politecnico di Milano, Italy. p.81

TA23 12:10 -12:25 MICROTUBULE MECHANICAL PROPERTIES BY MEANS OF NORMAL MODE ANALYSIS. **Marco Agostino Deriu**, Mechanics Department, Politecnico di Torino, Italy. p.82

TA24 12:25 -12:40 SIMULATION OF BIOMATERIAL FLOW THROUGH POROUS MEDIA. **René Widmer**, Institute for Surgical Technology and Biomechanics, University of Bern, Bern, Switzerland. p.83

TA25 12:40 -12:55 SIMULATION OF MICROCIRCULATORY DISORDER BY MALARIAL INFECTION USING A PARTICLE METHOD. **Takami Yamaguchi**, Dept. Biomedical Engineering, School of Biomedical Engineering. p.84

TA26 12:55 -13:10 FINITE ELEMENT SIMULATION OF THE HUMAN TRACHEA IN HEALTHY AND PATHOLOGIC SITUATIONS. **Manuel Doblaré**, Group of Structural Mechanics and Material Modelling (GEMM). Aragon Institute of Engineering Research. CIBERBBN (ICS), Spain. p.85

11:40 -12:40 TB#2: Cardiovascular system -heart

TB21 11:40 -11:55 TOOLS TO UNDERSTAND THE PUMPING MECHANISM OF EMBRYONIC HEARTS. **Frédéric Maes**, University College Ghent, Biomechanics Research Group, Belgium; Gent University, IBItech, Belgium. p.87

TB22 11:55 -12:10 NUMERIC INTEGRATED APPROACH FOR SHEAR INDUCED THROMBOEMBOLIC POTENCY OF PROSTHETIC HEART VALVES. **Umberto Morbiducci**, Politecnico di Torino, Italy. p.88

TB23 12:10 -12:25 MULTI-PHYSICS COUPLING IN THE HEART. **Nicolas Smith**, Computing Laboratory, University of Oxford, Oxford, UK. p.89

TB24 12:25 -12:40 AN IMPLICIT NUMERICAL METHOD FOR CARDIAC ELECTROMECHANICS SIMULATIONS. **Pras Pathmanathan**, University of Oxford Computing Laboratory, UK. p.90

14:30 -15:30 TA#3: Orthopedic Bioengineering

TA31 14:30 -14:45 LOADING OF THE TEMPOROMANDIBULAR JOINT AFTER ARTIFICIAL JOINT IMPLANTATION ON THE OPPOSITE SIDE. **Zdenek Horak**, Laboratory of Biomechanics, Fac. of Mechanical Eng., CTU in Prague, Czech Republic. p.92

TA32 14:45 -15:00 MATERIAL PROPERTIES SENSITIVITY OF THE LUMBAR DISC UNDER COMPRESSION: A FACTORIAL STATISTICAL APPROACH. **Malandrino Andrea**, Institute for Bioengineering of Catalonia, Barcelona, Spain. p.93

TA33 15:00 -15:15 THE CEMENT-BONE INTERFACE: A COMPARATIVE EXPERIMENTAL AND FINITE ELEMENT STUDY. **Ruth Wilcox**, Institute of Medical and Biological Engineering, University of Leeds, Leeds, UK. p.94

TA34 15:15 -15:30 FRONTAL PLANE LOWER LIMB ALIGNMENT USING FUNCTIONALLY DETERMINED JOINT CENTERS AND AXES. **William R. Taylor**, Julius Wolff Institut and CMSC, Charité – Universitätsmedizin -Berlin, Germany. p.95

14:00 -15:30 TB#3: Cardiovascular system -vascular

TB31 14:00 -14:15 SELF-REGULATION OF RED BLOOD CELL TRANSPORT IN CAPILLARY NETWORKS. **Dominik Obrist**, Institute of Fluid Dynamics, ETH Zurich, Switzerland. p.97

TB32 14:15 -14:30 ON THE PATIENT-SPECIFIC COMPUTATIONAL MODELLING OF BLOOD VESSEL. **Estefanía Peña**, Baquedano Group of Structural Mechanics and Materials modelling. Aragón Institute of Engineering Research. University of Zaragoza, Spain. p.98

TB33 14:30 -14:45 FINITE ELEMENT SIMULATIONS OF STENTING IN A STENOSED BIFURCATION. **Francesco Migliavacca**, Laboratory of Biological Structure Mechanics, Structural Engineering Department Politecnico di Milano, Milan, Italy. p.99

TB34 14:45 -15:00 PATIENT SPECIFIC FINITE ELEMENT STUDY OF STENT FRACTURE AFTER PERCUTANEOUS PULMONARY VALVE IMPLANTATION. **Silvia Schievano**, UCL Institute of Child Health & Great Ormond Street Hospital for Children, London, UK. p.100

TB35 15:00 -15:15 RUPTURE-RISK EVALUATION OF AORTIC ANEURYSMS BY FINITE ELEMENT PROBABILISTIC ANALYSIS. **Simona Celi**, Dept. Mechanical, Nuclear and Production Engineering, University of Pisa, Italy. p.101

TB36 15:15 -15:30 RULE-BASED SIMULATION OF RESTENOSIS IN STENTS. **Colin Boyle**, Trinity Centre for Bioengineering, School of Engineering, Trinity College Dublin, Ireland. p.102

15:30 - 16:00 PLENARY LECTURE

P7 15:30 – 16:00 Cellular Modelling: Experiments and simulation. Yoshihisa Kurachi, Osaka University, Japan, p.18

17:00 -18:30 TA#4: Experimental methods for models validation

TA41 17:00 -17:15 TIME DEPENDENT INVERSE FEA OF SUPERFICIAL PORCINE SOFT TISSUE USING MR SECTIONS -A PILOT STUDY. **Andrew Sims**, The University of New South Wales, Australia. p.104

TA42 17:15 -17:30 MUSCULOSKELETAL MODELLING OF A SKI TRAINING EXERCISE: MODEL VALIDATION BY EMG ACQUISITION. **Nicola Petrone**, Department of Mechanical Engineering, University of Padova, Italy. p.105

TA43 17:30 -17:45 IN VIVO PHASE CONTRAST MRI VALIDATION OF CFD-BASED BLOOD FLOW RATE ESTIMATES IN DOPPLER ANALYSIS. **Raffaele Ponzini**, CILEA, Italy. p.106

TA44 17:45 -18:00 MECHANICAL TESTING OF LONG BONES: HOW CAN FE MODELS AND IN VITRO TESTS HELP EACH OTHER? **Luca Cristofolini**, Facoltà di Ingegneria, Università di Bologna, Italy; Laboratorio di Tecnologia Medica, Istituto Ortopedico Rizzoli, Bologna, Italy. p.107

TA45 18:00 -18:15 VALIDATING SUBJECT-SPECIFIC FINITE ELEMENT MODELS OF LOWER LIMB BONES IN BENDING AND TORSION. **Enrico Schileo**, Laboratorio di Tecnologia Medica, Istituto Ortopedico Rizzoli, Bologna, Italy. p.108

TA46 18:15 -18:30 IDENTIFICATION METHOD OF SUBJECT-SPECIFIC CORNEAL MATERIAL CONSTANTS AND INTRAOCULAR PRESSURE. **Masao Tanaka**, Graduate School of Engineering Science, Osaka University, Japan. p.109

17:00 -18:30 TB#4: Modelling internal organs

TB41 17:00 -17:15 SEMI-ANALYTICAL METHOD FOR CALCULATION OF PRESSURE DROP IN HEALTHY AND DISEASED LUNG. **Pierre-Antoine Muller**, Air Liquide CRCD Research Center, Medical Gases Group, France. p.111

TB42 17:15 -17:30 NEW PERCUTANEOUS PULMONARY VALVE DEVICE: FINITE ELEMENT TESTING IN PATIENTS' IMPLANTATION SITE. **Claudio Capelli**, UCL Institute of Child Health & Great Ormond Street Hospital for Children, London, UK. p.112

TB43 17:30 -17:45 A SYSTEMS ENGINEERING SIMULATOR FOR PATHOPULMONARY PHYSIOLOGY RESEARCH. **Anup Das**, Department of Engineering, University of Leicester, UK. p.113

TB44 17:45 -18:00 MULTI-SCALE MODELING OF LUNG PARENCHYMA. **Lena Wiechert**, Institute for Computational Mechanics, Technische Universität München, Germany. p.114

TB45 18:00 -18:15 MODELLING OF TEMPERATURE FIELD IN A TISSUE WITH A TUMOR SUBJECTED TO EXTERNAL ELECTROMAGNETIC FIELD. **Marek Paruch**, Department for Strength of Materials and Computational Mechanics, Silesian University of Technology, Poland. p.115

TB46 18:15 -18:30 MODELLING OF LOCAL AND GLOBAL RENAL FUNCTION IN THE PHYSIOME CONTEXT. **Randal S. Thomas**, IBISC, CNRS FRE 3190, Evry F-91000, France. p.116

Friday 18th September 2009

09:00 - 09:30 PLENARY LECTURE

P8 09:00 – 09:30 The VPH/Physiome Project infrastructure. **Peter J. Hunter**, Auckland Bioengineering Institute, University of Auckland, New Zealand, p.19

09:30 - 10:00 PLENARY LECTURE

P9 09:30 – 10:00 Using microfluidics to study coordinated cell population behavior. **Roger Kamm**, Massachusetts Institute of Technology, Department of Biological Engineering, USA. p.20

10:30 -11:30 FA#1: Modelling mechanobiology processes

FA11 10:30 -10:45 FEM AND CFD-BASED MODEL TO ANALYZE MECHANICAL STIMULATION OF OSTEOGENESIS WITHIN PLAGGLASS SCAFFOLD. **Jean-Louis Milan**, Institute for Bioengineering of Catalonia, Technical University of Catalonia, Barcelona, Spain. p.118

FA12 10:45 -11:00 POTENTIAL FUNCTIONS TO DESCRIBE MECHANICAL CELL-CELL INTERACTIONS. **Jeremy Cope**, Department of Computer Science, University of Sheffield, Sheffield S3 7HQ, UK. p.119

FA13 11:00 -11:15 TRABECULAR BONE REMODELING SIMULATION CONSIDERING OSTEOCYTIC RESPONSE TO FLUIDINDUCED SHEAR STRESS. **Taiji Adachi**, Department of Mechanical Engineering & Science, Kyoto University, Japan. p.120

FA14 11:15 -11:30 COMPUTATIONAL SIMULATION OF TISSUE DIFFERENTIATION IN A BONE INGROWTH CHAMBER: THE EFFECT OF VASCULARITY. **Hanifeh Khayeri**, Trinity Centre for Bioengineering, School of Engineering, Trinity College Dublin, Ireland. p.121

10:30 -11:30 FB#1: Cellular modelling

FB11 10:30 -10:45 FLAME/COPASI: AN INTEGRATED COMPUTATIONAL FRAMEWORK FOR MULTISCALE MODELLING. **Rod Smallwood**, Department of Computer Science, Sheffield University, UK. p.123

FB12 10:45 -11:00 DEVELOPMENTS OF COARSE GRAINING DNA MODELS FOR SINGLE NUCLEOTIDE RESOLUTION ANALYSIS. **Kentaro Doi**, Department of Mechanical Science and Bioengineering, Toyonaka, Osaka 560-8531, Japan. p.124

FB13 11:00 -11:15 GENERIC AGENT BASED EPITHELIAL CELL MODEL. **Des Ryan**, Department of Computer Science, University of Sheffield, UK. p.125

FB14 11:15 -11:30 SHAPE INDEX: NEW PARAMETER OF PANCREATIC BETA-CELL FUNCTION IN SUBJECTS AT RISK FOR DIABETES? **Andrea Tura**, Institute of Biomedical Engineering, CNR, Padua, Italy. p.126

11:40 -13:10 FA#2: Musculoskeletal system -cell

FA21 11:40 -11:55 A NESTED DUAL POROSITY FE MODEL FOR CORTICAL BONE. APPLICATION TO A ROOSTER ULNA EXPERIMENT. **M^aAngeles Pérez Ansón**, Group of Structures and Materials Modelling. Aragón Institute of Engineering Research (I3A), University of Zaragoza, Spain. p.128

FA22 11:55 -12:10 VALIDATION OF AN IN SILICO BONE ADAPTATION MODEL BY MEANS OF EXPERIMENTAL IN VIVO LOADING DATA. **Friederike Gerhard**, Institute for Biomechanics, ETH Zürich, Zürich, Switzerland. p.129

FA23 12:10 -12:25 ANALYSIS OF TRABECULAR STRUCTURE REMODELLING FOR PATHOLOGICAL LOAD CASE. **Krzysztof Scigala**, Division of Biomedical Engineering and Experimental Mechanics, Wrocław University of Technology, Poland. p.130

FA24 12:25 -12:40 AN APPROACH TOWARDS PATIENT-SPECIFIC BONE REMODELLING SIMULATION IN OSTEOPOROSIS. **Luís Santos**, IDMEC – Instituto Superior Técnico, Technical University of Lisbon, Portugal. p.131

FA25 12:40 -15:55 MULTI-CELL SIMULATIONS OF GASTRULATION AND SOMITOGENESIS USING COMPUCELL3D. **Randy Heiland**, Indiana University, USA. p.132

FA26 12:55 -13:10 REMODELLING RATE VARIATION CAN ACCOUNT FOR SUBJECT SPECIFIC BONE ADAPTATION. **William R. Taylor**, Julius Wolff Institut and CMSC, Charité – Universitätsmedizin -Berlin, Germany. p.133

11:40 -12:40 FB#2: probabilistic and optimisation methods

FB21 11:40 -11:55 MODELING ANATOMIC VARIABILITY FOR APPLICATION IN PROBABILISTIC SIMULATION OF LUMBAR SPINE BIOMECHANICS. **Anthony J Petrella**, Computational Biomechanics Group, Colorado School of Mines, USA. p.135

FB22 11:55 -12:10 OPTIMIZATION OF A BUOYANCY-DRIVEN MICRODEVICE THROUGH COMPUTATIONAL ANALYSES. **Gabriele Dubini**, Laboratory of Biological Structure Mechanics, Dept. of Structural Engineering, Politecnico di Milano, Milan, Italy. p.136

FB23 12:10 -12:25 PROBABILISTIC FINITE ELEMENT SIMULATIONS OF ELASTOSONOGRAPHY FOR BREAST LESIONS DETECTION. **Simona Celi**, Dipartimento di Ingegneria Meccanica, Nucleare e della Produzione, Università di Pisa. p.137

14:30 -15:30 FA#3: Tissue adaptation

FA31 14:30 -14:45 LOAD INDUCED BONE ADAPTATION MONITORED WITH IN VIVO MICRO-COMPUTED TOMOGRAPHY. **Floor Lambers**, Institute for Biomechanics, ETH Zurich, Zurich, Switzerland. p.139

FA32 14:45 -15:00 THE PREDICTION OF CORTICAL AND TRABECULAR BONE REMODELLING IN AN IN VIVO MODEL OF BONE ADAPTATION. **Webster Duncan James**, Institute for Biomechanics ETH Zürich, Zürich Switzerland. p.140

FA33 15:00 -15:15 DEVELOPMENT OF MULTISCALE CABABILITY FOR CELL BASED MODELLING OF EPITHELIAL TISSUE. **Goodarz Khodabakhshi**, The Department of Computer science, The University of Sheffield, UK. p.141

FA34 15:15 -15:30 HIERARCHICAL BONE REMODELING MODEL WITH PERMEABLE MICROSTRUCTURES. **Pedro Coelho**, FCTUNL, Portugal. p.142

14:00 -15:30 FB#3: New numerical methods and tools

FB32 14:15 -14:30 STRUCTURED TREE OUTFLOW BOUNDARY CONDITIONS FOR 3D LUNG SIMULATIONS. **Andrew Comerford**, Institute for Computational Mechanics, Technische Universität München, Germany. p.144

FB33 14:30 -14:45 COMPUTATIONAL ANALYSIS OF SHOULDER ARTHROPLASTY: BONE REMODELLING AND JOINT WEAR. **Carlos Quental**, IDMEC -IST, TU Lisbon, Portugal. p.145

FB34 14:45 -15:00 MORPHOLOGICAL STUDY OF OVINE SPINAL FACET JOINTS. **Mohd Juzaila Abd Latif**, School of Mechanical Engineering, University of Leeds, Leeds, LS2 9JT, UK. p.146

FB35 15:00 -15:15 CLINICAL SOFTWARE DEVELOPMENT: WHY RESEARCH SYSTEMS FAIL TO TRANSLATE INTO CLINICAL SERVICE. **Steven Wood**, Sheffield Teaching Hospitals NHS Foundation Trust, UK. p.147

FB36 15:15 -15:30 PULLOUT STRENGTH OF ORTHOPEDIC SCREWS CAN BE ACCURATELY ESTIMATED FROM A NOVEL IN SILICO TECHNIQUE. **Andreas J. Wirth**, Institute for Biomechanics, ETH Zurich, Zurich, Switzerland. p.148

15:30 - 16:00 PLENARY LECTURE

P10 15:30 – 16:00 Mathematical models for the circulatory system. **Alfio Quarteroni**. Ecole Polytechnique Federale de Lausanne, Switzerland and Mox-Politecnico di Milano, Italy. p.21

17:00 -18:30 FA#4: Orthopaedic biomechanics

FA41 17:00 -17:15 STRONGER IMPLANTS DO NOT CAUSE STRESS-SHIELDING IN THE FIXATION OF HIP FRACTURES VALIDATED FINITE ELEMENT ANALYSIS AND CADAVER TESTS. **Sebastian Eberle**, Trauma Center Murnau, Biomechanics Laboratory, Germany. p.150

FA42 17:15 -17:30 INVESTIGATION OF INFLUENCE LOCATION OF MOBILE TYPE ARTIFICIAL DISC REPLACEMENT ON THE LOWER CERVICAL SPINE LOADING AND STABILITY. **Lenka Jirkova**, CTU in Prague, Fac. of Mechanical Eng., Laboratory of Biomechanics, Czech Republic. p.151

FA43 17:30 -17:45 IN VIVO ARTICULAR CONTACT ANALYSIS IN A TKA -A FINITE ELEMENT STUDY. **Bernardo Innocenti**, European Centre for Knee Research, Smith&Nephew, Leuven, Belgium p.152

FA44 17:45 -18:00 EVALUATION OF OSTEOSYNTHESIS OPTIONS AND FRACTURE HEALING PROGRESS FROM CT BASED FEA. **Julia Koerber**, Biomechanics Research Laboratory, BGU Murnau, Germany. p.153

FA45 18:00 -18:15 DESIGN OF TREATMENT STRATEGIES FOR AN ATROPHIC NONUNION CASE IN FRACTURE HEALING. **Liesbet Geris**, Division of Biomechanics and Engineering Design, K.U.Leuven, Belgium p.154

FA46 18:15 -18:30 THE ROLE OF BONE ARCHITECTURE ON IMPLANT ANCHORAGE. **Davide Ruffoni**, Institute for Biomechanics, ETH Zurich, Zurich, Switzerland. p.155

17:00 -18:30 FB#4: biomedical signals and instrumentation modelling

FB41 17:00 -17:15 NUMERICAL SIMULATION OF THROMBUS ASPIRATION IN REALISTIC MODELS OF CATHETER TIPS. **Gabriele Dubini**, Laboratory of Biological Structure Mechanics -LaBS, Dept. of Structural Engineering, Politecnico di Milano, Milan, Italy. p.157

FB42 17:15 -17:30 IN SILICO BIOREACTOR FOR SIMULATING TISSUE ENGINEERING USING A MULTI AGENT MODEL. PRELIMINARY RESULTS. **Laura Gaetano**, Politecnico di Torino, Torino, Italy. p.158

FB43 17:30 -17:45 AN OVERVIEW OF COMPUTATIONAL MODELLING IN NEONATOLOGY. **Luiz Wrobel**, School of Engineering and Design, Brunel University, Uxbridge, UK. p.159

FB44 17:45 -18:00 A REAL-TIME HAEMODYNAMICS-BASED TEMPERATURE MODEL FOR HYPOTHERMIC PATIENTS. **Martin Krueger**, Institute of Biomedical Engineering, Universität Karlsruhe (TH), Germany. p.160

FB45 18:00 -18:15 CFD ANALYSIS FOR VORTEX DESIGN IN MICROMIXERS. **Francesco Mastrangelo**, Department of Mechanics, Politecnico di Torino, Italy. p.161

FB46 18:15 -18:30 A BOUNDARY ELEMENT MODEL OF VASCULAR MICROBUBBLE TRANSPORT IN GAS EMBOLOThERAPY. **Joseph L. Bull**, University of Michigan, USA. p.162

Poster Session A

Page	NAME/SURNAME	Title
165	Bruno Bisceglia	Exposure of cell culture to 1f electric fields. Induction of alkaline phosphatase activity
166	Bruno Bisceglia	Capacitively coupled electric fields treatment of spine. Evaluation of electric field in tissues
167	Ruth Wilcox	A parametric finite element evaluation of prophylactic vertebroplasty
168	Stephen Ferguson	Depth and time dependent poisson ratio of cartilage explained by a fiber embedded biphasic model
169	Brandon G. Santoni	Modeling of the transverse post-yield behavior of bovine cortical bone
170	Andreas Vetter	Temporal patterns of different tissue types during fracture healing: experiment vs. Simulation
171	Hans Van Oosterwyck	Porous versus detailed models for the prediction of oxygen profiles in a bone engineering scaffold
172	Simone Tassani	3d registration scheme of microtomographic volumes for the assessment of trabecular bone fracture
173	Ruth Wilcox	A morphological validation method for micro finite element models of bone
174	Massimiliano Baleani	The effect of specimen geometry on the mechanical behaviour of human cortical bone
175	Adelaide de Vecchi	Computational modelling of congenital heart defects for clinical and surgical intervention planning
176	Alison Jones	Simulation of the anterior longitudinal ligament within spinal segments: a sensitivity study
177	Ameet K Aiyangar	Effect of lumbar fusion surgery on the moment arms of the multifidus: a biomechanical modeling study
178	Debora Testi	Vph2_viewer: visualisation and fusion of biomedical cardiac data
179	Elisa Magosso	Neural bases of crossmodal spatial attention: a neural network study
180	Marco Pirini	A mass model of interconnected thalamic populations including both tonic and burst firing mechanism
181	Saulo Martelli	Modelling the mechanical effect of muscles: the lower limb mechanism
182	Yasin Draher	Sensitivity of Bipedal Dynamic Behaviors to CPG-oscillator gains
183	David Lunn	A new method using warped gait data to create subject specific musculoskeletal models for cadaveric bone samples
184	Rita Stagni	Subject-specific tibio-femoral contact estimation during step up/down motor task
185	Mariam Kiran	Exploring the use of social bulletin boards in adaptive agents for fast changing environments
186	Mariam Kiran	Using the learning window in agent memory to reduce complexity in reactive agents
187	Duncan Payne	An efficient and accurate plotting tool for 3d curve analysis in biological samples

Poster Session B

Page	NAME/SURNAME	Title
189	Lorenza Mattei	Experimental procedure for wear model validation: from macro to micro analysis
190	Sami Tarsuslugil	Experimental validation of finite element models of thoracolumbar vertebrae
191	Sophie Rausch	Inverse analysis based determination of material parameters for alveolar parenchyma on different scales
192	Ewelina Swiatek-Najwer	Free-hand sonographic system for bone correction planning
193	Marek Jasinski	Numerical evaluation of changes in retinal perfusion rate during laser irradiation
194	Seishin Takao	Evaluation of therapeutic response to radiotherapy based on tumor geometry
195	A. Motroni	Innovations in medical image processing for the design of custom medical devices and implants
196	Masako Himeno	Cfd analysis of determinant for carotid bulb geometry
197	Diana Massai	Sensitivity of wall shear stress to temporal discretisation in carotid bifurcation models
198	Diego Gallo	A multiscale model of carotid bifurcation haemodynamics
199	Marine Pichelin	Prediction of aerosol deposition within lungs: 3d cfd simulation coupled with analytical modelling
200	M ^a Angeles Pérez Ansón	Bone remodelling on hip resurfacing prosthesis with different cement mantle thicknesses
201	Brendan Frehill	Long-term stability analysis of augmented knee arthroplasty using bone remodelling algorithms
202	M ^a José Gómez Benito	Monitoring fracture healing in sheep: an in vivo study
203	Holger Schmid	Modelling the influence of transmural changes in the mechanical environment to growth
204	John Leicester Williams	What causes paradoxical anterior translation in total knee replacements?
205	John Antoni	The interval and fuzzy analysis of thigh bone with artificial implant
206	Nir Trabelsi	P-fe investigation on the influence of isotropic or anisotropic material models on the mechanical response of the proximal femur
207	Antonio DiCarlo	Progressive coarsening & refining techniques for integrative biomedical computing
208	Nenad Filipovic	Prediction of plaque development in coronary arteries using coupling fe and dpd method
209	Oussama Jarrousse	Efficient volume preservation for a modified massspring system in myocardium mechanical modelling
210	Pras Pathmanathan	A computational study of the mechanical behaviour of discrete tissue models
211	Víctor Alastrué	A micromechanical model to predict damage in soft biological tissues. Application to arterial modelling
212	Daniel Kemmoku	A self adaptative prosthesis using techniques of biocad modeling

Invited Contributions

MODELLING THE NEURAL ADJUSTMENTS IN MUSCLE FATIGUE

Dario Farina¹, Jakob L. Dideriksen¹, Martin Bækgaard^{1,2}, Roger M. Enoka²

1. Center for Sensory-Motor Interaction (SMI), Department of Health Science and Technology, Aalborg University, Aalborg, Denmark

2. Department of Integrative Physiology, University of Colorado at Boulder, CO, USA

Introduction

Muscle fatigue is the exercise-induced reduction in the maximal force-generating capacity of the neuromuscular system. Due to the constraints of experimental approaches, models have been used to evaluate the adjustments that occur during fatiguing contractions (e.g., Giat, et al., 1993; Liu, et al., 2002), including changes in motor unit activity (Bigland-Ritchie, et al., 1983) and in the force expressed by muscle fibers (Thomas, et al., 1991).

In this lecture we present a novel model that simulates a population of motor units during sustained contractions. This model is based on the mathematical description of motor unit recruitment and rate coding proposed by Fuglevand et al. (1993A), with the inclusion of time-varying parameters to simulate fatigue. Moreover, a control algorithm was developed to estimate the descending drive needed to maintain a target force over time.

Methods

The motor unit force and motor neuron model proposed by Fuglevand et al. (1993) was adapted to simulate muscle fatigue during sustained isometric contractions. A proportional-integral-derivative (PID) control system was implemented to generate a target force profile at the output of the model with varying model parameters. A compartment metabolite model of the intra- and extracellular milieu was implemented to drive most of the fatigue-induced changes, and peripheral afferent feedback was included in the motor neuron model. The accumulation of metabolites in the extracellular environment, as predicted by the model, directly affected the force production capacity of muscle fibers and the afferent input to the motor neurons.

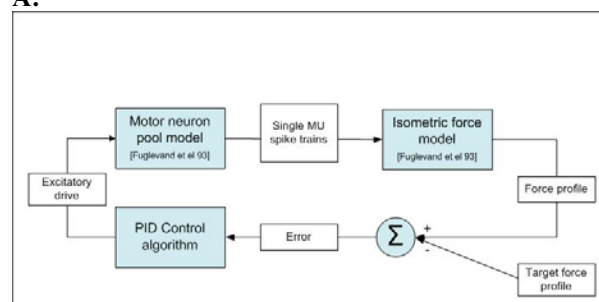
Fig. 1a shows the model structure and Fig. 1b the metabolic compartment model. The model was intended to characterize the first dorsal interosseus muscle, which was assumed to comprise 120 motor units (Fuglevand, et al., 1993). The simulations had a sampling period of 1 ms, the metabolite model was computed every 500 ms, and the PID controller provided a command at sampling rate of 3 Hz.

Results

The model predictions were compared with published experimental results. The time-to-task failure predicted by the model was similar to the experimental observations. At 20% of the maximal force, for example, the model predicted a time to

failure of 522 s, which is similar to experimental results (534 ± 195 s) reported by Fuglevand et al. (1993B). The model also predicted most of the experimentally observed neural adjustments that occur during sustained submaximal contractions, including motor unit recruitment and derecruitment, changes in discharge rates, and changes in recruitment thresholds.

A:



B:

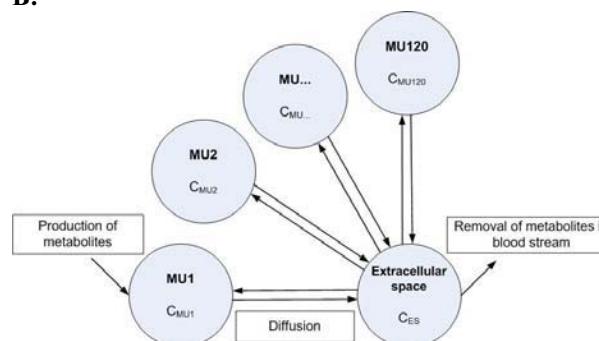


Figure 1: A. Model structure. B. Simplified structure of the compartment model used to describe the accumulation of metabolites during fatiguing contractions.

Conclusion

A model of motor unit recruitment and rate coding has been expanded to incorporate exercise-induced changes in muscle properties and in the excitatory drive received by the motor neuron pool. The approach augments our understanding of the physiological mechanisms that occur during fatiguing contractions.

References

- Bigland-Ritchie et al, J Physiol 340:335-346, 1983
- Fuglevand et al, J Neurophysiol 80:2470-2489, 1993A
- Fuglevand et al, J Physiol 460:549-572, 1993B
- Giat et al, IEEE Trans Biomed Eng 40:664-674, 1993
- Liu et al, Biophys J 82:2344-2359, 2002
- Thomas C. K. et al, J Neurophysiol 65: 1501-1508, 1991

HIERARCHICAL POROELASTICITY: MOVEMENT OF INTERSTITIAL FLUID BETWEEN POROSITY LEVELS IN BONES

Stephen C. Cowin(1), Gaffar Gailani(1, 2) and Mohammed Benalla(1, 2)

1. *The New York Center for Biomedical Engineering & The Departments of Biomedical & Mechanical Engineering, The School of Engineering of The City College and The Graduate School of The City University of New York, New York, NY 10031, U.S.A.*
2. *Mechanical Engineering and Industrial Design, New York City College of Technology*

Abstract.

The governing equations for the theory of poroelastic materials with hierarchical pore space architecture and compressible constituents undergoing small deformations are developed. These equations are applied to the problem of determining the exchange of pore fluid between the vascular porosity and the lacunar-canalicular porosity in bone tissue due to cyclic mechanical loading and blood pressure oscillations. The result is basic to the understanding of interstitial flow in bone tissue that, in turn, is basic to understanding of nutrient transport from the vasculature to the bone cells buried in the bone tissue and to the process of mechanotransduction by these cells. A formula for the volume of fluid that moves between the lacunar-canalicular and vascular porosity in a cyclic loading is obtained as a function of the cyclic mechanical loading and blood pressure oscillations. Formulas for the oscillating fluid pore pressure in both the

lacunar-canalicular and the vascular porosity are obtained as functions of the two driving forces, the cyclic mechanical straining and the blood pressure, both with specified amplitude and frequency. A general observation is that the vascular porosity and the lacunar-canalicular porosity are greatly different. The lacunar-canalicular porosity is a relatively high-pressure domain characterized by a relatively small pore size and no vascular vessels. On the other hand the vascular porosity is a relatively low-pressure domain characterized by a relatively large pore size that contains vascular vessels. The model shows that, although the two porosities exchange fluids, their influence on one another in terms of pressure change is small. The results of this study also suggest a vascular porosity permeability lower than 10^{-11}m^2 and perhaps a little greater than 10^{-10}m^2 . Previous estimates of this permeability have been as low as 10^{-14}m^2 .

TOWARD INTEGRATED MANAGEMENT OF CEREBRAL ANEURYSMS

Alejandro Frangi (1,2,3), Ignacio Larrabide (2,1), Mari Cruz Villa (1,2), Minsuok Kim (1,2), José María Pozo (1,2), Chong Zhang (1,2), Hernán Morales (1,2), Arjan Geers (1,2), Eleonora Flore (1,2)

Center for Computational Imaging & Simulation Technologies in Biomedicine (CISTIB)

1. *Universitat Pompeu Fabra (UPF), Spain*; 2. *Networking Center for Biomedical Research on Bioengineering, Biomaterials and Nanomedicine (CIBER-BBN), Spain*; 3. *Institució Catalana de Recerca i Estudis Avançats, Spain*

Introduction

This keynote lecture will overview work carried out at the Center for Computational Imaging & Simulation in Biomedicine (CISTIB) from Universitat Pompeu Fabra in Barcelona. This work has been performed predominantly under the umbrella of the European Project @neurIST (www.aneurist.org) and the Spanish Technology Platform CDTEAM (www.cdteam.org). Such projects entail some of the visionary concepts behind the Virtual Physiological Human (www.vph-noe.eu).

The ultimate goal behind these projects is moving towards *integrated management of cerebral aneurysms* where *all relevant information* is taken into account in the context of diagnosis and prognosis. Although joint work with other partners in these projects look into the federation of information and computational resources [Dunlop 2008], our own work is primarily focused on developing image- and biomechanics-based diagnostic and prognostic indexes. On the one hand, one is interested in personalized risk assessment of aneurysm rupture, particularly associating it to image-based morphodynamical features of cerebral aneurysms [Hernández 2006, Millán 2007, Zhang 2009] as well as to image-based computational characterization of intra aneurysmal flows [Cebal 2005, Radaelli 2008, Geers 2009]. On the other hand, these projects aim also to develop techniques and systems for optimization of the design and virtual implantation of medical devices like stents and coils used for aneurysm embolization [Radaelli 2008, Larrabide 2008, Kim 2009].

We argue that much technical progress and pre-clinical evaluation have been made towards facilitating the uptake of this technology in clinical practice and that there is a need for multicenter clinical trials involving also technical specialists. After such studies, we anticipate that these tools could become part of standard clinical workflows.

Methodology

The best way to present our methodology is in the form of a data processing pipeline, which proceeds in two main stages. The first stage consists in generating anatomical and, subsequently, flow models of patient specific data. This stage processes the data originating in radiological images and combines it with domain knowledge about the physics, physiology and biology of the cardiovascular systems. From this first stage, diagnostic indexes of morphology and hemodynamics can be derived and

these can be associated to clinical events like aneurysms rupture or reopening. The second stage consists in the virtual implantation of specific devices [Larrabide 2008, Kim 2009], which in turn need to be modelled and the study of the course of hemodynamics after virtual implantation. This stage allows us to study alternative scenarios before treatment in a way that integrates patient-specific knowledge derived from images and biomechanics as well as device-specific information.

Results

A summary of our most recent results will be provided which will cover both illustrations of the application of our techniques as well as some of our efforts to validate the proposed methods or assess their sensitivity to various critical variables.

Discussion

Current state of the art of medical imaging, image computing, and computational biomechanics and physiology already allow today tackling a number of important clinical questions as well as supporting medical device optimization and personalization. Streamlining large and complex processing change workflows reveals sometimes as a challenging problem for more aggressive take-up of these technologies. Validation of these tool chains in large clinical trials and establishment of the associations between computational indexes and clinical outcome still remain an area of further effort.

In order to ease the clinical workflows, availability of such computational tools is at least as important as the IT infrastructures that underpin and enable data and computational resource federation.

Acknowledgements

This work has been partially funded by the European Commission (@neurIST Project IST-FP6-027703) and from CDTI-MICINN (CDTEAM Project). Support from Philips Healthcare BV is also acknowledged.

References

- Bogunovic et al., SPIE Med Imag. 6914:91419, 2008.
- Cebal et al., IEEE Trans Med Imag. 24:457-67, 2005.
- Dunlop et al., Stud Health Tech Inform. 138:173-7, 2008.
- Geers et al., IEEE Int Symp Biom Imag, in press, 2009
- Hernandez et al., Med Image Anal, 11:224-41, 2006.
- Kim et al., IEEE Int Symp Biom Imag, in press, 2009
- Larrabide et al., Lec Not Comp Sci 5247:790-797, 2008.
- Millán et al., IEEE Trans Med Imag, 26:1270-82, 2007.
- Radaelli et al., J Biomech, 41:2069-8, 2008.
- Zhang et al., IEEE Trans Med Imag, in press, 2009.

COMPUTATIONAL MODELLING AND SIMULATION

IN HEART RHYTHM RESEARCH

Blanca Rodriguez

University of Oxford, United Kingdom

In 1962, Denis Noble published the first mathematical model of a cardiac action potential based on the Hodgkin-Huxley formulation. Since then, computational cardiac electrophysiology has developed into a mature discipline in which advanced computational, mathematical and engineering techniques are used to investigate heart rhythm mechanisms in health and disease.

A large body of research in computational cardiac electrophysiology has aimed at investigating the mechanisms of cardiac arrhythmogenesis. The main reason for this is the huge burden cardiac arrhythmias impose to society, as they can often result in sudden cardiac death. In fact, sudden cardiac death subsequent to lethal ventricular arrhythmias is the leading cause of mortality in industrialised societies.

The causes of lethal cardiac arrhythmias are numerous but in 80% of victims, the heart rhythm disturbances arise in consequence of a mismatch between cardiac oxygen supply and demand (myocardial ischaemia) due to coronary heart disease.

In other cases, lethal arrhythmias can be caused by unwanted side effects of drugs (cardiac toxicity), in patients with otherwise healthy hearts. The potential risk of a drug causing lethal arrhythmias is of great concern to both pharmaceutical industry and regulatory agencies and also represents a huge socio-economic burden.

In this presentation, we will describe the development of multiscale models of ventricular electrophysiology, and we will illustrate their use in the investigation of the mechanisms of ventricular arrhythmias caused by ischaemic disease and drug cardiotoxicity. The ultimate goal of the research described here is to contribute to the improvement of the diagnosis and treatment of cardiac arrhythmias to reduce the burden they impose to society.

INTEGRATING MACRO WITH MICRO SCALE TRANSPORT IN THE SMALL INTESTINE: A MULTIGRID LATTICE-BOLTZMANN MODEL

James G. Brasseur (1,2), Yanxing Wang (1), Gino G. Banco (1), Amit C. Aliani (2), Thomas Neuberger (2), Nadine B. Smith (2), Andrew G. Webb (2)

1. Department of Mechanical Engineering, Pennsylvania State University, USA;
2. Department of Bioengineering, Pennsylvania State University, USA;

Introduction

Nutrient and pharmaceutical absorption rely on highly coupled multiscale transport and mixing processes that span several orders of magnitude from the lumen scale (~ 1 cm), to the villi scale (~ 100 μm), to the cellular scale (~ 1 μm), and ultimately to the molecular scale. Nutrient contents are mixed with secretions and transported axially and radially within the gut by macro-scale contractions that are of two basic types: peristaltic and segmental. It is not clear whether these two motility patterns act in concert or independently to effect digestion. However, absorption cannot occur until molecules are presented to the epithelial cells that line micro-scale “villi,” finger-like protrusions that are under controlled motion. Disease can interfere with the rate of radial nutrient transport and lead to malabsorption [Fase, 1985]. We are analyzing the hypothesis that villi motion is necessary to reduce the time scale for nutrient molecules to reach the epithelium [Levitt, 1992], and that disease interferes with villi motion and leads to malabsorption.

Methods

We developed our models within the lattice-Boltzmann (LB) “mesoscale” numerical framework [Chen, 1998], incorporating important advances from the literature and introducing new advances for application to scalar transport within a multigrid LB structure with complex moving boundaries. The continuum level is obtained from discretized moments of a particle distribution function. The space-time-velocity discretization requires a uniform fixed grid, over which can be superposed complex boundary shapes. We have extended the multigrid LB strategy of Yu [2002] to include scalar concentration, predicted using the “moment propagation method” of Merks [2002]. Because our dynamics are driven by complex surface motions, accuracy is critical. We generalized the second-order boundary conditions for fixed boundaries [Lellemand, 2003] to moving boundaries [Ladd 1994] with scalar/scalar-flux boundary conditions.

Results and Discussion

In figure 1 we show examples visualizations of nutrient scalar transport for two model studies. The upper figure is from a study of macroscale scalar

transport and absorption associated with mixtures of peristaltic and segmental contractions of the small intestine. The lower figure shows a 2D cavity flow with moving lid used to model the macro-micro scale couplings in the gut between moving micro-scale “villi” and a macro-scale eddying motion. The uptake of nutrient scalar at the surface of the villi is enhanced by villi motion due to the formation of a “micro-mixing layer.”

The lattice-Boltzmann framework is ideally suited to model internal friction-dominated flows with complex moving surface and passive scalar transport, and to predict scalar uptake at surfaces. The multigrid scalar strategies work beautifully. We have recently extended the study to full 3D.

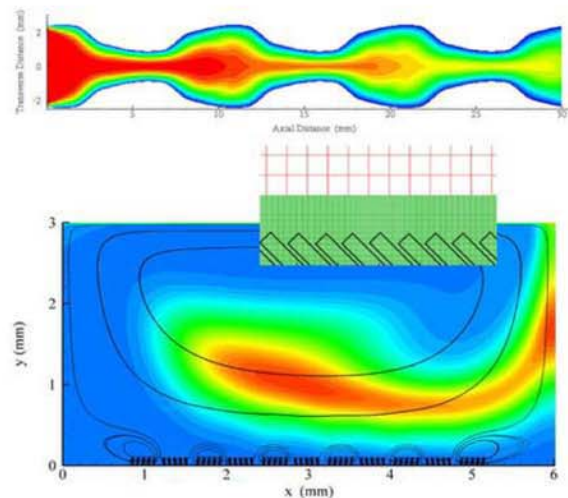


Figure 1: Upper figure: transport from mixed peristaltic and segmental contractions of the gut. Lower figure: a model so study the enhancement of scalar absorption from motility of micro-scale villi. The multigrid is shown in the inset.

Acknowledgements

This work was supported under NSF grant CTS-056215.

References

- Chen S, Doolen, Ann Rev Fluid Mech, 30:329-364, 1998.
- Frase LL, et al, Gastroenterology 88:478-484, 1985..
- Ladd AJC, J Fluid Mech 271:285-309, 1994.
- Lallemand P, Luo L, J Comput Phys 184:406-421, 2003.
- Levitt MD, et al, Amer J Physiol 262:G593-G596, 1992.
- Merks R, et al, J Comput Phys 183:563-576, 2002.
- Yu D, et al, Int J Num Meth Fluids 39: 99-210, 2002.

CELLULAR MODELLING: EXPERIMENTS AND SIMULATION

Yoshihisa Kurachi

Osaka University, Japan

Progresses in experimental understandings are one of the keys to develop the useful cellular models. And the developed models inversely will aid further understandings of the cellular mechanisms by providing us with the tools which allow us to examine a variety of possible perturbations on the interested cellular events. I would like to introduce our experiences in this line of thinking.

1) G protein-control of cardiac K^+ channels: Upon application of acetylcholine, a cardiac K^+ channel is activated to decelerate the heart beat. The activation of the K^+ channel is mediated by the $\beta\gamma$ subunits of PTX-sensitive G proteins (G_K) coupled to m2- or A1-receptors in cardiac cell membrane. This system is subject to further functional and special controls. In the functional aspect, we recently found that the activity of G_K is regulated by RGS proteins in an apparent voltage-dependent manner, which forms the relaxation behavior of K_G channel current. The RGS proteins are inactivated with binding of PIP₃ in the resting state. Ca^{2+} /CaM complex that is formed by depolarization-induced Ca^{2+} influx across cell membrane binds to RGS in a competitive manner against PIP₃. This causes de-inhibition of RGS activity. The activated RGS stimulates GTPase activity of $G\alpha$, resulting in the decrease of $G\beta\gamma$ and thus activity of K_G at depolarized potentials. With this understanding of the mechanism for relation-behaviour of K_G , we could have estimated the physiological dynamics of receptor-G protein cycle. This allows us modelling of the kinetic behaviour of K_G channel activity. With the model, we could have developed a model to obtain insights of temporal and also voltage-dependent behaviour of K_G .

2) β -Adrenergic modulation of Cardiac Calcium Channels: Cardiac L-type Calcium channels are dramatically enhanced under beta-adrenergic stimulation. It has been thought that an increase of functional number of the channel is the only mechanism for this modulation. However, it was found recently that beta-stimulation dramatically modulate and attenuate the voltage-dependent inactivation (VDI) of Ca channel. We have developed a model for Ca channel possessing VDI as well as CDI

(calcium-dependent inactivation). The VDI was measured using outwardly flowing K^+ current at highly positive potential. With taking the attenuation of VDI into account, the simulation results indicated that the inactivation process of Ca channel is purely controlled by CDI under beta-stimulation. The further experimental analyses of CDI mechanism also indicated the need for microstructure-based modelling of Ca^{2+} dynamics to understand the calcium channel inactivation mechanism.

Acknowledgements

These works have been supported by GCOE program for in silico Medicine and grants in aid for scientific research from the Ministry of Education, Science, Culture and Sports of Japan.

References

- Yamada M et al (1998) G protein regulation of potassium ion channels. *Pharmacol Rev* 50(4): 723-760.
- Ishii M et al (2002) PIP₃ inhibition of RGS protein and its reversal by Ca^{2+} /calmodulin mediate voltage-dependent control of the G protein cycle in a cardiac K^+ channel. *Pro Natl Acad Scie USA* 99(7): 4325-4330.
- Kurachi Y, Ishii M (2004) Cell signal control of the G protein-gated potassium channel and its subcellular localization. *J Physiol* 554: 285-294.
- Findlay I et al. (2008) Physiological modulation of voltage-dependent inactivation in the cardiac muscle L-type calcium channel: A modelling study. *Prog Biophys Mol Biol* 96: 482-498
- Kawazu T et al (2008) Microstructure-based Monte Carlo simulation of Ca^{2+} dynamics evoking cardiac calcium channel inactivation. *J Physiol Sci* 58(7): 471-480.

THE VPH/PHYSIOME PROJECT INFRASTRUCTURE

Peter J. Hunter

Auckland Bioengineering Institute, University of Auckland, New Zealand

Introduction

The application of computational methods from the physical and engineering sciences to the fields of physiology and medical science is relatively new but expanding rapidly [Hunter, 2003]. One stimulus to this expansion has been the International Union of Physiological Sciences (IUPS) Physiome Project, another has been the European Virtual Physiological Human (VPH) project. In the US the NIH is contributing through the Multi-Scale Modeling (MSM) consortium.

The biggest challenge for computational physiology is to build personalized (e.g. patient-specific) models that link integrated organ level function (typically accessible in a clinical setting via imaging devices such as MRI or CT) to protein level function (accessible clinically via blood, saliva, urine or biopsy samples). It is at the protein level that diseases and drugs operate, but the function of proteins is as dependent on the cell and tissue environment in which they operate as it is on the genes that encode their sequence. Our quantitative understanding of normal and pathological physiology, and of course our ability to improve the diagnosis and treatment of disease, is therefore highly dependent on linking protein, cell, tissue and organ function through multi-scale modeling.

Methods

To facilitate model sharing and collaboration on multi-scale model development, a major current focus of the VPH/Physiome project is to develop markup languages, model repositories and open source software. CellML [Hunter, 2005; www.cellml.org] and its associated model repository [Lloyd, 2008; www.cellml.org/models] is designed to encode the ordinary differential and algebraic models that are typical of cell physiology (ion channels, calcium transport, metabolic pathways, signaling pathways, myofilament mechanics, gene regulation, etc) or lumped parameter systems physiology models that represent the integrated behaviour of organ systems. Spatially varying anatomically based models (such as finite element models) are similarly encoded in a markup language standard called FieldML [Christie, 2008; www.fieldml.org].

Discussion

The talk will present the above framework for computational physiology and also discuss some of the current challenges in multi-scale modeling of various organ systems.

Acknowledgements

Thanks to the many people who have contributed to the work reported here from the Auckland Bioengineering Institute, the Wellcome Trust Heart Physiome Project (Auckland and Oxford Universities), the European VPH Network of Excellence and the euHeart consortium. Thanks also to the NZ Foundation for Research, Science and Technology.

References

- Christie, R., Nielsen, P.M.F., Blackett, S., Bradley, C. and Hunter, P.J. FieldML: Standards, tools and repositories. *Phil.Trans. Roy. Soc.* In press 2009.
- Hunter, P.J. and Borg, T.K. Integration from proteins to organs: The Physiome Project. *Nature Reviews Molecular and Cell Biology*. **4**, 237-243, 2003.
- Hunter, P.J. and Nielsen, P.M.F. A strategy for integrative computational physiology. *Physiology*. 20,316-325, 2005.
- Lloyd, C.M., Lawson, J.R., Hunter, P.J., Nielsen, P.F. The CellML Model Repository. *Bioinformatics* Vol. 24 no. 18, pp 2122–2123, 2008.

USING MICROFLUIDICS TO STUDY COORDINATED CELL POPULATION BEHAVIOR

Roger D. Kamm (1,3), Vernella Vickerman (2), Ryo Sudo (1), Seok Chung (1)

1. Massachusetts Institute of Technology, Department of Biological Engineering, USA;
2. Massachusetts Institute of Technology, Department of Chemical Engineering, USA;
3. Massachusetts Institute of Technology, Department of Mechanical Engineering, USA

Introduction

Despite the fact that most biological processes in higher-level organisms occur within a complex environment involving multiple cell types and numerous biochemical and biophysical factors, the *in vitro* experiments used extensively in the past to study these phenomena typically involve only one or two cell types and have limited capability for the control of multiple factors [Meyvantsson, 2008]. As a result, questions often remain regarding the physiological relevance of *in vitro* testing under such constrained conditions.

Microfluidic systems offer an ideal platform in which to control and study coordinated cell behaviour, leading to a level of structural organization as is found in vascular networks or organs [Vickerman, 2008][Chung, 2009]. Here we explore several examples of such coordinated behaviour captured in a microfluidic device and with the potential to be simulated by numerical models.

Methods

Experiments are performed in one of several variations on the basic design shown in Fig. 1. “Gel regions” are designed to simulate the extracellular matrix; “access channels”, analogous to vessels of the vascular or lymphatic circulations, provide conduits for cells, medium and pressure control. Various arrangements of these elements have been used in our laboratory to simulate, for example, liver function, tumour angiogenesis and cancer cell intravasation.

Models to simulate these phenomena require, at a minimum, field equations to describe the fluid flow and chemical distributions around cells, solution of the intracellular response of individual cells to stimuli, and the ability of cells to signal via autocrine or paracrine pathways. They must also allow for stochasticity in the responses of individual cells to external stimuli, representing the variability of cell behaviour between different cell types or even among cells of the same population.

Results and Discussion

Angiogenesis. Plating microvascular cells on one face of a collagen gel and controlling the concentrations and gradients of various growth factors, vascular networks have been grown *in vitro*.

Liver tissue engineering. A combination of three cell types – hepatocytes, endothelial cells, and stellate cells – have been introduced under spatial and temporal control in order to maximize their interaction, and promote the vascularization of hepatocyte tissue by an endothelial network.

Tumor cell intravasation. Tumour cells placed in one channel of a microfluidic system are shown to communicate with an endothelial monolayer grown in an opposite channel. Signals exchanged between the two cell types lead to sprouting of microvessels, and induce migration of tumour cells.

Acknowledgements

Support from the US National Science Foundation (EFRI) and the Singapore-MIT Alliance for Research and Technology is gratefully acknowledged.

References

- Meyvantsson et al, *Ann Rev Anal Chem*, 1: 423-449, 2008.
 Vickerman et al, *Lab Chip* 8: 1468-1477, 2008.
 Chung et al, *Lab on a Chip* 9: 269-275, 2009.

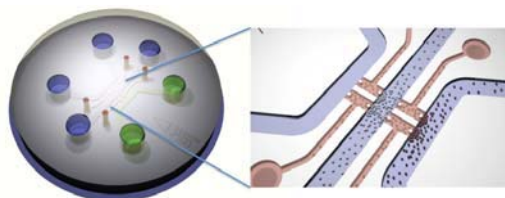


Figure 1: Microfluidic platform showing entire device (right) with filling ports, and the region containing access channels and gel regions, seeded with cells.

MATHEMATICAL MODELS FOR THE CIRCULATORY SYSTEM

Alfio Quarteroni

*Ecole Polytechnique Federale de Lausanne, Switzerland
and MOX-Politecnico di Milano, Italy*

Introduction

In this presentation I will address the role of mathematics in understanding and simulating fluid dynamics and mass transport processes in the physiological and patho-physiological functions of the human cardiovascular system. These phenomena are indeed correlated with the origin of some major cardiovascular pathologies, and, besides, they influence the efficacy of the treatments to heal the arteries from their diseases. Our research activity covers several aspects of the mathematical modeling and numerical simulation of the cardiovascular system; these include the fluid-mechanical interaction between blood flow and arterial wall deformation, as well as the transfer of drugs and chemicals.

Models for biochemical interactions

Concerning the study of pathogenesis, we consider for instance the arteriosclerotic disease that consists in degenerative changes in the arteries, characterized by thickening of the vessel walls and accumulation of calcium with consequent loss of elasticity and lessened blood flow. Based on the knowledge that abnormal accumulation of macromolecules such as low density lipoprotein (LDL) or other atherogens in the arterial wall is an important component of the atherosclerotic disease processes, the quantification of the transport phenomena is required. On this basis, it is world-wide accepted that an improved understanding of vascular mass transport phenomena and the influence of fluid dynamics will have a significant impact on public health.

Starting from suitable mathematical equations and their computer resolution, we are able to compute quantities such as wall shear stresses and mass fluxes, which are correlated with the development of the aforementioned pathologies.

As regards the analysis of medical treatments, we focus on the study of drug eluting stents by means of numerical simulations. Drug eluting stents (DES) are apparently simple medical implanted devices used to restore blood flow perfusion into stenotic arteries. However, the design of such devices is a very complex task because their performance in widening the arterial lumen and preventing further restenosis is influenced by many factors such as the geometrical design of the stent, the mechanical properties and the bio-compatibility of the metal struts, the bio-compatibility of the stent outer surface and finally by the chemical properties of the drug that is released. All these topics are relevant for an effective stent design.

In this framework, mathematical modeling and numerical simulation techniques play a relevant role in understanding what are the most appropriate choices for the optimal design of DES. Nevertheless, because of the complexity of the problem, computer simulation turn out to be an effective tool provided that very efficient algorithms are applied. The main computational difficulties arise from the need to deal with phenomena that take place on multiple scales in space and time.

Concerning the space scales, we remind that DES for cardiovascular applications are miniaturized metal structures that are coated with a micro-film containing the drug that will be locally released into the arterial walls for healing purposes. The thickness of this film generally lays within the range of microns. As regards the time scales, we observe that the release of drug is deliberately very slow. In general, it persists until a few weeks after the stent implantation.

Models for mechanical interactions

The mechanical interaction of blood flow with the arterial wall is the key mechanism responsible for the propagation of pressure waves from heart to peripheral vessels and has a fundamental role in regulation blood pressure in the whole cardiovascular system. Such interaction introduces different spatial and temporal scales, since the pressure propagation speed is much larger than the characteristic blood velocity and size of large arteries.

In the study of blood flow and blood/artery interaction, one is typically interested on local flow features of the flow, which are correlated with the origin and development of major cardiovascular pathologies such as atherogenesis or growth and rupture of aneurisms. On the other hand, local changes in geometry or mechanical properties, as may appear as consequences of surgical interventions, might induce partial reflection of pressure waves and have global effects on the whole cardiovascular system, which should be properly accounted for to achieve reliable numerical simulations.

The geometrical multiscale approach that we have proposed and investigated allows to obtain a model that includes at the same time local and global features and consists in coupling network models for the arterial tree with the local fluid-structure model to describe in detail specific regions of interest. This idea is extremely attractive and has great potentials as a tool to assist in surgical planning being able to simulate both local and global consequences of a surgery intervention.

Oral Presentations

Musculoskeletal system – organ

A MORPHOMETRIC RECONSTRUCTION OF A DISARTICULATED JUVENILE PELVIS

P J Watson (1), P O'Higgins (2), M J Fagan (1), C A Dobson (1)

1. *Department of Engineering, University of Hull, UK;* 2. *Department of Anatomy, Hull York Medical School, University of York, UK*

Introduction

The use of micro-CT data to produce accurate 3D biomechanical and finite element (FE) models of bone structures is increasingly commonplace and well documented [Curtis *et al*, 2008; Kupczik *et al*, 2007; Li *et al*, 2007]. However, when modelling bones of the young or from archaeological or fossilised material, anatomical form is often disrupted through disarticulation at epiphyses or through damage. This is especially challenging with juvenile specimens where ossification is incomplete and a significant proportion of the structures can be cartilaginous. This paper presents an innovative approach for reconstruction of incomplete scan data, to produce digitised bone models which replicate anatomical arrangements of bone and cartilaginous materials. Statistical and warping tools utilising geometric morphometric methods (GMM) (Bookstein, 1989; Dryden *et al*, 1998; O'Higgins, 2000; Zelditch *et al*, 2004) are used to create a model of the complete juvenile hemipelvis, from scan data of each of its three constituent bones, minus the triradiate cartilage.

Method

The three disarticulated bones of the left hemipelvis of an 8yr old were separately μ CT scanned and, together with fused pelvic CT data for a 19yr old, digitised into volumetric models.

Using morphometric data from juvenile pelvic structures, (detailing 27 landmark locations for a range of ages), the fused 19yr old pelvis was then warped to the geometry of a 10yr old (selected to be similar in size and shape to the 8 year old), using thin plate splines, a part of the GMM toolkit (Bookstein, 1989). This warped geometry provided a template to facilitate reconstruction of the disarticulated bones of the 8yr old. By merging all overlying models, the geometry of the cartilaginous acetabulum was estimated.

Results

A final digitised model of a complete 8yr old hemipelvis was created, comprising the separate bones articulating around a cartilaginous acetabulum and pubic symphysis (see Fig 1).

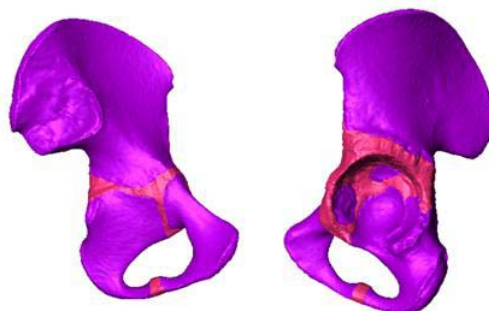


Figure 1: Complete 8yr old hemi-pelvic structure

Discussion

This modelling method has been applied successfully to the reconstruction of a hemipelvis from original disarticulated bony components. The anatomical accuracy of the reconstructed hemipelvis is dependent on the geometry of the warped template, which could be improved through additional landmarks. Validation techniques for the method are currently being explored.

Multivariate regression analyses of registered dense landmark data from a suitable sample offers great potential in facilitating the rapid building of models representing a range of ages.

The reconstruction of juvenile hemipelvis geometries is part of a larger study investigating the structural development of pelvic trabecular bone from pre-natal to adulthood. The resulting FE models will be physiologically loaded to ascertain strain distribution in the bone. Preliminary results of the validation and the FE modelling will be presented at the conference.

Acknowledgements

The authors gratefully acknowledge Prof. S.Black of the Department of Anatomy and Forensic Anthropology, University of Dundee, for kindly providing access to the Scheuer collection.

References

- Curtis *et al*, *The Anatomical Record*, 291:491-501,2008.
- Kupczik *et al*, *Journal of Anatomy*, 210:1, 41-53, 2007.
- Li *et al*, *Journal of Biomechanics*, 40:2758-2766, 2007.
- Dryden *et al*, *Statistical Shape Analysis*, 1998.
- O'Higgins, *Journal of Anatomy*, 197:103-120, 2000.
- Zelditch *et al*, *Geometric Morphometrics for Biologists: a Primer*, 2004.
- Bookstein, *IEE Trans.Pattern Anal. Mach. Intell.*, 11:567-585, 1989.

WHO BENEFITS FROM INTEGRATIVE BIOMEDICAL RESEARCH? THE SOCIO-ECONOMIC ASSESSMENT METHOD OF VPHOP

Karl A. Stroetmann (1), Veli N. Stroetmann (1), Rainer Thiel (1), Marco Viceconti (2)

1. *empirica Communication and Technology Research, Germany*
2. *Laboratorio di Tecnologia Medica, Istituti Ortopedici Rizzoli, Italy*

Introduction

The most significant clinical and societal impact of integrative biomedical research is expected from a more precise quantification of disease risks and the development of optimal pathways for treatment. Methods assessing the clinical and socio-economic impact are rarely applied to more complex technologies, such as predictive and multiscale modelling. The EU funded *Osteoporotic Virtual Physiological Human* (VPHOP) research project, part of the *Virtual Physiological Human* (VPH) European initiative [Kohl, 2008], will create a patient-specific hypermodel to predict the absolute risk of bone fracture much more accurately than predictions based on current clinical practice.

The project developed an innovative, multilevel generic methodological framework to assess the clinical and socio-economic impact of multiscale and predictive modelling technologies.

Methods

The assessment framework was built by constructing a method-mix of benefit cost analysis (BCA), health economic analysis of care pathways, and disease cost simulation models. The beneficial impact of the VPHOP predictive technology may involve costs and benefits on two levels: firstly, earlier and more focused interventions lead to a reduction of the individual as well as social costs of osteoporotic fractures while improving quality of life; secondly, costs and benefits associated with the diagnosis, treatment and rehabilitation need to be assessed as well.

Results

A commonly agreed clinical pathway reflecting the present standard of optimal care was supplemented by a benefit-cost dimension to provide a tool for collecting the required basic clinical, economic and organisational data. Once the new multiscale predictive technology has been validated in a clinical context, the resulting modified new pathway represents the initial tool for comparatively estimating the expected overall impact of the new clinical technology.

Analytically, the increased accuracy of the predictive technology leads also to the prevention

of fractures. These benefits are calculated on the basis of transition probabilities between health states that are typical of osteoporosis. In addition, a decision-analytic [Briggs, 2006; Martin 2007] and scenario-oriented simulation model is conceptualised and integrated with a patient's flow in both old and new clinical pathways. The methodological consolidation is achieved by applying results and data from the clinical pathway analysis and its integrated disease modelling in a holistic cost-benefit analysis.

Discussion

The developed assessment method allows identifying relevant costs and benefits for all stakeholders, from patient to healthcare provider to policy decision-maker, and thereby provides a tool to appraise the overall value of multiscale modelling for society. Health technology assessment is increasingly used to realise optimum benefit from and encourage the efficient use of health technologies. This new assessment method also allows deriving more clearly-defined business models, thus enhancing clinical as well as industrial exploitation of biomedical research.

Acknowledgements

VPHOP is a project co-funded by the European Commission's Seventh Framework Programme. The research reported upon in this presentation has either directly or indirectly been supported by the European Commission, Directorate General Information Society and Media, Brussels. The results, analyses and conclusions derived there from reflect solely the views of its authors and of the presenter. The European Community is not liable for any use that may be made of the information contained therein.

References

- Kohl, P., Coveney, P., Clapworthy, G., and Viceconti, M. The virtual physiological human. Editorial. *Philos Transact A Math Phys Eng Sci* 366: 2987, 2008.
- Briggs, A., Claxton, K., and Sculpher, M. J. Decision modelling for health economic evaluation. Oxford University Press, Oxford, 2006.
- Martin S., Schramm W., Schneider B., Neeser K., Weber C., Lodwig V., Heinemann L., Scherbaum W.A., Kolb H. Epidemiology of Complications and Total Treatment Costs from Diagnosis of Type 2 Diabetes in Germany (ROSSO 4). *Exp Clin Endocrinol Diabetes*. 2007 Sep; 115(8):495-501.

PREDICTING THE FEMORAL NECK RISK OF FRACTURE: TOWARDS A MULTISCALE PROBABILISTIC APPROACH

Fulvia Taddei (1), Saulo Martelli (1), Enrico Schileo (1), Marco Viceconti (1)

1. Laboratorio di Tecnologia Medica, Istituto Ortopedico Rizzoli, Italy

Introduction

Bone fractures in the elderly represent a well-acknowledged and heavy social burden [Cole, 2008]. At present, the definition of fracture risk is usually based only on densitometric measurements and epidemiological parameters [Kanis, 2007]. These protocols are not technology-demanding, but their predictive ability is limited, since they include a single, lumped structural parameter and do not consider the effect of loading. Subject specific Finite Element (FE) models, generated from Computed Tomography (CT) data, have shown to be a powerful tool for the estimation of bone strength [Bessho, 2007; Schileo, 2008]. However, the estimation of fracture risk in a bone segment should take into account the combination of both intrinsic (structure and material) and extrinsic (loading) factors. This is intrinsically a multiscale problem but the development of a corresponding multiscale model of the human musculoskeletal system able to accurately predict the risk of bone fracture is still a grand challenge [STEP, 2007].

A first FE organ-level probabilistic study

A preliminary FE probabilistic model of the proximal femur was developed to investigate the determinants of femoral neck fracture risk during various loading conditions.

A validated procedure was used to build the base FE model from CT data. Different loading conditions, representative of frequent motor tasks, were simulated and a Monte Carlo analysis was run including the patient variabilities of bodyweight, level of osteoporosis, and load intensity level. The resulting peak principal strain in the FE analyses was used to monitor the risk of bone failure.

The results showed that when simple and not too demanding motor tasks were simulated, under the assumption of an optimal neuro-muscular control, no fracture was predicted for any level of osteoporosis. On the contrary, a 4% of fractures were predicted for an unbalanced condition, where the hip joint reaction, taken from experimental measurements [Bergmann, 2001], showed the highest variability.

The results suggested the importance of considering the occurrence of “anomalous” motor tasks as well as understanding the influence of different motor control strategies on the bone loading conditions.

A two-level multiscale approach

A body-level musculo-skeletal model of the lower limbs of a specific subject was coupled with the FE model of the right femur of the same cadaver specimen, obtained from CT data.

An innovative approach was applied to estimate, for the instant of maximum hip joint reaction, all possible combination of muscles forces that satisfy the equilibrium equations, corresponding to different activation strategies. The space of solutions was sampled and a Monte Carlo simulation was run to investigate how the predicted variability influenced the femoral neck fracture.

Preliminary results showed very different muscle activation patterns, to the point that several muscles varied between silence and full activation. This reflected in a huge variation of the FE predicted risk of fracture that ranged between 0.7 and 2.1.

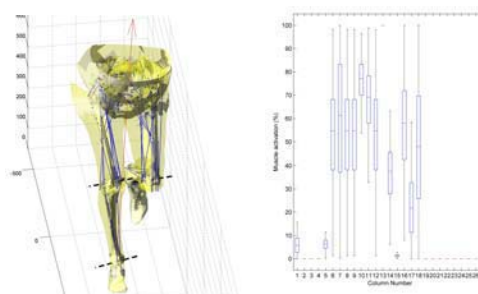


Figure 1: on the left the MS model in the instant of peak hip joint reaction, on the right the variability of each muscle activation.

Discussion

The obtained results, although with the limitations of the presented studies, highlighted the importance of adopting a multiscale approach for the prediction of the risk of fracture in the femoral neck. In addition they showed the necessity of including a probabilistic description of the possible occurrence of “anomalous” motor tasks and a probabilistic description of the possible co-contraction schemes since they may greatly influence the stress state experienced by the bone segment.

Acknowledgements

This study was partially supported by EC-funded projects LHD (IST-2004-026932) and VPHOP (Grant #223865).

References

- Bergmann et al, J Biomech, 34: 859-71, 2001.
- Bessho et al, J Biomech, 40: 1745-53, 2007.
- Cole et al, Curr Rheumatol Rep, 10: 92-6, 2008.
- Kanis et al, Osteoporos Int, 18 : 1033-46, 2007.
- Schileo et al, J Biomech, 41: 356-67, 2008.
- STEP, <http://www.europhysiome.org/roadmap>.

FINITE ELEMENT FEMUR GENERATION USING MORPHING AND SPHERICAL PARAMETERIZATION TECHNIQUES

Najah Hraiech(1,2), Michel Rochette(1), Fulvia Taddei(3), Marco Viceconti(3)

1. ANSYS France, Villeurbanne, France; 2. LTSI, Inserm 642, Université de Rennes 1, France; 3. Laboratorio di Tecnologia Medica, Istituto Ortopedico Rizzoli, Bologna, Italy.

Najah.Hraiech@ansys.com

Introduction

An accurate prediction of the failure load and location of osteoporotic bones can be obtained using personalized FE models [Schileo, 2008]. Therefore one would need to simulate a personalized model, to better predict the behavior of organs in diagnostic and surgery planning. Nowadays, automatic model generation represents a very active research topic in surgical treatment and simulation. Different methods for reconstructing such models directly from CT scans have been addressed in the recent years by researchers [Viceconti, 2003], yet few of those approaches have been transferred to practice. An alternative to direct, time-consuming, step-wise reconstruction would be to take a carefully designed and annotated database of existing femur models, and to derive new femurs by adapting selected prototypes from this database to the new CT scans using a morphing technique. Because morphing is a bijective transformation, this approach could also permit to map element connectivity and even spatial distribution of bone mineral density (BMD) from the generic to the specific model..

In the following we present an approach of such a morphing technique, which is an extension of a recently proposed morphing technique for proximal femurs [Hraiech, 2008].

Method: 3D Femur Mesh Morphing

In [Hraiech, 2008], we described a fast and accurate method to generate patient specific models for proximal femurs, based on a constrained morphing (through Radial Basis Function (RBF) regression) of a template mesh, . The method takes as input a tetrahedral template mesh of proximal femur region, and a set of reference anatomical landmarks (10 nodes for the example of fig. 1). Then, it is sufficient to define the corresponding anatomical landmarks on a triangulated surface (STL, usually derived from a CT scan) of a specific femur, and the method generates automatically the tetrahedral volume mesh. In this paper we extend this method to the whole femur. To achieve this aim, the morphing of the surface mesh, which was originally performed on a planar parameterization of the proximal femur, is now replaced by a morphing on a spherical domain.

In detail, we map both femurs (the skin of the tetrahedral template mesh and the STL) onto two spheres using the method described in [Saba, 2005], and then we apply RBFs regression, centered by the set of pre-selected anatomical landmarks, to morph the spherical parameterization of the generic mesh into the spherical parameterization of the patient geometry. The resulting “morphed” spherical mesh, which matches the anatomical landmarks of the STL, is then correlated with the STL sphere. As a result we obtain the local coordinates of each node of the mesh in the target triangles, and by projecting them on the surface of the patient geometry we derive the resulting triangular mesh of the whole femur. Combining this result with a second RBF interpolation in 3D, we compute the tetrahedral mesh of the patient geometry; fig.1 shows one of the resulting meshes.

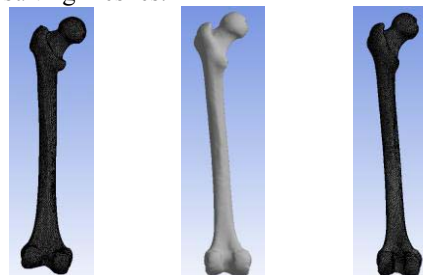


Fig.1: (Left) tetrahedral generic mesh, (middle) patient geometry, and (right) resulting patient mesh.

This new method offers a great benefit for building an exhaustive database of femurs: the shape, and possibly in future implementations even BMD parameters, to define a generic template could be easily extracted from a population of real femurs using standard principal component analysis.

Results and Discussion

Using a template tetrahedral mesh and 10 anatomical points, we tested the process on 8 different femurs. Preliminary results are encouraging. We are currently preparing an extensive evaluation of the method on a larger database (approx. 100 femurs; courtesy of Istituto Ortopedico Rizzoli, Italy).

References

- Hraiech N. et al. ISBI, 1561-1564, 2008.
- Saba S. et al. SMI '05, 258-267, 2005.
- Schileo et al., J Biomech 41:356-67, 2008.
- Viceconti and Taddei, CritRevBiomedEng31:27-72, 2003

Data management and modelling tools

PHYSIOMESPACE: DIGITAL LIBRARY SERVICE FOR BIOMEDICAL DATA

Debora Testi (1), Paolo Quadrani (2), Marco Viceconti (3)

1. *SuperComputing Solutions, Italy*; 2. *CINECA, Italy*; 3. *Laboratorio di Tecnologia Medica, Istituti Ortopedici Rizzoli, Italy*

Introduction

PhysiomeSpace (www.physiomespace.com) is a digital library service designed to help researchers to share their biomedical data and models. The service allows the users to share their data, but also to search for data owned by other users, and download them after authorisation.

The service is composed by a client application, which allows to import almost any type of biomedical data, visualise and annotate the data, upload data to the repository and download the data already selected with the web interface. Then, the user can manage his/her uploaded data by accessing the repository via a web interface. This interface allows the user to complete the data annotation, share the data with other PhysiomeSpace users, search for new data, and select data for downloading into the local computer (Figure 1).

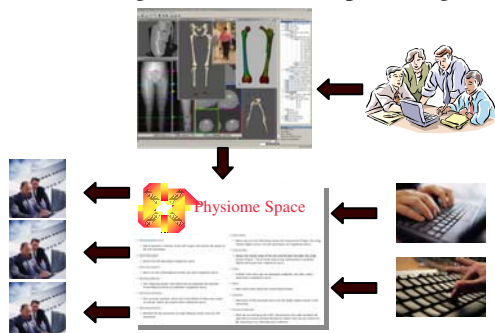


Figure 1: PhysiomeSpace user's experience

The PhysiomeSpace modules communicate each other via web services with the infrastructure schematised in Figure 2.

The client application: PSLoader

PSLoader is an application developed based on the Multimod Application Framework, an open source framework for the rapid development of computer-aided medical applications (www.openmaf.org). The C++ code has been then extended with Python scripts to allow communication with the other infrastructure services.

The application is a desktop application that, after user authentication, allows him/her to import a long series of biomedical data (DICOM, stl, finite element mesh, motion analysis etc.), and to visualise them with a series of specialised views (orthoslice, arbitrary slice, isosurface, etc.). Then the data can be curate with a series of metadata which aims to provide a coherent set of concepts to

be used for the annotation of the resources stored in the digital library and to provide the information framework for the searching and retrieving of resources, and the creation of complex workflows (i.e. traceability).

The user can then select one or more data and upload them into his/her repository sandbox.

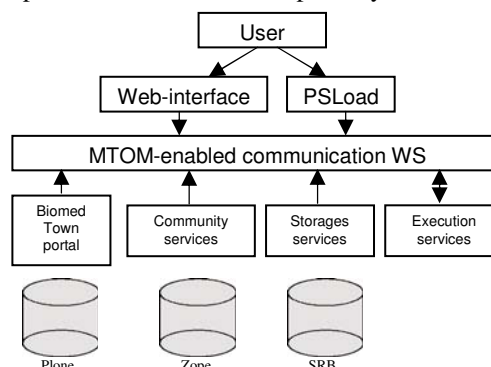


Figure 2: PhysiomeSpace architecture

The web-interface

The user can access the repository also via browser through a web-interface which is hosted on the BiomedTown portal (www.biomedtown.org).

The user can there manage his/her loaded data, complete the metadata curation, and share each data with other PhysiomeSpace users.

Once shared the data can be downloaded by whom has permissions to, and searched by any other PhysiomeSpace user. Specific search mechanisms have been implemented and exposed to allow the user the look for the data in the most efficient way according to his/her specific needs.

When a data of interest is found, the user can ask permissions to the data owner to download it and, once granted for access, download locally the file using PSLoader.

Conclusions

PhysiomeSpace is an advanced service which allows researchers to share their biomedical data. The basic system functionalities are freeware and will be continuously improved and expanded to provide a better and better service to its users.

Acknowledgements

This work has been partially funded by the ICT for Health Unit of the European Commission in the LHDH project (FP6-2004-IST-4-026932).

PHYSIOMESPACE: EXECUTION SERVICES TO REMOTELY PRE-PROCESS AND PREVIEW BIOMEDICAL DATA

Debora Testi (1), Xia Zhao (2), Enjie Liu (2), Gordon Clapworthy (2)

1. SuperComputing Solutions, Italy; 2. University of Bedfordshire, UK

Introduction

PhysiomeSpace (www.physiomespace.com) is a digital library service designed to help researchers to share their biomedical data and models. The service allows the users to share their data, but also to search for data owned by other users and download them after authorisation.

Though this is very powerful, the users previously lacked any tool to preview or eventually pre-process the data before downloading.

To overcome these limitations, PhysiomeSpace has been enriched by the development and integration of Execution Services. These are executed remotely and provide the users with functionalities to pre-process and preview the data stored in the digital library.

For example, a user may find a CT scan of a femur but the volume is at a very high resolution (and consequently of a huge size), and the user does not know if it is the whole femur or only a part. Before downloading it, the user can launch a remote operation to preview the volume, and after making sure that the whole femur is indeed represented, to resample the volume to the resolution he/she needs. The result is still stored in the digital library but can then be locally downloaded and used.

Execution services description

Execution services take advantage of current Web Services [Alonso, 2003] technologies that prompt for building and integrating distributed applications in open-standard, platform-independent and loosely-coupled style. Services encapsulating core data-processing functionalities can be accessed remotely through the Internet.

According to these data-processing functionalities, 6 groups of Execution services have been designated and developed, as shown in Figure 1. *Import* and *Export* services are used to translate data from different formats (e.g. dicom, stl, vrm) into a unified standard and to store them in the digital library. *Creation* services allow users to create datasets from scratch. *Modification* services provide functions to process datasets, such as resample-volume, decimate-surface, etc. *Preview* services allow users to remotely preview data as surface, slice or volume, etc. *Measurement* services measure data without creating new data in the library, such as measure-volume.

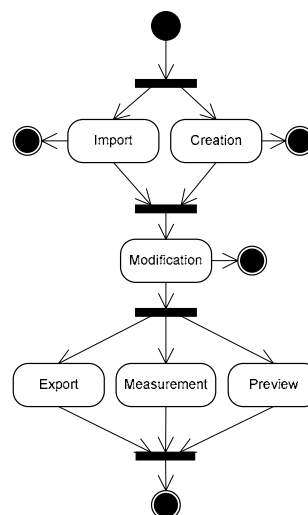


Figure 1: Execution services and data flows among them

In addition, a flow of data-processing functions, such as *extractisosurface-then-decimatesurface*, can be formed using Web service composition technology. The Web Service Business Process Execution Language (WSBPEL) [Jordan, 2007] is used to build new workflow services by choreographing basic Execution services. On one hand, the composite services prompt reusability, and on the other, they can significantly reduce the complexity for users who wish to access an extended series of services.

Conclusions

The execution services described represent an advanced and useful add-on to the digital library in its progress towards a complete web-based service.

Acknowledgements

This work has been partially funded by the ICT for Health Unit of the European Commission in the LHDL project (FP6-2004-IST-4-026932).

References

- Alonso G et al, *Web Services: Concepts, Architectures and Applications*, Springer-Verlag, Berlin, Germany, 2003.
- Jordan D et al, *Web Services Business Process Execution language Version 2.0*, OASIS Standard, 2007, online: <http://docs.oasis-open.org/wsbpel/2.0/wsbpel-v2.0.pdf>.

STRUCTURAL IMAGING OF CORONARY VASCULAR-MYOCARDIAL RELATIONSHIP AND MODEL GENERATION

Jack C. J. Lee (1), Bruce H. Smaill (2), Nicolas P. Smith (1)

1. Computing Laboratory, University of Oxford, UK; 2. Bioengineering Institute, University of Auckland, New Zealand

Introduction

The mechanical *crosstalk* between coronary flow and contracting myocardium is a phenomenon that plays a fundamental role in cardiac perfusion and function. It describes the interplay between pressure and deformations in vessels and tissue [Westerhof, 2006] that leads to systolic coronary flow impediment and reversal, and has been suggested to contribute to the heightened subendocardial vulnerability to ischemic damage. Crosstalk is a local and heterogeneous process that depends on a large number of factors including, at minimum, the combined anatomical structures of vasculature and myocardium, coronary and ventricular pressures, cardiac contractility, coronary compliance and resistance. Model characterisation of these complexities has much to benefit from a biophysically-accurate finite element model that allows rigorous and detailed assessments against experimental studies. Such a model has not been available to date due to a lack of detailed anatomical information.

In this study, we aimed to address this deficiency by employing novel imaging techniques to characterise cardiac and vascular microstructures and demonstrate model building via automated image processing algorithms.

Methods

Structural imaging of myocardium and coronary vasculature of a complete rat heart LV transmural block was achieved using a custom-built automated extended volume confocal imaging device [Sands, 2005]. The sample specimen was perfused with vascular casting polymer, dehydrated and embedded in resin to be dual-channel imaged in sequential serial planes at 1 μ m isotropic resolution, alternated with removal of the uppermost layer of tissue.

The resulting vascular images were segmented into a binary mask. A modified form of voxel-coding based centerline tracking algorithm [Zhou, 1999] was then employed to extract a graph representation of the vascular topology, and post-processed with a minimum spanning tree-based reduction algorithm. The images of myocytes were acquired into a separate channel and the fibre orientation angles were estimated using a previously described method [Karlson, 1998].

Results

The vascular network extracted from the transmural block is shown in figure 1. The ~140,000 segments occupied approximately 15% of the total volume. The transmural distribution of average fiber angles were found to vary approximately linearly between 60° (endo) to -60° (epi), consistent with previous estimates. The angles vessel segments form with the surrounding myofibers were calculated in the fiber plane, as shown in figure 2.

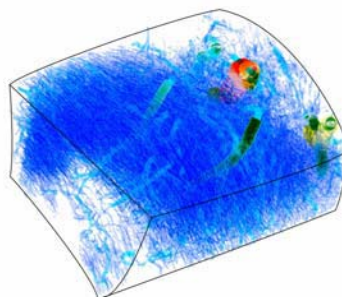


Figure 1: Extracted vascular network and outlines of the tissue block (endocardial surface on the left).

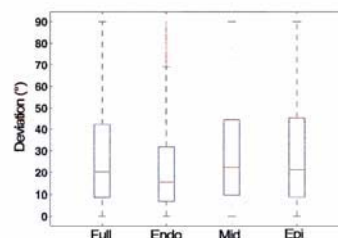


Figure 2: Vessel-myofiber alignment angles.

Discussion

The model extraction capability of the proposed technique has been demonstrated on a complex and heterogeneous cardiac and coronary microstructure. The future application of this technique to functional implication studies in biomechanical models is currently under way.

References

- Karlson et al, Anat Rec, 252(4):612-625, 1998.
- Sands et al, Micro Res Tech, 67:227-239, 2005.
- Westerhof et al, Physiol Rev, 86:1263-1308, 2006.
- Zhou et al, IEEE Trans Visual Comput Graph, 5(3):196-209, 1999.

DESIGN OF A GRID INTERFACE FOR THE HIGH-PERFORMING PARALLEL FINITE ELEMENT SOLVER PARFE

Peter Arbenz (1), Sumit Paranjape (1)

1. Computer Science Department, ETH, Zurich, Switzerland

Introduction

The goal of the ParFE project is to develop massively parallel solvers for finite element (FE) problems arising from bone modeling [Sala, 2006]. The computationally intensive phase is the solution of the linear system

$$A x = b \quad (1)$$

arising from the FE discretization of the linear elasticity equations. In fact, although the equations their discretization techniques are well-known, much has to be done to solve them efficiently for real-life problems, especially on parallel, distributed memory computers. Several issues arise. First, the application must be able to read large mesh files from disk, compute the desired solution and write it to disk again. Then, an optimal solution technique must be determined.

The approach followed by ParFE developers consists in applying powerful multilevel preconditioners based on smoothed aggregation procedures. We provide both matrix-free and matrix-ready approaches (that is, our preconditioners can both solve the assembled linear system or use the element-by-element matrix-vector product).

ParFE is written in C++, and it is based on several high-performance libraries for scientific computing, mostly BLAS, LAPACK, MPI, ParMETIS, [Trilinos](#) and [HDF5](#). ParFE is usually executed on massively parallel machines like Cray XT or IBM Blue Gene.

A Grid Interface

The basic idea of grid computing is the sharing of resources. In order to make available ParFE to a dedicated group of people we design an interface to make available ParFE on the HPC facility at the Swiss Supercomputer Center (CSCS). This will make the modeling of large scale bone structures easy for the people in the group.

The interface will be based on the GridSphere portal framework that provides an open-source portlet based Web portal [GridSphere] which in turn is based on the Globus toolkit [Globus]. The prototype portal will provide a simple and secure



Figure 1: The Cray XT-3 at CSCS

means to submit ParFE jobs to CSCS. It in particular authenticates users through username and password. It only accepts actions of the user according to his/her permissions. The portal is accessed through a web browser. The web interface accepts parameters that it will forward to ParFE jobs like, e.g., the number of processors needed, and files that contain input data for one or several jobs. The user does not have to bother about the actual start of a ParFE job. Jobs that are submitted to HPC centers like the CSCS are typically scheduled through queuing systems. There are no interactive jobs. It may take some time (minutes to days) until a job is finished. The grid interface then notifies the user by an email message about job completion and whereabouts of the output. (The volume of the output prevents it from being sent as an attachment.) The grid interface provides the user with information on the job status (queued, running, completed), project accounting, but also with some statistics on the available machines, in order to direct the execution process.

References

- [Arbenz, 2008] P. Arbenz, R.Müller, ERCIM News 74: 31-32, 2008.
- [Arbenz, 2008] Arbenz et al., *Internat. J. Numer. Methods Engrg.* 73: 927-947, 2008.
- [GridSphere] <http://www.gridsphere.org>
- [Globus] <http://www.globus.org>
- [Sala, 2006] Sala et al., PARFE, a fully-parallel μ -FE code. <http://parfe.sourceforge.net/>

Musculoskeletal system - body

MUSCLE WRAPPING USING FINITE ELEMENT CONTACT DEFINITIONS

Philippe Favre (1,2), Jess G Snedeker (1,2)

1. Orthopaedic Research Laboratory, University of Zürich, Balgrist, Switzerland;

2. Institute for Biomechanics, ETH, Zürich, Switzerland

Introduction

Representation of a realistic muscle path is central in musculoskeletal modelling, as this directly influences the respective muscle moment arm, line of action and force. Two methods have typically been described to solve this intricate issue. The centroid method represents the muscles by deformable line segments wrapping on simplified geometries. This method solves quickly and has been shown to deliver realistic moment arms. However, the approximate underlying geometry and fixed “via points” must be set in advance for each joint configuration [Garner, 2000]. Second, wrapping on anatomically precise bone geometries has been achieved with sophisticated 3D volumetric finite element (FE) models of the muscle [Blemker, 2005]. While this approach could eliminate many artificial boundary conditions, its complexity may be excessive for muscle force estimation simulations. With the intention to combine the advantages of both methods, we have developed an intermediate technique relying on the contact detection capabilities of commercial FE packages.

Methods

The 3D surface geometry of the humerus and scapula were imported to Marc Mentat (MSC Software, Santa Ana, CA) from the *Bel repository* and set as rigid bodies. The bones were held fixed in the joint configuration of interest.

Ten line segments represented the rotator cuff muscles, each as series of beam elements (Fig.1). One end of each segment was attached to the insertion site on the humerus, and the segment was oriented perpendicular to the humerus surface at the attachment site. Boundary conditions were defined to move the other segment end to the respective origin point on the scapula, deforming and wrapping the muscle strings on the bony surface. Touching contacts between the bones (except for the acromion and coracoid) and all muscles prevented penetration. To avoid slipping, friction had to be introduced between the bone and the muscles. The direction of the muscle at the last point of contact with the humerus defines the line of action vector, and the moment arm could be directly computed as its distance to the humerus center.

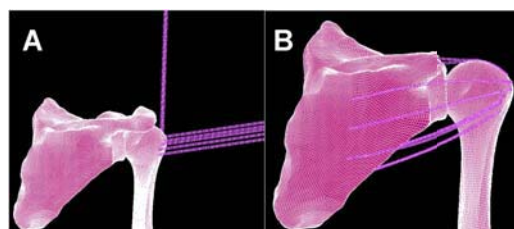


Figure 1: Model configuration before (A) and after (B) muscle wrapping.

Results

Wrapping could be simulated in a variety of joint positions without user intervention or tuning of the model. The resulting abduction moment arms during humerus elevation were comparable to published in vitro or modelling data (Fig. 2).

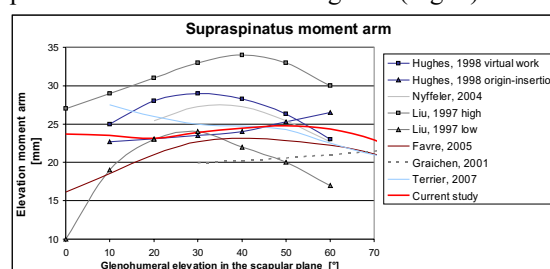


Figure 2: Supraspinatus elevation moment arms compared to published data.

Discussion

This method yields realistic muscle moment arms for the tested positions, solves in few minutes for 10 muscle segments on a standard desktop PC, does not require artificial underlying geometries nor prior measurement of input data. The main limitation is an arbitrarily assigned muscle-bone friction to achieve a realistic outcome, but this may be preferable to the use of more artificial constraints like via points or stub obstacles.

This technique is now being extended to all glenohumeral muscles and combined with a muscle force estimation algorithm [Favre, 2005] to build an integrated, actively stabilized, FE model of the glenohumeral joint.

References

- Blemker et al, Ann Biomed Eng, 33: 661-73, 2005.
- Favre et al, Clin Biomech, 20:822-33, 2005.
- Garner et al, Comput Methods Biomech Biomed Engin, 3:1-30, 2000.

ASSESSMENT OF EFFECTIVE CONNECTIVITY IN TETRAPLEGIC AND HEALTHY SUBJECTS BY USING A NEURAL MASS MODEL

Filippo Cona (1), Melissa Zavaglia (1), Laura Astolfi (2,3), Fabio Babiloni (2,3), Mauro Ursino (1)

1. Department of Electronics, Computer Science, and Systems, University of Bologna, Cesena, Italy; 2. Department of Human Physiology and Pharmacology, University of Roma "La Sapienza", Italy; 3. IRCCS Fondazione Santa Lucia, Roma, Italy

Introduction

The execution of simple motor or cognitive tasks by the brain requires the participation of multiple cortical regions, which are functionally and mutually interconnected. In this work, a neural mass model is used to estimate the connectivity among three cortical regions of interest (ROIs) (the cingulate cortex (CMA_L), the primary motor area (MIF_L), and the supplementary motor area (SMAp_L)) during a simple imagery foot movement task. A new method, based on a genetic algorithm, is implemented to provide an automatic fitting between model and real power spectral densities (PSDs).

Methods

The model of a single ROI was obtained by modifying equations proposed by [Wendling, 2002]. It consists of four neural groups communicating via excitatory and inhibitory synapses. In order to simulate the overall task, we considered five ROIs which are interconnected through long-range excitatory connections: three simulate the CMA_L, the MIF_L and the SMAp_L and exhibit an intrinsic oscillation in the beta range. Other two ROIs (simulating a thalamic region (LF) and a pre-frontal region (HF)) intrinsically oscillate in the alpha and gamma range, respectively. High-resolution scalp EEG data were acquired in five healthy volunteers and five tetraplegic patients; scalp EEG was propagated to the cortex via a propagation model, to infer cortical electrical activity in three ROIs. A fitting between model and real EEG PSDs was realized via an original genetic algorithm.

Results

Results demonstrate that the model can fit real spectra quite well (see Figure 1) reproducing the presence of three rhythms (in the alpha, beta and gamma ranges). The stronger connections are those from the cingulate cortex to the primary and supplementary motor areas (Figure 2, right panel). This result suggests that the CMA_L has a pivotal role during the task. Tetraplegic patients exhibit higher connectivity strength on average (+12%), with significant statistical differences in some

connections (Figure 2, left panel). In particular, connections from the thalamus and from the pre-frontal cortex are significantly higher in the tetraplegic group.

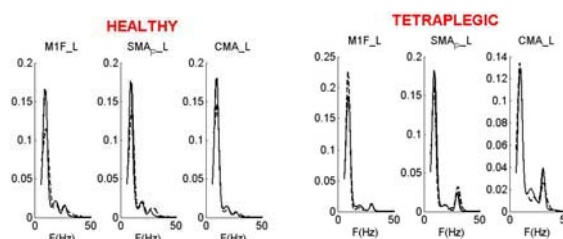


Figure 1: Example of the comparison between real (dashed line) and simulated (continuous line) PSDs in one healthy and one tetraplegic subject.

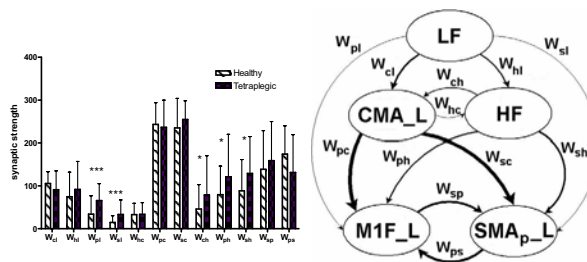


Figure 2: Connectivity weights estimated on five healthy subjects and five tetraplegic patients (left panel). Connectivity weights are proportional to the line thickness (right panel).

Discussion

The present work represents a first attempt to reproduce the presence of multiple rhythms in three ROIs involved in motor tasks, and their variability, using a simple model of interconnected populations. An innovative aspect of this work is that connectivity is not obtained starting from empirical black-box equations, but using an interpretative model, which attempts to mimic real neurophysiological aspects. Encouraging results concern the capacity to obtain reliable PSD spectra, by acting on a few parameters representing the connection weights, and to detect significant differences between the two classes.

References

Wendling et al, Eur J Neurosci, 15:1499-1508, 2002.

3D MODELING OF PATIENT-SPECIFIC MUSCULOSKELETAL SYSTEM USING MRI IMAGES AND THE EOS[®] SYSTEM

Jérôme Hausselle, Amine El Helou, Erwan Jolivet, Ayman Assi, Dominique Bonneau, Wafa Skalli

LBM, Arts et Metiers ParisTech, UMR CNRS 8005, France

Introduction

3D musculo-skeletal models are widely used to evolve from gait analysis to joint loads estimation [Delp, 1990, Erdemir, 2007]. However, there is still a need to improve subject specificity of such models, usually obtained by rescaling a generic model. In particular, muscle-tendon lengths and muscle moment-arm lengths need to be better estimated [Scheys, 2008]. Medical images have been used allowing an evolution towards patient-specific models [Blemker, 2005]. In these models, muscles are rigidly transformed from one position to the other. This study aimed at defining a patient-specific model based on MRI images and the use of the EOS[®] system, taking into account muscle shape changes between the MRI and EOS[®] positions.

Methods

The EOS[®] system has been used to get biplanar X-rays of a healthy male subject, leading to the 3D model of his lower limb skeleton [Südhoff, 2007]. This enhanced bone model also provided muscle origin and insertion points. MRI images have been taken and 42 lower limb muscles have been reconstructed (Figure 1.a), based on a reduced set of images [Assi, 2008, Jolivet, 2008]. Several anatomical landmarks have also been identified.

For each bone, a local coordinate system has been defined, allowing the calculation of transformation matrices between the MRI and EOS[®] positions (Figure 1.b).

The first step used a rigid transformation between the bones to get muscle origin and insertions points in the MRI position, before transforming the whole MRI model (3D muscles and insertion points) into the EOS coordinate system.

The second step involved the use of the skin envelopes of the legs, reconstructed from both the MRI images and the biplanar X-rays (Figure 1.c). A non-linear kriging method was then used to take into account skin deformation and to transform muscle shapes.

Results

The developed method allowed the transformation of muscles from MRI to EOS[®] position, giving a

patient-specific musculoskeletal model of the lower limbs. This method also took into account muscle shapes changes from the lying to the standing position.

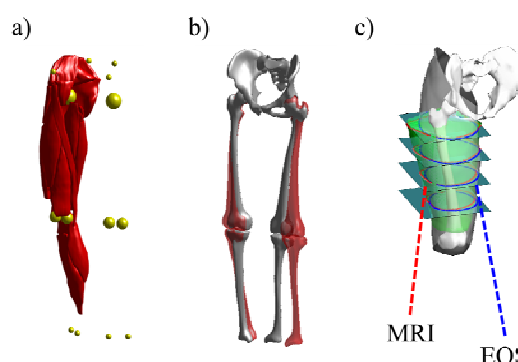


Figure 1: a) 3D muscles (right leg only for visual purpose) and anatomical landmarks from MRI images. b) Bones in EOS[®] (gray) and MRI (red) positions. c) Skin envelopes of the thigh, from MRI images and EOS[®] X-rays.

Discussion

The goal of this study was to develop a method to model patient-specific lower limb musculo-skeletal system, based on MRI images and the EOS[®] system. This method also took into account soft tissues shape changes from lying (MRI) to standing (EOS[®]) position. By combining motion analysis and such patient-specific model it should be possible to get realistic dynamical musculoskeletal models during motion, improving the accuracy of muscles moment arms and muscle-tendon lengths calculation.

Acknowledgements

The authors would like to thank the Louis Mourier Hospital and Dr. Dion for providing the MRI images.

References

- Assi et al, *Gait & Posture*, 28(2):S12-S13, 2008.
- Blemker et al, *J Biomech*, 39:1383-1391, 2005.
- Delp et al, *IEEE Trans Biomed Eng*, 37:757-767, 1990.
- Erdemir et al, *Clin Biomech*, 22:131-154, 2007.
- Jolivet et al, *Comput Methods Biomech Biomed Engin*, 11:281-290, 2008.
- Scheys et al, *Gait & Posture*, 28:640-648, 2008.
- Südhoff et al, *J Biomech*, 40(2):S346, 2007.

PREDICTING THE WHOLE MUSCLE ACTIVATION SPECTRUM COHERENT WITH A GIVEN MOTION TASK: A FEASIBILITY STUDY

S. Martelli (1), F. Taddei (1), A. Cappello (2), E. Schileo (1), S. Van sint Jan (3), A. Leardini (4), M. Viceconti (1)

1. *Laboratorio di Tecnologia Medica, Istituto Ortopedico Rizzoli, Bologna, Italy*
2. *Dipartimento di Elettronica, Informatica e Sistemistica, Università di Bologna, Italy*
3. *Laboratory of Anatomy, Biomechanics and Organogenesis, Université Libre de Bruxelles, Belgium*
4. *Laboratorio di Analisi del Movimento, Istituto Ortopedico Rizzoli, Italy*

Introduction

Muscle forces predicted through musculo-skeletal models have been recently used to predict skeletal or implants stress patterns [Jonkers, 2008] although current inverse dynamics models are known to underestimate the role of muscle co-contractions [Raikova, 1999]. Nevertheless recent studies showed the high contribution of muscle co-contractions to joint reaction forces [Bergmann, 2004] suggesting a dramatic increase on skeletal stresses. The knowledge of the whole space of possible activation strategies during a pre-defined action would give insight in understanding the critical condition the skeleton might face. However, the current limits of experimental techniques to measure in-vivo muscle forces make the numerical methods the only viable approach for this purpose. Aim of the present study is to propose a method to numerically identify and sample the whole muscle activation space for a given action of the musculo-skeletal mechanism of the lower limb.

Methods

The musculo-skeletal model of the lower limbs of a cadaver was generated in the frame of the EC-funded project LHDL based on CT and dissection data. The muscle system scheme was defined by registering a published atlas [Kepple, 1998] onto the skeletal geometry. The tetanic value of muscle forces were derived from the measured physiological cross section area (PCSA). A volunteer was selected to best match the cadaver anatomy and 3D motion of the lower limb was recorded during walking (Vicon Motion Capture, Oxford UK) together with the ground reactions. The relevant final skeletal kinematics was derived using a global optimisation method. The frame of the hip reaction peak was identified through preliminary simulations and selected for studying the whole muscle activation spectrum. An orthonormal base of activation patterns was computed from the redundant equilibrium equation. The boundary of the admissible muscle forces domain was sampled by generating 1E5 random linear combination of base vectors. Thus, for each vector, the two points on the boundary were

computed. The variation of muscle forces and of hip reaction was calculated.

Results

Very different muscle activation patterns were predicted, in which several muscles varied between silence and fully activation. The consequent hip reaction force was predicted between 3.1 and 14 times bodyweight (BW) (Fig.1).



Figure 1: Left, the musculo-skeletal model. Right, variation of the hip muscle signals and of the hip reaction force.

Discussion

The proposed method allowed sampling the whole space of solutions for a given activity. Results showed that very different muscle activation patterns are coherent with the same body action producing high variation of the hip reaction. Current results suggest that equivalent activation patterns are likely to produce dramatically different skeletal stresses, highlighting the limits of current optimisation methods to solve the muscle indeterminacy. The proposed methods represent a possible approach to identify and study critical condition of skeletal stresses.

Acknowledgments

The study was partially funded by the project LHDL, IST-2004-026932

References

- Bergmann, et al, *Langenbecks Arch Surg* 389:53-9, 2004.
 Jonkers, et al, *J Biomech* 41:3405-13, 2008.
 Kepple, et al, *J Biomech* 31: 77-80, 1998.
 Raikova, *J Biomech* 32:689-94, 1999.

THE INTERACTION BETWEEN MUSCULOSKELETAL LOADING, POSTURAL STABILITY AND MUSCULAR CONTROL

W.R. Taylor, N.B. Singh, I. Kutzner, G. Bergmann

Julius Wolff Institut, Charité – Universitätsmedizin Berlin, Germany

Introduction

With osteoporosis now affecting an estimated 75 million people, a major concern has become the incidence of falls in elderly individuals, particularly since falling contributes to some 90% of hip fractures [Nevitt et al. 1991]. Knowledge of the internal loading conditions during stumbling alone indicate that hip contact forces of over eight times body weight are produced during instances of subject instability, even without the additional impact of falling [Bergmann et al. 2004].

The inherent process of sub-maximal activation of multiple motor units during voluntary contraction results in an inability of musculature to generate purely constant forces, causing force fluctuation particularly during isometric contractions [Enoka and Fuglevand 2001]. The maintenance of postural stability requires the complex interaction of both sensory and motor systems [Lord et al. 2003], leading to sway during standing. Ageing has been shown to adversely affect both the control of forces [Enoka et al. 2003] and postural stability [Prieto et al. 1996], and it is therefore likely that subjects with deficits in muscular control and lower levels of postural stability would be less able to avoid stumbling or control falling. Their exposure to large joint contact forces, and possible overloading of the joint, would therefore be increased, particularly during uncontrolled or less stable activities.

The vision of the project is to understand the relationship between muscular control and propensity to stumble and fall. Quantification of an individual's ability to control loading of the lower limb, could then identify individuals who are more susceptible to overloading their joints, and possible fracture. In this sub-section of the larger study, we aim to understand the relationship between a subject's ability to control force production in the lower limb and their postural stability. Furthermore, in specific cases, a more complete understanding of the interaction between internal and external loading conditions may be gained through synchronously examining the *in vivo* joint contact forces and external loading during specific control tasks.

Methods

To assess the control of external forces, subjects are tested in both stable and unstable postures. To investigate subjects in a stable position, isometric sub-maximal knee extensions are performed in a seated posture on a dynamometer (Biodex 3 Pro, Biodex Medical Systems Inc., USA, sampled at 3000 Hz). The target extensor torques are provided in real-time as a visual force feedback and participants are instructed to match the torque level. To assess subjects in an unstable posture, participants are required to stand on one leg on a force platform (AMTI OR6-7-1000, USA, 1000 Hz) and control an external force level using the contralateral limb.

An additional, unique group of patients with instrumented knee implants [Heinlein et al. 2007], are to be recruited to perform the force control tests in both stable and unstable positions, while synchronously measuring internal knee contact forces *in vivo*. Investigation into the internal forces required to perform control tasks may allow an understanding of the interaction between internal and external loading conditions in postures of varying stability

Discussion

Preliminary data indicates that a deeper understanding of the interaction of postural stability, muscular control and the internal loading conditions of the lower limb must be gained before a more accurate categorisation of subjects who are susceptible to joint overloading can be obtained.

Acknowledgements

This project was partially funded by the EU under FP7 (VPHOP)

References

- Bergmann et al, Lang. Arch Surg. 389(1):53-9, 2004
- Enoka and Fuglevand, Muscle Nerve. 24:4-17, 2001
- Lord et al, Physical Therapy. 83(3): 237-52, 2003
- Nevitt et al, J Gerontol 46:M164, 1991
- Prieto et al, IEEE Trans Biomed Eng. 43: 956-966, 1996
- Heinlein et al, J. Biomechanics, 40:S4-S10, 2007.

ON MEASURING 3-D *IN VIVO* KINEMATICS, VISUALIZING, AND MODELLING THE CARPAL BONES OF THE WRIST

Joseph J. Crisco (1), Evan Leventhal (1), Michael Rainbow (1), Douglas Moore (1), G. Elisabeta Marai (2), David Laidlaw (2), Scott Wolfe (3)

1. Department of Orthopaedics, Brown University/Lifespan, USA; 2. Department of Computer Science, Brown University, USA; 3. Hospital for Special Surgery, USA

Introduction

The skeletal human wrist is composed eight irregular sized and shaped carpal bones, whose motion was first studied shortly after the discovery of X-rays [Bryce, 1896]. However, the mechanics of the carpus remain incompletely understood due in part to their anatomical and functional complexity. Our group's efforts have focused on developing methods for accurately measuring and visualizing the 3-D *in vivo* kinematics of the carpal bones. These methods address the inherent limitations of 2-D and cadaveric studies. More recently we have developed algorithms to examine carpal ligament and cartilage function. In this presentation we provide an overview of our methods and the results of several of our studies.

Methods

With IRB approval, wrists of healthy subjects (15 males; 15 females; ages 21-34) were imaged across a range of wrist positions with a GE helical CT scanner (GE Medical, Milwaukee, WI). Carpal bones, radius, ulna, and proximal metacarpals were segmented and registered among the subject's multiple CT volume images using tissue-classified distance fields [Marai, 2006]. 3-D kinematics of each bone were described using helical axis of motion variables. Ligament fiber length was computed as the shortest path from origin to insertion, with the constraint that ligament fibers not penetrate bony surfaces.

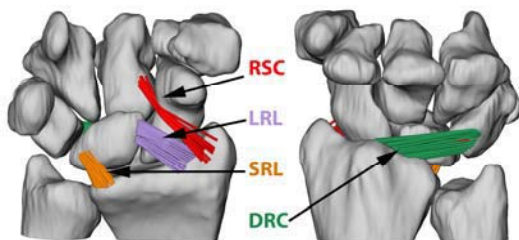


Figure 1: Palmar (left) and dorsal (right) views of the carpal bones and ligament fibers whose elongation as a function of wrist motion was analyzed.

Results

In the proximal row, the scaphoid and lunate primarily flexed or extended in all directions of

wrist motion. Along the path of the dart thrower's motion (DTM), scaphoid and lunate motion was significantly less than in any other direction of wrist motion ($P < 0.01$) [Crisco, 2005].

Wrist motions into flexion and those involving radial deviation significantly ($P < 0.0001$) elongated the dorsal radiocarpal (DRC). Fibers of the radioscaphoidcapitate (RSC) elongated significantly during wrist motions from flexion to extension ($p < 0.0001$).

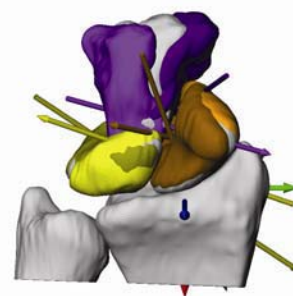


Figure 2: The minimal motion of the scaphoid and lunate bone during DTM visualized in a palmar view of wrist radial extension (dark colors), ulnar flexion (light colors), and neutral. The scaphoid, lunate, and capitate rotation axes are colored similar to the corresponding carpal bone.

Discussion

The ability to accurately measure 3-D carpal bone motion *in vivo*, to determine ligament elongation and cartilage thickness maps have allowed us to test several novel hypotheses. We have demonstrated that carpal bone function is far more complex than the existing row or column models predict, and that the DTM of the wrist elicits a unique pattern of carpal bone motion, which provides new insight into this wrist motion's functional and evolutionary significance. Compiling our anatomic, kinematics, ligamentous and cartilaginous dataset into a complete model of the carpus is continuing.

Acknowledgements

Funded by NIH HD052127, AR44005, AR0053648.

References

Bryce, J Anat Physiol, 31:69, 1896. Crisco et al, JBJS, 85:2729-40, 2005. Marai et al, IEEE Trans. Medical Imaging, 25:177-187, 2006.

VPH NoE special session

VIRTUAL PHYSIOLOGICAL HUMAN: INTEGRATIVE STUDIES

Patricia Lawford (1), Andrew Narracott (1), Bart Bijmens (2), Jordi Villà i Freixa (3), Bindi Brook (4), Margarita Zachariou (4), Vanessa Díaz (5), Katherine Fletcher (6)

1. University of Sheffield, UK; 2. CISTIB, Universitat Pompeu Fabra, Spain; 3. IMIM, Universitat Pompeu Fabra, Spain; 4. University of Nottingham, UK; 5. University College London, UK, 6. University of Oxford, UK

The barriers encountered by academic institutions when setting up interdisciplinary programmes have been identified in a number of studies, for instance (1). Obstacles include; the lengthy start-up time required, the increased administrative overhead faced when breaching traditional departmental boundaries and concerns about the quality of the training. There is significant concern that, unless carefully managed, increased breadth could be translated into weakness if the depth in which topics can be covered is compromised.

There is also a widespread perception within academic institutions that support for interdisciplinary research is stronger than that for interdisciplinary teaching. Whilst, for many institutions, this may indeed be the case; research success will ultimately drive an increasing demand for training. Young scientists must be provided with the skills required to expand and sustain an area of developing research and to facilitate its subsequent translation into industrial or clinical practice.

The Virtual Physiological Human (VPH), encompassing all aspects of complex physiological modelling and data management, is a prime example of a rapidly developing area of multidisciplinary research with complex training needs.

The development of a training strategy for researchers wishing to undertake careers in VPH-related research is one of the goals of an EU funded Network of Excellence (VPH-NoE) (2). In order to foster an educational path or VPH model of training, the VPH NoE has conducted a number of information gathering activities and training initiatives.

This presentation will summarise the routes currently followed by researchers working on VPH-related fields including reference to; the current education environment in Europe, existing programmes and the educational profiles of researchers already working in this field. Emphasis will be placed on multidisciplinary approaches and the specific requirements of a VPH training model.

In terms of training initiatives, current plans include;

- a series of Study Groups (multidisciplinary workshops), and
- VPH Training Modules.

These two activities are summarised below and will be discussed in more detail during the session.

The first VPH Study Group is dedicated to the “Regenerative aspects of epithelial tissue/cells” and will take place at the University of Nottingham, UK (29th June - 3rd July, 2009). Researchers from academic, clinical and industrial laboratories have been invited to present technical problems for study in ‘brain storming’ sessions with leading modellers from the academic community. Short-term goals focus on engendering novel interdisciplinary approaches and on the development of new theoretical models. Long-term goals include follow-up activities such as; meetings focussing on emerging topics which show promise for research output, publications and/or clinical/industrial uptake, ongoing collaborations or grant proposals. One generic outcome will be an assessment of the most challenging aspects of delivering both the short- and long-term goals. This will be the subject of a follow-up report but the key points will be presented in this session.

A prototype VPH training module will be directed at existing graduate students studying at VPH NoE core-member institutions and will use existing training material from world-leading research teams. This represents the first stage in the development of a pan-EU VPH graduate training initiative and the foundation of a sustainable strategy for an integrative VPH Training Programme.

This work is partially funded by the European Community's 7th Framework Program (VPH-NoE, grant agreement n° 223920)

1. Academy of Medical Sciences and the Royal Academy of Engineering, Systems Biology: a vision for engineering and medicine, February 2007

2. VPH NoE, Integrative Action Plan, March 2009

VPH NOE WORKPACKAGE 2 - EXEMPLAR PROJECTS

S. Randall Thomas

IBISC, CNRS FRE 3190, Evry F-91000, France

Abstract

A key objective of the VPH (Virtual Physiological Human) Network of Excellence is the development of a VPH ToolKit. The principal challenge recognized in development of this ToolKit is the establishment of transversal, or horizontal, connections between the usual domains of investigation. In order to push development of the ToolKit in the direction of this transversal integration, the NoE supports a small number of Exemplar Projects (EPs). These are independently funded projects (National or EU) that accept to enter the VPH "arena" rather than remaining isolated in the usual manner. They commit to interaction with the WP3 team (i.e., VPH ToolKit development) towards the dual goals of horizontal and vertical research integration. They must specify both what they need from the VPH ToolKit and what they can contribute, such as data (experimental, clinical, benchmark output...), models (subject to validation procedure to be worked out), and resources/software for the ToolKit.

Five research areas exploiting existing expertise of VPH NoE core members were identified during development of the NoE. The VPH NoE allocated 12 person-months to each of these "seed" EPs (seedEPs) in the first year of the NoE to enable early feedback for WP3 ToolKit development. Two or three new EPs will be awarded in each of years 2, 3 and 4 of the NoE, through a competitive grant mechanism within the NoE.

Individual EPs will be strictly focused on integration of VPH-related research which addresses an area of need, fostering new collaborative links, benefiting from transfer of skills from 'neighboring' VPH activities, with the mandate to make output (models, data repositories) available to the VPH community as widely as possible, and with the expectation that such support will contribute to the ability of the recipients to obtain follow-on funding. The VPH NoE will aim to promote the sharing of data across the VPH community, including the development of appropriate standards and infrastructure to enable this. Furthermore, EPs selected for funding will

help to define the needs for the VPH ToolKit and be early adopters of relevant output of the VPH ToolKit development (WP3), thereby contributing to the development of an integrated set of tools for the VPH. The concrete implementation of these tools towards the goals of vertical and horizontal integration will be an essential step in honing them for actual use, and (where appropriate) the EPs should provide a thorough testing ground.

In this talk, and with this underlying goal in mind, I will summarize the five seedEP projects and their expressed technical needs and contributions in terms of the WP3 ToolKit development. I will then briefly describe the first group of new Exemplar Projects (selected in Spring 2009). The primary criterion for selection of these was to fill identified key gaps in both the technological requirements and in coverage of the horizontal and vertical links among the various physiological levels (gene-to-organism) and organ systems.

Acknowledgements

The author's research is funded by: the European Community's 7th Framework Program (VPH-NoE, grant agreement n° 223920), and the French National Research Agency (ANR projects SAPHIR (ANR-06-BYOS-0007-01), and BIMBO (ANR-08-SYSC-002-04)).

IMPLEMENTING A TOOLKIT FOR THE VIRTUAL PHYSIOLOGICAL HUMAN (VPH) COMMUNITY

Sharon Lloyd (1), Jonathan Cooper (1)

1. University of Oxford, UK

Background

A key deliverable from the VPH Network of Excellence (NoE) project is a “VPH ToolKit” which was described in the project Description of Work as “*a technical and methodological framework that will support and enable VPH Research through the creation, accumulation, and curation of VPH research-related 'capacities'.*”

The focus of VPH NoE activities is the coordination and development of interoperable ToolKit components based on common standards (for data and models) and frames of reference (through the use of ontologies and atlases). We work with exemplar projects (EPs) and the wider VPH community to ensure that solutions deployed are fit for purpose. The Requirements and Technology Assessment Exercise (RTAE) has clarified the role of the ToolKit and it is clear that it must build on the extensive work being undertaken for specific scientific problems, bringing much of this to wider use and understanding.

This session will describe the foundational work which has been undertaken in 2009 to commence the process of delivering such a ToolKit, by providing essential structures from which a wider portfolio of tools, services and methods may be developed in the future. In each area of the ToolKit these activities culminate in the placement of two key cornerstones – standards and knowledge. The four subsequent releases during the lifetime of the NoE will build on this foundation, in order to meet the needs identified in the RTAE.

ToolKit Version 1

The focus of the first version of the ToolKit, released in July 2009, is on the selection and development of standards, including work on training and support for their use, for example through assisting EPs in marking up models, or extending the support for markup languages in existing tools. A key activity is to work towards enabling data and model interoperability. The use of ontologies is crucial, and so one component of the first release of the ToolKit is the definition of a VPH reference dataset and ontology standard for anatomy (in collaboration with relevant groups such as the FMA, OBO and NCBO). The first version of the ToolKit also includes releases of some specific tools, such as further development of imaging and data fusion frameworks, and facilities for accessing high performance computing resources.

In order to encourage the sharing of knowledge and wider dissemination of relevant tools and services, a community website has been developed. This is interactive, enabling VPH researchers to contribute to as well as benefit from the evolving resource, and will provide a structure to aid in placing work within the context of the VPH as a whole.

The VPH ToolKit should also comprise a deployed infrastructure offering numerous services to allow VPH-I projects to access compute resources, share datasets, run workflows, access data translation services and so on. Work is progressing on a prototype platform for exposing clinical data. Many aspects of infrastructure provision are beyond the scope of the NoE itself and will be tackled by other projects; the VPH Roadmap document will indicate particular needs, for example addressing usable security for research and clinical users.

We will describe in more detail our vision for the ToolKit, the work undertaken, what this will enable users to benefit from, and how to be involved. There will be an opportunity for discussion to gather feedback on the direction taken.

ToolKit Validation and Refinement

It has been imperative that the ToolKit team work closely with both the EPs and other VPH researchers to ensure that tools and services provided through the ToolKit are refined in accordance with the needs of the community. Later work will aim to ensure validation and refinement for a more clinical user-base. Following the release of this foundational phase of the ToolKit, we will again survey the community to determine gaps in knowledge and changes in requirements. This will ensure an iterative approach to development and support for VPH research.

Acknowledgements

We acknowledge the extensive work of the VPH NoE ToolKit team for providing input to the material for this abstract. The financial support of the European Commission is gratefully acknowledged. Material in this abstract reflects only the authors' views and the Commission is not liable for any use that may be made of the information contained herein.

References

VPH NoE Consortium, http://www.vph-noe.eu/vph-repository/doc_download/51-vph-noe-requirements-and-technology-assessment-exercise, 2008.

Musculoskeletal system - tissue

THE POTENTIAL OF FLAT-PANEL FLUOROSCOPY CT TO QUANTIFY VERTEBRAL TRABECULAR ARCHITECTURE IN VIVO

Lars Mulder (1), Bert van Rietbergen (1), Niels Noordhoek (2), Keita Ito (1)

1. Biomedical Engineering, Eindhoven University of Technology, Eindhoven, the Netherlands; 2. Philips Healthcare, Best, the Netherlands

Introduction

Osteoporotic fractures should be prevented rather than treated. This requires an accurate diagnosis of bone strength. The overall aim of the EU-funded VPHOP research project is to obtain an improved patient-specific assessment of the current and future risk of fractures by using multiscale hypermodels based on multi-level imaging methods that also include the bone micro-architecture. These images are used to determine bone strength either directly (using micro-finite element methods) or indirect from structural parameters [van Rietbergen, 1995]. This requires imaging methods that can resolve trabecular architecture in vivo at the hip and vertebra. Current methods, however, do not provide sufficient detail. Recently, high-resolution flat-panel fluoroscopy with CT applicability has been developed. These devices can potentially be used to resolve the bone architecture at the hip and vertebrae and the main goal of this study is to assess the potential of such a device, XperCT (Philips Healthcare) to visualize trabecular bone.

Materials and methods

A set of human cervical vertebrae (C1-C4) was scanned with a high-resolution XperCT prototype resulting in reconstructions with a voxel size of 150 μm and with a microCT 80 (Scanco Medical AG, Switzerland), voxel size: 37 μm . The reconstructions of C3 of both scans were similarly oriented using image registration to allow selection of identical cylindrical volumes of interest (Fig. 1). To assess trabecular architecture, the volumes were segmented using a global threshold and the influence of a Laplace-Hamming (LH) filter was studied. The segmented volumes were transformed into finite element models and a compression simulation was used to predict bone stiffness (E).

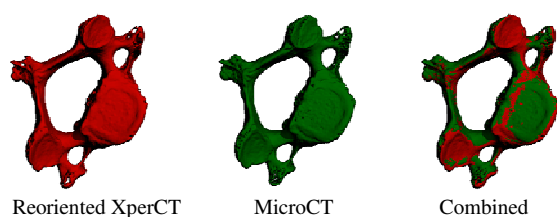


Figure 1: XperCT and microCT reconstructions of C3 and the combined ones after image registration.

Results

Image registration of the C3 vertebrae resulted in a good match (Fig. 1). This is especially appreciated by comparing matching slice reconstructions from both scans (Fig. 2) in which individual trabeculae can be easily recognized. The Laplace-Hamming (LH) filter improved the quantitative results: bone volume fraction, stiffness and trabecular separation were quantified fairly accurate (Table 1).

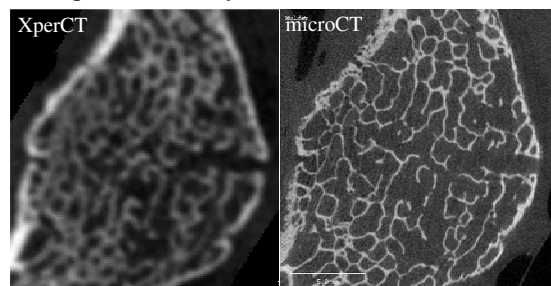


Figure 2: Reconstructed slice from XperCT (left) and microCT (right).

Table 1	XperCT	XperCT (LH)	microCT
BV/TV [%]	55.3	26.1	24.6
Tb.Th [mm]	0.77	0.41	0.20
Tb.N [mm^{-1}]	0.91	1.01	1.20
Tb.Sp [mm]	0.89	0.89	0.80
Conn.D [mm^{-3}]	0.27	0.91	3.51
E [N mm^{-1}]	47,452	10,651	14,791

Discussion and conclusion

The Laplace-Hamming filtering implemented here already dramatically improved the results, but it is likely that by using more sophisticated filtering algorithms or local thresholding schemes based on edge detection, bone architecture and strength prediction will further improve. Earlier studies with pQCT devices, have demonstrated that trabecular thickness e.g. can be well measured at 150 μm when correction factors are used [Laib, 1999].

Although more work is warranted to establish the accuracy of XperCT, this study demonstrates the potential clinical application of XperCT as a tool for assessing trabecular bone morphology and strength at the hip and vertebra.

References

- van Rietbergen et al, J Biomech, 28:69-81, 1995.
- Laib et al, Bone, 25:35-39, 1999.

SIMULATION OF TISSUE DIFFERENTIATION IN SCAFFOLDS FOR BONE TISSUE ENGINEERING

C. Sandino (1,2), J.A. Planell (1,2), D. Lacroix (1)

1. Institute for Bioengineering of Catalonia, Barcelona, Spain

2. Universitat Politècnica de Catalunya, Barcelona, Spain.

Introduction

Mechanical stimuli can be used to improve the process of tissue differentiation in the development of biomaterials for bone tissue engineering. In *in vitro* studies, perfusion flows are used to transport cells into the scaffolds and to stimulate them. Compressive loads applied to the scaffolds are also used to stimulate cells. The specific microscopic stimuli into the scaffolds can be determined using the Finite Element (FE) method. Micro CT based FE models of scaffolds with different morphology have shown the strong relation between the architecture of the samples and the mechanical stimuli distribution into the porous materials [1,3]. The objective of this study was to simulate the effect of unconfined compressive loads and perfusion flows in tissue differentiation within the pores of a scaffold for bone tissue engineering.

Methods

A calcium phosphate cement scaffold with amorphous porosity was studied. A tissue differentiation algorithm was developed using two independent FE models [3]. In one analysis a compressive load was simulated and octahedral shear strain was computed. In another analysis a perfusion fluid flow through the interconnected pores of the scaffold was simulated and fluid shear stress was computed. In each iteration of the algorithm (Fig.1), mechanical stimuli were calculated using the FE analyses and the differentiated tissue for every element was determined using a mechano-regulation concept [2]. An iterative process was applied until homeostasis was achieved. Compressive load was equivalent to 0.5% of total strain. A parametric study using inlet fluid velocities of 1, 10, 100, and 1000 $\mu\text{m/s}$ for the fluid flow was made.

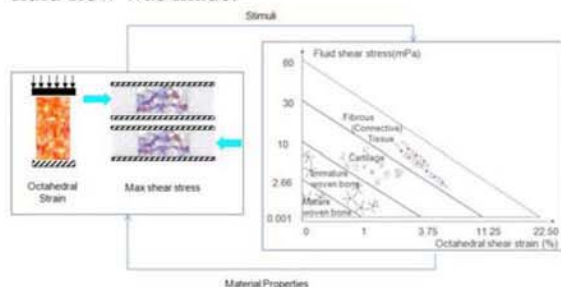


Fig. 1. Tissue differentiation simulation based on the solid and fluid flow analyses.

Results

Inlet fluid velocity is a significant factor in tissue differentiation; its variation can result in a totally different tissue distribution (Fig. 2, left). According to the pore size and interconnectivity, different types of tissue are predicted across the sample (Fig. 2, right). When inlet velocity is 1 $\mu\text{m/s}$ only mature bone forms and appears in the small well-interconnected pores. When increasing inlet velocity mature bone is predicted in the tubes of the bioreactor and in well-interconnected pores; immature bone and fibrous tissue appears in some regions. When inlet velocity is 1 mm/s, tissue is not predicted in the small well-interconnected pores because of high stimuli. The maximum quantity of mature bone predicted is 87% when an inlet velocity of 10 $\mu\text{m/s}$ is applied.

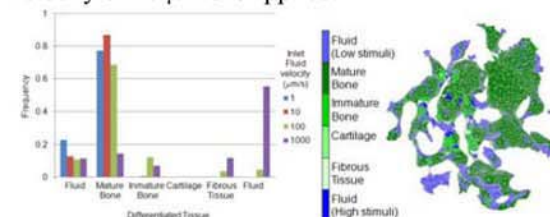


Fig. 2. Left: Frequency of differentiated tissue for different inlet velocities. Right: Tissue distribution into the interconnected pores of the scaffold when inlet velocity is 100 $\mu\text{m/s}$. Iteration 20.

Discussion

Discriminating the pores and the solid phase of the scaffold in the simulation allows to determine regions feasible for tissue differentiation according to the macro mechanical loads applied. The performance of the scaffolds for bone tissue engineering can be studied in terms of its morphology and the optimal mechanical conditions used in the bioreactor can be determined.

Acknowledgements

Funding from the European Commission (SmartCaP NMP3-CT2005-013912) is acknowledged.

References

- [1] Cioffi et al, Biotech and Bioeng, 93: 500 – 510, 2006.
- [2] Prendergast et al, J Biomech, 30: 539 – 548, 1997.
- [3] Sandino et al, J. Biomech, 41:1005-1014, 2008

STRAIN MAPPING FOR TIME-LAPSED MICROSTRUCTURAL IMAGING OF BONE FAILURE – A VALIDATION STUDY

David Christen (1), Romain Voide (1), G. Harry van Lenthe (1), Steven Boyd (2), Ralph Müller (1)

1. Institute for Biomechanics, ETH Zürich, Zürich, Switzerland; 2. Schulich School of Engineering, University of Calgary, Calgary, Canada

Introduction

Image guided failure assessment (IGFA) using micro-computed tomography (μ CT) is an important tool for a better understanding of trabecular bone failure. Computing local strain maps based on time-lapsed three-dimensional images will help in the evaluation of IGFA experiments. Here we present and validate a novel 3D strain mapping technique based on deformable image registration.

Method

Given two μ CT images, one of an unloaded sample and one of a loaded sample, the displacement was computed for every voxel using deformable image registration. In a first step, digital volume correlation (DVC) was used to align regions of the images. For a finer and more localized alignment of the images, the ‘Demons’ deformable image registration algorithm was implemented [Thirion *et al*, 1998], [Pauchard *et al*, 2008]. Based on the Gaussian filtered displacement field, the Green-Lagrange strain tensor was finally calculated.

IGFA compression tests of five cylindrical aluminum foams were used for validation. Additionally, μ CT images were digitally deformed using displacements computed from voxel-based linear elastic micro-finite element (μ FE) analysis. Using structural decomposition [Stauber and Müller, 2006], the maximal strain was computed for every structural element, i.e. for each rod and plate, for both FE and strain mapping.

Results

When the samples were digitally compressed by 1% strain, a linear correlation of $R^2 = 0.90 \pm 0.03$ was found between the applied displacements and the ones measured by the image registration. The accuracy of the registration was four-fold better than the voxel size (7 μ m and 30 μ m, respectively). The maximal effective strain per structural element computed by strain mapping and FE respectively showed a correlation of $R^2 = 0.43 \pm 0.14$.

Discussion

While strain computed by μ FE indicates deformed regions within individual trabeculae, strain maps based on image registration can only characterize structures with an accumulation of strain. To limit

the difference in localization, displacement fields have to be accurate and very localized.

Further experiments are planned to determine the accuracy of the deformable registration and strain mapping in human trabecular bone, to find optimal parameter sets and to investigate possible effects of the image resolution or large displacements. However, the preliminary results suggest that strain mapping is an effective tool for the characterization of regions with high strains, i.e. local strains above 3 times nominal strain.

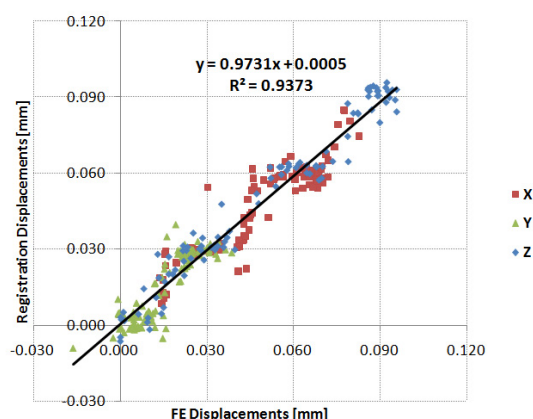


Figure 1: Linear regression analysis of the digitally applied displacements and the displacements measured by deformable image registration.

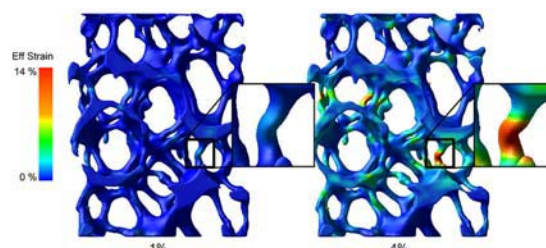


Figure 2: Strain maps from IGFA compression tests using aluminum foam and applied strains of 1% (left) and 4% (right).

References

- Pauchard *et al*, J Biomech, 41:2946-53, 2008.
- Stauber and Müller, Bone, 38: 475-484, 2006.
- Thirion *et al*, Med Image Anal, 2: 243-260, 1998.

Cellular modelling

THE EPITHELIOME PROJECT: MULTI-PARADIGM, MULTISCALE MODELLING OF CELLS AND TISSUES

Rod Smallwood

Department of Computer Science, University of Sheffield, UK

Introduction

Predictive modelling of the interaction of individual cells has received little attention. Cells self-assemble into fully-differentiated tissue. This building of functional structures from autonomous cells is central to human biology, from embryology, growth, cell turnover, to wound repair and the development of malignancy. Cell biology, molecular biology, genomics, proteomics are providing, in a qualitative, reductive manner, the data to answer these questions. To understand the mechanisms in a predictive manner requires the integration of this data through computational models. Epithelial tissues are relatively simple but nevertheless exhibit a number of very important clinical problems (e.g. wound healing and the development of malignancy), and there are good biological models for data input and validation. The aim of the Epitheliome Project is to develop a computational model of cell behaviour within the context of tissue architecture, differentiation, wound repair and malignancy.

Discussion

Detailed discussion of the components of the Project will be found in other presentations and in the references. This presentation will provide an overview of the philosophy underlying the project, and indicate the approach used to develop multiscale models of tissue when starting from a cell-based perspective. In principle, the individual-based approach used for modelling the cellular interaction could be used in a hierarchical manner, so that only a single modelling paradigm would be needed. However, the pragmatic (sensible!) approach is to make use of existing models where appropriate, which requires the modelling framework to be able to import or link to other modelling paradigms e.g. CellML and SBML models; finite element models.

The underlying premise is that the structure and function of all tissues is a result of the interaction of individual cells – the cell is the smallest entity that contains all the necessary machinery for growth and division, and there is no information store above the level of the cell – so an understanding of emergent behaviour at the cellular level is essential. The physics of cell behaviour is also essential – not just in the obvious case of muscle behaviour, but

throughout the spectrum of cellular interaction. Cells grow, divide, form bonds, all of which exert forces on their neighbours and organise and re-organise tissue structure. Cells are exquisitely sensitive to applied forces, and there is substantial evidence for the influence of the physical environment on cell phenotype.

The result is that emergent behaviour at the cellular level, which is the result of biochemical behaviour at sub-cellular level and physical interaction between the cells and their environment, has to inform the continuum properties of the tissue.

Acknowledgements

The Epitheliome Project has been funded by the EPSRC (Engineering and Physical Sciences Research Council).

References

- The Epitheliome Project <http://www.epitheliome.org.uk>
- Coakley S, Smallwood R and Holcombe M (2006) *Scientiae Mathematicae Japonicae* 64:185-198
- Pogson M, Smallwood R, Qvarnstrom E, Holcombe M (2006) 85(1):37-45
- Smallwood R H, Holcombe W M L and Walker D C (2004) *Journal of Molecular Histology* 35:659-665
- Sun 2007 Sun T, McMinn P, Coakley S, Holcombe M, Smallwood R, MacNeil S (2007) *J Roy Soc Interface* 4:1077-1092
- Sun T, McMinn P, Holcombe M, Smallwood R, MacNeil S (2008) *PLoS ONE* 3(5): e2129 doi:10.1371/journal.pone.0002129
- Walker D C, Georgopoulos NT and Southgate J in *Foundations of Systems Biology in Engineering*. 2007: Stuttgart, Germany.
- Walker DC, Georgopoulos NT, Southgate J. *BMC Syst Biol*. 2008; 2:102. PMID: 19036127.
- Walker D C, Southgate J S, Hill G, Holcombe M, Hose D R, Wood S M, MacNeil S and Smallwood R H (2004) *BioSystems* 76:89-100
- Walker D C, Hill G, Wood S M, Smallwood R H and Southgate J (2004) *IEEE Trans Nanobioscience* 3:153-163
- Walker D, Sun T, Macneil S, Smallwood R (2006) *Tissue Eng*. 12(8):2301-2309
- Walker D, Wood S, Southgate J, Holcombe M, Smallwood R (2006) *J Theor Biol*. 242:774-789

AN AGENT-BASED MODEL OF 'ANTISOCIAL' CELLS

Dawn Walker(1), Nikolaos Georgopoulos(2), Saquib Shabir(2), Jenny Southgate(2)

(1)Department of Computer Science, University of Sheffield, Sheffield S3 7HQ, U.K.

(2) Department of Biology, University of York, York, YO10 5YW, U.K.

Introduction

Biological tissues are not fixed heterogeneous structures, but consist of large populations of biological cells which interact in complex ways to generate emergent properties, including structure and function. The agent-based modelling paradigm, where each individual cell is represented by an equivalent computational entity or *software agent*, provides an intuitively natural computational representation of such a system.

E-cadherin is a protein expressed on the surface of normal epithelial cells that plays a key role in mediating intercellular adhesion via calcium-dependent homotypic interactions [Baumgartner, 2000]. The presence of stable, E-cadherin-mediated contacts plays a role in regulating proliferation and migration of cells. Loss of function of E-cadherin is associated with malignant progression. We describe the development of an agent-based computational model to explore how interactions of normal cells and those with diminished E-cadherin expression may affect population growth dynamics.

Methods

We have further developed the agent-based model of individual cells previously described elsewhere [Walker, 2004]. The observed or hypothesised behaviour of the individual cells can be represented by logical rule sets that determine the responses of the virtual cells (software agents) to various stimuli. In this case, rule sets represent cell migration, intercellular adhesion (both E-cadherin mediated and transient contacts) and proliferation. E-cadherin expression and extracellular calcium concentration determine the probability of any pair of cells forming a stable bond, which in turn affects the proliferative and migratory behaviour of these cells.

An initial population of 200 virtual cells was 'seeded' onto a 1mm x 1mm substrate. Each cell was assigned a variable representing its endogenous E-cadherin expression (1= normal or, 0= no endogenous expression). For each simulation, a particular fraction of the population was designated to express either normal (EC-N) or zero levels (EC-A). The model was run iteratively with rule sets applied to each agent in turn, up to a maximum of 300 iterations (1 iteration = 30 minutes). Simulations were repeated with the virtual exogenous calcium concentration set to 2mM

(physiological level, stable bonds likely for EC-N cells) or 0.09mM (very low, stable bonds unlikely even for EC-N cells). Cell numbers, locations and states were recorded at each iteration.

Results

Figure 1a shows the growth curves obtained from simulated 100% normal and 100% abnormal populations. It can be seen that the model predicts the differences in population growth observed in EC-N cells in 0.09 and 2mM calcium, which are observed experimentally (figure 1b).

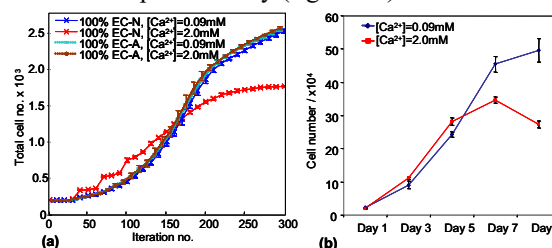


Figure 1 Growth curves derived from (a) agent model and (b) in vitro experiments on normal bladder epithelial cells.

As anticipated, these differences are less apparent for EC-A cells. At the level of individual cells, we observed that as well as exhibiting different adhesive and migratory behaviour to their normal counterparts, EC-A cells also modulate the behaviour of the normal cells with which they interact.

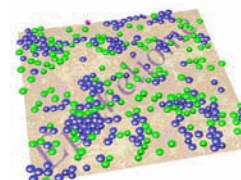


Figure 2 Simulated population consisting of 50% EC-N and 50% EC-A cells after 50 iterations (25 hours)

Discussion

We have described how an agent-based model can be used to understand the behaviour and interactions of normal epithelial cells and mutant cells that lack a particular cell surface adhesion protein that is frequently lost during malignant progression. We are currently developing an in vitro system to further validate the predictions of this model.

References

Baumgartner et al, PNAS USA, 2000 97(8): 4005-4010
Walker, D. et al, Biosystems, 2004. 76(1-3): 89-100.

MICROFLUIDIC DIELECTRIC SPECTROSCOPY CYTOMETER: MODELLING AND OPTIMIZATION

Federica Caselli, Paolo Bisegna, Franco Maceri

Department of Civil Engineering, University of Rome "Tor Vergata", via del Politecnico 1, 00133 Rome, Italy. Email addresses: {caselli, bisegna, maceri}@ing.uniroma2.it

Introduction

Dielectric spectroscopy is a non-invasive method suitable for the characterization of living biological cells (e.g., analysis of normal and malignant white blood cells [Ermolina, 2001], or morphological inspection of erythrocytes [Asami, 2008]).

Nowadays, thanks to microfabrication techniques, it is possible to perform single-cell dielectric spectroscopy by means of microfluidic cytometers [Gawad, 2004; Morgan, 2007].

Figure 1(a) shows the schematic representation of a state-of-the-art microfluidic cytometer: ac signals applied to the top microelectrodes generate an electric field in the microchannel; when a cell passes through the device, an impedance variation is measured which depends on the specific cell characteristics (size, morphology and dielectric properties).

In this work an innovative design for the microfluidic cytometer is proposed by exploiting the basic principle of Electrical Impedance Tomography (EIT) [Bayford, 2006]: instead of just two pairs of opposite electrodes, two arrays of electrodes are conceived (Figure 1(b)), allowing a greater versatility in the stimulation pattern. In particular, rotating spatially-harmonic distributions of electric current can be applied at the device surface, thus enabling a thorough testing of the dielectric cell response.

Methods

The ability of the proposed device to detect cell structure and morphology is investigated by means of mathematical modelling and computer simulation. Both red blood cells of different morphology (normal erythrocytes, echinocytes, spherocytes) and cells with nucleus (e.g., white blood cells) are considered. Cell membranes are modelled as two-dimensional interfaces exhibiting a capacitive behaviour [Bisegna, 2008].

Several stimulation current patterns in the radiofrequency range are implemented as Neumann boundary condition, and the resulting surface voltage distribution is computed. The finite element method is employed, in order to take into account the complex geometrical and structural features of different cell types. Numerical computations are performed with COMSOL Multiphysics™.

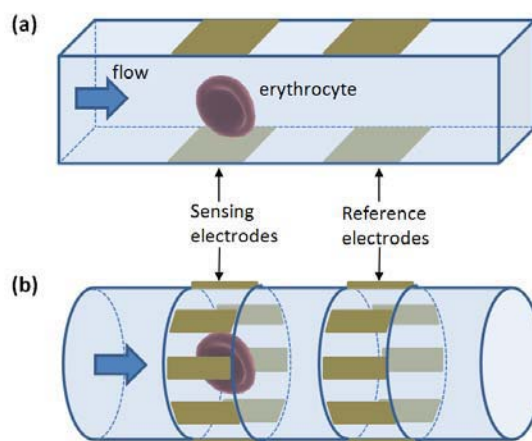


Figure 1 Schematic representation of: (a) classic microfluidic cytometer and (b) proposed device.

Results and discussion

The various stimulation patterns applied to each cell yield an ensemble of impedance spectra. Simulation results show that such an ensemble strongly depends on cell features, as dielectric properties, size, shape, nuclear-cytoplasmic ratio, and thus it constitutes a sort of cell fingerprint. As a consequence, the experimental measurement of that ensemble allows to reliably recover quantitative information on the above significant cell properties, by using reconstruction algorithms developed for EIT. The proposed design, enabling several stimulation patterns, is therefore outperforming with respect to the classic system, with very limited stimulation capability.

Future research will be devoted to the electronic design of the device and to the implementation and optimization of reconstruction algorithms. A further improvement will be obtained by substituting each strip electrode in Figure 1(b) with an array of point electrodes, thus enhancing the axial resolution.

References

- Ermolina I. et al, IEEE Trans Diel Elec Insul, 8(2):253-261, 2001.
- Asami K. et al, Phys Med Biol, 53:2553-2564, 2008.
- Gawad S. et al, Lab Chip, 4:241-251, 2004.
- Morgan H. et al, J Phys D: Appl Phys, 40:61-70, 2007.
- Bayford R.H., Ann Rev Biomed Eng, 8:63-91, 2006.
- Bisegna P. and Caselli F., J Phys D: Appl Phys, 41(11):115506, 2008.

CYTOSKELETON REORGANIZATION OF SPREAD CELL ON MICRO-PATTERNED ISLANDS: A FUNCTIONAL MODEL

Yannick Loosli (1,2,3) Jess Snedeker (1,2)

1. Orthopedic Research Laboratory, University of Zürich, Balgrist, Switzerland;

2. Institute for Biomechanics, ETH, Zürich, Switzerland;

3. RMS Foundation, Bettlach, Switzerland

Introduction

Understanding how cells interact with their neighborhood is of paramount importance for externally directing cellular behaviors (e.g. growth, migration, cycle, differentiation, etc.) The mechanical coupling between the cell cytoskeleton (CSK) and cell substrate operates via the connection of focal adhesion (FA) complexes to actin stress fibers (SFs). The organization of these components, among others, increases cell adherence, stabilizes the cell shape and affects its mechano-transduction properties. Therefore being able to understand the driving forces behind FA and SF allocation constitutes a powerful tool for predicting cell fate. The use of microfabricated surfaces that have been functionalized with binding ligands is a well established approach to investigate this behavior, and provides an ideal experimental benchmark for modeling purposes [Pathak, 2007]. The proposed model is based on the cell tendency to optimize its adhesive pre-stress and its total surface by varying the SF contractibility.

Methods

For this multi-objective optimization (cell pre-stress and cell surface) a 2-dimensional objective function was defined as the square of the differences (i) between the computed total FA size and a target value that corresponds to the total surface of cell FAs and (ii) between the SFs defined cell area with the maximal spreading surface (here corresponding to the island surface). The system variable was a vector composed of the strain (ϵ) existing in each SF. To compute the objective function, the linear relationship between the FA size and the SF force (generated by ϵ), was used ($\beta=5.5 \text{ nN}\mu\text{m}^{-2}$) [Balaban, 2001]. The strain was assumed to be related to the force via Hooke's Law with $EA=45\text{nN}$ (A: SF cross section; E: SF elastic modulus). An additional force was included to the outer-SF that simulated the membrane inward pulling effect. Further constraints related to maximum and minimum values of single SF and FA were applied. The modeled adhesive surfaces were defined similar to available experimental literature [Pathak, 2007], as depicted on figure 1.

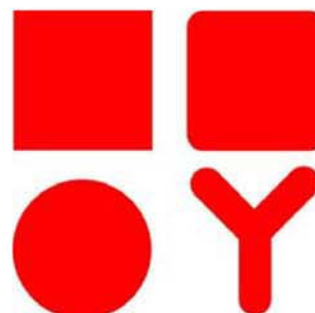


Figure 1: Adhesive surface geometry in red with an approximately $900\mu\text{m}^2$ area.

Results

FA location and FA interconnectivity via SFs were in agreement with reported experiments. As expected we observed denser FAs at regions of high curvature (or corners) on the periphery of the cell. SFs at non-adhesive edges were favored.

Discussion and Conclusion

This model was driven by a set of biophysical constraints and structure-function rules that were able to replicate a realistic CSK structure of spread cells on widely varying substrate geometries. The applied phenomenological approach to modeling cell mechanisms allows insight into how cells might reorganize themselves, with downstream consequences for mechano-transduction.

A major limitation of this model is the lack of a time dependent variable which could otherwise offer insight to cell dynamics and CSK kinetics. Another simplifying assumption is the neglected role of CSK microtubules which may influence the cell-substrate force balance. Nonetheless, this model can reasonably predict resultant FA and SF distributions in spread cells with a few essential constraints that have been experimentally quantified.

References

- Pathak et al, J. R. Soc. Interface, 5:507-524, 2007.
- Balaban et al, Nat Cell Biol, 3:466-472, 2001.

FINITE DEFORMATION BASED MODEL OF CYTOSKELETON

Eligiusz Postek (1), Rod Smallwood (2), Rod Hose (3)

1. University of Sheffield, Department of Computer Science, UK; 2. University of Sheffield, Department of Computer Science; 3. University of Sheffield, Medical Physics and Clinical Engineering, UK

Introduction

The cytoskeleton is modelled as a tensegrity structure. It consists of tendons and struts [Stamenovic, 2005]. The basic tensegrity structures are developed from icosahedron.

The cells undergo finite deformations behaviour and their response to loading conditions is visco-elastic.

These types of structures are sensitive to initial prestressing what is intuitively natural since without the initial stress state they would not exist. The other factors affecting the mechanical behaviour of the cell are the constitutive parameters and positions of the nodes, in fact, the shape of the cell.

Methods

The generic incremental FE equation is formulated in the Updated Lagrangian frame [Kleiber, 1997] and reads

$$\left(\int_{\Omega'} \mathbf{B}_L^T \bar{\boldsymbol{\tau}} \mathbf{B}_L^T d\Omega' \right) \Delta \mathbf{q} + \int_{\Omega'} \mathbf{B}_L^T \Delta \mathbf{S} d\Omega' = \int_{\Omega'} \mathbf{N}^T \Delta \mathbf{f} d\Omega' + \int_{\partial\Omega'_\sigma} \mathbf{N}^T \Delta \mathbf{t} d(\partial\Omega'_\sigma) \quad (1)$$

where \mathbf{B}_L^T and \mathbf{B}_L are the nonlinear and linear operators, \mathbf{N} is the shape functions matrix, $\Delta \mathbf{S}$ is the stress increment, $\bar{\boldsymbol{\tau}}$ is the Cauchy stress matrix, $\Delta \mathbf{q}$ is the displacement increment, $\Delta \mathbf{f}$ and $\Delta \mathbf{t}$ are the body forces and the boundary tractions increments. The integration is done over the domain Ω and its boundary Ω_σ .

The constitutive model is visco-elastic such as the stress increment depends on total stress \mathbf{S} , the shear modulus (G), the bulk modulus (K) and the strain increment $\Delta \mathbf{E}$ as follows

$$\Delta \mathbf{S} = \mathbf{D}^{const}(\mathbf{S}, G, K) \Delta \mathbf{E} \quad (2)$$

with the relaxation function

$$G(t) = G_o + \sum_{i=1}^n G_i \exp\left(\frac{-t}{\lambda_i}\right) \quad (3)$$

where t is the time and λ_i are the relaxation times of the particular parallel dampers. These above describe the generalized Maxwell model.

Exemplary results and discussion

The icosahedron tensegrity structure is presented in Fig. 1. The CSK is fixed at the surface and is tested for the uni-axial extension. We adopted the

following data, namely, height of the cell 64 μm , cross-sectional areas of the tendons (filaments) 10nm², cross-sectional areas of the struts (microtubules) 190 nm², Young's moduli of the tendons 2.6GPa and the struts 1.2GPa, initial prestressing forces 20 nN, maximum loading 0.1N, relaxation time 1.0 sec, G_V/G_o ratio 0.91 (case A) and 0.1 (case B).

We investigated the stiffening effect during extension and up to buckling and postbuckling equilibrium paths in compression. Our interests were focused on visco-elasticity effects and geometrically imperfect system.

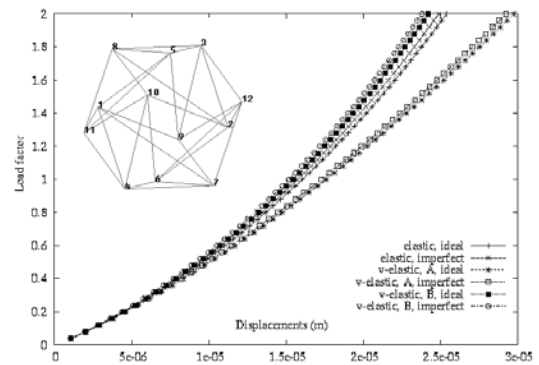


Figure 1: Icosahedron based tensegrity structure, tension test, materials elastic and visco-elastic, perfect and imperfect geometries.

The tension tests demonstrate stiffening of the structure. We can see that the considered imperfection pattern (moving the node under the force in the plane perpendicular to it) slightly stiffens the CSK. Considering the visco-elastic cases the low value of the shear ratio stiffens the structure while the high value of the shear ratio softens the CSK.

The cell model is an element of a matrix of cells. We observe the effects of imperfections, in this case different materials in the cell on the behaviour of the cell assembly under tension and compression tests.

References

- Stamenovic D., Acta Biomaterialia, 1:255-262, 2005.
- Kleiber M. et al, Parameter Sensitivity in Nonlinear Mechanics: Theory and Finite Elements, Wiley & Sons, 1997.

DISPERSION EFFECTS OF ACTIVE CONTRACTILE FILAMENTS IN SMOOTH MUSCLE CELLS

Sae-Il Murtada (1), Martin Kroon (1), Gerhard A. Holzapfel (1, 2)

1. Royal Institute of Technology (KTH), Department of Solid Mechanics
Osquars Backe 1, SE-100 44 Stockholm, Sweden
2. Graz University of Technology, Institute of Biomechanics
Center of Biomedical Engineering, Kronesgasse 5-I, A-8010 Graz, Austria

Introduction

When intracellular calcium ion concentration increases in smooth muscle cells, chemical cross-bridges are bound between the thin (actin) and the thick (myosin) filaments causing sliding between the filaments which gives rise to contraction. The relationship between the chemical activation and the mechanical contraction is still not well understood, but is important for the understanding of smooth muscle related diseases such as atherosclerosis, asthma and incontinence.

Methods

A chemomechanical model is proposed which couples a biochemical four-state latch model by Hai and Murphy [Hai and Murphy, 1988] with a mechanical model based on the classical Hill's model. The contractile filaments are assumed to be arranged in series with a dispersion constituting a network of long fibres inside the layers of smooth muscle cells. The mechanical model of the contractile filament is described by the strain-energy function

$$\Psi_f = \frac{\mu_f n}{2} [(\alpha I_1 + (1 - 3\alpha)I_4)^{1/2} - 1 + \bar{u}_{fc}]^2$$

where μ_f is a material parameter, n is the level of cross-bridge activation, α is a dispersion parameter [Gasser et al., 2006], I_1 and I_4 are the first and fourth invariants and \bar{u}_{fc} is the internal variable describing the contraction.

Layers of smooth muscle cells are modelled as contractile filaments surrounded by a matrix consisting of elastin and collagen fibres using the proposed model and a continuum-based model [Holzapfel et al., 2000] to describe the matrix. The dispersion parameter is defined through comparisons with experimental studies of the underlying structure of actin and myosin filaments in smooth muscle cells [Walmsley and Murphy, 1987]. By fitting the model with isometric experiments performed under different pre-stretches [Rembold and Murphy, 1990] the material parameters could be defined.

Results

The proposed model is able to predict experimental results for a varying intracellular calcium ion concentration and different pre-stretches, and the dispersion of the contractile filaments had a significant influence on the results.

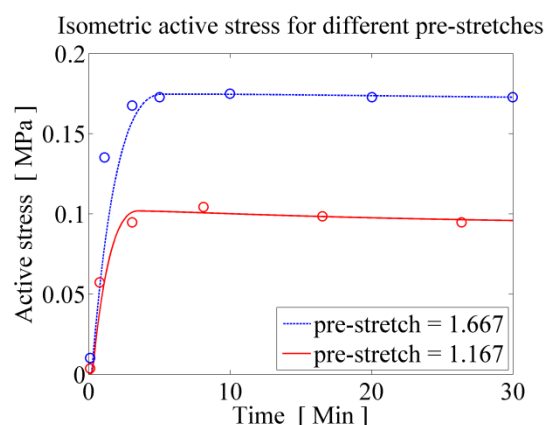


Figure 1: Active stress during isometric contraction for two pre-stretches. The circles represent experimental data [Rembold and Murphy, 1990] and the curves represent the model results.

Discussion

The proposed mechanical model coupled with an existing chemical model is able to predict active stress during isometric contraction for different pre-stretches. The contractile filament model has only three material parameters. It is able to consider the dispersion of the contractile filaments through the structural parameter α which turned out to have a significant effect on the mechanochemical response of the smooth muscle cell.

Acknowledgements. We wish to thank Anders Arner from KI, Stockholm for his helpful comments and the Swedish Research Council for the financial support of SM.

References

- Gasser et al., J R Soc Interface, 3:15-35, 2006.
 Hai and Murphy, J Appl Physiol, 254:C99-106, 1988.
 Holzapfel et al., J Elast, 61:1-48, 2000.
 Rembold and Murphy, Circ Research, 66:1354-1361, 1990.
 Walmsley and Murphy, Am J Physiol, 253:H1141-H1147, 1987.

Musculoskeletal system - constituent

SIMULATION OF THE MINERAL HETEROGENEITY OF BONE IN HEALTH AND DISEASE

Carolin Lukas (1), Peter Fratzl (1), Paul Roschger (2), Klaus Klaushofer (2), and Richard Weinkamer (1)

1. Max Planck Institute of Colloids and Interfaces – Department of Biomaterials, Potsdam, Germany;

2. Ludwig Boltzmann Institute of Osteology at the Hanusch Hospital of WGKK and AUVA Trauma Center Meidling, Vienna, Austria

Introduction

Trabecular bone changes its structure and therefore its material properties due to the processes of remodeling and mineralization. Within the picture of a BMU (= Basic Multicellular Unit) trabecular bone remodeling can be described as bone resorbing cells removing small bone packets from the surface. After a time lag of a few weeks a new bone packet is deposited by bone forming cells. Within the subsequent mineralization process the initially unmineralized bone increases its mineral content in time as described by the so-called *mineralization law*. For healthy humans the mineralization law is characterized by a fast increase in mineral content in the first few weeks (primary mineralization) followed by a much slower secondary mineralization [1]. The outcome of remodeling and mineralization is a dynamically changing patchwork of bone packets with different mineral content. This material heterogeneity can be described by a probability distribution of the mineral content called *bone mineralization density distribution (BMDD)* [2]. Measurements of the BMDD (e.g. with the backscattered mode of an electron microscope [3]) showed that for healthy humans the BMDD is bell-shaped and virtually independent of age [4]. Changes in bone turnover and/or disorders in the mineralization process lead to significant deviations from this healthy BMDD. The aim of the work was to establish a mathematical connection between the processes of remodeling and mineralization, and the shape of the BMDD. Interpreting the BMDD in terms of mechanical properties allows connecting changes in the BMDD with changes in bone material quality.

Methods

The mathematical model is based on a continuity equation of the BMDD [1] including a source term corresponding to bone resorption. Bone deposition is modelled as the boundary condition at zero mineral content. The mineralization kinetics are reflected by a velocity with which a bone packet of given mineral content shifts to larger values of the mineral content in the BMDD diagram. Changes in

the rate of bone turnover have to consider the time lag between an increase/decrease in resorptive and formative fluxes of bone volume. This model approach was extended to allow the description of mineralization disorders as a time dependent mineralization law.

Results

In cases where the (measured) BMDD does not change significantly in time, a steady-state solution of the model allows deducing the underlying mineralization law. The case of a patient with a disorder in the phosphate control is compared to the healthy case [5]. Knowing the change in bone turnover or the change in the mineralization law as a function of time, the full time evolution of the BMDD can be obtained numerically [6]. Results presented include the cases of increased bone turnover at menopause, the reduction of turnover due to antiresorptive therapy, and the outbreak of mineralization disorders. Transiently strong deviations from the shape of the healthy BMDD can be observed, leading in extreme case to a very homogeneous distribution of the bone mineral or to a double-peak of the BMDD.

Discussion

The given examples should demonstrate the important information about the kinetics of bone remodeling and mineralization, which is included in the BMDD. Our mathematical model opens the possibility to extract some of this information. With the availability of medications with a known effect on bone turnover, the predictive model can be used for a therapeutic manipulation of the BMDD.

References

- [1] D. Ruffoni et al., *Bone* **40**, 1308, 2007.
- [2] P. Roschger et al., *Bone* **42**, 456, 2008.
- [3] P. Roschger et al., *Bone* **23**, 319, 1998.
- [4] P. Roschger et al., *Bone* **32**, 316, 2003.
- [5] K. Nawrot-Wawrzyniak et al, *Calcif Tissue Int*, accepted, 2009
- [6] D. Ruffoni et al., *J Bone Miner Res* **23**, 1905, 2008.

ASSESSMENT OF BV/TV DISTRIBUTION IN VERTEBRAE FOR SPECIMEN SPECIFIC AND STATISTICAL MODELLING

Sarawat Rehman (1), Nagitha Wijayathunga (1), Ruth Wilcox (1)

1. Institute of Medical and Biological Engineering, University of Leeds, U.K.

Introduction

Subject-specific finite element (FE) models of the spine are increasingly being developed to enable one-to-one validation against experimental specimens. There has also been a recent drive to develop stochastic models of the spine that can represent subject variance, with the longer term aim of predicting the performance of new interventions across a patient cohort. A number of authors have examined the distribution of trabecular bone within the vertebra by measuring parameters such as (bone volume)/(total volume) (BV/TV) and have found significant variation between different regions of the vertebral body [Hulme, 2007]. The aim of this study was to determine if the BV/TV parameter could be used as a basis for developing statistical models of the vertebrae for predicting stiffness. The objectives of this study were twofold: 1) to examine if localised BV/TV measurements could be used to determine elastic properties of bone within vertebrae by comparison between specimen-specific finite element (FE) models and corresponding experimental tests, 2) to evaluate the distribution of BV/TV in different specimens and establish if similar trends occur in all cases.

Methods

Seven vertebrae from five cadaver spines were imaged using microCT at 74µm resolution. Four vertebrae were tested under axial compression in the laboratory [Wijayathunga, 2008]. FE models were generated from the corresponding µCT images using proprietary software (ScanIP/FE, Simpleware, UK) with a maximum element size of 2mm. The µCT images were segmented at a constant threshold to capture the bone tissue and the BV/TV value determined for each element volume. For all the elements, the elastic modulus was related to the element BV/TV value using a linear conversion factor. An iterative approach was used to determine the optimum conversion factor that minimised the error between the predicted model stiffnesses and those determined experimentally. For three T12 vertebrae, BV/TV was also determined and compared across eight defined vertebral body regions.

Results

The finite element model predictions of stiffness were in good agreement with the values measured experimentally, with a root mean square error of 9.6%. Distribution of mean BV/TV was varied across the vertebral body regions with a mean of $19\% \pm 0.05\%$ and range of 13% to 29%. No clear trends were seen between specimens (Figure 1).

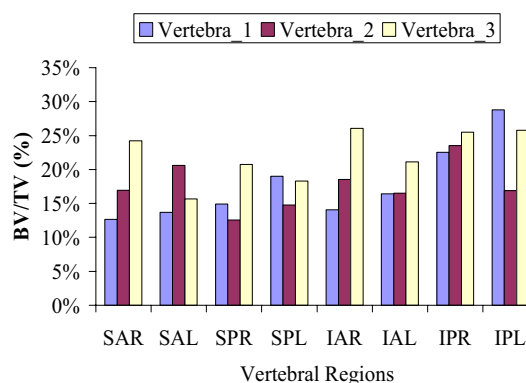


Figure 1: Distribution of BV/TV across eight T12 vertebral body regions denoted by superior (S), inferior (I), anterior (A), posterior (P), right (R) and left (L).

Discussion

The good agreement between FE models and corresponding experimental tests demonstrated that the BV/TV parameter can be used to determine the elastic properties of bone when applied on an element-by-element basis. Although trends have been predicted previously [Hulme, 2007] in the distribution of BV/TV, the large intra-specimen variations in found in this study show the need for a specimen-specific approach to capture individual variation.

If statistical models are to be built to represent sets of patients, then further analysis of components and features based on larger data sets is required.

Acknowledgements

This work was funded by the Engineering and Physical Sciences Research Council.

References

- Hulme et al, Bone, 41:946-957,2007.
- Wijayathunga et al, J Eng Med, 222:221-228, 2008.

CONTACT MECHANICS OF A DISCRETE FIBER-REINFORCED CARTILAGE MODEL

Patrik Christen (1), Stephen J. Ferguson (1), Salman Chegini (1)

1. Institute for Surgical Technology and Biomechanics, University of Bern, Bern, Switzerland

Introduction

The orientation of articular cartilage (AC) collagen fibers is depth-dependent, often referred to as Benninghoff's arcades [Benninghoff, 1925]. The mechanical response of AC depends primarily on the principal matrix components of collagen and proteoglycan [Wilson, 2007]. Thus, collagen fibers play an important role for understanding the mechanical behavior of AC, especially for the contact of cartilage layers.

Fiber-reinforced models have been proposed to more accurately describe the mechanical behavior of AC. To date, there are two different kinds of fiber reinforcement, discrete reinforcement using non-linear springs and continuum reinforcement [Wilson, 2005].

This work presents the first 3D finite element contact model of two fiber-reinforced cartilage layers and the first application of this to hip joint geometry with biphasic matrix material properties.

Method

Based on the discrete fiber reinforced model of [Chegini, 2008], primary and secondary fibers were created for the hemispherical cartilage layers using a Matlab routine and embedded into a solid matrix within ABAQUS finite element software. To compare different material models, a hip joint model was created with linear-elastic, biphasic, and biphasic fiber-reinforced materials. The labrum was modeled orthotropic and with low permeability in the fiber-reinforced model.

The maximum load during walking activity was applied to the created hip models according to in vivo data [Bergmann, 2001]. To determine the mesh size and fiber density relationship an indentation test model was created.

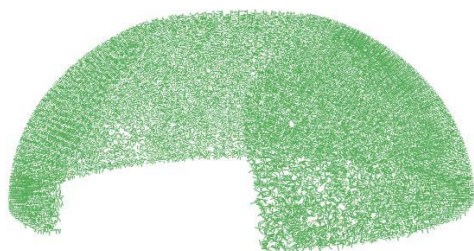


Figure 1: Fiber-embedded acetabular cartilage layer.

Results

Von Mises stress in the solid matrix was highest in the linear-elastic model (1.4 MPa) and very low in the biphasic models (0.05 MPa). Highest values occurred at the labrum-cartilage interface of the fiber-reinforced model and at the articular surface and the bone-cartilage interface of the linear elastic model. In the fibers, highest values occurred at the bone-cartilage interface (12.9 MPa) in the hip joint model and in the superficial zone (3.7 MPa) of the indentation test model. Contact pressure of the linear-elastic model (2.5 MPa) was comparable with the summation of fluid pressure and matrix stress of the biphasic models (2.2 MPa).

Discussion

The hip joint model showed contact pressure in the range of experimental data and previous models. The indentation model showed only slightly higher stress in the fibers compared to the poroviscoelastic fibril-reinforced model from [Wilson, 2004].

The hip joint model showed the equivalence between short-time biphasic and incompressible elastic material responses as also reported by [Ateshian, 2007] and load sharing between solid and fluid fractions. Most of the load was applied to the fluid fraction, as also showed by [Macirowski, 1994]. The biphasic transversely isotropic contact model from [Donzelli, 1999] predicted peak stresses at the cartilage surface and the cartilage-bone interface, which is in agreement with our model and with observed sites of cartilage fibrillation.

The developed method facilitates the automatic embedding of primary and secondary fibers within arbitrary 3D cartilage layers. Fiber density and distribution are defined within the seeding routine. Future work will focus on the incorporation of joint-specific direction dependence of fiber orientation.

References

- Ateshian et al, J Biomech Eng, 129:405-12, 2007;
- Benninghoff, Zellforsch, 763-862, 1925; Bergmann et al, J Biomech, 34:859-71, 2001; Chegini et al, CMBBE, 2008 ; Donzelli et al, J Biomech, 32:1037-47, 1999 ; Macirowski et al, J Biomech Eng, 116:10-8, 1994;
- Wilson et al, Biom & Mod in Mechbio, 6:43-53, 2007;
- Wilson et al, Medical Eng & Physics, 27:810-26, 2005.
- Wilson et al, J Biomech, 37:357-66, 2004.

ISOLATION, LOADING AND ESTIMATING THE POROELASTIC PROPERTIES OF A SINGLE OSTEON

Gaffar B. Gailani¹, Stephen Cowin², Luis Cardoso²

1. Department of Mechanical Engineering and Industrial Design, New York City College of Technology, USA; 2. Departments of Mechanical and Biomedical Engineering, City College of New York, New York, USA

Abstract

Measurement of the permeability of a single osteon is still one of the most challenging tasks in bone mechanics because of the size of the osteon and the limitations or absence of the tools that can take a direct measurement. Determining the poroelastic properties and the permeability of an osteon is a critical element in understanding fluid flow occurring in cortical bone and its role in bone nutrition and mechanotransduction, it also provides insight into the nature of the elastic response of osteons. In this communication, we present the development of a new procedure to isolate the osteon, design a mechanism for loading the osteon and compare the results of the stress relaxation test in *unconfined* compression experiment with the analytical results for a compressible transverse isotropy model that we developed previously, [Gailani, 2008]. These experimentally determined values for the permeability and mechanical properties have shown reasonable agreement with the previously reported experimentally and theoretically estimated value.

Introduction

Any attempts to understand and model the biomechanical properties of bone must be firmly rooted in a knowledge of the structure of bone on both the ultrastructural and microstructural levels of organization. Mechanical properties of bone are determined by a multiplicity of material and structural properties such as tissue mineralization, size and composition of mineral crystals, anisotropy...etc. Time varying mechanical loads applied to bone generate fluid pressure gradients in the lacunar canalicular porosity (PLC) that contribute to the interstitial fluid flow. The osteon (average diameter is 250 micrometers) is composed of a central Haversian canal (average diameter is 50 micrometers) housing a blood vessel and is surrounded by alternating mineralized collagen lamellae.

Methods

Many attempts were made to isolate the osteon, [Ascenzi, 1968, Frasca 1976] and reported different techniques. In this work the Micro-CT ((SkyScan

Corp., Belgium) was used with the Micro-lathe (Central Machinery, Inc.) to isolate the osteons of a bovine femur. The loading was done for stress relaxation by the system shown in Figure 1 below. The pico-motor used has a resolution below 30 nm.

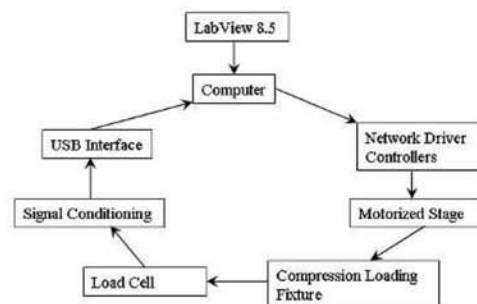


Figure 1: Loading the osteon [Gailani,2009]

Results & Discussion

The curve fitting of the analytical to the experimental data (using Matlab Tool box) with strain rate of 10^{-4} /s have shown a value of the permeability in the order of $O(10^{-24})$ m² and a reasonable values for the drained poroelastic (E_1 , E_3 , ν_{12} , ν_{13} , ν_{32}) compared to the previously reported ones. The permeability value has a reasonable agreement with the previously reported ones of [Zhang, 1998; Smit, 2002; Oyen, 2008],

Acknowledgements

This work was supported by grants from NSF (NSF/CUNY AGEF # 0450360 and NSF-MRI 0723027). The authors also acknowledge the support from PSC-CUNY Research Award Program (PSC-CUNY-60014-38-39; 69486-00 38, PSCREG-39-1103) and CUNY-LSAMP

References

- Ascenzi et al, Anat. Rec, 161: 377 – 391, 1968.
- Frasca et al, Acta. Anat., 95:122-129, 1976.
- Gailani et al, J. Mech. Of Mater., 40(6): 507 – 523, 2008.
- Gailani et al, J. Biomech. Engr., Submitted
- Oyen, J. Mater. Res., 23: 1307 – 1314, 2008.
- Smit et al, J. Biomech., 35: 829-36, 2002.
- Zhang et al, J. Biomech. Eng., 120:697-703, 1998.

CAN HUMAN TISSUE MINERAL DENSITY BE ASSUMED CONSTANT?

Simone Tassani (1,2), Caroline Öhman (1,2), Massimiliano Baleani (1), Fabio Baruffaldi (1), Marco Viceconti (1)

1) *Laboratorio di Tecnologia Medica, Istituti Ortopedici Rizzoli, Bologna, Italy*

2) *Engineering Faculty, University of Bologna, Italy*

Introduction

Bone Mineral Density (BMD) is one of the most used parameter in the clinical practice. It is used to estimate the mechanical strength of bone and the risk of fracture in critical anatomical sites. Furthermore, it is applied in computational application to derive material proprieties of bone tissue. However, BMD cannot identify if the variation in bone density is related to a modification of Tissue Mineral Density (TMD), a decrease of Bone Volume (BV) or a combination of the two. TMD is defined as the degree of bone-tissue mineralization [Kazakia, 2008]. While it is widely known that BV changes passing from cortical to trabecular bone, it is still debated if TMD is a constant or not. This study was aimed to investigate whether TMD can be assumed as a constant.

Methods

From two female donors, without musculoskeletal disorders, 55 cylindrical specimens were extracted from different anatomical site: 38 trabecular specimens (diameter 10mm, height 20mm) and 17 cortical specimens (diameter 2.8mm, height 14mm). A micro tomographic device (micro-CT) was used to determine the bone volume fraction (BV/TV) of every specimen. Two different acquisition protocols, based on two morphometric phantoms, were used. Trabecular bone specimens were acquired using a published protocol [Perilli, 2008]. Cortical specimens were acquired using pixel size 8 μ m, tube voltage 80kVp, tube current 120 μ A. All specimens were ashed and ash density (ρ_{ash}) was measured following a previous published protocol [Öhman, 2007]. TMD was computed as the ratio between ρ_{ash} and BV/TV, as described in equation (1).

$$TMD = \frac{\text{Ash Mass}}{\text{Bone Volume}} = \frac{\rho_{ash}}{BV/TV} \quad (1)$$

Mann-Whitney statistical analysis was performed to verify whether TMD of trabecular and cortical bone were significantly different. Furthermore a regression analysis was performed between ρ_{ash} and BV/TV.

Results

The results showed that the TMD of trabecular ($1.29 \pm 0.17 \text{ mg/mm}^3$) and cortical ($1.24 \pm 0.03 \text{ mg/mm}^3$) bone were not statistically different ($p=0.74$). The linear regression between ρ_{ash} and BV/TV is shown in Figure 1.

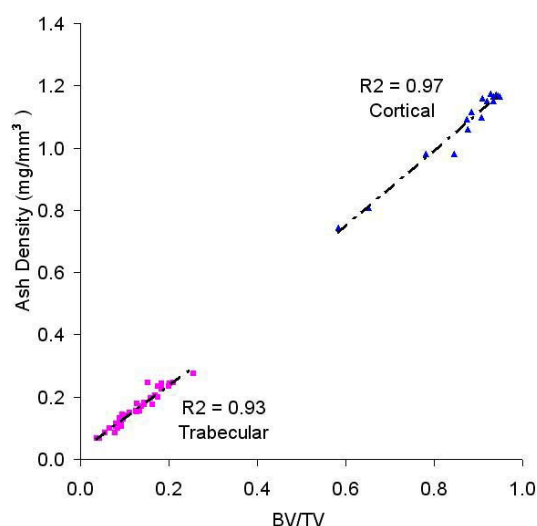


Figure 1: Linear regression between Ash Density and BV/TV.

Discussion

These results are limited by the restricted donor number. However the results, although preliminary, suggest that TMD can be supposed constant in non pathological bone tissue. If these results will be confirmed by further studies on larger sample sizes (donor number), computational models could manage TMD as a constant and only vary the bone volume in relation to clinical densitometric analysis.

Acknowledgements

This work was supported by the EC (project numbers: IST-2004-026932 (acronym: LHDL) and MRTN-CT-2006-035763 (acronym: 3D Anatomical Human)).

References

- Perilli et al, J Biomech 41(2): 438-46.2008.
- Öhman et al, J Biomech 40(11): 2426-33.
- Kazakia et al, Med Phys 35(7): 3170-9

OSTEON CLASSIFICATION IN HUMAN FEMUR, TIBIA AND FIBULA SHAFT BY CIRCULARLY POLARIZED LIGHT

Alina Beraudi, Massimiliano Baleani, Susanna Stea, Sara Cremonini, Marco Viceconti
 Laboratorio di Tecnologia Medica, Istituto Ortopedico Rizzoli, Italy

Introduction

Mechanical properties of the long bones and their functional adaptation are usually studied at organ [Cristofolini, 2007] and tissue level [Ohman, 2007]. However, it has been observed that there are correlations between the tissue loading condition and the microscopic organization of the bone, both in terms of composition and microstructural properties [Goldman, 2005]. Recently, models of the human cortical bone have been developed [Predoi-Racila, 2008]. The validation of these model needs of the microstructural physical properties at each architectural level. The aim of this work is to investigate collagen fiber orientation in long bones of lower limb to verify if collagen fiber orientation is regionally dependent.

Methods

A sample of each long bone of the lower limb (femur, tibia, and fibula) was obtained from the donor program of the Université Libre de Bruxelles. The bones were harvested from old female subjects without musculoskeletal pathologies. Serial transverse cross-sections were cut from each bone segment at different levels of the shaft. The anatomical orientation was marked on each cross-section before it was embedded in polymethylmethacrylate. A thin slice of 100 μm thickness was cut from each cross-section and prepared for microscopy analysis. Each slice analyzed by circularly polarized light microscopy. The osteons were classified referring to their collagen fiber orientation: transversal, T; alternated, A; and longitudinal-hooped, LO [Bigley modified, 2006].

The collected data were analysed by means of an ANOVA analysis with F test was applied to determine the effect of anatomical, cortical thickness and distance from the mid-section.

Results

In all the three analysed bones, osteonal pattern distribution was not significantly affected by the anatomical quadrant of section or by the cortical wall thickness, while the distance from the mid-section was significantly effective. Moving toward the diaphyses the percentage of osteons transversal type increased, at the expense of longitudinal-hooped osteons in femur and tibia and of alternated osteons in fibula. The alternated pattern of orientation is always the most numerous and apparently constant along the shaft of in femur and tibia.

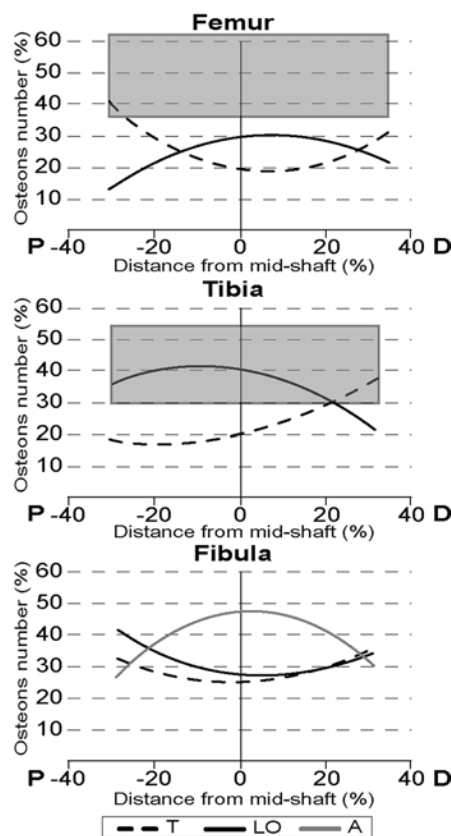


Figure 1: The percentage of each type of osteon as a function of the distance from the mid-level of bone

Discussion

These preliminary results suggest that there may be a pattern in orientation of collagen fibers, which may be correlated to the loading conditions the bone tissue undergoes. Although this findings have to be analysed in a larger sample size, a not-random osteon type distribution has to be considered in bone tissue models.

Acknowledgements

This work was partially supported by the European Community (project n° IST-2004-026932; LHDL).

References

- Cristofolini L. et al, J Biomech, 40:2837-2845, 2007
- Ohman C. et al, J Biomech, 40: 2426-2433, 2007
- Goldman HM et al, J Anat, 206: 127-139, 2005
- Predoi-Racila M et al., Stud Health Technol Inform, 133: 208-215, 2008
- Bigley RF et al, J Biomech 39: 1629-1640, 2006

Cardiovascular system - neurovascular

A MATHEMATICAL CEREBROVASCULAR MODEL INCLUDING THE CIRCLE OF WILLIS AND CORTICAL ANASTOMOSES

Mauro Ursino (1), Massimo Giannessi (1)

1. Department of Electronics, Computer Science, and Systems, University of Bologna, Italy

Introduction

An important characteristic of brain hemodynamics is its heterogeneity, i.e. blood flow to different brain regions can be independently regulated by active mechanisms and passively redistributed via anastomotical paths.

Methods

In this work, a mathematical model of cerebral hemodynamics and intracranial pressure (ICP) dynamics, developed in previous years [Ursino, 2000], is significantly extended to account for heterogeneity in cerebral blood flow (CBF). The model includes the circle of Willis, six regional districts (perfused by the six main cerebral arteries), distal cortical anastomoses, venous circulation (with a collapsible terminal portion), the cerebrospinal fluid circulation, and the intracranial pressure-volume relationship. Moreover, blood flow in the six regions is independently regulated by autoregulation and CO₂ reactivity.

Results

A first group of simulations was performed to simulate the transient hyperaemic response (THR), i.e. the transient increase in ipsilateral blood flow velocity at the end of partial internal carotid artery (ICA) occlusion, in a normal subject.

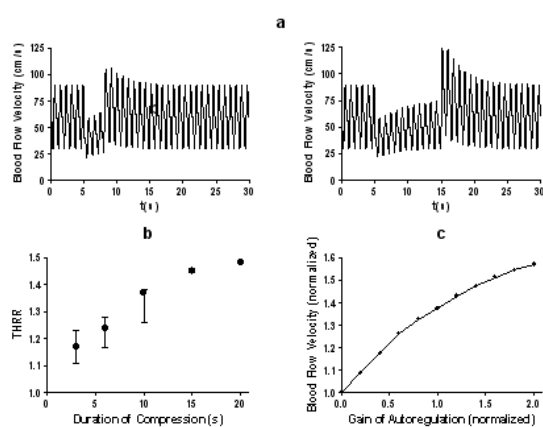


Figure 1: THR computed with the model after the release of an ICA compression of different duration and assuming different values for the autoregulation gain.

Since this test is often used to assess the autoregulation strength and dynamics, simulations have been repeated with different durations of the occlusion and with different values of the autoregulation gain. Results agree with data in the literature (Fig. 1b) and highlight the existence of a quasi-linear relationship between THR and the autoregulation gain (Fig. 1c). Subsequently, the model was used to simulated blood flow distribution in intracranial arteries during unilateral ICA stenosis, with and without CO₂ pressure changes (Fig. 2), or unilateral stenosis of the middle cerebral artery (MCA). Results suggest that local blood flow regulation is progressively lost in a MCA territory during ipsilateral severe stenosis (in the most serious cases one can observe a steal phenomenon) and that the anterior communicating artery plays the major role to redistribute blood flow toward the ischemic territory.

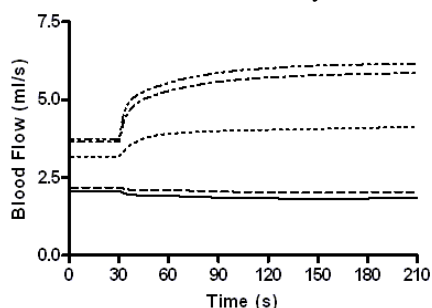


Figure 2: Time pattern of blood flow in the ipsilateral ICA following a step increase in arterial CO₂ pressure. Five cases are shown, characterized by different degree of stenosis of the ICA.

Discussion

An important function of the present model is to provide a quantitative framework for the analysis of the complex relationships between severity of an ICA stenosis, CBF regulation and morphology of the circle of Willis. The model can be of value to interpret cerebral hemodynamics during clinical tests or pathological conditions characterized by asymmetry in cerebral hemodynamics.

References

- Cavill et al, Br J Anaesth, 81:317-321, 1998.
- Ursino et al, Am J Physiol, 279:H2439-H2455, 2000.

A COMPUTATIONAL MODEL FOR BLOOD FLOW IN PATIENT-SPECIFIC CEREBRAL VENOUS TREE

Harvey Ho, Kumar Mithraratne, Peter Hunter

Bioengineering Institute, University of Auckland, New Zealand

Introduction

Compared with large arteries, the blood pressure in veins is much lower, the wall of large veins is thinner and some of them are collapsed [Fung, 1996]. Many investigators have studied flow in collapsible vessels e.g. in [Shapiro, 1977][Pedley, 2000][Elad et al, 1991] etc. In particular, the self oscillation phenomenon (“flutter”) and the shock wave formed when the flow transits from the subcritical state to supercritical state, are well documented and some mathematical models are suggested [Pedley, 2000].

However, unlike its arterial counterpart the research on blood flow in a venous tree is still rare. This is largely due to the fluid structure interaction (FSI) nature in large veins and the possible shock waves formed in some venous segments in the tree. This work is not an answer to these complex processes either, but as an initial model simple enough to make computation feasible for a patient-specific venous tree, e.g. by assuming: (a) a venous segment is either (partially) collapsed or expanded but not both; (b) the external pressure is uniform across the venous tree. We show that such a model can capture some important hemodynamic features when blood flows through the venous tree.

Methods

Vascular tree construction: Using an open source tool CMGUI, some 402 nodes are selected manually along the centreline of venous tree in a 3D CTA image. The cross-section area at each node is defined as a *field*. 1D cubic Hermite elements are then constructed along these nodes to represent the cerebral venous tree starting from intracranial venous sinus to superior vena cava (min diameter: 1.5mm) (Figure 1a). This tree consists of 42 venous segments and 30 bifurcations.

Mathematical model: The governing equations for a single vessel can be formulated as: [Pedley, 2000]

$$\frac{\partial A}{\partial t} + \frac{\partial VA}{\partial x} = 0 \quad (1)$$

$$\frac{\partial V}{\partial t} + V \frac{\partial V}{\partial x} = -\frac{1}{\rho} \frac{\partial P}{\partial x} + \frac{R(A)V}{\rho} \quad (2)$$

$$P - P_e = KF(A/A_0) \quad (3)$$

Eq. (3) is also called the Tube Law where K is bending stiffness, F is a dimensionless function differentiating collapsed and expanded vascular

status. The above hyperbolic system is solved using a MacCormack finite difference scheme. The fixed pressure boundary condition (15mmHg) is prescribed from inlets, and a pulsatile pressure (0-3mmHg) from outlet, respectively.

Bifurcation model: a bifurcation model similar to [Smith *et al*, 2000] is incorporated to predict flow distribution, pressure gradient and velocity across branches, thus the whole venous tree.

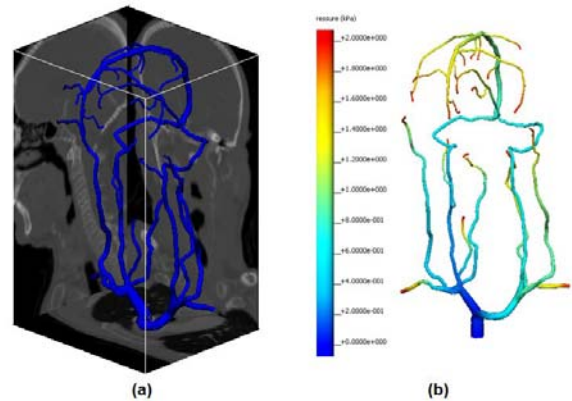


Figure 1: (a) Reconstructed venous tree from a CTA image; (b) Pressure distribution in the tree.

Results

It takes less than 5 minutes to compute P , V and A along the tree during a cardiac cycle. The computed data at some typical venous sites are shown in Table 1. The results indicate that both superior vena cava ($A/A_0=53\%$) and jugular vein ($A/A_0=12\%$) are partially collapsed.

Name of Vein	$A(\text{cm}^2)$	$V(\text{cm/s})$	$P(\text{mmHg})$
Sup. Sagittal Sinus	0.48	0.4	13.65
Left Jugular	0.28	7.4	5.0
Sup. Vena Cava	4.08	12.0	0.1

Table 1: A, V, P at 0.8s (cardiac cycle: 1s).

Acknowledgements

We thank Dr. A. Frangi for providing the CTA image.

References

- Fung, Chapter 4, pp. 206-252, Springer, 1996
- Pedley, Chapter 2, pp. 27-40, WIT press, 2000.
- Shapiro, J. Biomech. Eng., 99:126-147, 1977
- Elad *et al*, J. Biomed. Eng., 13:11-18, 1991
- Smith *et al*, SIAM J. App. Math., 62:990-1018, 2000

FAST VIRTUAL STENTING IN CEREBRAL ANEURYSMS: VALIDATION WITH FINITE ELEMENT ANALYSIS

**Eleonora Flore (1,2), Ignacio Larrabide (2,1), Giancarlo Pennati (4), Lorenza Petrini (4),
Alejandro Frangi (1,2,3)**

*Center for Computational Imaging and Simulation Technologies in Biomedicine (CISTIB) –
(1) Universitat Pompeu Fabra (UPF), (2) CIBER-BBN and (3) ICREA, Barcelona, Spain.
(4) Laboratory of Biological Structure Mechanics, Politecnico di Milano, Milano, Italy*

Introduction

Finite Element Analysis (FEA) has been widely used to investigate both the mechanical behaviour of vascular stents and the interaction between stents and the vessel wall [Migliavacca, 2002; Wu, 2008]. A different approach allowing the prediction of the stent released shape, useful for fluid dynamics analyses, is based on simplex deformable meshes [Larrabide, 2008]. In particular, this Fast Virtual Stenting (FVS) methodology has been successfully applied with fast execution times for virtual stent release in real vessel geometries. As this method does not explicitly consider all the structural issues, a proper assessment of its results is required. In this work we quantify the differences between FEA and FVS method.

Methods

A series of parametric models has been set, using one commercially available stent and idealized vessel geometries. Two straight vessels with different diameters, 4 mm (V_L) and 3.6 mm (V_S), have been chosen. For each one, three different necks, with a main dimension proportional to the vessel diameter, have been considered (N1 - rounded, 80%; N2 - rounded 60%; N3 - oval, 80%). Two other geometries (C1 and C2) with curvature on the vessel and an oval neck (N3) have been also considered. FEA simulations have been performed using ABAQUS/Standard (Simulia Corp, Providence, RI, USA) and a user-defined subroutine describing the behaviour of the Ni-Ti alloy [Auricchio, 2004] was used. In the first step of the analysis the devices are crimped and then left free to expand due to their superelasticity property. In the FVS method, a second order differential equation is used for moving the stent mesh under the effect of internal and external forces and taking into account geometric constraints for the specific stent. To assess the differences between both models, the stent released configurations has been compared for each scenario, computing the distance between corresponding nodes.

Results

Figure 1 shows a box plot presenting the global error when comparing FVS to FEA model in each

scenario, evaluated by computing the distance between corresponding nodes in the two models.

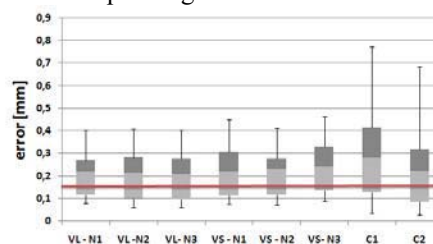


Figure 1: Box plot for the error between corresponding nodes in FEA and FVS models.

The average error (red line in Figure 1) is about 4% compared to the vessels diameters.

The largest errors correspond to the analyses run considering the vessel curvature, which that mainly affects the released stent configuration (Figure 2).



Figure 2: FEA (a) and FVS (b) final configuration of the stent in one of the curved vessel geometries

Moreover, the greatest difference between the two methods consists in the computational time. While FEA simulations required almost two hours each, executed on a Cluster (4CPUs each one with 4GB of memory), those executed with the FVS method on an Intel®Core™ Duo CPU T7300 2.00GHz with 2Gb of memory run in 9.125 ± 1.125 s.

Discussion

The results of this first validation of the FVS method show a quite fine match between the two methodologies in front of a huge reduction of computational time and costs gained. A further optimization of the algorithm parameters and a supplementary validation with patient specific vessel geometries is currently work in progress.

References

- Auricchio and Petrini, Int J Numer Meth Engng,; 61:807–836, 2004.
- Larrabide et al, MICCAI08 - Part II - LNCS 5242 - 790-797, 6th-10th September 2008, New York, NY, USA
- Migliavacca et al, Biomech Model Mechanobiol, 2(4):205-17, 2002
- Wu et al, J Biomech, 40(11):2580-5, 2007.

A NOVEL APPROACH FOR COMPUTATIONAL HAEMODYNAMIC CHARACTERISATION OF CEREBRAL ANEURYSMS

Alberto Marzo¹, Pankaj K Singh^{1,2}, Patricia Lawford¹, Umang J Patel², Stuart C Coley³, D Rod Hose¹

(1) Academic Unit of Medical Physics, School of Medicine and Biomedical Sciences, University of Sheffield, Sheffield, UK,

(2) Department of Neurosurgery, Royal Hallamshire Hospital, Sheffield, UK

(3) Department of Neuroradiology, Royal Hallamshire Hospital, Sheffield, UK

Introduction

Intracranial aneurysms (IA) are abnormal dilations of blood vessels, which may rupture with devastating consequences. Inspired by the importance of haemodynamics in the etiopathogenesis of IAs, several haemodynamic indices, including wall shear stress (WSS) and oscillatory shear index (OSI), have been identified as having an association with endothelial deterioration. Unfortunately, the exact nature of associations between these and the initiation, growth and rupture of IAs is poorly understood. Recent studies suggest a strong correlation between rupture and the complexity of intra-aneurysmal flow patterns [Cebal et al., 2005]. The definition of complexity used in these studies relies on a subjective interpretation of the flow fields; a method prone to inter-observer variability. Using concepts used in other applications, specifically Hunt's Q criterion [Hunt et al., 1988], and energy viscous dissipation (EVD), this study aims to quantify complexity to obtain a more objective characterisation of 3D flows within IAs.

Methods

Models for six typical IAs were reconstructed from rotational angiograms using the computational tool-chain being developed in the EU project @neurIST (www.aneurist.org). Flow fields were predicted by solving the transient Navier-Stokes equations, using the finite-control-volume software ANSYS®-CFX™. A coherent vortex in a complex flow field can be defined in regions where

$$Q = \frac{1}{2} (\|\Omega\|^2 - \|S\|^2) > 0 \quad (1)$$

Where Ω and S are vorticity and strain rate tensor respectively. Flow complexity is also directly related to viscous energy loss arising from complex vortices. The rate of EVD in an incompressible and Newtonian fluid is defined by

$$E = \mu \int \Phi dv \quad (2)$$

Where the Φ is

$$\Phi = 2 \left\{ \left(\frac{\partial u}{\partial x} \right)^2 + \left(\frac{\partial v}{\partial y} \right)^2 + \left(\frac{\partial w}{\partial z} \right)^2 \right\} + \left(\frac{\partial v}{\partial x} + \frac{\partial u}{\partial y} \right)^2 + \left(\frac{\partial w}{\partial y} + \frac{\partial v}{\partial z} \right)^2 + \left(\frac{\partial u}{\partial z} + \frac{\partial w}{\partial x} \right)^2$$

These haemodynamic indices were used to characterise the flow fields of the IAs examined.

Results

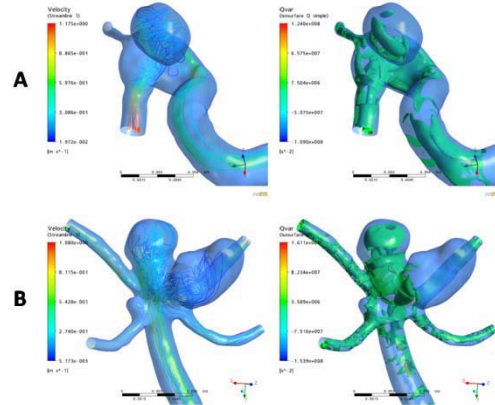


Figure 1: Streamlines (left) and Q iso-surfaces for 2 typical IAs.

	A	B
Viscous Energy loss rate [W]	8.0E-4	1.9E-3
Kinetic energy inflow rate [W]	1.2E-3	5.9E-3
Viscous energy loss %	0.7	32.0

Table 1: Rates of viscous energy loss for aneurysms A and B, and comparison with rate of inflow kinetic energy, at peak-systole.

Discussion

When the Q criterion was applied to flows in IAs, the resulting isosurfaces provided a better description of vortices as compared to conventional flow representations (Fig 1). As reported by Moyle et al [year], in a cardiac application, there are significant energy losses arising from vortices. Table 1 reports values of energy loss rates for two aneurysms. It is apparent that the subjectively more complex flow of aneurysm B (Figure 1) is also that affected by more substantial energy losses, both in absolute terms (1.9E-3W), and relative to the inflow kinetic energy at the neck of the aneurysm (32%). This study demonstrates that measurements of Q and EVD can provide a better and objective quantification of complex flow patterns, free from inter-observer variability.

Acknowledgements

The study was funded by European Commission, @neurIST (Grant No: IST-FP6-027703).

References

- Cebal et al. IEEE Trans Med Imaging. 24(4):457-467, 2005
- Hunt et al. Center for Turbulence Report. CTR-S88, 193-208, 1988.
- Moyle et al. Int J Numer Meth Fluids. 50:1357-1368, 2006.

NEW ORIENTATION DISTRIBUTION FUNCTIONS IN THE MICRO-SPHERE-BASED MODELING OF BLOOD VESSELS

M. A. Martínez, V. Alastrué, and M. Doblaré

Group of Structural Mechanics and Materials modelling.

Aragón Institute of Engineering Research. University of Zaragoza.

CIBER-BBN. Centro de Investigación Biomédica en Red en Bioingeniería, Biomateriales y Nanomedicina

Introduction

During the last years, the constitutive modelling of soft biological tissues has constituted a very active field of research. Usually, they are composed of an extra-cellular matrix formed by an isotropic high water content ground substance in which a network of elastin and collagen fibres is embedded. Commonly, these materials have been modelled as hyperelastic continua embedded into continuum mechanical formulations, whereas inclusion of structural tensors into constitutive laws is the most widely used technique to introduce anisotropy caused by fibres [1]. Nevertheless, the large variability concerning the mechanical behaviour and the particular composition exhibited by soft biological tissues requires the incorporation of representative structural information that includes the spatial probabilistic distribution of the fibers.

Methods

Microsphere-based models incorporate the individual response of the underlying material constituents so that the macroscopic behaviour is obtained by means of a computational homogenisation technique [2]. Incorporation of anisotropy present in blood vessels in microsphere-based models is achieved by means of the inclusion of an orientation density function (ODF) that weights the contribution of the micro-fibres in each direction of space respect to a preferred orientation direction \mathbf{a} [4]. Then, the macroscopic energy turns out

$$\psi = \langle n \rho \psi_f \rangle := \frac{1}{4} \int_{U^2} n \rho \psi_f dA \approx \sum_{i=1}^m \omega^i \rho^i \psi_f^i$$

where n is the micro-fibres density, ρ is the named ODF, and ψ_f represents the mechanical response of an individual micro-fibre.

Normalization the integral over the surface of the unit sphere is done by means of the factor $A_{U^2} = 4\pi$.

Amongst the several possibilities of ODFs to contemplate the spatial distribution, in this work

two of them are compared, the π -periodic Von Mises [3] and the Bingham function.

Results

The material parameters of the two ODFs introduced above are identified. For the least-squares-based iteration scheme, experimental data reported in [4] corresponding to human coronary arteries were used. Both ODFs present similar results, reproducing quantitatively the circumferential and axial experimental data.

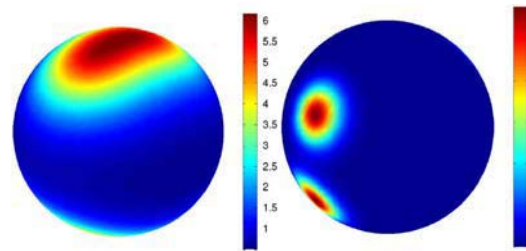


Figure 1: Von Mises ODF for the media and adventitia layers of a human coronary artery.

Discussion

The two ODFs presented in this work show similar results and fit adequately the experimental data. However the Bingham ODF offers a greater flexibility due to the higher number of parameters. Therefore, for the Bingham ODF only one family of fibers is needed when two are used for the Von Mises function.

Acknowledgements

The authors gratefully acknowledge research support from Spanish Ministry of Science and Technology through the research project DPI2007-65601-C03-00, and the Spanish Ministry of Health through Instituto Salud Carlos III (CIBER-BBN).

References

- [1] Gasser et al., J Roy Soc Interface, 3:15–35, 2006
- [2] Miehe et al., J Mech Phys Solids, 52:2617–2660, 2004
- [3] Alastrué et al, J Mech Phys Solids, 57:178-203, 2009
- [4] Holzapfel et al., Am J Physiol - Heart Circ Physiol 289:2048-2058, 2005

COMPUTATIONAL STUDY OF THE EFFECTS OF DRUGS ON GROWTH AND RUPTURE OF INTRACRANIAL ANEURYSMS

Pankaj K Singh^{1,2}, Alberto Marzo¹, Hannan Tahir¹, Tissa F Weeratunge¹, D Rod Hose¹, Patricia Lawford¹, Umang J Patel², Stuart C Coley³

(1) Academic Unit of Medical Physics, School of Medicine and Biomedical Sciences, University of Sheffield, Sheffield, UK

(2) Department of Neurosurgery, Royal Hallamshire Hospital, Sheffield, UK

(3) Department of Neuroradiology, Royal Hallamshire Hospital, Sheffield, UK

Introduction

Intracranial aneurysms (IA) are abnormal dilations of blood vessels. These may rupture, resulting in high morbidity and mortality. Whereas the exact reasons for IA formation and rupture are poorly understood, recent evidence indicates that haemodynamic indices such as wall shear stress (WSS) and oscillatory shear index (OSI), are important underlying factors. As the rheological properties of blood, including blood viscosity (BV), have a significant influence on the haemodynamics of an IA, it is suggested that factors affecting BV may in turn, affect growth and rupture. A number of studies have demonstrated the influence of drugs, including heparin, a widely-used antithrombotic agent, on BV [Hitosugi, 2001]. The current study investigates the sensitivity of WSS and OSI to heparin-induced changes in BV and discusses its possible long-term implications.

Methods

Five aneurysms in typical locations along the cerebral arteries were considered. Using the computational tool-chain being developed within the EU project @neurIST (www.aneurist.org), model geometries were reconstructed from clinical rotational angiograms and used to compute the WSS and OSI fields acting at the aneurysmal wall. Blood was assumed to be incompressible, with density $\rho = 1060 \text{ kg/m}^3$ and Newtonian, with viscosity $\mu_{\text{untreated}} = 0.0045 \text{ Pa}\cdot\text{s}$, for untreated blood, and $\mu_{\text{heparin}} = 0.0025 \text{ Pa}\cdot\text{s}$, for heparinised blood. This simulates the effect of heparin at an average therapeutic concentration of 0.0075 mg/ml. The 3D unsteady Navier-Stokes equations were solved by using the finite-control-volume software, ANSYS[®]-CFX[™].

Results

Contour plots of WSS and OSI show similar haemodynamic patterns for both values of BV, for all IAs studied (Figure 1). Whilst for both BV values, areas of low WSS remain confined within the dome and body of the aneurysms, zones of comparatively higher WSS were concentrated around the distal part of the neck and in areas within the aneurysmal body, where the jet generated at the base of the aneurysm impinges against its wall. Table 1 shows a quantitative comparison between minimum and maximum values of WSS and OSI, and areas where values for

these indices are outside their normal physiological range [Malek *et al*, 1999], for one of the aneurysms.

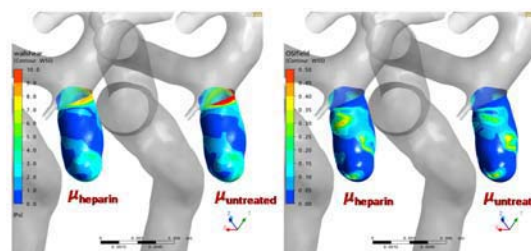


Figure 1: Time-averaged WSS (left) and OSI (right) contours in aneurysm for heparinised and non-heparinised blood.

	$\mu_{\text{untreated}}$	μ_{heparin}
WSS min [Pa]	0.025	0.014
WSS max [Pa]	14.7	9.5
Area of infra-physiological WSS (<0.4 Pa)	8.9%	10.5%
OSI max	0.41	0.44
Area of elevated OSI (>0.4)	0.03%	0.11%

Table 1: Quantitative comparison of effects of BV on WSS and OSI. Percentages are computed over the total aneurysmal area and WSS values are time-averaged along the cardiac cycle.

Discussion

Infra and supra-physiological values of WSS and OSI have been associated with endothelial cell loss, desquamation and derangement in activity of wall-growth regulators. BV, which directly affects these haemodynamic indices, can be influenced by various commonly used drugs, viz. aspirin [Vekasi, 2008], amlodipine [Linde *et al*, 1996], statins [Box *et al*, 2007], etc. Heparin is an anti-thrombotic agent commonly used as anticoagulant, has been shown to reduce BV by approximately 50% [Hitosugi, 2001]. The computed results reported in Table 1, show that heparin induces a significant increase in the areas of affected by infra-physiological WSS, and high OSI. Such regions carry a higher risk of deterioration of endothelial cell function and may lead to an increased risk of IA growth and rupture.

Acknowledgements

The study was funded by European Commission, @neurIST (Grant No: IST-FP6-027703).

References

- Box *et al*. Stroke. 38:1374-1376, 2007.
- Hitosugi *et al*. Thromb Res. 104(5):371-374, 2001.
- Linde *et al*. J Hum Hypertens. 10(3):199-205, 1996.
- Malek *et al*. JAMA 282:2035-2042, 1999.
- Vekasi. Clin Hemorheol Microcirc. 39 (1-4):385-389, 2008.

Musculoskeletal system – subject specific

SUBJECT-SPECIFIC P-FE ANALYSIS OF THE PROXIMAL FEMUR UTILIZING MICROMECHANICS-BASED MATERIAL PROPERTIES

Zohar Yosibash (1), Nir Trabelsi (1), Christian Hellmich (2)

1. Dept. of Mechanical Engineering, Ben-Gurion Univ., Beer-Sheva 84105, Israel

2. Inst. for Mech. of Materials & Structures, Vienna Univ. of Tech., A-1040 Vienna, Austria

Introduction

Novel subject-specific high-order finite element (FE) models of the human femur based on computer tomographic (CT) data are generated with two different methods for material properties determination: micromechanics and empirically based, both being determined from CT scans. FE results are validated through displacements and strain measurements on a femur harvested from a 54-y.o. female. To the best of our knowledge, this work is the first to consider an inhomogeneous Poisson ratio and the first to compare results obtained by micromechanics-based material properties to experimental observations on a bone. The p-FE models with the micromechanics-based material properties yield results which closely match the experimental observations and are in accordance with the empirically based FE models. Furthermore, these micromechanics-based material properties provide access to patient-specific distribution of the full anisotropic elasticity tensor components, as will be demonstrated herein.

Methods

A fresh-frozen femur was defrosted, CT-scanned, and thereafter exposed to in vitro experiments while displacements, loads, and strains were measured. Structural p-FE models mimicking the experiments were created from the CT-scans (see [Yosibash 2007] for details). Two different types of material properties were assigned to the p-FE model (a) Empirically based isotropic inhomogeneous Young modulus [Keyak 2003] with a constant Poisson's ratio of 0.3: $E_{Cort} = 10200\rho_{ash}^{2.01}$, $E_{Trab} = 5307\rho_{ash}^{2.01} + 469$ [MPa] (b) Micromechanically based inhomogeneous isotropic and anisotropic material properties constructed based on two consecutive steps (details are given in [Hellmich 2008 and Yosibash 2009]):

- Based on voxel average rules for the attenuation coefficients, each voxel was assigned a volume fraction occupied by water (marrow) and by solid bone matrix.
- By means of a micromechanical model based on stiffness properties of solid bone matrix and of water, the volume fractions were converted into voxel-specific orthotropic (and also transversely isotropic) stiffness tensor.

Results

To verify the accuracy of our CT-based p-FE models, a comparison between the experimental observations (strains and displacements) and the FE results was conducted when considering inhomogeneous isotropic material properties shown in Figure 1 and transversely isotropic material properties shown in Figure 2.

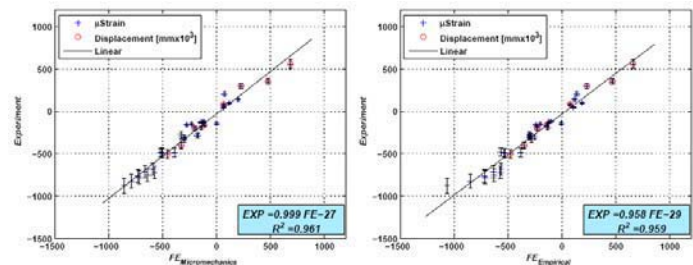


Figure 1: FE results vs experimental observations. Isotropic properties assigned by micromechanics-based (left) and empirically based (right)

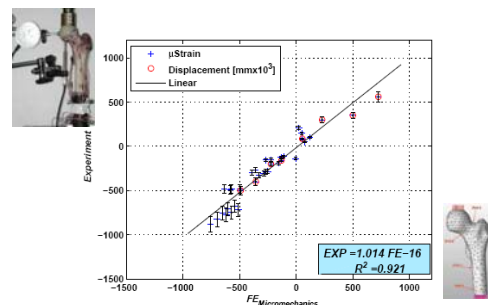


Figure 2: Micromechanics-based model - transversely isotropic cortical and isotropic head material properties.

Discussion

Micromechanics-based material properties determined from CT scans in conjunction with p-FEs show an excellent correlation to experimental observations, and are similar to these obtained with isotropic empirically derived material properties. The ability to determine anisotropic material properties by micromechanics-based model may be of major importance if one considers a more complicated state of stress on the bone involving shear and torsion.

References

- Hellmich, C. et al, Ann. Biomed. Eng. 36:108–122, 2008.
 Keyak, J.H. et al, J. Med. Eng. Phys 25:781–787N, 2003.
 Yosibash, Z. et al. J. Biomech. 40:3688–3699, 2007.
 Yosibash, Z. et al, Int. J. Multiscale Comp. Eng., In press 2009.

DEVELOPMENT AND VALIDATION OF SPECIMEN-SPECIFIC MICRO-CT BASED FINITE ELEMENT MODELS OF MOUSE TIBIAE

Antonia Torcasio (1), Leanne Saxon (2), Davide Ruffoni (3), G. Harry van Lenthe (1, 3)

1. *Division of Biomechanics and Engineering Design, K.U.Leuven, Leuven, Belgium;*

2. *Department of Veterinary Basic Sciences, University of London, London, UK*

3. *Institute for Biomechanics, ETH Zurich, Zurich, Switzerland*

Introduction

Bone has long been recognized to be capable of adapting its mass and structure in response to mechanical loading. Nevertheless, a quantitative understanding of the load-induced bone adaptation processes is still lacking. Where animal studies can provide detailed data on bone response, they only offer limited experimental strain data, mainly due to technical constraints in the size of strain gauges and in accessibility of the bone tissue under investigation. Hence, including micro-computed tomography (μ CT) based finite element (μ FE) models in the analyses seems useful because they allow the calculation of local tissue loading throughout the entire bone. Therefore, the aim of this study was to validate FE models for the assessment of tissue strain. Specifically, our aim was to validate μ FE models for the mouse tibia loading model [De Souza, 2005].

Methods

Ex vivo strain gauge measurements were carried out on tibia of three C57BL/6J mice (17 weeks of age). Strain was measured at the medial surface of the tibial midshaft with the tibia subjected to 10 N axial compression loading. Each tibia was imaged twice by μ CT (Skyscan 1172, Skyscan, Kontich, Belgium) using a 5 μ m nominal resolution; once with and once without strain gauge. After increasing voxel size to 20 μ m, the μ CT data were filtered using a constrained three-dimensional Gaussian filter to partially suppress the noise in the volumes. The data were binarized using a global threshold of 20% of maximum possible grey value. Image processing was performed using IPL (Scanco Medical, Brüttisellen, Switzerland). The location of the strain gauge with respect to the bone was defined by means of fully automated alignment routines. Micro-FE models (element size of 20 μ m) were created by a direct conversion of bone voxels to linear hexahedral elements. All elements in the μ FE models were given a tissue modulus of 12 GPa [van Lenthe, 2008] and a Poisson ratio of 0.3. The model was fixed at its distal end, and a force of 10 N was applied at the proximal end. The models were solved using ParFE, a dedicated large-scale finite element solver [Arbenz, 2008]. Strain was calculated at the location of the strain gauges.

Results

10 N loading resulted in measured strain between 1163 and 1437 microstrains. The measurements on the same animal were reproducible with 10 % variability. On average, the μ FE models consisted of 2.7 million elements and 3.1 million nodes, respectively. The strains as calculated by the μ FE models correlated highly to the experimentally measured strains ($R^2=0.90$).

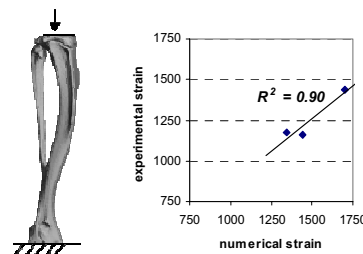


Figure 1: *Experimental vs numerical strain on the medial surface of the tibial midshaft.*

Discussion

We found a very strong correlation between measured and computed strains. Whether this will hold in general remains to be tested, as up to now we only analyzed 3 tibiae. The numerical results overestimated the experimentally measured strain values by an average of 18.9%. One potential reason may be that the soft tissues, which are not included in the μ FE models, reduce the load that is actually transferred to the bone. It may also be relayed to a slight underestimation of the tissue modulus. In conclusion, we have demonstrated that μ FE models can provide accurate estimates of tissue-level strains in mouse tibia when exposed to controlled mechanical loading. Such models can provide quantitative strain data which is necessary to establish relationships between local mechanical stimuli and local tissue response.

Acknowledgements

Computational time was granted by the Swiss National Supercomputing Centre (CSCS).

References

- Arbenz et al, *Int JNumerMethods Eng*, 73:927-947, 2008.
- De Souza et al, *Bone*, 37:810-818, 2005.
- van Lenthe et al, *Bone*, 43:717-723, 2008.

CONSTRUCTION OF A COMPLETE DIGITISED JUVENILE FEMUR FOR USE IN MUSCULOSKELETAL AND FINITE ELEMENT MODELS

D E Lunn, M J Fagan, C A Dobson,
Department of Engineering, University of Hull, UK

Introduction

It is widely accepted that bone adapts to its mechanical usage (Wolff, 1892), with optimization of trabecular architecture with respect to loading. Finite element (FE) modelling of the femur to investigate the relationship between trabecular growth and load patterns has been undertaken by a number of researchers (e.g. Ryan and Krovit, 2006; Qian *et al.*, 2009). However much of the research is based on the adult femur, with the development and structure of the juvenile femur receiving very little attention. The changing modes of locomotion and associated muscle loading that is characteristic of achieving human bipedal gait (e.g. crawling, toddler gait) are important considerations for fully understanding the development of the trabecular architecture. FE modelling of the juvenile femur is particularly challenging due to the fact that the ossification process is not complete until late adolescence, occurring at approximately 22 years (Scheuer and Black, 2004). Prior to this age, the femoral head and trochanters are frequently absent in dry bone specimens due to their original cartilaginous nature, as is evident in Figure 1; but to accurately predict the strain distribution through the bone, the cartilage must be represented in FE models. An additional consideration is the fact that the angulation of the femoral head and neck changes during the development process (Scheuer and Black, 2004). This must also be represented in any musculoskeletal or FE models. The current study uses geometric morphometric (GMM) warping techniques to construct a representative digitised model of the juvenile femur including cartilage, for use in musculoskeletal and FE modelling.

Method

Two cadaveric femur specimens were chosen for analysis from the Scheuer Collection (University of Dundee). These consisted of a juvenile sample (aged approximately 3 years (figure 1d)) where the trochanter and femoral head are disconnected due to absent cartilage, and a fully fused adult femur, (figure 1f). The samples have been μ CT scanned and digitised into volumetric models. To faithfully represent the complete construct of the juvenile sample including connective cartilage, GMM techniques (O'Higgins and Jones, 1998) will be employed using carefully chosen landmarks to warp the adult femur to a size similar to that of the 3 year old specimen. This warped model will be used as a

template to position the digitised models of the 3 separate bony samples comprising the juvenile specimen. Through merging the two models the geometry of the interspersing cartilage can be identified and assigned as a different material for subsequent FE analyses.

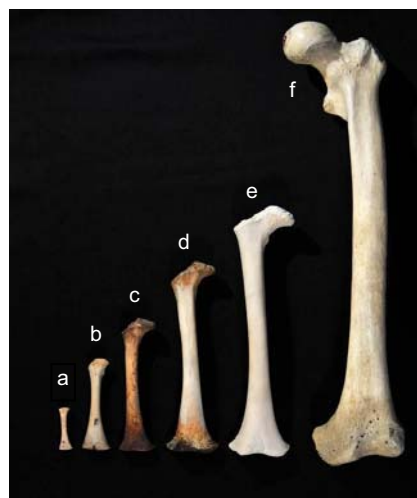


Figure 1: Transformation of a prenatal femur to an adult femur (not to scale). a) 4.6 months in utero; b) 6 months, neonatal; c) 1 year; d) 3-5 years; e) 7 years; f) adult femur.

Results and Discussion

Results from the warping procedure will be presented at the conference, along with potential validation techniques. The method has already been used in a related project on the juvenile pelvis although the femur presents different challenges due to the cartilaginous material forming much of the proximal and distal features of the bone.

It is the intention to use these results to in a musculoskeletal and gait analysis on the juvenile femur, which will be further implemented into a FEA to view the load responses and measure the correlation of strain distribution resulting from the loading due to different age related activities. The resulting strain distributions will be compared with the trabecular distribution during bone growth.

References

- O'Higgins P, *et al* (1998). *J Anat*, **193**: 251-272.
- Qian, J, G *et al* (2009). *Clin Biomech*, **24**: 47-52.
- Ryan, T, M *et al* (2006). *J Human Evol*, **51**: 591-602.
- Scheuer *et al* (2004). *The Juvenile Skeleton*, London: Elsevier.

A VALIDATION OF SUBJECT-SPECIFIC FINITE ELEMENT MODELS OF PROXIMAL FEMUR IN SIDEWAYS FALL CONFIGURATION

Lorenzo Grassi (1), Enrico Schileo (1), Fulvia Taddei (1), Mateusz Juszczak (1,2), Luca Cristofolini (1,2), Marco Viceconti (1)

1. *Laboratorio di Tecnologia Medica, Istituto Ortopedico Rizzoli, Bologna, Italy;*

2. *Engineering Faculty, University of Bologna, Italy*

Introduction

Proximal femur fractures are a severe problem among the elderly, because of their profound influence on patient morbidity, functional capacity and mortality. The majority of clinical studies indicate that sideways falls are a major determinant of proximal femur fractures [Parkkari, 1999].

Subject-specific finite element (FE) models from CT data are a promising tool to non-invasively assess the fracture risk induced by loading on bone segments. This technique has recently proved accurate in predicting experimentally determined strain levels and fracture conditions [Schileo, 2008; Bessho, 2007] under a simulated single-stance loading condition.

While subject-specific FE approaches have been proposed also to simulate sideways falls, a comprehensive validation study against experimental strain measurements is lacking.

The aim of the present study was to validate a subject-specific FE modelling technique against experimentally measured strains and failure properties, exploring the range of admissible sideways fall configurations.

Methods

Four unpaired cadaver femurs showing no deformities were obtained and CT scanned.

Subject-specific finite element models were built from CT data using a validated procedure [Schileo, 2008].

All the femurs were tested non destructively in vitro under four different loading scenarios, aimed at exploring the conditions of femur tilting in the transverse and coronal plane that can happen during a fall to the side (Figure 1a).

Finally, each femur was loaded to fracture in a typical side falling configuration (Figure 1b) [Backman, 1957]. The greater trochanter and the femoral head were supported by dedicated bone cement moulds to prevent local crushing while obtaining finite element reproducible boundary conditions. Fifteen triaxial strain gauges were positioned on each femur and two LVDTs were used to monitor femoral head displacement. Tests were conducted in order to obtain a strain rate higher than $50000\mu\epsilon/s$. During destructive tests, load-displacement curves as well as strain were

acquired at 2kHz to define failure load and strain behaviour; high speed movies (10000fps) were recorded to identify the location of fracture onset.

These data were used to assess the finite element models accuracy in predicting principal strains, fracture load and location.

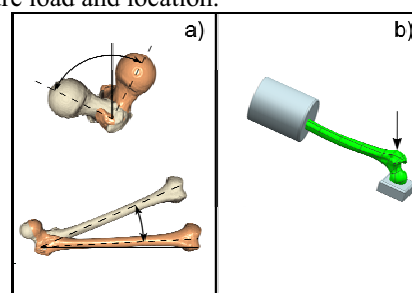


Figure 1: a) loading configurations: the angles spanned in the transverse and coronal plane b) a sketch of the load configuration to failure.

Results and Discussion

Preliminary results showed an acceptable agreement between experimentally measured and FE predicted strains and displacements.

The main limitation of the present work is that only four femoral specimens were used. The small sample size limits the possibility to make a more meaningful statistical analysis.

Another limitation concerns the loading rate applied to the specimens, which is lower with respect to a realistic fall. It should be noted that this difference could be overcome in the simulations applying a scaling factor [Carter, 1976], at least for the elastic tissue response.

Finally, having achieved with this study a validation of the FE models, the influence of other variables (such as the debated issue of muscle actions) on bone strength in case of a fall, could be now investigated through models.

Acknowledgements

This study was partially funded by the EC-funded project VPHOP (Grant #223865)

References

- Backman, S., Acta Radiol Suppl 146:1-166, 1957.
- Bessho, M. et al, J Biomech 40:1745-1753, 2007.
- Carter, D.R., Hayes, W.C., Science 194:1174-1176, 1976.
- Parkkari, J., et al, Calcif Tissue Int 65:183-187, 1999.
- Schileo, E et al, J Biomech 41:2483-2491, 2008.
- Schileo, E. et al, J Biomech 41:356-367, 2008.

Modelling human movement

SENSITIVITY ANALYSIS OF AN ENERGETIC MUSCLE MODEL APPLIED AT WHOLE BODY LEVEL IN RECUMBENT CYCLING.

Maria Cristina Bisi (1), Rita Stagni (1), Gianni Gnudi (1)

1. DEIS, University of Bologna, Italy

Introduction

Models of muscles were developed in order to analyse human movement in terms of motor control [Van Soest 1993] and metabolic energy expenditure [Umberger 2003]. Umberger proposed a phenomenological muscle energy expenditure model that predicts human energy rate consumption over the full activation range and for varying contractile conditions, for use both at single muscle level and whole body level [Umberger 2003].

The accuracy of any modelling approach also depends on the values of the assumed parameters.

A complete musculoskeletal model includes numerous parameters, often taken from literature. Muscle function was found to be strongly task dependent [Scovil 2006]. Sensitivity of energetic muscle models has not been studied yet. The aim of the present work was to further study the sensitivity of muscle model that can describe both mechanics and energetics during recumbent cycling for varying contractile conditions.

Methods

Model sensitivity to changes in muscle-tendon properties was determined using a 2D whole body model of recumbent cycling. The model was represented as a 7-segment mechanical linkage (feet, shanks, thighs and trunk), actuated by 9 muscles per leg. Each muscle-tendon model received neural signals and joint angles as inputs.

Inputs were collected experimentally: one healthy participant [25y, 1.86m, 90kg] performed 3 minute cycling tests on a recumbent cycle-ergometer (Technogym, Italy) at 3 different speeds (50-, 70-, 90rpm) and 3 different power levels (50-, 70-, 90W). Kinematic and EMG (BTS, Milan, Italy) data were acquired. EMG data were collected, rectified, filtered and normalized to Maximal Voluntary Contraction.

Musculoskeletal geometry described the relationship between joint angles and muscle-tendon lengths [Gerritsen 1998]. Muscle activation dynamics governed the transformation from the neural signal to a measure of muscle activation [He 1991]. Muscle contraction model was divided in a mechanical part [Van Soest 1993] and an energy expenditure part [Umberger 2003].

Soleus, gastrocnemius, vasti, gluteus and medial hamstrings were selected for the sensitivity analyses: they all play an important role in recumbent cycling.

We quantified the effect of small changes in muscle properties on model estimates of muscle forces, muscle energy expenditure rates and joint moments. Values of tendon rest length (*Lse slack*), muscle maximal force (*Fmax*) and percentage of fast twitch fibers (*%FT fibers*) were perturbed in the model with increments of 2.5% of the nominal value of the parameter, ranging from 2.5% to 10%.

The sensitivity of model outputs to changes in muscle properties was quantified by computing an integrated sensitivity ratio (ISR) [Redl 2007].

Results

Overall muscle force and joint moment estimates were more sensitive to changes in tendon slack length than to maximal muscle isometric force. Energy rate consumption was more sensitive to changes in *Lse slack* for soleus and gastrocnemius than in other cases. Results are shown in Table 1.

		vasti	soleus	gluteus	gastro	M. Ham
<i>Fmax</i>	Force	0.58	0.54	0.39	0.59	0.34
	Moment	0.58	0.50	0.36	0.30	0.33
	Energy	0.13	0.09	0.04	0.07	0.02
<i>Lslack</i>	Force	2.37	21.02	1.04	25.32	1.65
	Moment	2.11	5.93	0.92	8.28	1.55
	Energy	0.44	2.05	0.13	1.76	0.25
<i>%FT fibres</i>	Energy	0.25	0.27	0.55	0.43	0.39

Table 1: Highest ISR for each muscle and each changed parameter.

Discussion

Energetic model was found to be less sensitive to changes in tendon slack length, maximal isometric muscle force and percentage of fast twitch fibres than mechanical muscle model. Tendon slack length was found to be the most critical parameter in recumbent cycling for both energetic and mechanical model.

References

- Gerritsen KGM., Motor Control, 2, 206-220, 1998.
- He J. et al, IEEE trans auto control, 36(3):322-332, 1991.
- Redl C. et al, Hum Mov Sci, 26 306-319, 2007.
- Umberger BR., Comput Methods Biomech Biomed Engin, 6(2):99-111, 2003.
- Van Soest AJ et al, Biol Cybern, 69(3):195-204, 2003.

QUANTITATIVE EVALUATION OF GAIT ABNORMALITIES IN TYPE 2 DIABETIC PATIENTS

Valentina Agostini (1), Marco Knaflitz (1), Riccardo De Luca (2), Luciano Corgiat Mansin (2)

1. Department of Electronics, Politecnico di Torino, Italy; 2. Department of Metabolic Diseases and Diabetology, Ospedale Oftalmico di Torino, Italy

Introduction

Patients with diabetes show a higher fall risk than healthy controls. Diabetes is associated with gait alterations in older adults, even in absence of concomitant peripheral neuropathies, but limited information regarding potential explanatory factors exists [Allet, 2008][Brach, 2008].

The practice of regular physical activity is the usual recommendation of clinicians to these patients and several procedures are available for assessing the benefits of physical activity from a metabolic point of view [Boulé, 2001][Knowler, 2002]. However, there is a lack of operator-independent procedures able to assess the benefits of the physical activity in terms of improved walking ability.

We quantitatively evaluated the gait performances of a population of 27 patients suffering from type 2 diabetes. Patients were enrolled in a program of light intensity physical activity that committed themselves twice a week for four months. They were tested before the start and at the end of the program. A Gait Abnormality (GA) score - in baseline conditions and after the program completion - was assigned to each patient using statistical gait analysis in conjunction with a fuzzy classifier.

Methods

Three foot-switches (under the heel, the first and the fifth metatarsal heads) and a knee goniometer were mounted on each lower limb of the patient. A first trial walk lasting 1 minute was carried out to allow patients to get acquainted with the instrumentation. Then, they were asked to walk continuously at their natural pace for 2.5 minutes, back and forth along a straight track of 18 m, thus collecting more than a hundred of consecutive steps.

We used the Step32 system (DemItalia s.r.l., Italy) to acquire the signals and perform statistical gait analysis. Step32 automatically segments each gait cycle, rejects outliers, and classifies the cycle as “typical” - if it shows the usual sequence of phases (Heel strike – Flat foot contact – Push off – Swing) or as “atypical” - if there is a different sequence of gait phases. Average values of the duration of the aforementioned gait phases were obtained, along

with cadence and single and double-support percent duration. The degree of dispersion of the knee-joint angle curves (in the sagittal plane) gives information on the stability of the knee in the various gait phases. The knee joint angular velocity at initial contact was also evaluated.

The described parameters were used as inputs to build the membership functions of a fuzzy classifier that grades the gait abnormalities of the patients.

Results and Discussion

More than a half of patients (15 over 27) reduced the GA score on the left leg after the completion of the physical activity program, while one third of them (9 over 27) reduced it on the right.

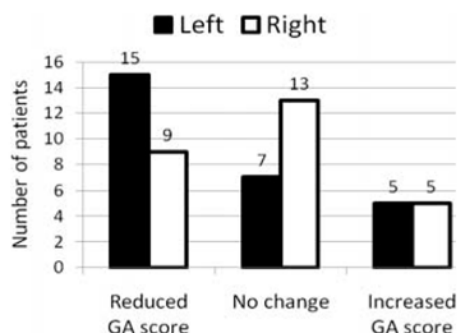


Figure 1: Changes of the Gait Abnormality (GA) score after the completion of the physical activity program.

These results demonstrate that even a light intensity activity program can be effective in improving the gait quality of diabetic patients. Therefore, it is possible to hypothesize that their falling propensity is consequently reduced. In conclusion, we believe that statistical gait analysis is a powerful tool to document the outcome of rehabilitation programs in patients suffering from gait disorders.

References

- Allet L et al, Diabetes Metab Res Rev, 24(3):173-191, 2008.
- Boulé NG et al, JAMA, 286:1218-1227, 2001.
- Brach JS et al, Phys Ther, 88(11):1365-1374, 2008.
- Knowler WC et al, N Engl J Med, 346:393-403, 2002.

3D JOINTS KINEMATICS WITH FLUOROSCOPY: ALGORITHM OPTIMIZATION

Luca Tersì (1), Rita Stagni (1), Silvia Fantozzi (1), Angelo Cappello (1)

1. Department of Electronics, Computer Science and Systems - University of Bologna, Italy

Introduction

A reliable knowledge of *in-vivo* joints kinematics in physiological conditions is fundamental in the clinical field. 3D fluoroscopy theoretically permits to achieve a millimetre/degree accuracy level in joint motion analysis. It has been widely used and applied to quantify the *in-vivo* kinematics of replaced [Zuffi, 1999] and intact joints such as knee, ankle or hip joints. To estimate the 6 degrees of freedom (DoF) pose of a segment, an iterative minimization algorithm is typically used. Different metrics can be used, but the process is highly dependent on the geometry of the bony segment analyzed and local minima could severely interfere with the final accuracy of the process. In the present study, thus, the convergence property of the minimization algorithm was analysed by means of computer simulations, in order to optimize the pose estimation in term of accuracy and computational weight with a focus on the upper limb.

Methods

The alignment algorithm implemented was based on 3D surface models and adaptive distance maps (DM) [Lavallée, 1995]. The fluoroscope was represented by a perspective projection model where the x and y axis were parallel to the image plane and z -axis perpendicular. The pose is then estimated minimizing with a Levenberg-Marquardt algorithm the euclidean root mean square distance (RMSD) between a surface model and a beam of lines connecting the X-ray source and the edge of the bone extracted in the projected image.

A high resolution model of the humerus was downloaded from the official site of the European project VAKHUM (contract #IST-1999-10954 <http://www.ulb.ac.be/project/vakhum/index.html>) and used in the experiments performed.

The model was placed in a reference pose (parallel to xy -plane, lateral view) and a flat shaded projection was generated. The complete contour was extracted and then used for the alignment. The DM had a resolution of 0.5 mm. The initial conditions for the minimization were in the domain around the projection pose, varying the translations (T) and rotations (Θ) between -10, -7, -3, 0, 3, 7, 10 mm or deg, resulting in 117649 permutations. The RMSD is a parabolic function of each DoF, the coefficient of the quadratic term (normalized convexity index, nci) of the fitting parabola has been calculated and represents an index of the

sensitivity of the method to the minimization of the relevant DoF. The convergence rate (cr) was calculated: the convergence was defined as a binary variable equal to 1 if the final deviations of the estimated DoF (all excepted T_z) were lower than a threshold equal to 0.5 or 1 mm or deg. The alignment was repeated on a random subset of 1000 starting poses (Table 1). The DM resolution was varied to 1 mm and the DoF were minimized all at the same time (*complete*) or in order of sensitivity (*sequential*).

Results

The algorithm could easily minimize the RMSD versus the single DoF for T_x , T_y , and Θ_z ($nci=2.8$, 0.6, 5.8 respectively), while the effect of Θ_x and Θ_y is influenced by the geometry of the bone ($nci=0.01$). Major problem affects T_z ($nci<0.001$): the distribution of the estimated T_z has a large deviation (75° percentile=6 mm) being less than 1mm or deg for the other DoF. The percentages of convergence are reported in Table 1.

	DM Res	type	cr _{th=0.5}	cr _{th=1}
a	0.5 mm	complete	72.9%	78.3%
b	1.0 mm	complete	61.6%	73.3%
c	1.0 mm	sequential	86.6%	94.3%
d	0.5 mm	sequential	95.3%	96.2%

Table 1: convergence rate with different thresholds.

Discussion

On long bones with cylindrical symmetries, the algorithm reacts to the alignment of the various DoF with different sensitivity. When the initial conditions are too far from the reference pose, if not conditioned, the pure algorithm can lead to false poses (low convergence rate). With sequential alignments, instead, the DoF with larger convergence domain are aligned in a first step, while the more critical DoF are minimized only when closed to reference pose. The convergence rate achieved is then excellent (up to 96%). Other features extracted from the contours might lead to start the minimization process always inside the convergence domain improving the reliability of the technique. A DM resolution of 1mm, with a sequential alignment, could be a good compromise when high computing performances are needed.

References

- Lavallée, S. et al. IEEE TPAMI 17(4): 378-390, 1995.
Zuffi, S. et al. IEEE TransMedImaging 18:981-991, 1999

AN EMG-DRIVEN MUSCULOSKELETAL MODELING APPROACH TO ESTIMATE ARTICULAR LOADING AT THE KNEE

Kurt Manal(1,2), Deepak Kumar (3), Katherine Rudolph (1,3), Thomas S. Buchanan (1,2)

1. Center for Biomedical Engineering Research, University of Delaware, USA

2. Department of Mechanical Engineering, University of Delaware, USA

3. Dept. of Physical Therapy, University of Delaware, USA

Introduction

The knee adduction moment has long been used as an indicator of knee joint loading. The magnitude of the moment has been shown to correlate with the severity and progression of knee osteoarthritis [Hurwitz, 2002], and as such has become an outcome measure of great interest to those studying gait mechanics. The relationship between the knee moment and joint loading is not straightforward, particularly when agonist/antagonist muscles are co-activated. Co-activation is believed to be a neuromuscular strategy to help stabilize the joint and is used by individuals with knee osteoarthritis [Schmitt, 2008]. Computational methods which account for subject specific neuromuscular activation patterns are important when studying articular loading. In this paper we present results of an EMG-driven modeling approach to predict articular loading for patients with different muscle activation patterns.

Methods

An EMG-driven musculoskeletal model was used to compute muscle forces at the knee during the stance phase of gait [Buchanan, 2006]. The muscle forces were used as inputs to a moment balancing algorithm to compute the contact forces necessary to balance the internal and external forces at the joint. Three adult male subjects participated in this study: one healthy, one with medial knee osteoarthritis (OA) and one with lateral OA. Gait kinematics and ground reaction forces were sampled using traditional methods (ie., video cameras and force platform). In addition, muscle activity was recorded from 3 of the 4 quadriceps, all 4 hamstrings and both gastrocnemii. Kinematic data were sampled at 120 Hz and EMG at 1080 Hz.

Results

Peak loads for the healthy subject and the individual with lateral OA approached 5 BW's, while smaller loads were noted for the subject with medial OA. The smaller values during late stance were associated with lateral compartment unloading during this time.

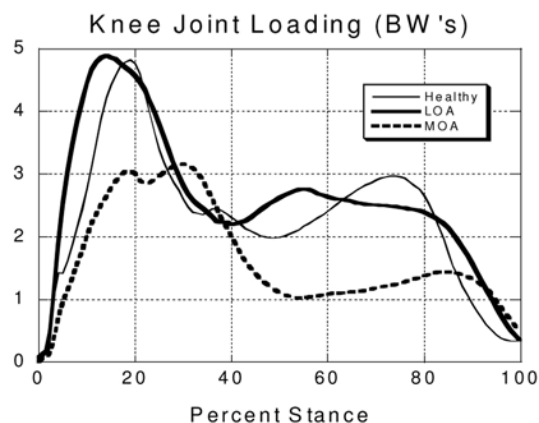


Figure 1: Total condylar loading during stance reported in bodyweights (BW's). LOA & MOA represent lateral & medial compartment OA. Each curve represents the average of 3 trials.

Discussion

The EMG-driven model predicted differential loading between the subjects with medial and lateral OA. Assuming joint moments of comparable magnitude, a smaller articular loading implies the muscles are supporting a greater proportion of the frontal plane moment. Quadriceps strength has been implicated as an important predictor of function in patients with medial compartment OA [Fitzgerald, 2004]. The subject with medial OA appears to have used more of a muscle balancing strategy compared to the individual with lateral OA. Additional work is underway to evaluate the efficacy of this modeling approach for investigating healthy and pathological gait.

Acknowledgements

Supported by NIH R01-AR48212 & P20-RR16458.

References

- Buchanan et al., J Appl Biomech. 20(4): 367-395, 2004.
- Fitzgerald et al., Arthr Care Res. 51(10): 40-48, 2004.
- Hurwitz et al., J Orthop Res. 20(1): 101-7, 2002.
- Schmitt et al., J Orthop Res. 26(9): 1180-5, 2008.

New numerical methods and tools

MULTISCALE MODELING OF TISSUE PERFUSION USING HOMOGENIZATION OF DUAL POROUS LAYERED MEDIA

Eduard Rohan, Vladimír Lukeš, Robert Cimrman

*Department of Mechanics, Faculty of Applied Sciences,
University of West Bohemia in Pilsen, Univerzitní 22, 30614 Pilsen, Czech Republic*

Introduction

Tracing the blood flow (BF) in tissues is important feature of the medical diagnosis, as it is related clearly to the transport of oxygen, nutrients and other chemicals. A standard method of the BF evaluation in brain is based on the CT or MRI dynamic investigation of the contrast fluid density; for reconstruction of such an experiment a mathematical model is needed which describes the transition times in the porous structure and, thus, makes the relationship between the measured contrast (fluid flow) input, output and the local density. We suggest a new approach which is based on a more refined modelling of the tissue microstructure; this should present an alternative to the ill-conditioned deconvolution technique [Koh, 2006].

Methods

We consider steady fluid diffusion in hierarchically arranged double porous media constituted by transversely periodic layers. In each layer, see Fig. 1, the reference periodic cell is composed of several compartments comprising the dual porous matrix, featured by permeability decreasing with the scale parameter, and several disconnected channels where the permeability is scale independent. Homogenization of the steady Darcy flow in such layer was done by the asymptotic analysis, using the periodic unfolding method [Griso, 2007].

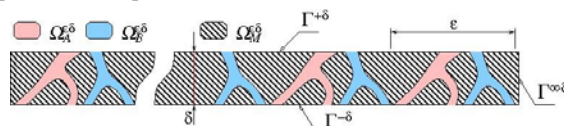


Figure 1: Layer decomposition according to the dual porous matrix (grey) and high conductive vessels (blue and red).

Results

The homogenized model of the single perfused layer transforms the 3D strongly heterogeneous medium (a thick layer) into 2D problem on the layer mid-surface. There the homogenized parallel flows in different compartments and the fluid redistributions are described, being represented at each point of the mid-surface by the pressure and

the overall drainage flux. Special interface conditions make possible to assembly the multi-layer model of the perfusion and, thus, to account for a complex hierarchical arrangement of the perfusion tree.

The limit model involves the homogenized permeabilities associated with the channels and the transmission and drainage coefficients associated with the mass redistribution between the microstructural compartments [Rohan,2009]. All these coefficients are evaluated using characteristic microstructure responses computed for the specific computational cells, cf. Fig. 2. Due to the layered organization of the medium (brain tissue), the 3D volume of a given heterogeneous body can be replaced by a finite number of 2D problems, each-one describing the homogenized fluid redistribution in the particular layer.

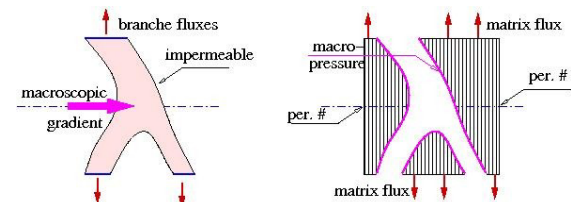


Figure 2: Scheme illustrating the microscopic problems

Discussion

The model is implemented in our FE code. The numerical examples will be discussed. The model will be extended by the convected diffusion of the tracer, which will allow to simulate the CT perfusion test at the multiscale problem.

Acknowledgements

The research supported by projects GACR 106/09/0740 and MSM 4977751303 of the Czech Republic.

References

- Griso G., Rohan, E. Ricerche di Mat., 56:161-188, 2007.
- Koh, T.S. et al. NeuroImage, 33:570-579, 2006.
- Rohan, E. Homogenization of the perfusion problem in a layered double-porous medium with hierarchical structure. Submitted, 2009.
- Showalter et al. J. Math. An. Appl. 295:191-210, 2004.

CFD SIMULATIONS TO PREDICT THE PERMEABILITY OF BIOLOGICAL AND SYNTHETIC CELLULAR MATERIALS

Giancarlo Pennati (1), Elena Bianchi (1), Margherita Cioffi (1), Davide Franco (1), Ilaria Chiapparini (1), Rossella Stoico (2), Simone Tassani (2,3), Fabio Baruffaldi (2)

1. Laboratory of Biological Structure Mechanics – LaBS, Dept. of Structural Engineering, Politecnico di Milano, Italy; 2. Laboratorio di Tecnologia Medica, Istituti Ortopedici Rizzoli, Bologna, Italy; 3. Engineering Faculty, University of Bologna, Italy

Introduction

Several biological (e.g. trabecular bone) and synthetic materials designed as tissue engineering scaffolds (e.g. metallic foams) show a porous cellular structure. Their structural properties have been well modelled [Gibson, 2005], whereas the flow behaviour has not been deeply investigated.

The permeability is an important property describing how fluids flow through cellular materials: for biological tissues and tissue-engineered scaffolds it plays a significant role in the nutrient and waste transport within the structure. Moreover, the efficacy of some mini-invasive procedures based on bone cement infiltration for the treatment of osteoporotic fractures depends on bone permeability properties [Baroud 2006].

Nevertheless, the experimental evaluation of the permeability properties is not always achievable since requires a specimen of the porous material.

In the present study a computational approach for modelling permeability of cellular solids, based on 3-D imaging coupled with CFD simulation, has been developed and validated with experiments.

Methods

Different cellular solids were investigated including a metallic foam (Reticulated Vitreous Carbon, RVC), femoral (both head FH and condyles FC) and vertebral (V) bovine cancellous bones.

The adopted approach to predict the velocity-pressure relationship, $v = v(\Delta P)$, of the materials consists of: 1) analysis of the microstructural features of the cellular solid (by using optical microscope or μ CT); 2) definition of a proper 3D periodic unit cell (tetrakaidecahedron with rods and plates); 3) CFD simulations of perfusion through a regular cellular material model with Newtonian (water, water and saccharose) and non-Newtonian fluids (two different liquid soaps).

The permeability values predicted by using the regular cellular model were compared with the corresponding values: i) calculated simulating the flow within some μ CT-based realistic models, ii) measured during experimental perfusions.

Results

The investigated materials showed wide ranges for microstructural features and permeability: porosity of 75-95%, trabecular diameters from 142 to 196 μm and permeability values with the tested fluids from 0.07 to 96 $\text{m}^4\text{N}^{-1}\text{s}^{-1}$.

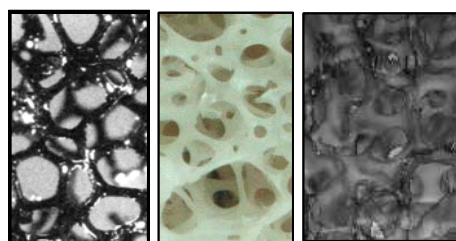


Figure 1: Microstructure analysis

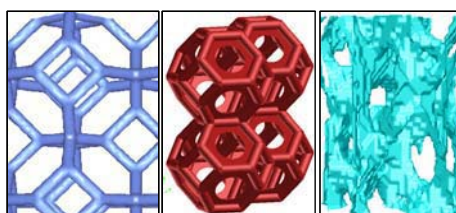


Figure 2: Computational models

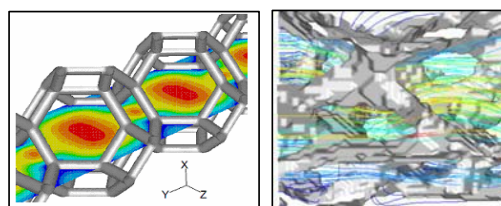


Figure 3: Computational results (velocity maps)

Discussion

The CFD results based on simplified regular cellular models allowed us to correctly predict actual values of permeability (errors always lower than 35%), taking into account the observed wide range (three magnitude orders) and the various microstructures (rod and plates).

The μ CT-based realistic models gave similar results but required much high computational times.

References

- Baroud G. et al, Spine 31, 22:2562-2568, 2006.
- Gibson, J Biomech, 38:377-399,2005.

MICROTUBULE MECHANICAL PROPERTIES BY MEANS OF NORMAL MODE ANALYSIS

Marco A. Deriu (1), Monica Soncini (2),
Alberto Redaelli (2), Franco M. Montecchi (1)

1. Mechanics Department, Politecnico di Torino, Italy; 2. Bioengineering Department, Politecnico di Milano, Italy

Introduction

The cellular microtubules (MTs) are hollow cylinder-shaped biopolymers of the cytoskeleton. Due to their unique mechanical properties they play important roles in regulating the cytoskeleton dynamic response in several stress conditions (e.g. cell compression, stretching and mitosis).

Despite the experimental efforts done to assess the mechanical properties of MTs, this topic is still debated since the experimental measurements cannot provide the desired atomic resolution needed for a thorough understanding of the MTs mechanical behaviour. Computational molecular modelling allows the investigation of the MT mechanical properties at the molecular scale.

In this work a Coarse Grain (CG) model of the whole MT is developed by means of Normal Mode Analysis (NMA), in order to characterize MT properties such as the bending stiffness, Young's modulus and persistence length on the basis of MT atomistic details.

Methods

Starting from the atomic structure of the tubulin dimer (1TUB.pdb) properly refined by means of molecular dynamics simulations, the MT (Fig.1a) was modelled as an Elastic Network (EN).

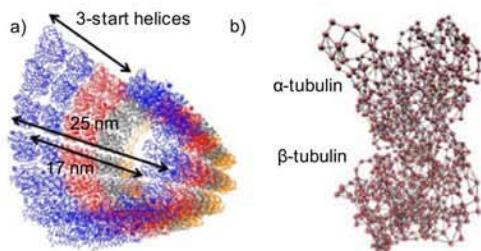


Figure 1. MT atomic structure (a). EN model (b).

In the EN model each tubulin residue is represented by a node in the position of the carbon C_{α} (Fig.1b). Nodes are connected if they are closer than a cut-off distance of 1.2 nm. Several MT ENs were modelled with different length (80-160 nm). Due to the huge number of atoms C_{α} in each MT EN model (more than 100,000 atoms), the Hessian matrix of the EN potential energy function (in the harmonic approximation) was inverted following the block normal mode approach [Tama, 2000]. Mechanical

properties were obtained directly from the resulting eigenvalues and eigenvectors applying the theory of elastic beams [Adamovich, 2008].

Results

Results in terms of Young's modulus as function of the MT length are shown in Figure 2 (right).

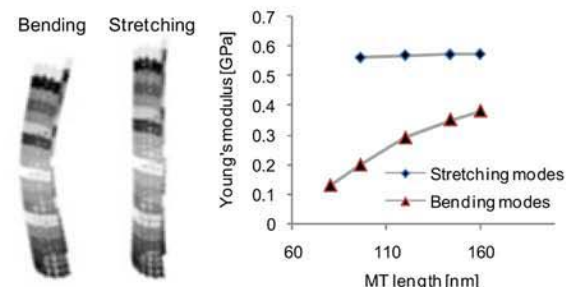


Figure 2. Young's modulus vs. MT length as calculated from the 1st stretching mode (diamonds) or from the 1st bending mode (triangles).

Discussion

From stretching modes for MT lengths up to 160 nm we found a Young's modulus of about 0.6 GPa non-length dependent (Fig.2 - diamonds) and close to the experimental data (0.1-2.5 GPa) obtained by observing long MTs fluctuating (24-60 μ m) under the thermal motion [Howard, 2001]. The Young's modulus calculated by bending modes varied with the length in a range 0.13-0.35 GPa (Fig. 2 triangles). The Young's modulus dependence on the MT length shows up the MT as a strongly inhomogeneous and anisotropic structure in which the lateral interaction among monomers, much weaker than the longitudinal ones, let adjacent protofilaments slide during the bending of short MTs. Thus the Young's modulus calculation under the hypothesis of isotropic and homogeneous material (i.e. from MT bending) is reliable just for very long MTs where the high number of lateral interactions among protofilaments avoids large shear displacements and the Young's modulus dominates the elastic behaviour.

References

- Howard, J., 2001, Sinauer, Sunderland.
- Tama et al. *Protein Struct Funct Genet*, 41:1-7, 2000.
- Adamovic et al., *Biophys. J.*, 94:3779-3789, 2008.

SIMULATION OF BIOMATERIAL FLOW THROUGH POROUS MEDIA

René P. Widmer (1), Stephen J. Ferguson, PhD (1)

1. Institute for Surgical Technology and Biomechanics, University of Bern, Bern, Switzerland

Introduction

In vertebroplasty, bone cement is injected into fractured and osteoporotic vertebrae for stabilization. Three categories of factors that influence cement flow in the vertebral body can be identified: (i) bone and fracture-related parameters, (ii) cement properties, and (iii) injection methods. The most common bone cement used today is polymethylmethacrylate (PMMA). With PMMA, the main characterizing parameter is viscosity.

Flow in porous trabecular bone can be described by a modified version of Darcy's law relating the Darcy flux q to the pressure gradient ∇P , the intrinsic permeability K and the viscosity μ :

$$q = \frac{K}{\mu} \nabla P \quad (1)$$

During the injection process, bone marrow, fat and blood are substituted by PMMA, i.e. a biofluid with viscosity μ_1 is replaced by a biomaterial with viscosity μ_2 , μ_2 depending on time and further parameters.

In this work a computational model has been developed and implemented to simulate the flow of two immiscible fluids in a porous media. A finite element approach has been chosen to numerically solve the PDE given in Eq. (1). In a first step, simulations were performed of well-controlled experiments conducted on an artificial vertebra model, in which PMMA was injected into a porous aluminium foam filled with a simulated biofluid (Fig. 1).

Methods

The development of the model involved the following steps: 1) Derivation of the governing equations and their weak formulations; 2) Development of a dedicated fluid volume tracking algorithm with a mixed boundary representation; 3) Implementation of the computational model in the open source finite element framework *libMesh* [Kirk, 2006]; 4) Simulation setup, preparation and meshing of the artificial vertebra using a regular, three dimensional mesh; 5) Model parameter assignment: (i) viscosity of PMMA was described using a power law capturing its rheological properties, (ii) butter filling the interstitial space of the porous aluminium foam structure (mimicking the biofluid) was modelled as a Newtonian fluid; 6) Computational simulation of the cement injection

process according to the protocol of [Loeffel, 2008].

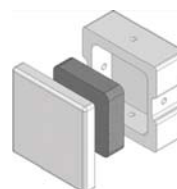


Figure 1: Injection experiments and simulations are based on an artificial vertebra model.

Results

Pressure curves and spreading patterns (Fig. 2) arising from the proposed computational model matched the experimental data published by [Loeffel, 2008], validating the developed methodology. The model demonstrated high numerical stability and efficiency.

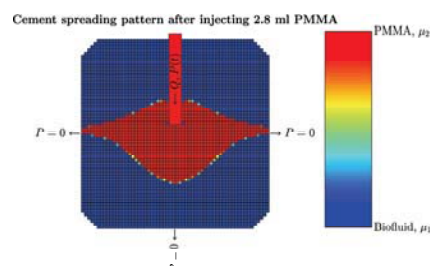


Figure 2: Representative cement spreading pattern obtained from the injection simulation ($\mu_2 \ll \mu_1$).

Discussion

The presented computational model establishes the foundation for a platform to study injection strategies and evaluate contributions of several procedural parameters. Ongoing work involves consideration of morphological bone properties for the region-specific anisotropic permeability calculation.

Acknowledgements

Support from the European Commission is acknowledged (Project FP7-ICT-223865-VPHOP).

References

- Kirk B. et al, Engineering with Computers, 22:237–254, 2006.
- Loeffel M. et al, Spine, 33:1352–1359, 2008.

SIMULATION OF MICROCIRCULATORY DISORDER BY MALARIAL INFECTION USING A PARTICLE METHOD

Takami Yamaguchi (1), Hitoshi Kondo(2), Yohsuke Imai(2), Takuji Ishikawa(2)

1. Dept. Biomedical Engineering, School of Biomedical Engineering; 2. Dept. Bioengineering and Robotics, School of Engineering, Tohoku University, Japan

Introduction

Malaria is one of the oldest and most serious infectious diseases on earth. It is reported that there are 500 million patients with 2 million deaths arising from malaria infection. When a parasite (*plasmodium*) invades and matures inside a red blood cell (RBC), the infected RBC (IRBC) becomes stiffer and cytoadherent. These changes are postulated to link to microvascular blockage. We simulated malarial microvascular blood flow disturbances by using a new particle method of biological solid-fluid interaction analysis specially developed for the analysis of malaria infection. Particle based spatial discretization and the sub time step time integration could provide us stable computations for the micro scale blood flow involving the interaction with many cells. We performed numerical simulation of stretching of infected red blood cells and results agreed well with experimental results. Our model successfully simulated flow of infected red blood cells into narrow channels.

Methods

All the components in the flow field, including plasma, RBC cellular membrane, and parasites are represented by particles. Fluid variables were calculated at the computational point and it was moved by the calculated advection velocity every time step. In contrast to mesh methods, the particle method does not require any computational meshes and the computation is stable even when many cells interacting with each other. In the particle method, the non-slip condition on the membrane is directly imposed by using the position and velocity of membrane particles. We use moving particle semi-implicit (MPS) method [Koshizuka, 1996] for solving Navier Stokes equations. In the MPS method, differential operators in the governing equations are approximated using the weight function, for example,

$$\nabla \phi_i = \frac{d}{n^0} \sum_{j \neq i} \frac{\phi_j - \phi_i}{|\mathbf{r}_{ij}|^2} \mathbf{r}_{ij} w(|\mathbf{r}_{ij}|), \quad (1)$$

$$\nabla^2 \phi_i = \frac{2d}{\lambda n^0} \sum_{j \neq i} (\phi_j - \phi_i) w(|\mathbf{r}_{ij}|), \quad (2)$$

where ϕ is a fluid variable, d is the space dimension number, n^0 is the reference particle number density, λ is the constant, \mathbf{r} is the position of particle, $\mathbf{r}_{ij} = \mathbf{r}_j - \mathbf{r}_i$, and w is the weight function.

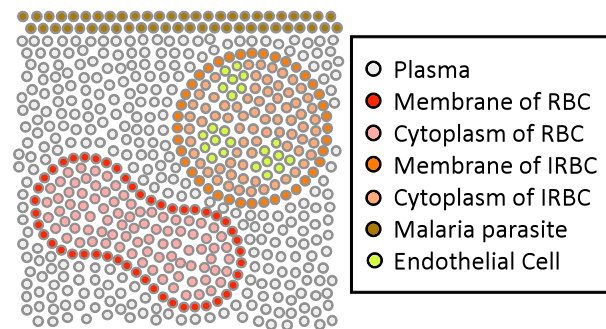


Fig. 1. Scheme of free mesh particle model of blood. All the components of blood are represented by finite number of particles (computational points). Velocity and pressure are calculated at the position of each particle and it is moved by the calculated advection velocity every time step.

Results and Discussion

We could build a numerical model of three-dimensional hemodynamics arising from malaria infection [Kondo, 2009].

To validate our model, we examined stretching of IRBCs. In the three-dimensional computational domain, we put an IRBC at initial time step. Then we stretch the IRBC horizontally with a stretching force. The governing equations are time-integrated until the axial and transverse diameters are well converged. By adjusting a small number of parameters, the numerical results agreed well with the reported experimental results [Suresh, 2005]. Our model successfully simulated flow of IRBCs into narrow channels as well. Particle based spatial discretization and the sub time step time integration can provide us stable computations for the micro scale blood flow involving the interaction with many cells.

References

- Koshizuka et al, *Nucl Sci Eng* 123:421-434, 1996.
- Kondo et al, *Ann Biomed Eng*, in press
- Suresh et al, *Acta Biomater* 1:15-30, 2005.

FINITE ELEMENT SIMULATION OF THE HUMAN TRACHEA IN HEALTHY AND PATHOLOGIC SITUATIONS

M. DOBLARE(1), A. PEREZ DEL PALOMAR(1), O. TRABELSI(1), M. MALVE(1), J.L. VILLALOBOS(2)

1. *Group of Structural Mechanics and Material Modelling (GEMM). Aragon Institute of Engineering Research. CIBER-BBN (ICS), Spain;*
2. *Department of thoracic surgery. Virgen del Rocio Sevilla, Spain*

Introduction

Human trachea can be affected by several disorders, stenosis, congenital malformations, cancer. The consequence of these disorders is the closing of the airways and therefore, the reconstruction of the airway has to be performed using endotracheal prostheses (Huang 2001). One of the most challenging aspects in thoracic surgery is the prediction of damage to the tracheal walls due to the implation of these prostheses. In this study a complete finite element model of the trachea has been developed. Different physiological conditions have been incorporated and the influence of the implantation of a prostheses has been analyzed.

Methods

The geometry of the trachea has been obtained from CT of a healthy man. The segmentation of the DICOM files was made using MIMICS, and the mesh using PATRAN. A fluid structure interaction approach was used to analyze the deformation of the wall when the air moves inside the trachea. A hexahedral-based grid for the trachea walls and a tetrahedral-based mesh for the fluid were used to perform the simulations with ADINA (Figure 1).

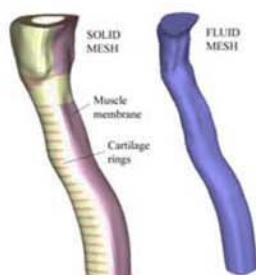


Figure 1: Finite element meshes of the tracheal walls and the fluid (air).

Samples of cartilage and muscle were dissected from human tracheas for histology and mechanical analysis procedures. The histology revealed that in the cartilage rings, the collagen fibers run randomly, therefore an isotropic material was use for them. However, for the muscular membrane the strain energy function proposed by Holzapfel was used since two othogonal family of collagen fibers

were found. Fluoroscopic images were used to build the swallowing movement. For the different ventilation conditions, the simulation of breathing and coughing was made. Finally, an endotracheal prostheses was introduced in order to estimate the stresses that may appear in the tracheal wall.

Results

The stresses and deformations for the different analyzed movements were computed. It was obtained that the most dangerous movement was the swallowing, because the trachea suffered large deformations and stresses. It was, in this case, where the highest stresses were obtained when implanting an endotracheal prostheses (Figure 2).

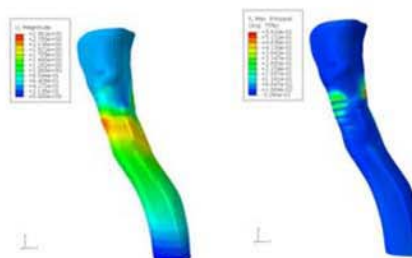


Figure 2: Displacement and maximum principal stresses in the trachea with a prostheses.

Discussion

The trachea is able to adapt itself to regulate the pressure during the different ventilation situations such as breathing or coughing. However, the most dangeorus movement for the thachea, specially when there is a prostheses is swallowing. In this case, it was obtained that the most loaded zones of the trachea are related with the clinically seen granulomas (Cosano et al, 2005), and therefore, this can be a usefull tool to predict damage to the tracheal wall and to design better prostheses.

Acknowledgements

This project was funded by Carlos III Health Institute, Spanish Ministry of Science and Innovation.

References

- Huang, *Ann Thorac Cardiovasc Surg*, 7(4):192-6, 2001.
 Cosano et al, *Arch Bronconeumol*, 41(6):322-7., 2005

Cardiovascular system - heart

TOOLS TO UNDERSTAND THE PUMPING MECHANISM OF EMBRYONIC HEARTS

Frédéric Maes (1,4), Francis Deboeverie (2), Bill Chaudhry (3), Peter Van Ransbeeck (1), Pascal Verdonck (4)

1. University College Ghent, Biomechanics Research Group, Belgium;
2. University College Ghent, TELIN, Belgium
3. Newcastle University, Institute of Human Genetics, UK;
4. Gent University, IBiTech, Belgium

Introduction

Congenital heart defects remain the most common birth defect in humans occurring in almost 1% of live births. The high prevalence of cardiac malformations can be partly attributed to the limited knowledge regarding the embryonic roots of cardiogenesis (Forouhar et al. 2006). The majority of the defects are believed to be influenced by both genetic patterning and mechanical stimuli such as the shear stress exerted by the blood flow on the developing heart (Hove et al. 2003).

The major cause of wall shear stress is the pumping of the heart itself. Our aim is to reveal the mechanism behind the intracardiac bloodflow in order to provide more insight in cardiac development.

Methods & Results

Using transmission light microscopy in combination with high speed image recording modalities we succeeded in mapping hearts of zebrafish embryo's, a model frequently used in developmental cardiology (Figure 1).

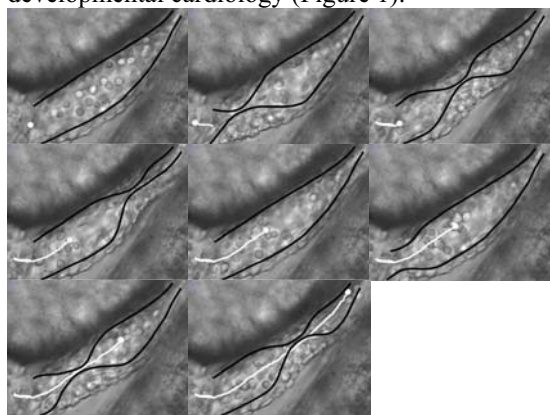


Figure 1: Image sequence with a time interval of 150 ms showing a track of one blood cell of a 30 hours post fertilization zebrafish embryo. The track is colored white, the heart wall is colored black.

We developed an automated algorithm based on pattern recognition to derive the cardiac output by tracking the motion of aortic blood cells in image sequences. Similar techniques are in current

development to automatically derive the motion of the cardiac wall.

Trying to understand the underlying players in the cardiac wall motion we used 2,3-butanedione 2-monoxime (BDM). This drug causes, in relative low doses, a reduction in cardiac output without affecting the number of heart beats per minute (Figure 2). This finding enable us to investigate the pumping mechanism by comparing the wall mechanics of a normal heart (control) with the wall mechanics of a heart with reduced efficiency (BDM 5mmol).

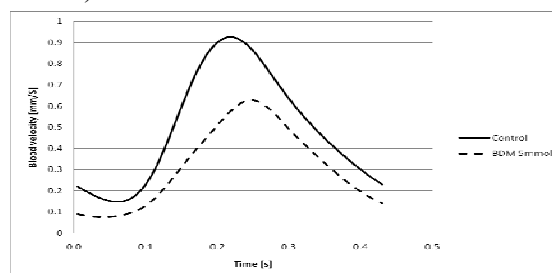


Figure 2: Graph showing the instantaneous aortic blood velocity of a zebrafish embryo (30 hours post fertilization)

Discussion & Conclusion

Microscopic observation of blood flow and wall motion in the embryonic heart is feasible, and will provide the necessary input for further modelling studies. We will use CFD (computational flow dynamics) to provide more detailed information on flow velocity distribution and wall motion mechanics. Modelling and follow up of these embryo's should enhance our insight into the role of mechanical stimuli in congenital heart defects.

Acknowledgements

The authors wish to acknowledge Sara Assecondi for her support in the algorithm development.

References

- Hove, J.R., et al., Nature, 421(6919): 172-177, 2003.
 Forouhar, A.S., et al., Science, 312(5774): p. 751-753, 2006.

NUMERIC INTEGRATED APPROACH FOR SHEAR INDUCED THROMBOEMBOLIC POTENCY OF PROSTHETIC HEART VALVES

Umberto Morbiducci (1), Diana Massai (1), Raffaele Ponzini (2), Matteo Nobili (3), Franco M. Montevvecchi (1), Danny Bluestein (4), Alberto Redaelli (3),

1. Politecnico di Torino, Italy; 2. CILEA, Italy; 3. Politecnico di Milano, Italy; 4. University of New York at Stony Brook, USA

Introduction

Shear-induced platelet activation can lead to an enhancement in the aggregation of platelets, increasing the risk for cardioemboli formation in blood flow through mechanical heart valves (MHVs). The optimization of the thrombogenic performance of MHVs could be facilitated by formulating a robust numerical methodology with predictive capabilities of flow-induced platelet activation. To achieve this objective, it is essential to quantify the link between realistic valve induced haemodynamics and platelet activation, and to integrate theoretical, numerical, and experimental approaches that allow for the thrombogenic risk estimation associated with a specific geometry and/or working conditions. Here we present a comprehensive analysis of the dynamics of platelet trajectories in the flow through a realistic model of bileaflet MHV, using information extracted from simulations performed by means of a FSI approach.

Methods

The investigated device is a commercial bileaflet MHV model (fig. 1). Simulation accounts for the motion of the valve leaflets using a fully coupled implicit FSI approach, previously developed and validated [Nobili, 2008].

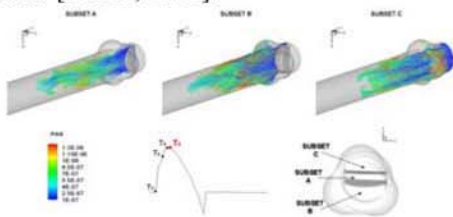


Figure 1: Evolving flow patterns of a particle set. Each particle set was separated into subsets A, B, and C in accordance with the orifice crossed by each evolving trajectory.

Platelets-like particles were released at different phases during systole (fig 1). For each seeded set, particle traces were tracked over the time interval between the time of injection and the end of systole. We estimated the performance of the valve in term of platelet activation by means of a mathematical model [Grigioni,2005] accounting for the cumulative load history sustained by formed elements, which was recently adapted for the

assessment of platelet activation state (PAS), quantifying the thrombogenic aspect of platelet prothrombinase activity [Nobili,2008]. Specifically, the k -th platelet activation state is expressed as:

$$PAS_k = \int_{t_0}^t Ca \left[\int_{t_0}^{\phi} \tau(\xi)^{b/a} d\xi + \frac{PAS_k(t_0)^{1/a}}{C} \right]^{a-1} \tau(\phi)^{b/a} d\phi$$

Over the whole set, we calculated also the mean PAS value for each time instant from the time of injection (PAS_{mean}).

Results and Discussion

Figure 1 shows the evolving intricate flow patterns of platelets moving through the valve during the deceleration phase. PAS_{mean} values calculated over platelets sets put in evidence that the level of activation depends upon the evolution of the flow through the valve. We introduce a graphic approach for comparing PAS predicted results, depending on the phases of the cardiac cycle (fig. 2). The diagram permits to evaluate the time intervals taken for each emitted platelet set to be activated at a certain level.

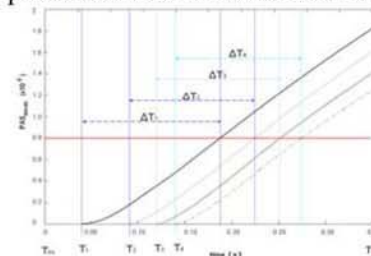


Figure 2: Graphic method for comparing PAS predicted results from dependence on the phases of the cardiac cycle.

Our approach allows for quantitative comparison of the potential PAS reached by platelets flowing through the valve at different time instants, taking into account the differences in exposure time among platelets during the various phases of the cardiac cycle. The proposed approach could be an efficient assessment tool for MHV performance.

References

- Nobili et al, J Biomech,41:2539-2550, 2008.
- Grigioni et al, Biomech Model Mechanobiol, 4:249-60, 2005.
- Nobili et al, ASAIO J, 54:64-72, 2008.

MULTI-PHYSICS COUPLING IN THE HEART

David Nordsletten (1), Steven Niderer(1), Jack Lee(1), David Kay(1), Nic Smith (1)

1. Computing Laboratory, University of Oxford, Oxford, UK

Introduction

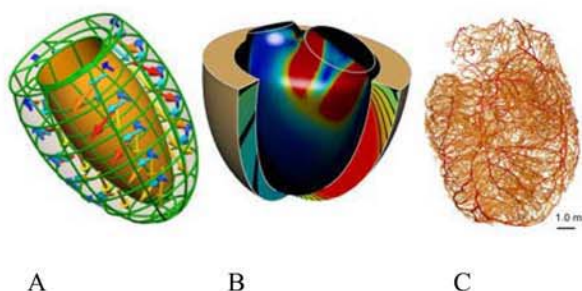
Inherent to the Physiome and Virtual Physiological Human (VPH) vision, and characteristic of the constituent research programs of the participating scientific community, is a shared interest in the concept of multi-scale and multi-physics coupling of previously distinct mathematical models. The VPH style of modelling, using explicit representations of the biophysical mechanisms within model equations, at each level in a modelling hierarchy, allows the coupling of equations between models to be cast in terms of the existing state variables of each model. This in turn facilitates the rapid development of models which link across physiological function and/or scales. When effectively applied, the resulting coupled model enables a valid analysis of an increased range of function, incorporating an enlarged set of the complex cause and effect relationships which exist in many physiological systems.

Methods

Through the application of finite element based models of the heart, which represent both cardiac anatomy and microstructure we have developed a multi-scale approach to simulating whole heart function. These anatomically based mathematical descriptions serve as spatial frameworks for embedding functional cellular models of electrical activation and the tension generation (Niederer et al 2006 Niederer and Smith 2007). Through this mathematical embedding the cellular model drives the spread of electrical waves and cardiac contraction within simulations of whole organ electromechanics. In parallel with the electromechanical models, coupled fluid mechanic representations of chamber and coronary blood flow have been developed to capture the influence of myocardial contraction, using linear and nonlinear mechanics theory, on fluid flow governed by the Navier-Stokes equations (Lee and Smith 2008; Nordsletten et al 2008). These coupled fluid mechanical models have been specifically applied within the chambers to quantify the two way fluid-structure interaction, between ventricular fluid dynamics and contraction, which is fundamental for understanding the cardiac pump function. Within the coronary vasculature, the interactions between contraction and the dynamics of perfusion have been simulated within the heart.

Results

The figure 1A below shows the application of coupled electromechanics where arrows indicate direction of work and the colour and magnitude of the arrows correspond to the rate of work. Figure 1B shows fluid velocity magnitude at the mid plane of the left ventricle cross-section, coloured from low (blue) to high (red). Figure 1C shows micro-CT imaging and segmentation of coronary vasculature through a maximum intensity projection of whole rat heart imaged at $21\mu\text{m}$ isotropic voxel dimension



A B C
Figure 1: A: Electromechanics solution B: Coupled fluid mechanical solution within the cardiac left ventricle C: Extracted coronary vascular mesh

Acknowledgements

This work has been supported by The United Kingdom Engineering and Physical Sciences Research Council (FP/F059361/1) and by the European Commission (FP7-ICT-2007-224495: euHeart).

References

- Niederer, S. A., P. J. Hunter, et al. (2006). "A quantitative analysis of cardiac myocyte relaxation: a simulation study." *Biophys J* 90(5): 1697-722.
- Niederer, S. A. and N. P. Smith (2007). "A Mathematical Model of the Slow Force Response to Stretch in Rat Ventricular Myocytes." *Biophys J* 92(11): 4030-4044.
- Nordsletten, D. A. a. S., N. P. and Kay, D. A. (2008). "Analysis of a non-conforming finite element method for fluid - solid mechanics." *SIAM J. Num. Anal.* in submission.
- Lee, J., P. Beighley, et al. (2007). "Automatic segmentation of 3D micro-CT coronary vascular images." *Medical Image Analysis* 11(6): 630-647.

AN IMPLICIT NUMERICAL METHOD FOR CARDIAC ELECTRO-MECHANICS SIMULATIONS

Pras Pathmanathan (1), David J. Gavaghan (1) and Jonathan P. Whiteley (1)

1. University of Oxford Computing Laboratory, UK

Introduction

Modelling cardiac electromechanics is an extremely challenging computational problem. It has been shown that explicit algorithms, using the finite element method, for solving such problems can display instabilities [Whiteley, 2007]. Here we describe a partially-implicit finite element approach which overcomes the issues of stability, yet is still computationally feasible. Using this new algorithm, we then identify features of the model which may be simplified (under particular conditions) without losing accuracy in the computations.

Methods

There are four general components of cardiac models of electrical activity coupled to the mechanical deformation: (i) ordinary differential equations (ODEs) representing cellular electrical activity; (ii) partial differential equations (PDEs) governing voltage propagation through the tissue (which together with (i) form the mono/bidomain equations for cardiac electrical activity); (iii) ODEs determining the active tension induced in the cell; and (iv) the PDEs of nonlinear elasticity which determine how the gross tissue deforms. (iii) is coupled to (iv) through the active tension multiplying a term which is added to the stress tensor. A simple explicit method for solving coupled electro-mechanics problems is to compute the electrical activity, and then calculate the induced active tension, and use this value when computing stresses in (iv); however this method can be unstable. Our new algorithm is based on the idea of computing the active tension as a function of the deformation at the next timestep, as opposed to the previous timestep. Given a solution to (i) and (ii) at the previous timestep, rather than solve the active tension ODEs (i.e. (iii)) using the current deformation, we embed the active tension ODEs into (iv) and always evaluate the active tension as a function of the deformation at the next timestep. This requires solving the active tension ODEs every time a trial deformation is used, and in particular, solving these ODEs every time a stress is computed. Thus the stress in this algorithm is not given in functional form (as in standard elasticity problems), but requires the solution of a set of

ODEs, to be evaluated at any point. We shall illustrate how this overcomes the issues of instability, and explain why this is the case. Such a method is in principle highly computationally expensive. However, using some computational tricks in how the active tension ODEs described in [Niederer, 2006] are solved, and since an implicit method allows relatively large timesteps, we can make this method computationally tractable.

Results

The method has been numerically validated to be stable in two and three dimensions. We have performed a series of numerical experiments in two dimensions. We have shown that a spatial stepsize in the mechanics mesh of the order of 1mm is acceptable to avoid losing accuracy, and that the timesteps used in the mechanics calculations can be two orders of magnitude greater than those in the electrical part of the simulation. We have also shown that, under certain conditions, the electrical activity can be decoupled from the mechanics without losing accuracy, as well as identifying simplifications which cannot be made.

Discussion

Modelling cardiac electromechanics is an extremely computationally challenging task which has received significantly less attention than cardiac electro-physiology. We have developed a new partially-implicit but computationally tractable algorithm for solving coupled cardiac electro-mechanical problems, which, because the active tension ODEs are embedded in the mechanics calculation and determined implicitly, does not exhibit any instabilities, and have qualitatively studied the numerical behaviour of the model.

Acknowledgements

PP is pleased to acknowledge the support of the EPSRC through grant EP/D048400/1, *New frontiers in the mathematics of solids*.

References

- Niederer et al, *Biophys. J.*, 90:1697-1722, 2006.
- Whiteley et al, *Bull. Math. Biol.*, 69(7):2199-2225, 2007.

Orthopaedic bioengineering

LOADING OF THE TEMPOROMANDIBULAR JOINT AFTER ARTIFICIAL JOINT IMPLANTATION ON THE OPPOSITE SIDE

Zdenek Horak (1), Tomas Bouda (1), Radek Jirman (2)

1. Laboratory of Biomechanics, Fac. of Mechanical Eng., CTU in Prague, Czech Republic;
2. Department of Stomatology, First Faculty of Medicine, Charles University in Prague, Czech Republic

Introduction

In clinical practice, the implantation of temporomandibular (TM) joint replacement is used to solve irreversible conditions of TM joint diseases. The result of such implantation is that the joint on the other side is overloaded, and after implantation of the first replacement, it is necessary to implant a replacement of the second joint afterwards. The objective of this work was to build a parametric FE study comparing the effect of the size of the mandible bone tissue resection, during the implantation of the TM joint replacement, on the loading of the joint on the other side.

Methods

The basis of the simulations was a simplified model of the mandible which was designed on the basis of the CT scans. The model was imported into the programme ABAQUS, in which the numerical analyses were carried out. The activity of all muscles in the model was represented using the 1D elements (see Fig.1). The occlusion was simulated for three basic situations: the occlusion on the incisor teeth I1, right and left first molar tooth M1. The muscular forces generated by individual muscles were determined from physiologic sections of individual muscles, which are mentioned in literature [Kolostra, 1992]. The magnitude of the forces of individual muscles [Kolostra, 1988, May, 2001] was defined so that they are equal to the forces generated at resulting occlusion force 300 N on the particular tooth.

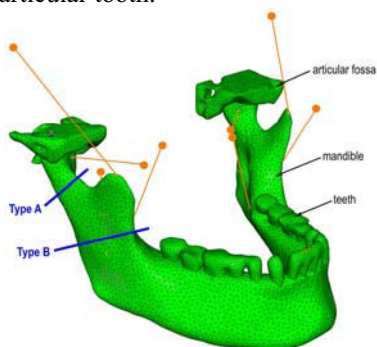


Figure 1: FE Model of the mandible and TM Joint. Muscles are represented by the orange lines. The type of the condylar resection is showed by the blue lines.

This magnitude of occlusion force was considered for all types of resections and the physiologic model. Models, which took into account set size of the resection and TMJ replacement, were consequently compared with the physiologic model. There were considered two simulations of mandible condyle resection (see Fig.1): right behind the caput mandibulae (Type A), when the m. pterygoideus lat. is removed, and behind the processus coronoideus mandibulae (Type B), when the m. masseter, m. temporalis, and m. pterygoideus lat. are removed.

Results

From the presented results obtained from FEM analyses for the version of occlusion on incisor teeth, the increase of resultant reaction force and all its components is measurable while increasing the size of resection. The same situation can be observed also for the variation of occlusion on the first left molar tooth. This result shows clearly that the function of the muscles after muscle resection must be substituted by other muscles. Therefore, the TM joint on the opposite side after implantation is overloaded.

Discussion

From the realised analyses is evident that removing the m. temporalis and m. masseter tendon has fatal consequences on the loading of the healthy TMJ on the other side. This result gives us scope for design of a more delicate construction of the TMJ implant, which could also enable smaller size of intervention into the system of muscles on the side of the implant, and thus, reduce the risk of damaging the opposite healthy TMJ.

Acknowledgements

The research was supported by the Czech Science Foundation project no. 106/07/0023 and by the Ministry of Education project no. MSM 6840770012.

References

- Kolostra, et al, J Biomech, 21:563-576, 1988.
- Kolostra, et al, J Biomech, 25:175-187, 1992.
- May et al, Clin Biomech, 16: 489-495, 2001.
- Biomet Inc at <http://www.biometmicrofixation.com>
- TMJ Concepts Inc at <http://www.tmjconcepts.com>
- TMJ Inc at <http://www.tmj.com>

MATERIAL PROPERTIES SENSITIVITY OF THE LUMBAR DISC UNDER COMPRESSION: A FACTORIAL STATISTICAL APPROACH

Andrea Malandrino (1), Josep A. Planell (1, 2), Damien Lacroix (1)

1. Institute for Bioengineering of Catalonia, Barcelona, Spain;
2. Universitat Politècnica de Catalunya, Barcelona, Spain.

Introduction

Poroelastic finite element (FE) modelling in spine biomechanics is based on a proper determination of solid and fluid material parameters from the literature. This task is often hard due to the large range of values reported [Nauman, 1999; Natarajan, 2004]. In this study, it was hypothesized that the permeability and stiffness values of some tissues in the IVD are critical for the overall response whereas other components do not influence significantly the IVD behaviour. The aim of this study was to determine through a ‘factorial design’ statistical approach the influence of each tissue material parameter within the IVD under compressive loads.

Methods

A FE model of an IVD with its adjacent vertebrae was obtained from a previously validated model of a spinal L3-L5 segment [Noailly, 2007]. Cartilage end-plate (CEP), nucleus pulposus (NP) and annulus fibrosus (AF) ground substance were modelled as isotropic poroelastic materials including hypoelastic collagen fibers for AF. Trabecular and cortical shell vertebral body (VB) layers were treated as orthotropic poroelastic materials. A fractional factorial design, consisting in 16 FE analyses, was performed varying six factors: Young’s moduli and permeabilities of AF and NP, permeabilities of CEP and VB. Each factor/material parameter was modulated among two levels according to extreme values within the range found in literature for tests in healthy and degenerated IVDs, as showed in Table 1. Compressive load was applied up to 1000 N for 16 hours and then removed for 8 hours. Responses in terms of displacement, pore pressure and fluid velocity were collected for each model (i.e. combination of factors). Statistical factorial analyses were performed to identify the significance of each factor in the specific response.

Factor	Low level	High level
TB permeability(mm ⁴ /N s)	26800	2000000
CEP permeability(mm ⁴ /N s)	0.0001	0.0014
AF permeability (mm ⁴ /N s)	0.00075	0.00187
NP permeability(mm ⁴ /N s)	0.00075	0.0014
AF Young’s modulus(MPa)	2.56	12.29
NP Young’s modulus (MPa)	1	1.66

Table 1: Factors and corresponding levels used in the statistical study.

Results

Viscoelastic disc behaviour was confirmed for all analyses and velocity and pressure results were in the same range found in experiments and other computational studies (Fig. 1). Anulus stiffness and cartilage end-plate permeability have a strong effect on the overall fluid- and solid-phase responses. Fig. 2 shows the effect of most important parameter variation in comparison with the experimental one. AF and NP stiffness variations were responsible of the absolute value of vertical displacement reached and CEP permeability effect was predicted in the 8 hours recovery phase.

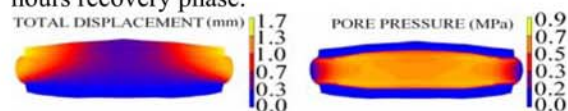


Figure 1: FE Results plots for one of the 16 models analyzed.

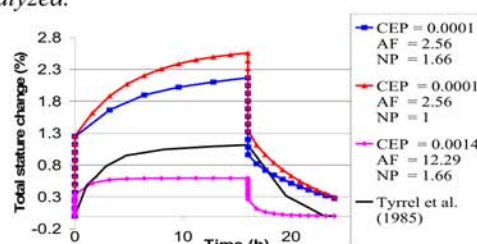


Figure 2: Results from model combinations of CEP permeability, AF and NP stiffness, compared with experimental ones.

Discussion

These results confirm the importance of CEP permeability variations (clinically due to degeneration and calcification) in fluid motion inside the disc and in its viscoelastic behaviour. To the authors’ knowledge, this is the first study exploring the importance of permeability in the IVD mechanical responses using a factorial analysis.

Acknowledgements

Funding is acknowledged from the European Commission under the DISC REGENERATION project (NMP3-LA-2008-213904).

References

- Natarajan et al, Spine, 29:2733-2741, 2004.
 Noailly et al, J Biomech, 40:2414-2425, 2007.
 Tyrrell et al, Spine, 2:161-164, 1985.

THE CEMENT-BONE INTERFACE: A COMPARATIVE EXPERIMENTAL AND FINITE ELEMENT STUDY

Y Zhao (1), A C Jones (1), V N Wijayathunga (1), Z M Jin (1), R K Wilcox (1)

1. Institute of Medical and Biological Engineering, University of Leeds, Leeds, UK

Introduction

In previous finite element (FE) studies of both joint replacement and vertebroplasty, the bone-cement interface has been represented in a simplified form by the properties of pure bulk cement. However a recent study has shown this to lead to a large overestimation in the predicted stiffness of the augmented vertebra [Wijayathunga, 2006]. The aim of this study was to compare different methodologies for representing the cement-bone interface using subject-specific models of trabecular-like specimens augmented with cement.

Methods

Three sets of six cylindrical specimens were cut from open cell polyurethane foam (Sawbone, Sweden). The first set was not augmented, the second was fully augmented with PMMA cement and the third was partially augmented in the centre of the specimen. All specimens were scanned using micro-computed tomography (Scanco μ CT80, Switzerland) and tested under axial compression.

Based on a previous convergence study [Zhao, 2007], FE models were built using the μ CT image greyscale data. From the first two sets, factors converting the greyscale to elastic modulus for each element of the pure sawbone and the cement-sawbone composite were determined. For the final set, FE models were generated by three different methods. Method I: both sawbone and cement regions were assigned single homogenous properties and a sensitivity study was undertaken on the effect of these properties; Method II: as Method I, except the elements in the sawbone region were assigned element-specific properties based on the image greyscale using the factors determined from the first two sets; Method III: elements in both the sawbone and cement regions were assigned element-specific properties based on the greyscale.

For both Method I and II, different properties of the cement region were defined and compared. Firstly, the properties of the cement region were defined as the same as those of pure cement (2500 MPa). Secondly an average elastic modulus was defined based on the mean greyscale value and the selected conversion factor (345 MPa).

Results

For the partially cemented specimens, the comparison between the predicted and experimentally measured stiffness values are shown in Figure 1 and the errors in Table 1. The lowest error was found with Method II ($E_{\text{cement}} = 345\text{MPa}$) and Method III. From the sensitivity study, doubling the modulus of the sawbone increased the overall stiffness by 90% but the maximum von Mises stress remained the same. Conversely, applying the same change to the cement region, the stiffness hardly increased and the stress increased by over 80%.

Method	I	I	II	II	III
E_{cement} (MPa)	2500	345	2500	345	varied
Error (%)	18.3	13.2	12.2	5.48	5.25

Table 1: Average errors between FE-predicted and experimentally-measured stiffness

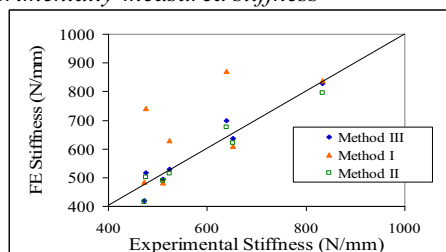


Figure 1: Agreement between FE and experiment

Discussion

This study showed the error in the FE model predictions using the greyscale-based method to define the cement-bone interface was $\sim 5\%$, rather than the commonly used methods ($\sim 18\%$) which are also likely to overestimate its stiffness. Good agreement was found where a homogenous value based on the mean greyscale was used for the whole cement region. The study also demonstrated that the apparent elastic modulus was dominated by the property of the sawbone, and high stiffness cement would only increase the maximum stress.

Acknowledgements

This work was supported by EPSRC and DePuy International Ltd

References

Wijayathunga J. Eng. Med. 222:221-228, 2008.
Zhao *et al.* Proc. BORS, UK, 2007.

FRONTAL PLANE LOWER LIMB ALIGNMENT USING FUNCTIONALLY DETERMINED JOINT CENTERS AND AXES

E.I. Kornaropoulos (1), W.R. Taylor (1), G.N. Duda (1), R.M. Ehrig (2), M.O. Heller (1)

1. Julius Wolff Institut and CMSC, Charité – Universitätsmedizin - Berlin, Germany

2. Zuse Institut Berlin, Germany

Introduction

Lower limb mal-alignment is thought to contribute to the onset and progression of osteoarthritis. Quantification of the degree of mal-alignment is important to allow planning of therapeutic interventions and to enable long-term assessment of disease progression. Standard imaging methods (X-rays/CT) for determining alignment expose patients to ionizing radiation, particularly if multiple follow-ups are required. The goal of this study was to evaluate a new imageless method against CT-based quantification of frontal plane alignment.

Methods

The position of reflective markers, attached to the lower extremity of 13 individuals (15 limbs), was tracked using an optical motion capture system (Vicon, Oxford, UK) during consecutive movement of the hip and knee joints through their entire ROM. Additionally, the marker configuration was captured for each subject in a static standing posture, where limb loading was monitored by a 6DOF force plate (AMTI). Based on published methods for the reduction of soft-tissue artefacts [Taylor, 2005] and for the functional identification of joint centres and axes [Ehrig, 2006-2007], the 3D positions of the hip joint centre, and the knee axis and center, were computed from the motion capture data. The ankle centre was geometrically defined after identification of the malleoli. The functional mechanical femoro-tibial angle (Functional-mFTA) was then calculated from the 3D positions of each of the three joint centres in the standing pose as a measure of frontal limb alignment and compared against the mFTA determined from three-joint CT scans of the hip, knee and ankle (CT-mFTA). The performance of the functional method was also compared against an approach where the hip and knee centres were approximated using regression methods (Regression-mFTA) as recently suggested [Hunt, 2008].

Results

Whilst the average Functional-mFTA ($1.3^\circ \pm 2.3^\circ$) was not significantly different ($p > 0.25$) from the CT-mFTA ($1.5^\circ \pm 2.1^\circ$), the Regression-mFTA ($4.7^\circ \pm 5.6^\circ$) showed a significant error ($p < 0.01$). The Functional-mFTA correlated significantly

($R=0.91$; $p < 0.0001$), with only a small bias (0.3°) and agreed better with the CT-mFTA than the Regression-mFTA ($R=0.76$; $P < 0.001$), which had a bias of 3.4° (Fig. 1).

Discussion

The results demonstrate that the mFTA can be quantified accurately using an imageless approach. Key prerequisites were the application of soft-tissue artefact minimizing procedures and precise methods for the functional determination of joint centres and axes. Comparing the two motion capture based methods, the functional approach offered greater accuracy over the regression methods. This new imageless method could help in reducing radiation exposure and could therefore become a valuable instrument for the quantification of frontal plane alignment for planning and monitoring of therapeutic interventions at the knee.

Figure and Tables

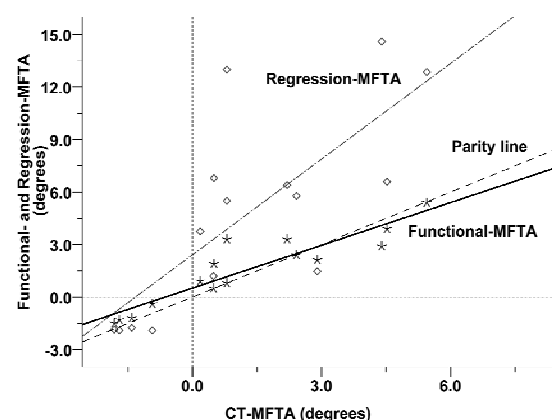


Figure 1: Scatter plot showing correlation of tested methods against CT-defined MFTA

Acknowledgements

This project was funded by the German Research Foundation (SFB 760) and the EU under FP6 (DeSSOS)

References

- Ehrig R. et al. J Biomech 39:2798-809, 2006.
- Ehrig R. et al. J Biomech 40:2150-7, 2007
- Hunt M. et al. Gait & Posture 27:635-40, 2008
- Taylor et al. J Orthop Res 23:726-34, 2005

Cardiovascular system - vascular

SELF-REGULATION OF RED BLOOD CELL TRANSPORT IN CAPILLARY NETWORKS

Dominik Obrist (1), Patrick Jenny (1), Alfred Buck (2), Bruno Weber (3)

1. Institute of Fluid Dynamics, ETH Zurich, Switzerland; 2. Division of Nuclear Medicine, University Hospital Zurich, Switzerland. 3. Institute of Pharmacology and Toxicology, University of Zurich, Switzerland.

Introduction

In capillary networks, blood must not be considered a homogeneous Newtonian fluid. Its rheology strongly depends on the density of red blood cells (RBC), i.e. the local hematocrit.

We devise a numerical model for plasma and RBC flow in a generic capillary network and show that there appears to be a self-regulation mechanism which leads to an inhomogeneous distribution of the flow rates and the local hematocrit. They differ strongly from the distributions that we would obtain for a homogeneous Newtonian fluid.

Methods

For a given distribution of RBC the local apparent blood viscosity in a capillary network can be modelled as $\mu_{app} = \mu (1 + K_T H_T)$ where μ is the viscosity of plasma, K_T is the apparent intrinsic viscosity and H_T is the local tube hematocrit [Pozrikidis, 2005]. With this information at hand, we can compute the pressure and flow in the whole capillary network using Kirchhoff's circuit laws [Boas, 2008]. These flow rates determine the velocity of the RBC until they arrive at a bifurcation. At that point, we use the simple rule that an RBC will enter the capillary vessel with the steepest local pressure gradient. This rule is supported by the experimental observation that RBC prefer the vessel with the highest local flow rate [Pries, 1989]. After an RBC has entered a new vessel the apparent viscosities, pressures and flow rates have to be recomputed.

We use these rules to simulate the plasma and RBC flow in a generic capillary network (Fig. 1) with a well-defined inflow at the bottom left corner and an outflow at the top right. Initially, one thousand RBC are randomly and uniformly seeded. After an initial transient, we reach a steady-state.

Results

In the steady-state configuration, the hematocrit reaches very high levels in the outer corners and there is almost no flow in these regions (Fig. 1). In contrast, there emerges a "highway" along the main diagonal with moderate hematocrit and a relatively high flow rate. This global result is related to the local observation that the flow rates in the vessels

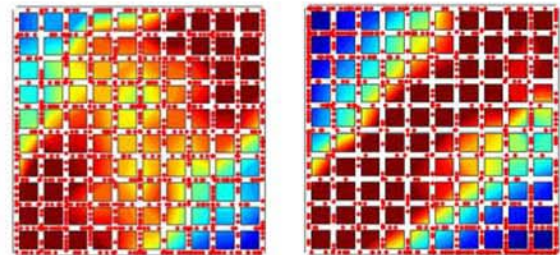


Figure 1: Generic capillary network (left: initial state; right: steady-state): red dots show the positions of RBC and colors indicate the local flow rates in the vessels (red: high velocities; blue: low velocities).

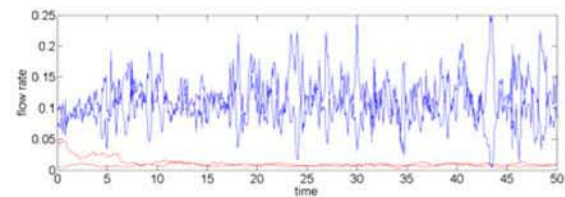


Figure 2: Flow rates versus time in vessels distal to a divergent bifurcation (red: bifurcation close to the top left corner; blue: center of the network).

distal to a divergent bifurcation fluctuate about the same mean value (Fig. 2).

Discussion

The observed flow rates are a direct result of the blood rheology and the bifurcation rule. Because an RBC enters the vessel with the higher flow rate, the local hematocrit of that vessel will increase. This leads to a higher apparent viscosity which decreases the flow velocity. This results in a self-regulating mechanism which ensures equal mean flow rates in the vessels distal to divergent bifurcations. Because of this self-regulation the distribution of the flow rates and the hematocrit across the network is different from the distribution that we would obtain for a homogeneous Newtonian fluid.

References

- D. A. Boas et al, NeuroImage, 40:1116-1129, 2008.
- C. Pozrikidis, Phys Fluids, 17:031503, 2005.
- A. R. Pries et al, Microvasc Res, 38:81-101, 1989.

ON THE PATIENT-SPECIFIC COMPUTATIONAL MODELLING OF BLOOD VESSEL

E. Peña, V. Alastrué, A. García, J.F. Rodríguez, M. A. Martínez and M. Doblaré

Group of Structural Mechanics and Materials modelling.

Aragón Institute of Engineering Research. University of Zaragoza.

CIBER-BBN. Centro de Investigación Biomédica en Red en Bioingeniería, Biomateriales y Nanomedicina

Introduction

Accurate determination of the biomechanical implications of vascular surgeries or pathologies on patients requires developing patient-specific models of the organ or vessel under consideration. In this regard, combining the development of advanced constitutive laws which mimic the behaviour of the vascular tissue with advanced computer analysis and medical imaging techniques provides a powerful tool for modelling vascular tissues on a patient specific basis. A framework for developing patient-specific models of blood vessel geometries obtained from medical imaging techniques is presented.

Methods

The multiplicative decomposition of the deformation gradient tensor is intensively combined with the Finite Element Method, in order to account for the residual stress present on those geometries. In addition, an algorithm to compensate the mismatching effect of the load on the medical images is also discussed [Alastrué et al, 2008].

The anisotropic behaviour of blood vessels comes from the existence of preferred directions of alignment of some of the micro-structural components that form the wall. A common assumption is that of considering two directions of fibres oriented in a helical manner with respect to the axial direction of the vessel [Holzapfel and Gasser, 2007]. In this work, a new approach for defining the fibre direction within the tissue is proposed based on the principal stress directions obtained from a previous analysis assuming isotropic material behaviour [Alastrué et al. 2009].

Results

The general framework is demonstrated in a realistic geometry of a carotid bifurcation. The example presented in this work shows that the incorporation of the residual stress dramatically affects the circumferential stress field, homogenizing the distribution and reducing the stress gradient. It also demonstrates that not accounting for the residual stress on a patient-

specific geometry can lead to completely different deformed configurations.

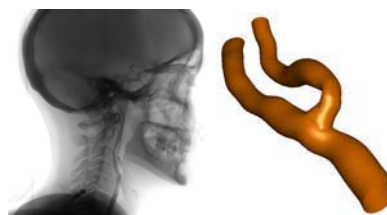


Figure 1: Images and reconstruction of a 3d patient-specific geometry of the human carotid bifurcation from angiographic images.

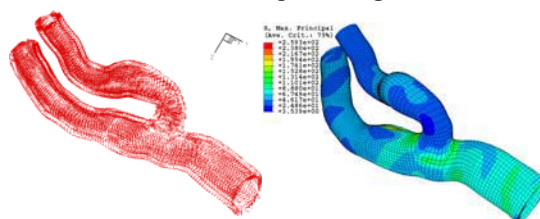


Figure 2: Fibre reconstruction and stress of a 3d patient-specific geometry of the human carotid bifurcation.

Discussion

The general framework proposed in this investigation proves to be feasible and valuable when dealing with realistic finite element simulations of patient specific geometries, allowing for incorporation of specific characteristics of the material structure and "in vivo" condition as is the case of the residual stress.

Acknowledgements

The authors gratefully acknowledge research support from Spanish Ministry of Science and Technology through the research projects DPI2007-63254, and the Spanish Ministry of Health through the research project FIS PI06-0446 and the Instituto Salud Carlos III (CIBER-BBN).

References

- Alastrué et al, J Biomech, 41:1773–1781, 2008.
- Alastrué et al, Commun Numer Meth Engng, In press, 2009
- Holzapfel and Gasser, Int J Cardiol, 116:78–85, 2007

FINITE ELEMENT SIMULATIONS OF STENTING IN A STENOSED BIFURCATION

Dario Gastaldi (1), Claudio Capelli (2), Lorenza Petrini (1), Francesco Migliavacca (1)

(1) *Laboratory of Biological Structure Mechanics, Structural Engineering Department Politecnico di Milano, Milan, Italy*

(2) *University College of London, Institute of Child Health, London, UK*

Introduction

Stenting of coronary bifurcated lesions is still an unresolved problem. Different techniques have been proposed to tackle this problem without a definitive solution. Aim of this work is to present a computational structural model based on finite element method able to reproduce a stenting procedure in a model of coronary bifurcation.

Methods

The model consisted of: *i*) a bifurcated coronary branch with three stenotic areas, *ii*) the balloon, and *iii*) the stent. A bifurcated coronary artery model was built as reported in Fig. 1. The artery has been modelled including three layers representing the intima, the media and the adventitia. Hyperelastic behaviour was adopted for the arterial layers and the parameter values of the constitutive laws have been adopted from the work of Holzapfel and colleagues [2005]. The plaques were modelled with hyperelastic behaviour till a values of 400 kPa where a stress was kept constant for increasing values of deformation. A semi-compliant balloon was modelled with an isotropic, linear-elastic material, with a Young modulus of 900 MPa and a Poisson coefficient of 0.3. The stent used in this study resembles the coronary Cordis BX-Velocity (Johnson & Johnson, Interventional System, Warren, NJ, USA) and was modelled as a homogeneous, isotropic, elasto-plastic material through a Von Mises–Hill plasticity model with a Young modulus of 193 GPa, a Poisson coefficient of 0.3 and a yield stress of 205 MPa. More information on the model can be found in a previous work from our laboratory [Gervaso, 2008]. The analyses were performed using the commercial code ABAQUS/Explicit v. 6.4. The large-deformation theory was used.

Results

Figure 1 shows four instants of the deployment of the stent in the main branch. Contact between the balloon and the artery are visible at the beginning of the inflation phase. The restoring of the vessel lumen is clearly visible after the balloon deflating and the elastic recoil of the artery. Figure 2 depicts

the stresses on the internal layer of the intima. The pattern of the stents on the two plaques is well detectable. Expansion of a second stent in the side branch (not shown) allowed to evaluate the interaction with the main stent. Its positioning inside the side branch is a crucial point in the restoration of the flow.

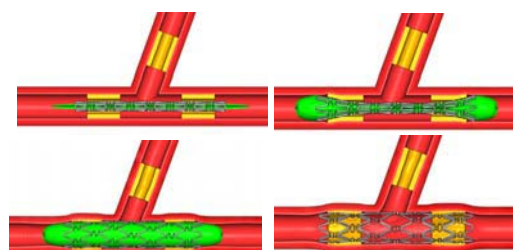


Figure 1: Expansion of the stent in the main branch.

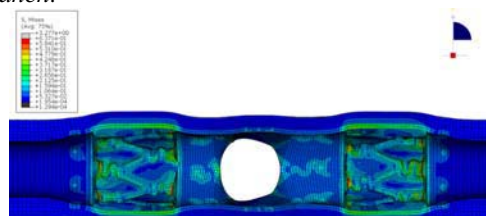


Figure 1: Stress distribution in the internal layer of the intima after the balloon deflation and the elastic recoil of the artery. The white hole is the side branch.

Discussion

The model here presented shows the feasibility to model a complex phenomenon as the stenting procedure in a bifurcation. Different configurations in the plaques position could be easily studied and their effects caused by different stenting techniques or stent model could be easily investigated in such a model. This model could also be a valid basis to study the fluid dynamics created by the expansion of stents in a bifurcation.

References

- Gervaso et al, J Biomech, 41:1206-1212, 2008.
- Holzapfel et al, Am J Physiol Heart Circ Physiol, 289:H2048-H2058, 2005.

PATIENT SPECIFIC FINITE ELEMENT STUDY OF STENT FRACTURE AFTER PERCUTANEOUS PULMONARY VALVE IMPLANTATION

Silvia Schievano (1), Andrew M Taylor (1), Claudio Capelli (1), Philipp Lurz (1), Johannes Nordmeyer (1), Francesco Migliavacca (2), Philipp Bonhoffer (1)

1. UCL Institute of Child Health & Great Ormond Street Hospital for Children, London, UK;
2. LaBS, Structural Engineering Department, Politecnico di Milano, Milan, Italy

Introduction

Stent fracture is a recognized complication following device implantation for all cardiovascular applications [Lim, 2008]. Percutaneous pulmonary valve implantation (PPVI) – a successful technique introduced in 2000 to treat right ventricular outflow tract (RVOT) dysfunction [Lurz, 2008] – is also subjected to this potentially adverse event. The PPVI device is made of a bovine jugular venous valve sewn into a balloon-expandable stent. During the development phase of this device, bench testing and animal experiments predicted valve degeneration with no stent fracturing. However, in our clinical experience, the opposite occurred – good valve function and 20% stent fractures.

The aim of this work was to analyse the shape and mechanical behaviour of the PPVI device when implanted into a patient RVOT, using finite element (FE) analysis.

Methods

Magnetic resonance data from a patient who underwent PPVI and had subsequent stent fractures was used to create a FE, rigid model of the implantation site. Simulated expansion of the PPVI stent into this RVOT geometry was compared with the free expansion of the PPVI stent up to a uniformly deployed configuration (conventional method employed in bench testing protocols), using FE analysis. PPVI biplane fluoroscopy images from the same patient were used to reconstruct the 3D shape and deformation of the stent *in-situ* (Fig. 1) and verify the FE geometrical results. Asymmetries were measured in the circumferential, radial and longitudinal direction, both in systole and diastole.

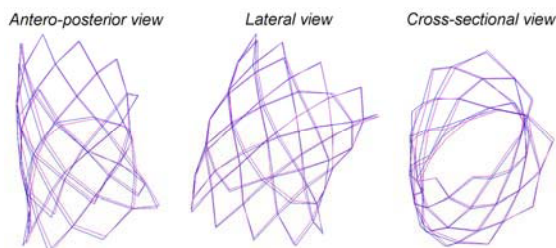


Figure 1: Fluoroscopy imaging 3D reconstructions of the stent in diastole (magenta) and systole (blue).

Results

Although a simplified FE model of the stent/implantation site interaction was adopted, this analysis gave useful information about the influence of the RVOT on the final geometry and mechanical performance of the stent. When deployed into the RVOT, the FE stent showed a non-uniform shape, similar to the geometry seen in the “real” fluoroscopy reconstructed stent, where the most expanded cells corresponded to the real fracture locations. This asymmetrical geometry, when compared to the free-expanded stent, resulted in higher stresses in the portion of the stent where fractures occurred.

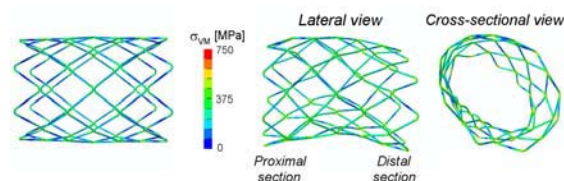


Figure 1: Stress distribution in the uniformly deployed stent (left) and in the stent expanded into the patient’s RVOT (right).

Furthermore, due to the cardiac pulsatile loading condition, fatigue fractures – that were not predicted in the free-deployed stent – developed in the asymmetrically expanded device.

Discussion

FE analysis of PPVI device deployment into a realistic implantation site anatomy clearly demonstrated that the interaction of the device with the RVOT influences the deployed shape of the stent. The asymmetrical expansion of the device, also proven by the 3D fluoroscopy reconstructions, changes the stent loading conditions. This methodology should be useful to predict the likelihood of stent fractures once a device has been implanted in a specific patient. If the risk of fractures is high, patient follow-up and monitoring may need to be increased to ensure device integrity.

References

- Lurz et al, *Circulation*, 117(15):1964-1972, 2008.
 Lim et al, *Radiology*, 249(3):810-819, 2008.

RUPTURE-RISK EVALUATION OF AORTIC ANEURYSMS BY FINITE ELEMENT PROBABILISTIC ANALYSIS

Simona Celi (1)(2), Francesca Di Puccio (1), Paola Forte (1), Sergio Berti (2), Massimiliano Mariani (2)

1. Dept. Mechanical, Nuclear and Production Engineering, University of Pisa, Italy
2. Institute of Clinical Physiology, National Research Council, Massa, Italy

Introduction

The aortic aneurysm (AA) is an irreversible and permanent dilatation of the aortic vessel. In clinical practice interventions are primarily decided on the basis of the maximum diameter criterion ($\phi_{critical} \approx 50-60$ mm). However, this is not a fail-safe criterion since some AAs rupture at a size smaller than the critical value and others grow up to a larger diameter without rupturing [Davies et al, 2002]. Several studies suggest the peak wall stress as a more reliable parameter for the evaluation of the risk of events [Vorp et al., 1998]; therefore to perform this assessment patient-specific geometry and material properties are required. In the literature simulations are often based, on one hand, on accurate geometry reconstruction from CT images while, on the other, on averaged material properties from different sets of patients. Moreover, even if investigations showed that asymmetry and geometry irregularities play a determinant role, sensitivity analyses have been performed only on ideal simplified models that cannot describe the complexity of the real geometry.

The aim of this study is to investigate, with statistical analyses, the relationships between the rupture-risk, different shapes and material properties to identify the parameters that mainly influence the peak stress. For this purpose a virtual 3D AA library was developed and simulations were performed by using a probabilistic technique implemented in the Ansys FE code.

Methods

CT images from our patients-database (70 cases) have been analysed. The main geometrical features of both thoracic and abdominal aortic diseases were identified and quantified to develop a virtual geometry library for the parametric finite element models. For each patient-geometry several parameters were collected such as the eccentricity (e) at three different sections and three ratios: F_ϕ between the dilated and the normal diameter, F_a between the minimum and the maximum axes of the dilated section and F_L between the length of the diseased portion and the dilated diameter. Both models with uniform and non uniform wall thickness were simulated. The thickness values

were obtained from the standard transesophageus procedures and from measurements on excised AAs. The thickness in the ventral area was less of the dorsal one of about 50%. Tissues were assumed to be incompressible, homogeneous, isotropic and hyperelastic. A homogeneous pressure of 16 kPa was applied to the luminal surface. The sensitivity of maximum stress with respect to geometric characteristics and tissue material properties was assessed by probabilistic analyses.

Results and discussions

The von Mises wall stress at the peak systolic pressure for a descending aorta deterministic configuration is plotted in fig. 1.a.

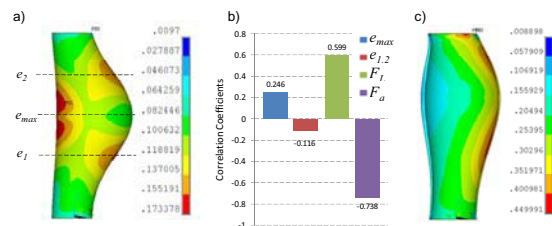


Figure 1: von Mises stress of a descending aorta model ($F_\phi=1.8$) and sections used for eccentricity evaluation (a); correlation coefficients (b); 3D model with non uniform thickness (c).

The sensitivity analysis for a model with uniform thickness shows that the von Mises stress is primarily affected by the F_L and F_a parameters with a positive and negative sign respectively, fig. 1.b. Eccentricities play less significant roles due to the small ranges of variability recorded for this type of aneurysm ($3 \leq e_{max} \leq 7$ mm; $0.6e_{max} \leq e_{1,2} \leq e_{max}$). For the 3D model with non uniform thickness, the peak stress is localised in the ventral area and the stress is primarily affected by e and by F_L , and the wall thickness ratio, fig. 1.c.

This study points out the importance of a probabilistic approach for aneurysm rupture-risk evaluation and the effect of morphology on peak stress estimation and localization.

References

- Davies et al, Ann Thorac Surg, 73: 17–28, 2002.
- Vorp et al., J. Vasc. Surg., 27: 632–639, 1998.

RULE-BASED SIMULATION OF RESTENOSIS IN STENTS

Colin J Boyle (1), Caitríona Lally (1,2), Patrick J Prendergast (1)

(1) Trinity Centre for Bioengineering, School of Engineering, Trinity College Dublin, Ireland;
 (2) School of Mechanical and Manufacturing Engineering, Dublin City University, Ireland.

Introduction

The efficacy of cardiovascular stents is limited due to the growth of tissue within the stent. Growth of tissue is termed 'restenosis' and is thought to be due, in part, to injury cause to the vascular tissue when the stent is deployed. Compression-induced necrosis and endothelial denudation attracts an inflammatory response which activates smooth muscle cells (SMCs) through degradation of the ECM by matrix metalloproteinases (MMPs).

Lattice-based simulation allows the complex interactions between several cell types, ECM and biochemical stimuli to be explicitly simulated. In this study, we aim to establish whether or not injury quantification using FEA can be combined with a lattice-based simulation of lesion growth to simulate restenosis within cardiovascular stents. We test the method by application to two stents with known differences in restenotic response.

Methods

The compressive stress shown to induce muscle cell necrosis in skeletal muscle [Linder-Ganz, 2006] was used as the injury threshold for vascular smooth muscle, and coupled with an FE model of stent expansion in a cylindrical vessel to calculate regions of injury.

The tissue growth domain surrounding the expanded artery was discretised into regular lattice points. Each point could store one cell (an endothelial cell (EC), or SMC), and the local environmental variables (ECM, MMP and growth stimulus).

The lattice points within each arterial element were found, and these were initialised with ECM=100% and SMCs were randomly seeded. Lattice points within injured elements were initialised with growth factor and MMPs, and SMCs were removed, simulating necrosis.

The lattice was updated iteratively based on assigned rules. SMC phenotype was quiescent if the local ECM was intact and synthetic otherwise. Synthetic SMCs proliferated and migrated by random walk, ECs proliferated over the lumen surface at a constant rate, and healed endothelium represented a barrier to further growth. ECM was produced by synthetic SMCs and degraded by MMPs at constant rates. The technique was applied to two stent designs: a four crown and six crown stent. The simulation was incremented to represent 180 days of lesion growth.

Results

Injured regions were localised around the stent struts. Matrix degradation in the injured zones was followed by neighbouring cell activation. The population doubling rate of the cells peaked at 7 days and dropped off after 50 days in both stents, with the four-crown stent producing higher proliferation rates. Synthetic cells migrated from injured regions to produce diffuse tissue accumulation (Figure 1). Reendothelialisation was complete at 115 days. The four-crown design produced maximum restenosis in the mid section of the stent, whereas the six-crown produced maximum restenosis at proximal and distal ends. Neointimal area at the midsection was 1.33 times greater in the four-crown design than the six-crown design.

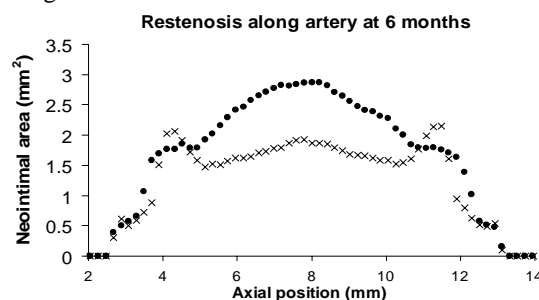


Figure 1. Simulated axial distribution of neointima in the four (•) and six-crown (x) stents.

Discussion

The simulations showed qualitative similarities with lumen formation found experimentally and clinically. In particular non-linear lesion growth (with initial rapid growth ending in lesion quiescence), early proliferation and non-uniform lesion area was found. The technique predicted a similar difference between stents as observed experimentally [Garasic, 2000], where the four-crown design induced 2-fold more neointima than the six-crown design *in vivo*.

Relevant assumptions are that the model assumed a constant endothelium healing rate, and did not include mechanoregulation or obstruction due to stent struts. The method was applied to simplified arterial geometries without stenosis.

References

- Linder-Ganz et al, J Biomech, 39:2725-32, 2006.
- Garasic et al, Circulation, 101:812-8, 2000.

Experimental methods for model validation

TIME DEPENDENT INVERSE FEA OF SUPERFICIAL PORCINE SOFT TISSUE USING MR SECTIONS – A PILOT STUDY

Andrew M. Sims (1), Timothy Stait-Gardner (2), William S. Price (2), John W. Morley (1,2), Mark Hoffman (1), Anne Simmons (1), Klaus Schindhelm (1)

1. The University of New South Wales, Australia;
2. The University of Western Sydney, Australia

Introduction

Many instances introducing a mechanical load into soft tissue result from compressive contact loading, e.g. pressure ulcers [Bouten, 2003] and heel strike impact [Miller-Young, 2002]. It is of clinical interest to accurately characterise the mechanical behaviour of soft tissues for a range of compressive loading scenarios.

The superficial soft tissues are comprised of layers of skin, subdermal fat and muscle, supported by the skeleton. The constitutive behaviour of soft tissues incorporates material non-linearity and large deformation kinematics [Fung, 1967]; hyperelastic models are commonly used for such simulations.

Although soft tissues have been studied over many decades [Fung, 1993], there is a paucity of published work on the mechanical properties of fatty tissue, which is mostly directed to the calcaneal fat pad [Miller-Young, 2002] and breast tissue [del Palomar, 2007].

This paper presents the initial sample results of a pilot study which characterised the mechanical properties of subdermal fat using a confined indentation test combined with magnetic resonance imaging and inverse finite element analysis.

Method

Porcine abdominal soft tissue was excised immediately post mortem. Indentation specimens were rotationally cut using a sharp cylindrical borer; subdermal fat was manually dissected by scalpel. Samples were mounted in a custom test rig with gelatine (10% by mass) being used to remove any voids in the sample and enforce a known fixed boundary condition for the constrained indentation experiment. The rig was placed inside a Bruker Avance 500MHz wide-bore NMR spectrometer. A series of MR section scans were performed while the sample was subjected to indentation/relaxation cycles (20min) by a 4mm radius spherical tipped PTFE indenter of known mass.

Threshold based segmentation (ScanIP, Matlab) was used to define and track material boundaries over time, hence determining indentation, $y(t)$.

A 2D axisymmetric FEA model (ANSYS) was developed which modelled gel and fat as incompressible isotropic hyperelastic viscoelastic

materials. The Matlab optimisation toolbox (fmincon) was used to determine the properties of the fat by minimising the objective function during the loading phases:

$$r(\mu, \alpha_i, \tau_i) = \|y(t) - y_{FEA}(t)\|$$

Results

Viscoelastic material deformations and properties were acquired from this experimental technique. Images and graphical results are shown in Figures 1 and 2 respectively. Optimised parameters for subdermal porcine fat are $\mu=0.70\text{kPa}$ for a Neo-Hookean model with Prony viscoelastic coefficients $\alpha=0.292$, with a relaxation constant of $\tau=150\text{s}$.

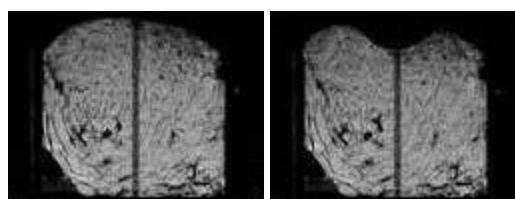


Figure 1: MRI images of reference (L) and indented (R) fat

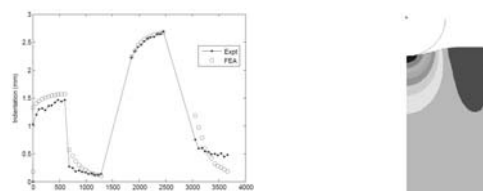


Figure 2: Optimised FEA results (L) and model (R)

Discussion

This experiment successfully determined the hyperelastic and Prony series viscoelastic constants of porcine subdermal fat from a series of MRI images and inverse FEA, thereby facilitating more comprehensive simulations of compressive loads on superficial soft tissues. These data are of the same order as breast tissue [delPalomar,2007]. Future work will consider the skin/fat/muscle composite.

References

- Bouten, C.V. et al, Arch Phys Med Rehabil, 84:616-9, 2003
- delPalomar, A.P. et al, Med Eng Phys, 30:1089-1097, 2008
- Fung, Y. C. Am J Physiol, 213: 1532-1544, 1967
- Fung, Y.C. Biomechanics: Mechanical Properties of Living Tissues, Springer-Verlag, 1993
- Miller-Young, J. E. et al, J Biomech, 35: 1523-31, 2002

MUSCULOSKELETAL MODELLING OF A SKI TRAINING EXERCISE: MODEL VALIDATION BY EMG ACQUISITION

Nicola Petrone (1), Oberdan Grotto (1), Alessandra Speranza (2)

1. Department of Mechanical Engineering, University of Padova, Italy; 2. Exercise Science Faculty, University of Padova, Italy

Introduction

Skiing is a very popular sport discipline involving a full body motion in an open environment. The muscular recruitment patterns at the lower limbs are related to the ski discipline, the skill levels and the snow properties: in most cases antigravitational muscles are reported to work in eccentric mode [Berg, 1999].

Motion Capture and EMG field data acquisition are very complex in such environment [Petrone, 2008]. Very few training devices are available to athletes for training away from slopes [Spitzenfeil, 2003].

On the other hand, the alpine ski disciplines are often related to different type of injuries, mostly occurring at the knee ligaments. After ACL reconstruction, several rehabilitation protocols are available, and of some interest are devices suitable for functional rehabilitation enabling to reproduce the field motion patterns at controlled load levels [Kvist J, 2004].

Aims of the present work were (i) to evaluate the muscular activation patterns developed by athletes on a popular ski training device, (ii) to compare the experimental EMG signals with the results of a numerical musculoskeletal simulation developed using the Anybody® SW and driven by markers trajectories collected by motion capture.

Methods

A BTS® motion capture system integrating 12 EMG channels, 2 force platform at each foot and 6 infrared cameras was used at 60 Hz for capturing the exercises on a commercial SkiEdge® training device. Several sessions were conducted on healthy skilled skiers and on skiers undergoing ACL reconstruction, tested 1 wk before and 8 wks after the surgery.

The markers trajectories and the reaction forces at the foot sole were used to drive the corresponding bony landmarks of the Anybody model after anthropometric scaling: inverse dynamic solution of the motion allowed to calculate the numerical muscle activation patterns that were compared with the experimental EMG muscle activity of 6 muscles (RF, VM, BF, TA, GASL, PERL) at each leg.

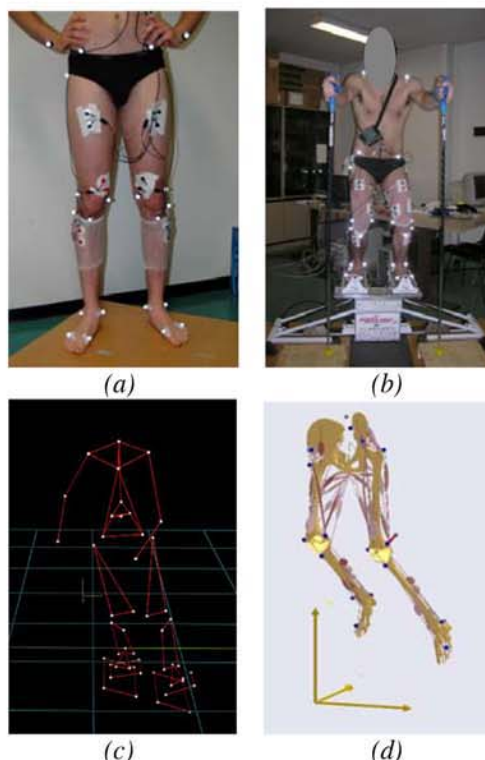


Figure 1:(a)EMG electrodes on a healthy tester; (b) SkiEdge test setup; (c) Motion Capture frame; (d) Anybody® model output.

Results & Discussion

Results of tests performed by healthy subject on the SkiEdge confirmed that low levels of muscle activation were obtained with respect to field EMG data: the device is unsuitable for high performance training. The numerical model was able to produce EMG patterns that were comparable with experimental EMG data and could be used for estimating the knee dynamic loads and moments. Finally, low load levels estimated at the knee joints during the training exercise could be positively considered for a rehabilitation protocol.

References

- Berg HE et al, Med Sci Sports Exerc. 31(7): 1065-7, 1999.
- Kvist J, Sports Med, 34: 269-280.
- Petrone N. et al, Science and Skiing IV, 2008.
- Spitzenfeil et al, Science and Skiing III, 204-215, 2003.

IN VIVO PHASE CONTRAST MRI VALIDATION OF CFD-BASED BLOOD FLOW RATE ESTIMATES IN DOPPLER ANALYSIS

Raffaele Ponzini (1), Christian Vergara (2), Giovanna Rizzo (3), Alessandro Veneziani (4), Alberto Redaelli (5), Angelo Vanzulli (6), Oberdan Parodi (7)

1. CILEA, Italy; 2. Università degli studi di Bergamo, Italy; 3. IBFM-CNR, Italy; 4. Emory University, USA; 5. Politecnico di Milano, Italy; 6. Ospedale Niguarda CàGranda, Italy; 7. Institute of Clinical Physiology CNR, Italy;

Introduction

In this work we carry out an *in vivo* validation of a method for estimating blood flow rate from the peak velocity, as it is usually done in single-wire Doppler catheter measurements. This method, originally proposed in [Ponzini, 2006], stems from the application of numerical analysis of the blood flow with Computational Fluid Dynamics (CFD) techniques. It proposes a new formula linking the maximum velocity and the flow rate by taking into account for heart pulsatility. In the new approach the Womersley number has been chosen as the link between mean and maximum velocity ('Womersley-based'); instead in more traditional ('a-priori') approaches a parabolic profile is considered valid for small and medium calliper districts, whilst the flat profile is used for large ones.

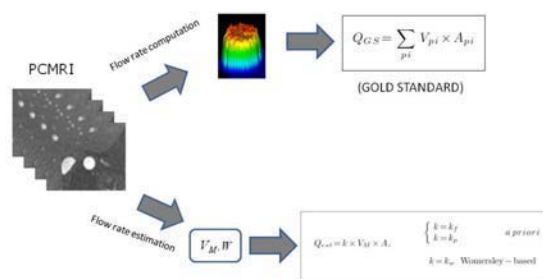


Figure 1: Overall schema of the *in vivo* validation protocol.

Methods

In figure 1 the protocol adopted is presented. Starting from the PCMRI images the gold standard value Q_{GS} of the blood flow rate has been computed by numerical integration of the local velocity field V_{pi} taken on each pixel pi of the lumen. More precisely, we set

$$Q_{GS} = \sum_{pi} V_{pi} \times A_{pi} \quad (1)$$

where A_{pi} is the area of the single intra-vessel pixel. On the other hand the estimate procedure is performed in all the considered cases mimicking the intravascular single-point Doppler data analysis

procedure and following the two different approaches:

- i. The *a-priori* approach (parabolic or flat depending on the vessel calliper).
- ii. The 'Womersley-based' approach.

The values of the estimated flow rates have been compared to their associated gold standard values Q_{GS} for a total of 30 observations (three arterial district for ten volunteers), covering a range of the Womersley number between 2.5 and 14.7.

Results

In figure 2 the mean values (among the ten subjects), with their variance, of the percentage of difference between the gold-standard and the estimates are shown in the three arterial districts using the three estimate approaches.

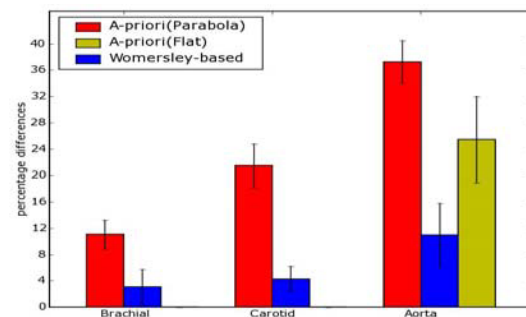


Figure 2: Mean performances of different approaches on blood flow rate estimate on the three arterial districts.

Discussion

The *in vivo* validation of the Womersley-based approach confirms:

- i. the validity of the new method for blood flow rate calculation;
- ii. the reliability of CFD modelling for hypothesis testing and data acquiring in hemodynamics.

References

Ponzini et al, Ultr. Med. Biol., 32(10):1545-55, 2006.

MECHANICAL TESTING OF LONG BONES: HOW CAN FE MODELS AND *IN VITRO* TESTS HELP EACH OTHER?

Luca Cristofolini (1, 2), Fulvia Taddei (2), Mateusz Juszczuk (1,2),
Enrico Schileo (2), Saulo Martelli (1,2), Marco Viceconti (2)

1. *Facoltà di Ingegneria, Università di Bologna, Italy;*

2. *Laboratorio di Tecnologia Medica, Istituto Ortopedico Rizzoli, Bologna, Italy*

Introduction

There is great interest in bone mechanics for two reasons: (1) explain and predict fracture of healthy and diseased (osteoporotic) bone; (2) improve the performance of prostheses. The mechanics of bony structures has been investigated for decades. While originally *in vitro* testing was the only viable option, nowadays most research is based on numerical models. The amount and quality of the information achieved by integrating subject-specific Finite Element (FE) models with *in vitro* testing is amazing.

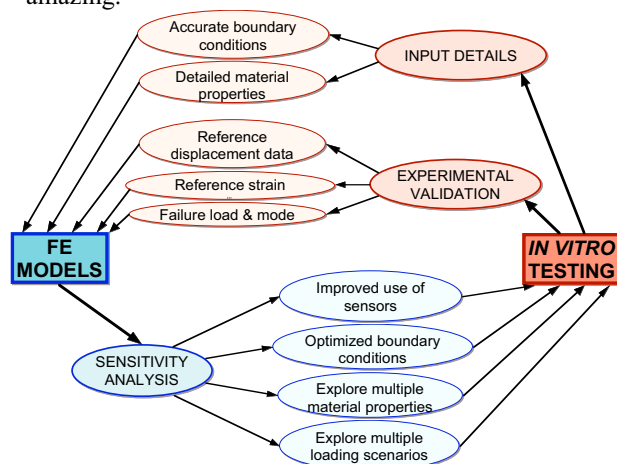


Fig. 1: Exchanges between FE models and experiments

FE models can exploit *in vitro* tests

In order to be meaningful, FE models require key input information (Fig. 1). When dealing with bones, this consists both of material properties (bone is inhomogeneous by nature), and accurately identified boundary conditions. This information can be provided by dedicated *in vitro* experiments. In addition, output of FE models must be checked to quantify closeness to “reality”. This is typically achieved by comparing experimentally measured vs. predicted strain or displacement. This can only be performed by designing an experiment to be carried out in parallel to the numerical simulation.

In vitro tests can exploit FE models

In vitro tests are costly and time-consuming. For this reason, any tool that can optimize an experiment is welcome (Fig. 1). All experimental measurements are affected by error. Specifically designed sensitivity analyses with FE models can

optimize the implementation of boundary conditions; and identify the best position of transducers such as strain gauges [Cristofolini, 1999]. Moreover, FE models can complement experimental measurements by exploring effect of varying some input variables, without the need of running the entire experiment all over again.

An example: the proximal femur

Eight pairs of human femurs were investigated in parallel using subject-specific FE models, and *in vitro* experiments. Six load configurations were derived from preliminary FE models to explore the physiological range, and spontaneous fracture [Cristofolini, 2007]. Subject-specific FE models of all femurs were built, deriving from CT data both geometry (10-noded tetrahedral meshes), and inhomogeneous material properties.

In vitro testing included: (1) to measure principal strain, each femur was instrumented with 15 triaxial strain gauges [Cristofolini, 2009]; (2) to measure 3D displacements, each femur was instrumented with LVDTs; (3) the position of each sensor was digitized and registered on the bone surface; (4) the actual position of the applied force was tracked with a dedicated transducer [Juszczuk, 2009]; (5) the point of fracture initiation was identified with hi-speed video [Cristofolini, 2007]

The agreement between FE and *in vitro* principal strain was 7% RMSE [Schileo, 2008a]; fracture was successfully predicted [Schileo, 2008b].

Conclusions

This experimental-numerical integrated approach is far more extensive and reliable than either method alone. Extremely relevant results were obtained both in the field of bone testing [Cristofolini, 2008], and of prosthetics [Viceconti, 2009].

Acknowledgements

EC grants: LHDL (IST-2004-026932), VPHOP (223865)

References

- Cristofolini *et al*, J Str Anal Engrn Des, 34(1): 1-15, 1999
- Cristofolini *et al*, J Biomech 40(13):2837-45, 2007
- Cristofolini *et al*, Phil Trans A Math Phys Eng Sci, 2008
- Cristofolini *et al*, Proc Inst Mech Eng [H], in press, 2009
- Juszczuk *et al*, Strain, in press, 2009
- Schileo *et al*, 41(11):2483-91, 2008a
- Schileo *et al*, J Biomech 41(2):356-67, 2008b
- Viceconti *et al*, J Mech Beh Biomed Mat 2: 120-7, 2009

VALIDATING SUBJECT-SPECIFIC FINITE ELEMENT MODELS OF LOWER LIMB BONES IN BENDING AND TORSION

Enrico Schileo (1), Paola Benegiamo (1), Lorenzo Grassi (1), Fulvia Taddei (1), Mateusz Juszczak (1,2), Luca Cristofolini (1,2), Marco Viceconti (1)

1. *Laboratorio di Tecnologia Medica, Istituto Ortopedico Rizzoli, Bologna, Italy;*
 2. *Facoltà di Ingegneria, Università di Bologna, Italy*

Introduction

The prediction of the mechanical strains induced in human bones is seeing the first pioneering applications to clinical practice [Taddei, 2004]. Subject-specific finite element (FE) models of bones from Computed Tomography (CT) data are the most used tool to achieve such predictions. It has been shown that they can bring to accurate strain predictions [Schileo, 2008] and even improve on the current clinical routines for the evaluation of fracture risk in the proximal femur and in the spine [Cody, 1999; Crawford, 2003]. Only few modelling studies focused on the diaphyses of long bones [Spruijt, 2006]. However, most common fractures do occur at those sites due to trauma, bone lesions or poor healing of a previous fracture. To the authors' knowledge, a validation study against experimental strain measurements on the diaphyses of lower limb bones is still lacking. We propose a combined experimental-numerical study to assess the ability of a FE modelling procedure previously validated for the proximal femur [Schileo, 2008], in predicting the strains induced in the femoral, tibial and fibular diaphyses by bending and torsion loads.

Methods

Pairs of femora, tibiae and fibulae were extracted from two donors, and CT scanned. FE models of all bones were generated according to the procedure described in [Schileo, 2008]. Anatomical frames were marked on each bone. Triaxial strain gauges were glued on each anatomical aspect: 15 on each femur and tibia, 8 on each fibula. Physiological loading conditions in the diaphysis of long bones are not always clearly identified (e.g. a debate is still open as to whether the fibula contributes to load bearing). Trauma loads can vary significantly, and might be intrusive or rotational in nature. For these reasons, in order to univocally identify the loading conditions, simplified loading configurations were chosen. Therefore, two controlled loading scenarios aimed at eliciting mainly bending and torsion were applied. Four point bending tests were conducted for both opposite directions in the frontal and sagittal plane (Fig. 1). Pure torsion was applied in both directions. Strains were acquired from strain gauges and displacements of relevant points measured by extensometers. A spatial registration between CT and experimental reference systems

was achieved (0.4 mm error) to effectively reproduce the boundary conditions in the FE models. Predicted displacements and strains were finally compared to the measured ones, deriving both correlations and error metrics.



Figure 1: Four point bending on a fibula: experiment and model.

Results and Discussion

Preliminary results indicate a satisfactory accuracy in the prediction of bending displacements (10% RMSE) and strains (Table 1). Strain prediction accuracy was improved when looking at the gauges in the bending direction, which are placed at the most stressed locations (e.g. medial and lateral aspect in medio-lateral bending). These findings corroborate the generality of the proposed subject-specific FE modelling procedure, originally devised for the proximal femur, that seem to be accurately applicable to all lower limb long bones.

<i>Exp vs. FEM</i>	<i>R²</i>	<i>RMSE%</i>	<i>Peak err%</i>
<i>All gauges</i>	<i>0.86</i>	<i>6.4%</i>	<i>93%</i>
<i>Bending direction</i>	<i>0.97</i>	<i>3.9%</i>	<i>36%</i>

Table 1: Strain correlations for bending loads (second cadaver).

Conversely, the prediction of strains induced by torsion is at the moment less satisfactory. This may be due to a mis-reproduction of boundary conditions or may even reflect an intrinsic limitation of the modelling procedure adopted: in fact, tissue anisotropy is not featured in the FE models, while it is likely to play a major role in torsion. Further studies are ongoing to clarify this aspect.

Acknowledgements

EC-funded projects LHDH (IST-2004-026932) and VPHOP (Grant #223865).

References

- Cody et al, J Biomech, 32:1013-20, 1999
- Crawford et al, Bone, 33:744-50, 2003.
- Schileo et al, J Biomech, 41:2483-91, 2008.
- Spruijt et al, Acta Orthop, 77:474-81, 2006.
- Taddei et al, Proc Inst Mech Eng [H], 217:111-9, 2004.

IDENTIFICATION METHOD OF SUBJECT-SPECIFIC CORNEAL MATERIAL CONSTANTS AND INTRAOCULAR PRESSURE

Masao Tanaka, Takeshi Matsumoto, Hisashi Naito, Hidemasa Tanaka

Graduate School of Engineering Science, Osaka University, Japan

Introduction

The quantification of the mechanical properties of cornea and the intraocular pressure is the first step for the precise preoperative planning/evaluation of keratomileusis. The direct in-vivo-measurement of intraocular pressure is applicable for animal study only, and Goldmann applanation tonometry is the standard for intraocular pressure measurement. However, it is well known that the pressure by applanation is much influenced by the central cornea thickness, the cornea curvature and so on. Concerning the material properties of cornea tissue, the conventional in vitro mechanical tests is the golden standard with no effective alternatives. Therefore, an evaluation method of the intraocular pressure and the material properties of cornea for individual patient is needed for the keratomileusis planning in practice.

Methods

Based on the finite element modelling of cornea as near-incompressible anisotropic hyperelastic material, the identification problems of intraocular pressure and material constants of cornea are formulated as optimisation problems. As the preliminary step for the identification problems, the estimation problem of cornea shape at natural state without intraocular pressure is formulated by referring the three-dimensional cornea shape of a subject in vivo under the presence of intraocular pressure his/her own as the minimization of the shape difference.

For the identification of intraocular pressure, the finite element simulation of Goldmann applanation tonometry is employed. In this problem, the intraocular pressure is identified by minimizing the error function defined between the simulated applanation force and the experimentally observed applanation force so as to reproduce the same cornea deformation with the same applanation force. For the identification of material constants of cornea, the error function of applanation force is recruited again and minimized. These three problems are coupling each other in terms of the natural shape under the absence of intraocular pressure, the material constants of cornea tissue, and the intraocular pressure of a subject under consideration. Therefore, these three optimisation problems are solved recurrently.

Results

Figure 1 is for the cornea shape under the absence of intraocular pressure estimated from the shape under the presence of pressure by tonometry with the material constants by inflation test [Anderson 2004]. Figure 2 is the sensitivity of the problem for the identification of material constants. These results show the rationale of the identification problems described.

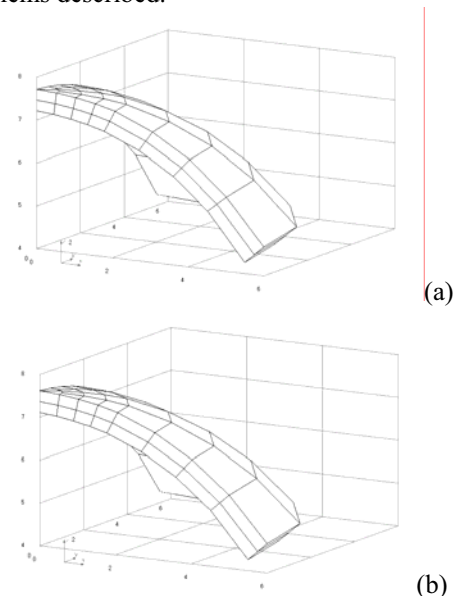


Figure 1: Cornea shapes under (a) presence and (b) absence of intraocular pressure. (one quarter)

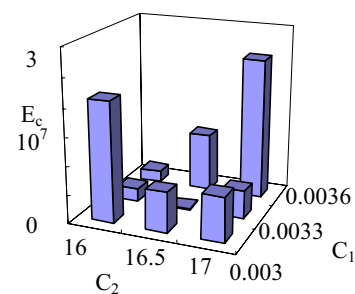


Figure 2: Applanation force error sensitive to material constant parameters

References

K. Anderson et al, J. Royal Soc Interface. 2004, 1(1):3-15, 2004.

Modelling internal organs

SEMI-ANALYTICAL METHOD FOR CALCULATION OF PRESSURE DROP IN HEALTHY AND DISEASED LUNG

Pierre-Antoine Muller (1), Ira Katz (1), Marine Pichelin (1), Georges Caillibotte (1)

1. Air Liquide CRCD Research Center, Medical Gases Group, France

Introduction

Decreasing the effort of breathing is a first importance issue in treatment and ventilation of lung diseased subjects – including severe asthmatics [Jolliet, 2002]. In order to mathematically evaluate the work of breathing the pressure drop is a good estimation of the resistance of gas flowing in the airways.

The objective of this work was to develop an analytical model for pressure drop in the lung. Pressure drop occurring in models of healthy and diseased (asthma) lungs are compared using successively air and Oxhel (78%-22% helium-oxygen mixture) as the breathed gas.

Methods

The basis of the lung models are a symmetric branching tree [Weibel, 1963]. The model of the asthmatic lung is obtained by applying a coefficient of constriction on the diameter of selected airways along the tree (e.g. figure 1).

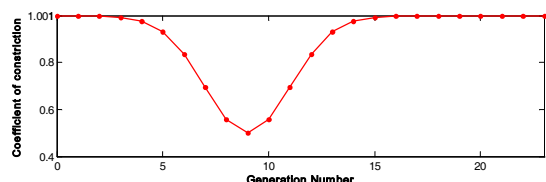


Figure 1: Coefficient of Constriction as a function of generation number

The pressure drop calculation method consists in separating pressure drop occurring in tubular branches and pressure drop due to bifurcations of the tree. Pressure drop in tubular branches is calculated using classical engineering formulas for pressure drop in pipes. As the variability of bifurcation geometries and flow regimes in the lung is very high, a correlation, giving pressure drop coefficient in bifurcations, was established by performing computational fluid dynamics (CFD) calculations on various bifurcation geometries and flow rates and implemented in the analytical model.

The model provides data on generational and cumulative pressure drop in physiological ranges of inhalation flow rates (see figure 2).

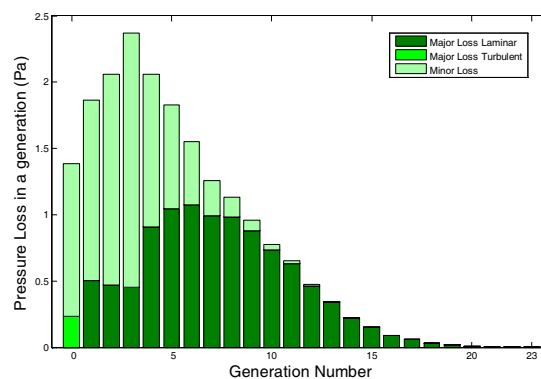


Figure 2: Generational Pressure Drop (Healthy lung – Air – Inhalation 25l/min)

Results

The model shows a decrease of pressure drop when using Oxhel compared to air both for healthy and diseased lungs. However, the decrease in pressure drop when Oxhel is used is much higher in the case of the diseased lung and for high ventilation rates.

Discussion

Even if several hypotheses were done on lung anatomy (healthy and diseased) and flow patterns, this model provides an estimation of the pressure drop in the lung due to the gas motion. It theoretically demonstrates a benefit in breathing Oxhel for diseased lungs; this is consistent with recent clinical data [Jaber et al., 2000]. This model provides a systematic methodology for understanding the role of airway resistance to the work of breathing to allow for the investigation of therapeutic gases in healthy and diseased lungs.

Acknowledgements

The authors gratefully acknowledge Dr A. Makarenko for his skilful assistance

References

- Jaber et al., Am J Respir Crit Care Med.,161:1191-1200, 2000
- Jolliet, Tassaux, J Respir Care Clin, 8:295-307, 2002
- Weibel, Springer-Verlag, 1963 (Book)

NEW PERCUTANEOUS PULMONARY VALVE DEVICE: FINITE ELEMENT TESTING IN PATIENTS' IMPLANTATION SITE

**Claudio Capelli (1), Francesco Migliavacca (2), Andrew M Taylor (1), Philipp Bonhoeffer (1),
Silvia Schievano (1)**

1. UCL Institute of Child Health & Great Ormond Street Hospital for Children, London, UK

2. LaBS, Department of Structural Engineering, Politecnico di Milano, Milan, Italy

Introduction

Since 2000, percutaneous pulmonary valve implantation has become a reality [Bonhoeffer, 2000], with over 800 patients already treated worldwide. However, due to morphological limitations [Schievano, 2007], the current device is suitable for only 13% of patients requiring treatment. A new device, which would potentially increase (>50%) the number of patients who could benefit from this minimally-invasive procedure, has recently been designed in collaboration with industry (Medtronic Inc., Minneapolis, USA). The main novelties of this device are an hourglass geometry and the use of self-expanding wires interwoven with a polymeric graft that should guarantee a greater adaptability of the device to different right ventricular outflow tract (RVOT) morphologies. The aim of this study was to mimic the implantation of this device in 50 selected patients using finite element (FE) modelling, in order to study the stent geometrical conformability and anchoring to the different implantation sites.

Methods

We retrospectively selected 50 consecutive patients with RVOT dysfunction. The study involved 3 phases, which were repeated for all 50 patients: 1) Magnetic resonance (MR) scan – 3D images of the patients' RVOT anatomies were acquired; 2) Imaging post-processing – MR data were elaborated to reconstruct a 3D volume of patients' RVOT; 3) FE analysis – Patients' reconstructed RVOT volumes were discretized and exported into FE structural software (Abaqus, Simulia, USA). Furthermore, a model of the new stent was designed and discretized with beam elements (Figure 1a). The analysis consisted of 2 steps. First, the stent was crimped inside the RVOT. Second, the stent was released, enabling contact with the RVOT. The expanded stent diameters and areas of contact with the RVOTs were measured.

Results

The stent, during the recovery of its elastic deformation and whilst in contact with the RVOT wall, adapted its shape to the patients' implantation site morphologies (Figure 1b).



Figure 1: FE model of the stent and an example of the stent implantation in a patient's RVOT.

Contact areas with the RVOT wall were identified in the distal and proximal struts of the stent for all patients (Figure 2).

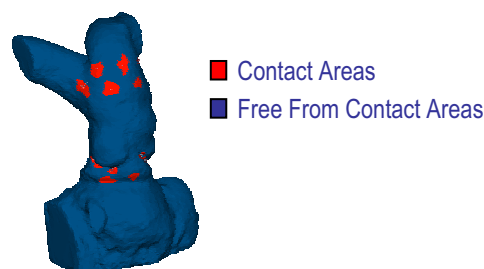


Figure 2: Map of the stent-RVOT contact areas.

Expanded diameters were measured at the distal, central and proximal section of the stent and an average diameter was calculated for each section. The central portion of the stent, holding the valve, was fully deployed in 48% of the patients. The proximal diameter guaranteed good anchoring in 22 patients whilst the distal diameter in 42 patients.

Discussion

Patient morphological reconstructions from MR images combined with FE analyses may help optimise a new device for percutaneous pulmonary valve implantation. Furthermore, FE analysis of stent implantation may help clinicians in the RVOT morphological suitability assessment and to evaluate the stability of the device in each individual patient, before the actual procedure is performed.

References

- Bonhoeffer P et al, Lancet, 21:1403-1405, 2000.
- Schievano S et al, J Cardiovasc Magn Reson, 9:687-695, 2007.

A SYSTEMS ENGINEERING SIMULATOR FOR PATHOPULMONARY PHYSIOLOGY RESEARCH

Anup Das and Declan G Bates, Department of Engineering, University of Leicester, UK.
Jonathan G Hardman, Department of Anaesthesia, Queen's Medical Centre, Nottingham, UK

Introduction

Mathematical and Computational simulation models across many fields of medicine could be better exploited by connecting them with the many powerful analytical tools currently available to systems and control engineers. These tools could be employed for the purposes of parameter estimation (system identification), verification and validation (robustness analysis) and structural investigation (numerical optimisation). In order to do this in an efficient manner, such simulation models need to be implemented in numerical computing environments such as MATLAB[®], since the corresponding analytical tools are themselves typically developed and applied in these environments. This poses a challenge for many simulation models used in medical applications, which may be extremely computationally intensive and are thus often coded using familiar and fast processing languages such as C++, FORTRAN or Pascal. In this paper, we describe the implementation of a detailed pulmonary physiology simulator, [Hardman, 2003] [McCahon, 2008], in MATLAB[®], highlight some of the corresponding modelling and computational challenges that arise, and illustrate the power of tools from control engineering to analyse the robustness and validity of the model against data from patient populations.

Methods

The core models in the simulator are designed to represent a dynamic in-vivo pulmonary situation using a mass-conserving, iterative, arithmetical set of equations based on well-established physiological principles. Designing the simulator as an iterative model allows the accurate representation of gradual changes in several parameters which are otherwise hard to estimate *in vivo*, but significantly increases the computational overheads associated with the simulation. Each iteration through the algorithm is indicative of a period of physiological time, and represents the movement of gas through the pulmonary system in that period of time. The overall system is modelled as comprising of a ventilator, anatomical deadspace, ventilated and perfused alveoli, cardiovascular system and a simplified representation of peripheral tissue.

The anatomical deadspace is divided into layers and no mixing between layers is assumed. In the perfused lung, all the gases come to a user defined level of equilibrium with pulmonary blood flow

based on the pressure gradient and the solubilities of gases in blood. It is assumed that there is no tension disparity in individual alveolar regions, i.e. centre of the alveolus compared to the alveolar capillary boundary. Complete mixing of gases within the alveoli is assumed. The pH of the blood is defined by the base excess, temperature and plasma CO₂ content. Each alveolar compartment can be attributed a specific pulmonary vascular resistance, bronchiolar resistance and compliance. Varying compliances for individual alveolar compartments can be considered. Bronchiolar resistance variations as a result of expansion of the lungs are included. The bronchiolar flow can be laminar or turbulent according to the Reynolds number. A common resistance to flow is included. Peripheral tissue O₂ transfer contains plain extraction of V_{O₂} (consumed O₂ during respiration) from the total O₂ volume of the tissue unit. During an iteration, peripheral capillary gas tensions reach a dynamic equilibrium with the tissue compartment. The acid base properties of blood are inferred simply through the pH and P_{CO₂} (CO₂ partial pressure in blood) levels. Small airway closure and the resultant recruitment pressure variation are integrated along with Hypoxic Pulmonary Vasoconstriction (HPV) under which pulmonary arterioles constrict in response to low alveolar oxygen tensions. Humidification and temperature effects on the inspired dry air concentrations are also incorporated.

Results

The credibility of the core models employed in the simulator has been established through discussion with experts and by validation against published clinical data [Hardman, 2000] [Hardman, 2003]. In this paper, we show how a new implementation of the model in a numerical computing environment facilitates significant further validation of the model using tools from systems and control engineering.

References

- Hardman, J.G. et al, *Anesthesia & Analgesia*, 90(3):614-618, 2000.
- Hardman, J.G. et al, *Anesthesia & Analgesia*, 97(6):1840, 2003.
- McCahon, R.A. et al, *British Journal of Anesthesia*, 101(3):358-65, 2008.

MULTI-SCALE MODELING OF LUNG PARENCHYMA

Lena Wiechert, Sophie Rausch, Wolfgang A. Wall

Institute for Computational Mechanics, Technische Universität München, Germany

Introduction

Mechanical ventilation of patients suffering from lung failure is a vital supportive therapy. Improper methods of ventilation, however, can cause overstraining of lung tissue resulting in additional and frequently lethal mechanical and inflammatory injuries. These so-called ventilator-induced lung injuries (VILI) occur mainly at the alveolar level of the lung. In order to bring more light into the involved phenomena, we have started to establish a comprehensive three-dimensional computational model of lung parenchyma [Wiechert, 2008].

Methods

For a geometric description of a ventilatory unit, we utilize assemblages of tetrakaidehedra representing individual alveoli. Random inter-alveolar connections are established with the help of a novel labyrinthine algorithm.

For the mathematical description of alveolar soft tissue behavior, a polyconvex hyperelastic constitutive law accounting for general histologic information is employed.

Pulmonary alveoli are covered by a thin, continuous fluid film with a monomolecular layer of surface active agents (the so-called surfactant) located on top of it. To model the influence of this liquid lining, we established a surface coupling of structural and interfacial mechanics [Wiechert, 2009]. The highly nonlinear and dynamic nature of surfactant is taken into account using an adsorption-limited constitutive model that relates surface stresses to the interfacial concentration of surfactant molecules [Otis, 1994].

In order to prescribe physiologically reasonable boundary conditions (bc) to the modeled ventilatory units, alveolar assemblages are embedded in a global, homogenized lung model by means of a computational multi-scale approach. We established a nested solution technique that extends existing approaches to coupled and dynamic scenarios inherent to (mechanical) ventilation.

Results and Discussion

Since global parenchyma and local alveolar models are simulated simultaneously in course of the developed multi-scale approach, a mutual information transfer is enabled. Figure 1 shows exemplarily the overall heterogeneous deformation of an idealized lung tissue strip due to locally

different interfacial configurations. This phenomenon is known to occur in case of lung failure.

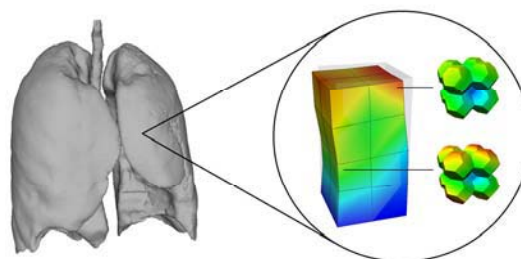


Figure 1: Simulation of the overall inhomogeneous behavior of a lung tissue strip due to local alveolar heterogeneities. Exemplary alveolar micro-structures are shown enlarged compared to original size.

By embedding local alveolar micro-structures in the homogenized lung parenchyma, boundary conditions are derived inherently considering the influence of surrounding tissue. Therefore, local alveolar deformation can be simulated more realistically with our model compared to previous approaches not considering this interdependence effect (cf. Figure 2 for a comparison of bc).

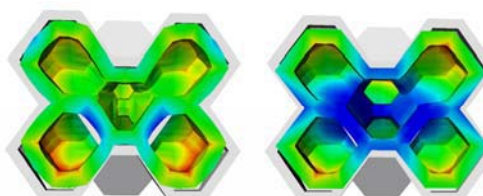


Figure 2: Overall deformation of alveolar assemblages under surface tension of interior liquid linings. Left: without specified bc. Right: bc derived in a nested multi-scale simulation.

While only homogenized material parameters for parenchyma could be determined from experiments up to now, the introduced method in combination with an inverse analysis will also allow the identification of local properties of alveolar walls for the first time. Based on that, local in vivo alveolar stresses and strains can be quantified, providing essential insights in the mechanisms of VILI.

References

- Wiechert et al, ESAIM Proc, 23 :98-113, 2008.
- Wiechert et al, J Eng Mech, in press, 2009.
- Otis et al, J Appl Physiol, 77:2681-2688,1994.

MODELLING OF TEMPERATURE FIELD IN A TISSUE WITH A TUMOR SUBJECTED TO EXTERNAL ELECTROMAGNETIC FIELD

Ewa Majchrzak, Marek Paruch

Department for Strength of Materials and Computational Mechanics,
Silesian University of Technology, Poland, e-mail: marek.paruch@polsl.pl

Introduction

Hyperthermia (42-46°C) is a therapeutic method that utilizes different technologies to obtain an artificial increase in temperature of certain types of cancer, such a skin cancer [Lv, 2005]. In the paper the heating of tissue induced by two external plate electrodes is modelled. Tissue contains a tumor with embedded nanoparticles in order to concentrate heat deposition at the tumor region and to avoid the damage of healthy tissue surrounding the tumor. The aim of investigations is to determine transient temperature field in the domain considered and to estimate the effect of nanoparticles concentration on the heating area assuring the damage of tumor region.

Formulation of the problem

The simplified 2D electromagnetic field and transient temperature field induced by two external electrodes in the biological tissue containing a tumor with magnetic nanoparticles (as shown in Figure 1) are considered.

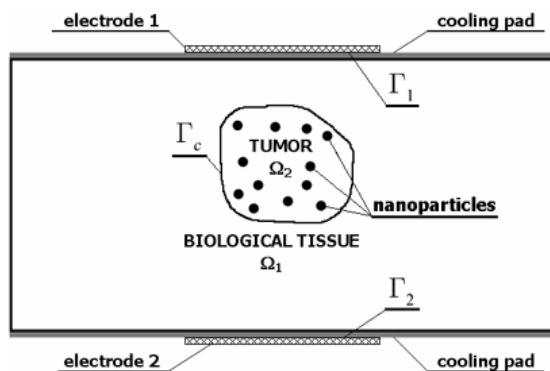


Figure 1: Hyperthermia system.

The electric potential inside the healthy tissue and tumor region is described by the system of Laplace equations supplemented by adequate boundary conditions [Lv, 2005; Majchrzak, 2008]. The temperature field in the domain considered can be determined using the system of Pennes equations

$$c_e \frac{\partial T_e}{\partial t} = \lambda_e \nabla^2 T_e + G_{Be} c_B [T_B - T_e] + Q_{met e} + Q_e \quad (1)$$

where $e = 1, 2$ correspond to the healthy tissue and tumor region, respectively, c_e is the volumetric specific heat of tissue and tumor [$J/(m^3K)$], T_e denotes the temperature, t is the time, λ_e [$W/(mK)$] is the thermal conductivity, $k_e = G_{Be} c_B$ (G_{Be} [1/s] is the perfusion rate, c_B [$J/(m^3K)$] is the volumetric specific heat of blood), T_B is the supplying arterial blood temperature, $Q_{met e}$ is the metabolic heat source and Q_e is the source function connected with the electromagnetic field.

Heat generation Q_1 [W/m^3] due to the electromagnetic dissipated power in healthy tissue (domain Ω_1) depends on the conductivity σ_1 [S/m] and the electric field \mathbf{E}_1 [Lv, 2005]

$$Q_1 = \sigma_1 |\mathbf{E}_1|^2 / 2 \quad (2)$$

The tumor region with embedded magnetic particles is treated as a composite and due to the assumed homogeneity of Ω_2 the mean value of electrical conductivity σ_2 of this sub-domain can be approximated as $1/\sigma_2 = (1-\theta)/\sigma_2' + \theta/\sigma_3$, where σ_2' , σ_3 are the electrical conductivities of tumor and particles, respectively, and $\theta = n\pi r^2$ is the concentration of particles (n is the number of particles, r is the radius of particle). Under the assumption that P_t is the tumor area one has

$$Q_2 = \frac{\theta}{P_t} P_{SPM} + \frac{P_t - \theta}{P_t} \frac{\sigma_2 |\mathbf{E}_2|^2}{2} \quad (3)$$

where P_{SPM} is the heat generation connected with the superparamagnetism.

On the stage of numerical computations the boundary element method for nonhomogeneous domain (tumor and healthy tissue) has been applied.

Results

Introduction of nanoparticles causes the control increase of temperature in the tumor region.

Acknowledgements

This work was supported by Grant No N N501 3667 34 from the Polish Ministry of Education and Science.

References

- Lv et al, IEEE Transactions on Nanobioscience, Vol. 4, No 4, 284-294, 2005.
- Majchrzak et al, Acta of Bioengineering and Biomechanics, Vol. 10, No 2, 29-37, 2008.

MODELLING OF LOCAL AND GLOBAL RENAL FUNCTION IN THE PHYSIOME CONTEXT

Jérôme Bazin, Samira Bakiri, Thibault Grosse, and S. Randall Thomas

IBISC, CNRS FRE 3190, Evry F-91000, France

In the context of IUPS Physiome project, and its European manifestation, the Virtual Physiological Human, we present results for modelling of renal physiology on two levels: a model of renal distal tubule transport targeting effects on arterial blood pressure, and a library of kinetic transporter and other local models for the renal physiome, for implementation in our integrated multi-organ 'core model environment' [Thomas 2008; Defontaine 2005].

A library of detailed local models for the Renal Physiome. There exists a rich literature of mathematical models of various aspects of renal function at all scales from the kinetics of membrane channels and coupled transporters, inclusion of these in tubule models of segmental reabsorption/secretion along the nephron, to models of tubuloglomerular feedback regulation and renal hemodynamics, and medullary models of nephrovascular solute and water recycling involved in the urine concentrating mechanism. However, there has been scant effort at integrating these detailed 'local' models into global descriptions of renal function sensitive to hormonal and neural controls and relevant to questions of the role of the kidneys in whole organism processes such as blood pressure regulation. This is the goal of our core modelling environment.

Via the dependence of salt excretion on arterial pressure (PA), known as the 'pressure-natriuresis relation' or the 'renal function curve' [Guyton 1987, 1990a, 1990b], the kidney is responsible for setting the long-term level of PA. As a consequence, the kidney is necessarily involved in the genesis of hypertension, as reflected in the fact that genetic polymorphisms linked to hereditary hypertension invariably involve the kidney. In particular, several hypertension-related defects involve gain-of-function mutations in membrane proteins responsible for salt reabsorption in the late portions of the nephron. Major anti-hypertensive drugs, such as the thiazides, act by inhibiting these transporters. However, the effectiveness of such drugs depends on several other steps in the salt reabsorption process, including especially the Na,K-ATPase, which in turn depends on connections to the cytoskeleton.

In order to explore these scenarios *in silico*, we present a model of distal tubule transport based on kinetics of the implicated membrane channels and transporters (Andersen et al. 1985; Chang & Fujita 1999, 2001; Monroy et al. 2000; Weinstein 1995, 2005). This involves the constitution of a library of available kinetic descriptions for membrane channels and transporters (and their various isoforms) in the different cell types along the nephron. We will present simulation results relevant to the role of polymorphisms of alpha-adducin (a cytoskeleton protein associated with the Na,K-ATPase in distal tubule cells) in the effectiveness of thiazide diuretics.

Acknowledgements

The research presented here has received funding from: the European Community's 7th Framework Program (VPH-NoE, grant agreement n° 223920), and the French National Research Agency (ANR projects SAPHIR (ANR-06-BYOS-0007-01), CorBioMath (ANR-05-BLAN-0247-06), and BIMBO (ANR-08-SYSC-002-04)). We also acknowledge the contribution of numerous workshops organized by the GdR STIC-Santé CNRS 2647/INSERM.

References

- Andersen, O. S., J. E. Silveira, et al. *J Gen Physiol* 86(2): 215-34, 1985.
- Chang, H. and T. Fujita, *Am J Physiol* 276(6 Pt 2): F952-9, 1999.
- Chang, H. and T. Fujita, *Am J Physiol Renal Physiol* 281(2): F222-43, 2001.
- Defontaine, A., A. I. Hernández, and G. Carrault, *Lecture Notes in Computer Science*, pp. 394-403, 2005.
- Guyton, A. C., *Hypertension* 10(1): 1-6, 1987.
- Guyton, A. C., *Am J Physiol* 259(5 Pt 2): R865-77, 1990a.
- Guyton, A. C., *Hypertension* 16(6): 725-30, 1990b.
- Monroy, A., C. Plata, et al., *Am J Physiol Renal Physiol* 279(1): F161-9, 2000.
- Thomas, S. R. et al., *Philos Transact A Math Phys Eng Sci* 366(1878): 3175-97, 2008.
- Weinstein, A. M., *Am J Physiol Renal Physiol* 289(4): F699-720, 2005.
- Weinstein, A. M., *J Gen Physiol* 105(5): 617-41, 1995.

Modelling mechanobiology processes

FEM AND CFD-BASED MODEL TO ANALYZE MECHANICAL STIMULATION OF OSTEOGENESIS WITHIN PLA-GLASS SCAFFOLD

Jean-Louis MILAN, Josep A. PLANELL, Damien LACROIX

Institute for Bioengineering of Catalonia, Technical University of Catalonia, Barcelona, Spain

Introduction

Porous biodegradable scaffolds made of polylactic acid (PLA) and calcium phosphate glass provide temporary architectural patterns for bone formation and open new perspectives in engineering and surgery of osteocartilaginous tissue. For instance, tissue formation may be stimulated mechanically within scaffolds submitted to appropriate loadings. A numerical model based on finite element method (FEM) and computational fluid dynamics (CFD) is proposed here to analyze the cell-scale mechanical stimuli within a PLA-Glass scaffold penetrated by a fluid phase and submitted to dynamic compression.

Methods

A FEM model was created from reconstruction of a 6mm-diameter and 7mm-height cylindrical PLA-Glass scaffold rendered by micro tomography [Navarro2006]. PLA ($E=3.6$ GPa) and Glass (71 GPa) phases were identified in the model and material properties were assigned. CFD model was created to represent the fluid phase ($\mu=1.45 \cdot 10^{-3}$ Pa.s) within the scaffold pores. A confined compression of 5% was simulated at a strain rate of $5 \cdot 10^{-3} \text{ s}^{-1}$ in the FEM-CFD model considering uncoupled fluid-structure scheme: the compression of the scaffold alone was computed in the FEM model under static conditions (Abaqus, Simulia) while the fluid flow induced by dynamic compression was computed in CFD model neglecting scaffold deformation and considering a Newtonian fluid in laminar flow (Fluent, Ansys).

Results

Under static compression of 5% the FEM model deforms by a spatial reorganization of internal pore walls involving modes of deformation of buckling and bending and introducing concentration of strain and stress in thinnest walls. A reaction force of 180 mN is generated indicating an overall stiffness of 130 kPa. Shear strain of [100;10,000] μstrain is also generated on 51% of total surface area of scaffold (Figure 1). Under dynamic compression of 5% at strain rate of $5 \cdot 10^{-3} \text{ s}^{-1}$ fluid flows through scaffold pores at velocities of [0.005;0.15] mm/s generating shear stresses of [0.5;5] mPa on 80% of total surface area of the scaffold (Figure 2) while 48% of the total surface area is submitted to fluid flow shear stress between [1;2] mPa.

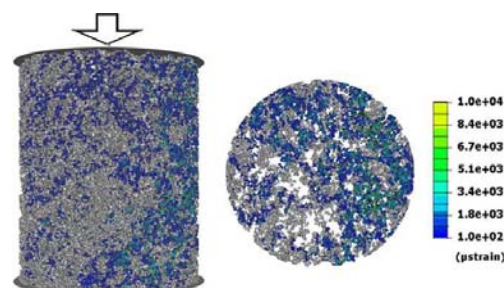


Figure 1: Shear strain distribution in FEM model under 5% static compression.

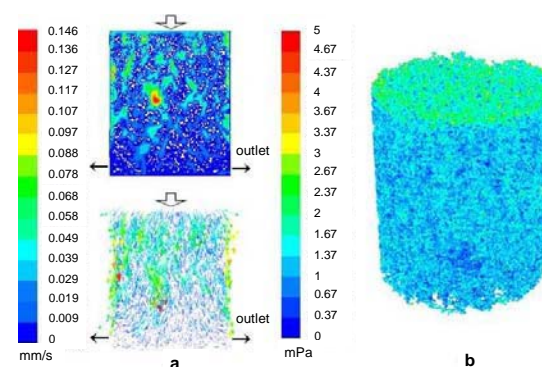


Figure 2: Fluid flow in CFD model under dynamic compression of 5% at a strain rate of $5 \cdot 10^{-3} \text{ s}^{-1}$. a) Velocities. b) Shear stress on scaffold surface

Discussion

Following Prendergast et al. (1997) and Porter et al. (2005) the mechanical environment generated in the PLA-Glass scaffold by dynamic compression of 5% at strain rate of $5 \cdot 10^{-3} \text{ s}^{-1}$ may stimulate bone formation. Strain rate of $5 \cdot 10^{-4} \text{ s}^{-1}$ may promote cell proliferation while strain rate of $5 \cdot 10^{-2} \text{ s}^{-1}$ may be detrimental. This model may therefore provide additional information to in vitro bioreactor studies [Charles-Harris2008] and identify the appropriate mechanical loading stimulating bone formation.

Acknowledgements

Financial support from Spanish Ministry of Science and Innovation (MAT 2005 - 07244) is acknowledged.

References

- Navarro et al., Adv Polym Sci, 200:209-31, 2006.
- Porter et al. J Biomech 38:543-549, 2005.
- Prendergast et al., J. Biomech 30:539-548,1997.
- Charles-Harris et al., J Mater Sci Mater Med 19:1503-13, 2008.

POTENTIAL FUNCTIONS TO DESCRIBE MECHANICAL CELL-CELL INTERACTIONS

Jeremy Cope (1), Dawn Walker (1), Rod Smallwood (1), Rod Hose (2)

1. Department of Computer Science, University of Sheffield, Sheffield S3 7HQ, UK;
2. Department of Medical Physics & Clinical Engineering, University of Sheffield, Sheffield S10 2JF, UK

Introduction

There is a growing body of evidence suggesting that the mechanical environment of the cell is a key determinant of cell behaviour (see e.g. [Assoian, 2008]). Conventional biomechanical models of biological tissues are usually continuum-based. However, real tissues are not homogenous or smoothly varying. They are made up of discrete parts and even one cell behaving differently can make a qualitative difference to their macroscopic properties. For example, a single cancer cell in a group of normal cells will grow into a tumour given the right circumstances. In a continuum model, such localised differences are smeared out by the averaging effect and disappear.

Agent- or individual-based modelling (IBM) can overcome this shortcoming by using software agents to model individual cells (e.g. [Walker, 2004]). An agent, in this context, is a self-contained unit of software, which obeys a built-in set of rules describing how it may alter its state and interact with its environment. To make use of this, a formal method of describing physical cell-cell interactions is needed.

Methods

Potential functions are commonly used in molecular dynamics (MD) simulations, and have been used by [Newman, 2005] to describe behaviour on a subcellular level. They quantify the potential energy of a given configuration of particles, and can be differentiated with respect to the position of each particle to give a force that can be used to simulate the time-evolution of the system.

An array of identical cells, described as points in a hexagonal close packed configuration was generated. Each cell was allowed to interact only with its nearest neighbours, and the potential energy of each interaction was defined as a function of the distance r between the two points. An increasing series of strains was then applied to the block as a whole and the stress at equilibrium calculated to give a stress-strain curve.

This was repeated for two different potential functions (with appropriate values for constants): a simple quadratic potential given by

$$U_1(r) = k(r - r_0)^2 \quad (1)$$

and a generalized Morse potential given by

$$U_2(r) = U_0 \exp\left(-\frac{r}{\xi_1}\right) - V_0 \exp\left(-\frac{r}{\xi_2}\right) \quad (2)$$

Results

Even this simple model is able to capture key macroscopic behaviours expected of biological tissue.

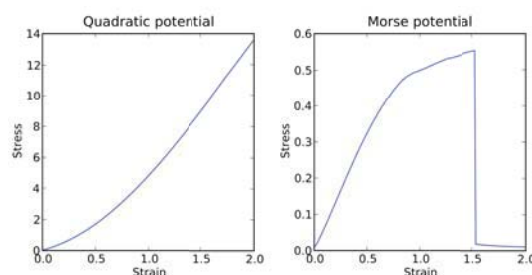


Figure 1: Typical stress-strain curves given by the models described above

The quadratic potential demonstrates the classic J-shaped curve of a polymeric material, caused by gradual alignment of bonds along the direction of tension. The Morse potential shows strain-softening and eventual failure caused by gradual failure of individual bonds.

Discussion

Despite the simplicity of this model it is able, from an individual-oriented description, to reproduce the properties expected of a biological tissue. Potential functions show great promise to provide an abstract and widely applicable description of the physical interactions between biological cells. The next stage will be to develop potential functions that reproduce empirical results on the tissue level based on theory from cell-level results.

References

- Assoian & Klein, Trends Cell Biol, 18(7):347–352, 2008
 Newman, Math Biosci Eng, 2(3):613-624, 2005
 Walker et al, Biosystems, 76(1-3):89-100, 2004

TRABECULAR BONE REMODELING SIMULATION CONSIDERING OSTEOCYTIC RESPONSE TO FLUID-INDUCED SHEAR STRESS

Taiji Adachi (1, 2), Yoshitaka Kameo (1), Masaki Hojo (1)

1. Department of Mechanical Engineering & Science, Kyoto University, Japan

2. Computational Cell Biomechanics Team, RIKEN, Japan

Introduction

Under dynamic loading, bone matrix deforms and its stress/strain field generates fluid flow in the lacuno-canalicular system. This interstitial fluid flow induces shear stress on the cell process membrane that is believed to stimulate the mechanosensitive osteocytes [Weinbaum, 1994]. In this study, we proposed a rate equation for the trabecular bone remodeling considering fluid-induced shear stress in the lacuno-canalicular system. Based on the rate equation, computational simulation of trabecular bone remodeling was conducted for a single trabecula under cyclic uniaxial loading, in which the fluid flow and pressure field were analyzed based on the poroelasticity [Cowin, 1999].

Methods

Interstitial fluid flow induced by bone matrix deformation was analyzed using a finite element method based on poroelasticity. For the simplicity, the bone matrix was assumed to behave as an isotropic elastic material. To clearly demonstrate the basic mechanisms of the complex trabecular bone adaptation by remodeling, a simplified mathematical model taking into account the mechanosensing and communication by osteocytes was proposed here.

A framework of the model for the trabecular bone remodeling is the followings. Mechanical loading applied to bone induces bone matrix deformation and pressure gradient in the interstitial fluid that drives the fluid flow. The osteocytes at \mathbf{x}_b respond to the fluid-induced shear stress τ_p , and deliver its mechanical signal:

$$S_{oc}(\mathbf{x}_b) = \int_{\Omega} w_S(l) |\tau_p| d\Omega \quad (1)$$

to the neighboring cells through the intercellular network system. That is, the cells on the trabecular surface at \mathbf{x}_{sf} are regulated by the integrated signal:

$$S_{sf}(\mathbf{x}_{sf}) = \int_{\Omega} w(l) S_{oc}(\mathbf{x}) d\Omega. \quad (2)$$

The proposed remodeling rate equation is applied to a single trabecula (Fig.1a) under cyclic uniaxial loading. As boundary conditions, a shear-free condition is applied to the lower surface, and the free fluid flow across all the trabecular surfaces is assumed. On the upper end, cyclic loading $F(t) = -a \sin(2\pi ft)$ ($a = 0.1$ MPa, $f = 1$ Hz) is applied.

Results and Discussion

Morphological change of the trabecula and distribution of the flow-induced shear stress are illustrated in Fig.1. At the initial state (Fig.1a), higher shear stress at the both ends with an acute angle generate large mechanical stimulus to the osteocytes and significant bone deposition. As a result of remodeling, shear stress near the trabecular surface became uniform and the remodeling reached equilibrium with a morphology aligning along the loading direction at 30 days (Fig.1d).

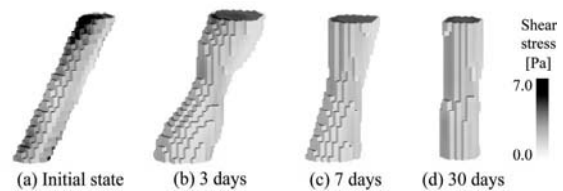


Figure 1: Morphological change of a trabecula and distribution of fluid-induced shear stress.

The seepage velocity in the 30-day-trabecula is shown in Fig.2, in which the velocity distributes nonuniformly near the trabecular surface, even after the trabecula aligns along the loading direction. This result indicates that the internal structure, such as canaliculi, after new bone deposition is locally regulated independently from the global trabecular orientation. This nonuniformity indicates that the remodeling history, formation/resorption influenced by loading conditions, remains in the trabeculae, suggesting that anisotropy of the permeability may locally affect adaptive remodeling process.

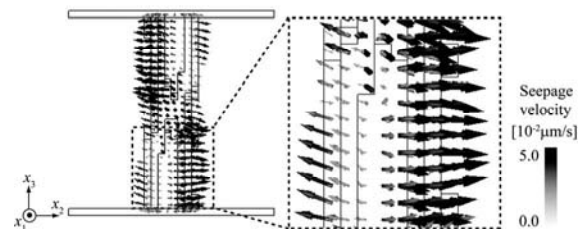


Figure 2: Seepage velocity at $t = 1.0s$ at 30 days.

This research was supported partly by the MEXT, Japan.

References

- Weinbaum S. et al., J. Biomech., 27(3): 339-360, 1994.
Cowin, S. C., J. Biomech., 32(3): 217-238, 1999.

COMPUTATIONAL SIMULATION OF TISSUE DIFFERENTIATION IN A BONE INGROWTH CHAMBER: THE EFFECT OF VASCULARITY

Hanifeh Khayyeri (1), Sara Checa (1), Magnus Tagil (2), Patrick J. Prendergast (1)

1. Trinity Centre for Bioengineering, School of Engineering, Trinity College Dublin, Ireland;

2. Department of Orthopaedics, Lund University Hospital, Lund, Sweden

Introduction

Angiogenesis plays a key role in the bone formation process. Newly formed capillaries provide cells with sufficient oxygen and nutrients required for bone cell survival and proliferation [Checa 2009]. Previous mechanobiological simulations of tissue differentiation inside a mechanically controlled bone chamber were only able to corroborate stem cell fate based on only mechanoregulation to a certain degree [Khayyeri, 2008]. An issue with corroboration of mechanobiology theories is that, even in well controlled environments, tissue differentiation patterns differ considerably between specimens. Since oxygen diffusion is limited to few hundred micrometers from capillaries, the random nature of the vascular network and growth has a significant effect on the patterns of newly formed bone [Checa, 2009] and might be largely responsible for the variable nature of the tissue differentiation process. Here we investigate whether cell differentiation based on mechanoregulation *and* site-specific vascularity can capture the effects of mechanical loading on the tissue differentiation process inside the bone chamber as seen in the animal experiments [Tagil, 1999]. In particular our aim in this paper is to determine what degree of variability may be attributed to the random nature of vascularization, and to determine if it can explain the variability seen in experimental results.

Methods

To model cell activities, a rule-based 3D lattice approach [Perez, 2007] was adopted, where each point of the lattice represented a position a cell could occupy. The cells in this lattice could migrate, proliferate, apoptose and differentiate randomly [Perez, 2007] in 3D and form new capillaries, all depending on the mechanical environment (determined using poroelastic FE-analysis in Abaqus). Cell differentiation was regulated by a biophysical stimulus (determined as a combination of fluid flow and shear strain [Prendergast, 1997]) and the local vascularity. Depending on the level of stimulus, mesenchymal cells were differentiated into osteoblasts, chondrocytes and fibroblasts. In regions of poor vascularity cells under an appropriate mechanical stimulus would follow a chondrogenic rather than an osteogenic pathway [Checa, 2009].

Simulations corresponding to the *in vivo* bone chamber experiments [Tagil, 1999] were performed, where the chambers were kept unloaded for 3 weeks allowing mesenchymal and endothelial cells to grow in and then subjected to a mechanical load of 2 MPa, every 12 hour, for another 6 weeks.

Results and Discussion

After 9 weeks of simulation, the loaded chamber is well vascularized and filled with mainly fibroblasts and small amounts of osteoblasts and chondrocytes; whereas the simulation of the control chamber (unloaded for 9 weeks) predicts only osteoblast differentiation.

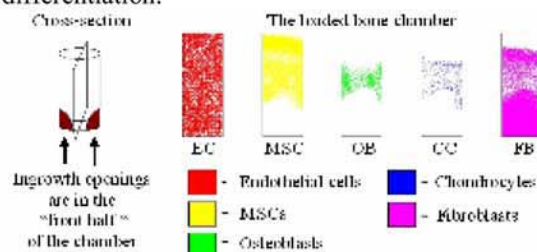


Figure 1: The rectangles illustrate the cross-section of the bone chamber with the ingrowth holes located at the bottom left. The coloured lattice points show the cell phenotypes in the loaded bone chamber after 9 weeks of simulation.

The model was able to predict the chondrocyte differentiation in the loaded chamber, which is often found in the specimens. Although the inclusion of angiogenesis in the model contributes to more variability in the simulations, the model was not able to capture the inter-specimen variability of the experiments. This raises the question whether tissue differentiation is genetically variable in an animal population.

Acknowledgements

The authors would like to thank Inger Martensson for her technical assistance in the laboratory. This project has been funded by Science Foundation Ireland Principal Investigator Award.

References

- Checa et al, Biomed Eng, 37:129-145, 2009
- Khayyeri et al, IFMBE proceedings, 2008
- Perez et al, J Biomech, 40:2244-2253, 2007
- Prendergast et al, J Biomech, 30:539-548, 1997
- Tagil et al, J Orth Res, 17:200-204, 1999

Cellular modelling #2

FLAME/COPASI: AN INTEGRATED COMPUTATIONAL FRAMEWORK FOR MULTISCALE MODELLING

Salem Adra¹, Rod Smallwood¹, Mike Holcombe¹

1. Department of Computer Science, Sheffield University, Kroto Research Institute, Broad Lane, Sheffield, S3 7HQ, UK

Introduction

Agent-based modelling facilitates research in complex systems and provides a complementary approach to understanding complex biological systems. FLAME (Flexible Large-scale Agent Modelling Environment) [Coakley, 2007] (www.flame.ac.uk) is an agent-based modelling framework developed at the University of Sheffield and has been successfully used to model the emergent behaviour of various biological systems (e.g. keratinocyte colony formation [Sun, 2007] and urothelial cells [Walker, 2004]). One of the main features of FLAME is that it automatically generates parallel and serial executable code for the model specification defined by the user (in XML format).

In order to increase the usability of FLAME and encourage the reusability of curated models, it was important to improve the connectivity of FLAME to other external solvers and to be able to import models specified in other widely used modelling languages such as SBML or CellML. In this paper we present an integrated computational framework which links FLAME to COPASI [Hoops, 2006] and allows the user to import SBML models (through COPASI) to be used as parts of agent-based models within FLAME.

COPASI

COPASI (Complex Pathway Simulator) [Hoops, 2006] (www.copasi.org) is a software application used for simulating and analyzing biochemical networks. COPASI provides many useful functionalities such as stochastic and deterministic time course simulation, steady state analysis, metabolic control analysis and optimisation of arbitrary objective functions. COPASI can also import SBML models and export ODEs into C code.

FLAME/COPASI Integration

An interface has been implemented which links FLAME and COPASI. COPASI models can now be initialised and called within FLAME to define and run time-course simulations of biochemical networks which can take place within the agents (e.g. intra-cellular signalling pathways) or the environment (e.g. inter-cellular reactions). The interface provides the following main functionalities:

(1) Setting up a COPASI model using FLAME generated code, (2) Updating a COPASI model

based on the agents' memory values and vice-versa, (3) Executing a COPASI model, and (4) Querying the COPASI report storing the simulation results.

```
<environment>
<var><type>double</type><name>calcium_level</name></var>
<var><type>double</type><name>substrate_width</name></var>

<!--*****COPASI DATA STRUCTURE*****-->
<datatypes>
<datatype>
<name>copasi_data</name>
<desc>Used by Cells to hold copasi data</desc>
<var><type>char_array</type><name>compartment</name></var>
<var><type>double</type><name>volume</name></var>
<var><type>char_array</type><name>metabolite</name></var>
<var><type>double</type><name>concentration</name></var>
</datatype>
</datatypes>
<!--*****-->

<functions><file>functions.c</file></functions>
</environment>
```

(a) model.xml

```
<states>
<environment>
<<calcium_level>1.3</calcium_level>
<<substrate_width>500.0</substrate_width>
</environment>

<tno>0</tno>

<xagent>
<name>keratinocyte</name>
<id>1</id>
<copasiData>{{PM,1,R1,20}, {PM,1,R2,20}, {PM,1,TGF_beta,0}}</copasiData>
<type>0</type>
<x>56</x>
<y>321</y>
<z>0</z>
<motility>1.2</motility>
<dir>2.3</dir>
</xagent>
```

(b) 0.xml

Figure 1 Snapshots from (a) a model specification file "model.xml" and (b) its initial state file "0.xml" which will be simulated by FLAME/COPASI.

Discussion

FLAME/COPASI is a useful modelling framework that has been used to simulate a multiscale model of skin wound healing process and gene regulation in E.coli. The approach adopted to link FLAME and COPASI is a simple yet efficient approach which maintains software modularity. Future work will include linking FLAME to other solvers, such as PCEnv and JSim.

Acknowledgements

We gratefully acknowledge financial support from EPSRC (UK) for this research.

References

Coakley, PhD Thesis, University of Sheffield, 2007.
 Hoops et al, Bioinformatics, 22: 3067-74, 2006.
 Sun et al, Journal of the Royal Society Interface, 4: 1107-1117, 2007.
 Walker et al, Biosystems, 76 (1-3): 89-100, 2004

DEVELOPMENTS OF COARSE GRAINING DNA MODELS FOR SINGLE NUCLEOTIDE RESOLUTION ANALYSIS

Kentaro Doi, Yukihiro Toyokita, Tomoaki Haga, Hirofumi Shintaku, Satoyuki Kawano

Department of Mechanical Science and Bioengineering, Toyonaka, Osaka 560-8531, Japan

Introduction

Various properties of double strand DNAs have received considerable attention from the technological aspects as well as the scientific one. In this study, we introduce coarse graining DNA models which realize the single nucleotide resolution and discuss their characteristics using molecular dynamics (MD) and Langevin dynamics.

Methods

In our model, as shown in Fig. 1(a), a continuous piece of base, sugar, and phosphoric group are substituted with one bead, and the beads are connected with springs. This is one of the simplest beads-spring model which has single nucleotide resolution. In another model, as shown in Fig. 1(b), base, sugar and nucleotide molecules are divided into two parts in which one for a base and another for a phosphate group and a sugar. These parts are connected with rigid rods. The rigid rods which constrain the lengths between the beads reduce the computational time. This model is available to describe the nature of the phenomena caused by a few factors such as charges on nucleotides, hydrogen bonds, and interactions between bases.

Results

At first, potential energy curves of hydrogen bonds between AT and GC base pairs are estimated using first-principles calculations. As shown in Fig. 2, these curves are fitted well with Morse type functions. Furthermore, the Mulliken charge on a phosphate group is estimated as -0.76 . The binding energy of hydrogen bonds in a GC pair is estimated to be 1.84 times larger than those in an AT pair. These properties are taken into account in our coarse graining models. Figure 3 presents a

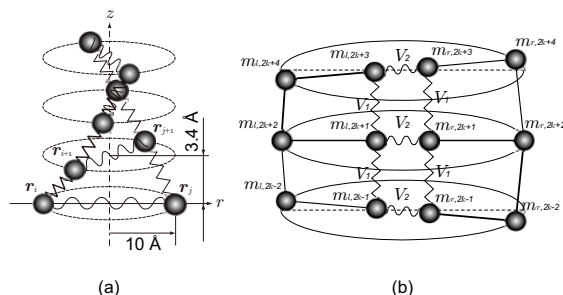


Figure 1: Schematic illustration of coarse graining double strand DNA fragments.

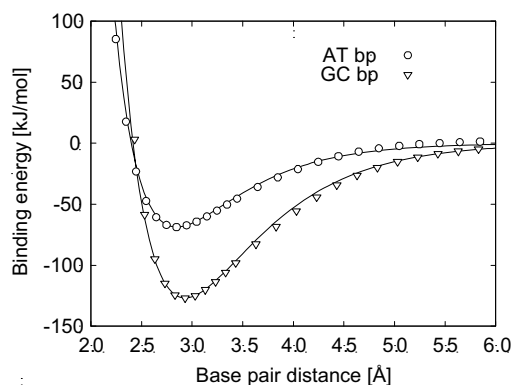


Figure 2: Binding energy curve of hydrogen bonds between AT and GC base pairs.

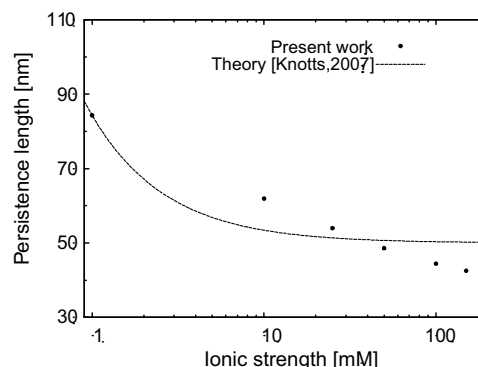


Figure 3: Persistence length as a function of ionic strength; comparison between present work and Poisson-Boltzmann theory.

computational result of persistence lengths depending on the ionic strength in solution. The present result is compared with that by other methods and reasonably agrees with them [Knotts, 2007].

Discussion

Our coarse graining DNA models are confirmed to represent the temperature dependency of melting phenomenon considering the base sequences. This result is attributed to the nature that weak interactions via hydrogen bonds are broken by the thermal fluctuation. Our model succeeds to represent the phenomena depending on the proportion of AT and GC base pairs.

References

T.A. Knotts IV et al, J Phys. Chem. 126:084901-1-084901-12, 2007.

GENERIC AGENT BASED EPITHELIAL CELL MODEL

Desmond Ryan (1), Rod Smallwood (2)

1. & 2. Department of Computer Science, Kroto Research Institute, North Campus, Broad Lane, University of Sheffield, S3 7HQ, UK;

Abstract

In this paper, we describe how a previously developed agent based model [Walker, 2004 & 2006] is extended to represent epithelial cellular processes and mechanisms in a new but physically realistic way. The basis of each cellular mechanism is the signalling pathway which triggers and modulates cellular rules such as migrate and stratify. The signalling pathway can be used to, not only, represent actual molecular pathways such as the MAPK pathway [Orton, 2005] but also any simple (or complex) physical process or rule. Each signalling pathway can be modulated by all other active pathways, and this model is coded flexibly so that the modulation matrices can be easily updated, as and when new data or insights appear. The model currently includes the following pathways: cell-substrate bond, cell-cell bond, EGFR-activated MAPK, and β -catenin pathways. And all cells can proliferate, migrate, stratify, differentiate and undergo apoptosis. The model, using the Flexible Large-scale Agent Modelling Environment or FLAME [Coakley, 2007], is deployed to investigate the effects of disabling certain rules or processes on the culture growth in both low and high calcium environments. Figure 1 shows the growth of a mono-layer of epithelial cells in a high calcium environment (on a 1000 micron square substrate) with all mechanisms active (top left), migration disabled (top right), proliferation disabled (bottom left) and juxtacrine signalling disabled (bottom right) for the same time point (at 29 hours). Figure 2 shows the growth of a mono-layer of epithelial cells in a low calcium environment with all mechanisms active (top left), migration disabled (top right), proliferation disabled (bottom left) and juxtacrine signalling disabled (bottom right) for the same time point (at 29 hours). The flexibility of the new model allows the interactions/modulations between the many signalling pathways and components to be easily specified and manipulated, rules can be turned on and off and indeed *in silico* predictions of the effects of agonists (activate components) and silencing RNA (used to block components) can be easily done without any code modification. The model is easily extendible to include other signalling pathways such as the canonical wnt pathways and Transforming Growth Factor Beta (TGF- β), and indeed this is now underway.

Figure and Tables

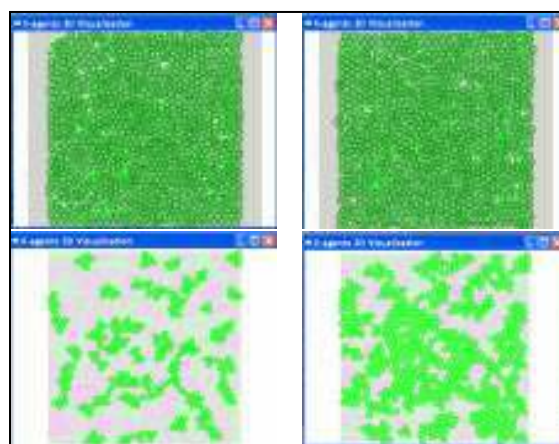


Figure 1: High calcium for normal growth (top left), migration off (top right), proliferation off (bottom left) and juxtacrine signalling off (bottom right). The light green background shows where cells have been and their limited motility in high calcium.

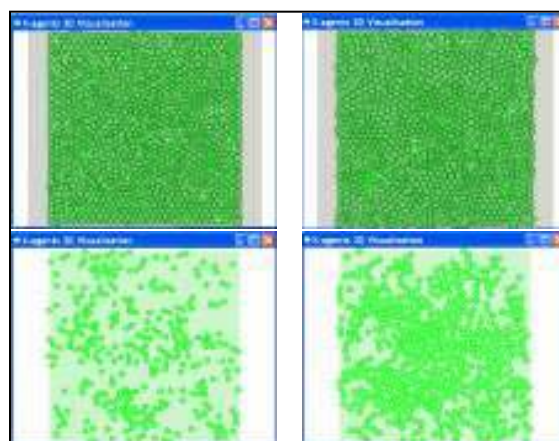


Figure 2: Low calcium for normal growth (top left), migration off (top right), proliferation off (bottom left) and juxtacrine signalling off (bottom right). The light green background shows where cells have been and their high motility in low calcium.

References

- Coakley, S, PhD thesis, University of Sheffield, 2007
- Orton, R et al, J Biochem, 392, 249-261, 2005
- Walker, D et al, Biosystems, 76, 89-100, 2004
- Walker, D et al, J Theor Biol, 242, 774-789, 2006

SHAPE INDEX: NEW PARAMETER OF PANCREATIC BETA-CELL FUNCTION IN SUBJECTS AT RISK FOR DIABETES?

Andrea Tura (1), Stefano Sbrignadello (1), Yvonne Winhofer (2), Giovanni Pacini (1), Alexandra Kautzky-Willer (2)

1. Institute of Biomedical Engineering, CNR, Padua, Italy; 2. Clinic of Internal Medicine III, Medical University of Vienna, Austria;

Introduction

It is known that insulin and C-peptide concentration curves from an oral glucose tolerance test (OGTT) may show different shapes (such as monophasic or biphasic), but possible meaning and potential usefulness of studying these discrepancies have been very poorly investigated so far. Aim of this study was the introduction of an index dependent on the shape of the OGTT curves and the assessment of its value in a group of women with former gestational diabetes (fGDM) with different degrees of glucose tolerance.

Methods

We analyzed 482 3h-OGTTs from fGDM women (age=35.2±0.2 years (Mean±SE), BMI=27.2±0.3 kg/m²) currently with normal (NGT, n=361, fasting glucose g₀=4.9±0.02 mM) or impaired (IGM, n=84, g₀=5.4±0.06) glucose tolerance, or even type 2 diabetes (T2DM, n=37, g₀=7.3±0.30). A shape index was computed from the glucose, insulin and C-peptide curve as the absolute value of the second derivative calculated at each time sample and then averaged over the whole OGTT interval (SHI_{GLU}, SHI_{INS}, SHI_{CP}, respectively). We then assessed possible differences of these parameters in the different groups of subjects (with ANOVA), and possible relationships (linear regression analysis) with known parameters of beta-cell function (Glucose Sensitivity, Gsens [Mari, 2002]; Insulinogenic Index, IGI [Tura, 2006]) and insulin resistance/sensitivity (HOMA-IR [Matthews, 1985]; OGIS [Mari, 2001]).

Results

SHI_{GLU}, SHI_{INS} were not different in NGT, IGM, T2DM. Conversely, SHI_{CP} was different in every group (SHI_{CP}=11.2±0.3 pM min⁻² in NGT, 9.6±0.7 in IGM, 6.6±0.5 in T2DM; IGM, NGT: P=0.04; IGM, T2DM: P=0.01; NGT, T2DM: P<0.0001). Similarly to SHI_{CP}, Gsens, HOMA-IR, OGIS were different in every group; IGI was not different in IGM, T2DM. In regression analysis SHI_{CP} showed significant relationship with Gsens (R=0.43, P<0.0001; Figure 1) and, though weak, with IGI (R=0.22, P<0.0001). No relationship was found with HOMA-IR and OGIS (P>0.36).

As regards the relationship between SHI_{CP} and Gsens, it was maintained even when considering NGT or IGM alone; only in T2DM the relationship was lost, possibly due to the modest number of subjects.

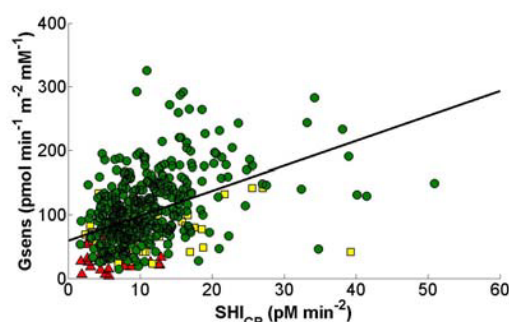


Figure 1: Relationship between SHI_{CP} and Gsens in all the subjects (circle: NGT; square: IGM; triangle: T2DM). Regression line: $Y=3.9X+59.3$.

Discussion

We introduced a new index, aimed at quantifying possible differences among subjects in the shape of the OGTT curves. To our knowledge, no study was performed before on OGTT shape in fGDM women, that is, a population at high risk for developing diabetes. We found that SHI_{CP} was different in groups with different degree of glucose tolerance, and it was related to known parameters of beta-cell function. Of note, SHI_{CP} seems to discriminate the different groups of subjects better than the widely used IGI. Compared to Gsens, SHI_{CP} does not require complex modeling analysis to be computed. We conclude that the assessment of OGTT curves shape may be relevant to calculate new simple empirical indices of beta-cell function.

Acknowledgements

In part supported by grants of Regione Veneto (Biotech DGR 2702/10-09-04) and Austrian Science Fund (P14515MED).

References

- Mari A et al, Diabetes, 51:S221-S226, 2002.
- Mari A et al, Diabetes Care, 24:539-548, 2001.
- Matthews DR et al, Diabetologia, 28:412-419, 1985.
- Tura A et al, Diabetes Res Clin Pract, 72:298-301, 2006.

Musculoskeletal system – cell

A NESTED DUAL POROSITY FE MODEL FOR CORTICAL BONE. APPLICATION TO A ROOSTER ULNA EXPERIMENT.

M. A. Pérez (1), P. Fornells (1), M. Doblaré (1), J. M. García-Aznar (1)

1. Group of Structures and Materials Modelling. Aragón Institute of Engineering Research (I3A), University of Zaragoza, Spain

Introduction

Bone is structured with a hierarchical network of porosities with quite different characteristic dimensions. Vascular porosity (PV) contains blood vessels and nerves and is associated with blood irrigation of the bone. The lacuno-canalicular porosity (PLC) is the network where the osteocytes are embedded and collagen-apatite porosity (PCA) is associated with the spaces between collagen and mineral in the bone matrix. All of these porosities are filled with bone fluid, but in PCA the fluid flow is negligible [Cowin, 1999].

Bone has also the property of adapting its structure to the mechanical environment in a process known as bone remodelling. The specific mechanical stimulus controlling this process is not completely understood, but current evidences suggest that it is related with lacuno-canalicular fluid flow and the shear stresses that exerts to the osteocytes. Fornells et al [2007] applied a dual porosity approach to compute fluid flow in both PV and PLC, but this macroscopic model is not able to analyze the fluid flow at the level of an osteon. In this work, a Russian doll poroelastic model [Gailani and Cowin, 2008] is implemented in FE to simulate bone fluid flow at PV and at the level of an osteon at the PLC. One model has been developed based on an experiment over a rooster ulna [Qin et al., 1998] in order to validate the approach presented herein.

Material and Methods

The Russian doll poroelastic formulation used in this work is the suggested by Gailani and Cowin [2008]. It is based on a poroelastic formulation for each porosity (PV and PLC) with a coupling term γ between them. It has been implemented in the commercial finite element software Abaqus. One mechanical load condition was simulated in order to check its potential. We simulated the experimental work of Qin et al [1998], where they determined the ability of a relative high-frequency and moderate-duration loading regime to maintain bone mass in a turkey ulna model of disuse osteopenia. A bending load was applied to a small sample of bone at the mid-diaphysis (Figure 1). Six bone sectors were considered, in each sector an osteon is assumed where the morphometric bone change will be analysed (Figure 1-(b)). The osteon was modelled as a cylinder (Figure 1-(c)).

Poroelastic properties and elastic ones were considered as in other studies of the literature [Fornells et al. 2007]. With this model we analyzed the pore fluid effective velocity at the level of an osteon and related it with the morphometric change of bone at the mid-diaphysis determined experimentally [Qin et al, 1998].

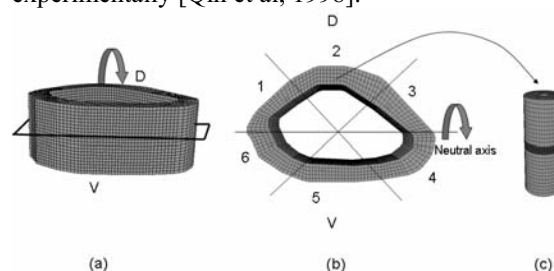


Figure 1: (a) FE model of the turkey ulna section under a bending load; (b) Cross section of (a) with the six osteons considered; (c) FE model of the osteons.

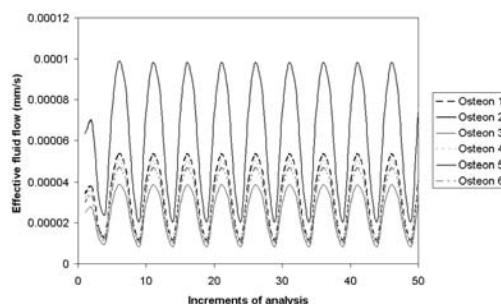


Figure 2. Effective fluid flow at PLC on the six osteons.

Results and Discussion

The effective fluid flow on the six osteons has been represented in Figure 2. The maximum fluid flow took place at the osteons 2 and 5 (coincident value). These regions corresponded with the higher morphometric change of bone determined experimentally. And the lower changed was produced at the region 6 and 3 as the computational approach predicted (Figure 2). Summarizing, the model proposed has been qualitatively correlated with the zones of bone formation observed in the laboratory.

References

- Cowin, J Biomech, 32,217-238,1999.
- Fornells et al, Ann Biomed Eng, 35,1687-1698,2007
- Gailani and Cowin, 9th Bone Fluid Workshop, 2008.
- Qin et al, J Orthp Res, 16, 482-489,1998.

VALIDATION OF AN *IN SILICO* BONE ADAPTATION MODEL BY MEANS OF EXPERIMENTAL *IN VIVO* LOADING DATA

Friederike A Gerhard, Floor M Lambers, Duncan J Webster, Gisela Kuhn, Ralph Müller

Institute for Biomechanics, ETH Zürich, Zürich, Switzerland

Introduction

Computational models can be of great help to understand the mechanisms of load induced bone adaptation. However, due to the nonexistence of suitable experimental *in vivo* data, a weakness of many existing models is their lack of quantitative validation. Here we propose for the first time a computational model which is validated using an *in vivo* model for load induced bone adaptation.

Methods

To induce *in vivo* bone adaptation, the 5th caudal vertebrae of 6 C57BL/6 mice were subjected to cyclic loading at 8N for 4 weeks and scanned weekly with *in vivo* micro-computed tomography (VivaCT) at 10.5 μm resolution. *In silico* trabecular bone adaptation was modelled, for each animal, by iteratively exposing the trabecular compartment of initial, thresholded VivaCT scans to a modified version of SIBA [1]. The model parameters were chosen so that the simulated bone volume fraction (BV/TV) of one sample at week 1 matched its experimental BV/TV. The model was then assessed by comparing experimental and simulated BV/TV for this animal at weeks 2, 3, and 4. Next, the simulations were run on the remaining 5 loaded animals and the resulting curves were compared to the experimental progression. Furthermore, curves of other structural indices were plotted, *i.e.* trabecular thickness (Tb.Th) and trabecular number (Tb.N). Group means were compared at each week using pairwise Student's t-test. Differences of $p < 0.05$ were considered significant. Visual assessment of formation and resorption sites was performed by an algorithm using rigid registration [2].

Results

Following the match at week 1 BV/TV was assessed in weeks 2, 3, and 4 for the same animal, giving absolute percentage errors of 1.8%, -1.2% and -4%. The time course of BV/TV for the group of 5 animals is shown in Figure 1. The mean of the percentage errors calculated for each animal were less than 10.1% over the 4 weeks, showing a slight saturation for the simulations being not yet evident in the experiment. For structural indices, maximum percentage errors in Tb.Th amounted to 6.6% and for Tb.N to 3.1%. None of the simulated mean values for BV/TV, Tb.Th and Tb.N differed significantly from the experimental mean values at any time stamp. Nevertheless, a visual comparison

of formation and resorption sites evident in both experiment and simulation uncovered local differences (Figure 2). The simulation showed less bone formation and barely any resorption sites compared to the experiment.

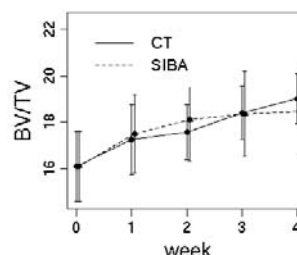


Figure 1: Time course for experiment (CT) and simulation (SIBA). Data are presented as mean \pm SE.

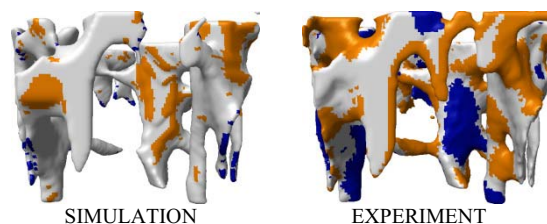


Figure 2: Visual representation of formed (yellow) and resorbed (blue) sites in the trabecular compartment after 4 weeks of simulation (left) and experiment (right).

Discussion

The presented algorithm was able to predict the increase in bone mass over a period of 3 weeks with an error of $<10.1\%$. No significant differences between simulations and experiment could be found for any parameter at any time point. Nevertheless, visual inspection revealed that the model does not yet represent the correct amounts of bone formation and resorption. This result indicates that a local regulation mechanism allowing bone resorption during the adaptation process needs to be incorporated. This finding could only be made through new visualization techniques and the availability of experimental *in vivo* loading data.

Acknowledgement

Funding from the European Union for the osteoporotic virtual physiological human project (VPHOP FP7-ICT2008-223865) is acknowledged.

References

- [1] Müller, Osteoporos Int, 2005
- [2] Gerhard et al., 2008 Annual Meeting of SSBE

ANALYSIS OF TRABECULAR STRUCTURE REMODELLING FOR PATHOLOGICAL LOAD CASE

Jerzy Bartodziej, Krzysztof Ścigala

*Division of Biomedical Engineering and Experimental Mechanics,
Wroclaw University of Technology, Poland*

Introduction

Adaptation of bone trabecular structure is described in series of numerical analyses, mostly by application of stress distribution non-homogeneity hypothesis [Adachi, 2002], [Adachi, 2005], [Bedzinski, 2002]. Resultant structures are characterised by high similarity to clinical observations, however mostly physiological loading situations are analysed. In clinical conditions, for example in many cases of varus knee deformation, pathological load leads to fractures in trabecular structure of medial tibia condyle [Pozowski, 2001]. In clinical practise those fractures are interpreted by overloading of trabecular structure, which outbalance bone tissue self-regeneration abilities. The main aim of presented analysis is to simulate cancellous bone remodelling, including damage accumulation effect.

Methods

Two – dimensional FE models of proximal part of tibia bone with initial homogenous and structurally isotropic structure of trabecules were created using own procedures and Ansys software. Load was applied to the models according to description of standing phase of gait proposed by Hurwitz [Hurwitz, 1998]. Simulation procedure was developed in form of two modules. In first module calculations of changes in bone structure according to model proposed by Adachi [Adachi, 2005] were carried out. Absorption and resorption of material on the surface of trabecules were carried out by changing of number finite elements in model. In second module calculation of damage accumulation were carried out. For each finite element in the model changes of elasticity modulus were calculated according to description proposed by Zioupos [Zioupos, 1996]. In case when change of elastic modulus was uncommonly high or stress value was higher than actual strength of element material element was deleted from the model.

Results

Resultant structures of trabecules in proximal tibia are highly non-homogenous and directed. There can be observed structures transferring load from overloaded medial articular surface to medial part of compact bone layer, as well as some additional

supporting structures of trabecules connecting medial condyle with opposite lateral part of compact bone layer. In the case of analysis including effects of damage accumulation in the structures under pathological load we can observe fractures of the trabecules in the region A (fig. 1).

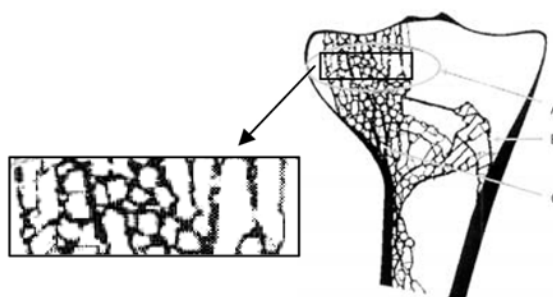


Figure 1: Resultant trabecular structure in the model of upper tibia

Fractures are mostly directed horizontally, and exist in whole medial condyle structure. In the region B also exists cracks in the one of the main, large trabecules, as well as in the region C, where structure developed in the response of varus tibia deformation.

Results

Comparative analysis of simulation results of trabecular remodelling with included and with included not effect of damage accumulation lead to conclusion so fractures of trabecules appears in multiple regions of analysed tibia model. However, existence of those fractures doesn't lead to significant changes in the main directions or density of trabecules distribution in the model. It can be concluded so in the range of presented analysis effect of damage accumulation is mostly very localised, small changes are observed in the close neighbourhood of fracture.

References

- Adachi T. et al, J Biomech, 35:1541-1551, 2002.
- Adachi T. et al, Med Eng & Phys, 27:305-311, 2005.
- Bedzinski R., Scigala K. CAMES, 10:353-358, 2003.
- Hurwitz D. et al, J Biomech, 31:423-430, 1998.
- Pozowski A. et al., Acta Biomech & Bioeng, 3:31-40, 2001
- Zioupos P. et al, Clin Biomech, 11:365 - 375, 1996.

AN APPROACH TOWARDS PATIENT-SPECIFIC BONE REMODELLING SIMULATION IN OSTEOPOROSIS

Luís Santos (1,3), Pedro Coelho (2), João E. Fonseca (3), Hélder C. Rodrigues (1), Paulo R. Fernandes (1)

1. IDMEC – Instituto Superior Técnico, Technical University of Lisbon, Portugal; 2. Department of Mechanical and Industrial Engineering, New University of Lisbon, Portugal; 3. Instituto de Medicina Molecular, University of Lisbon Medical School, Portugal

Introduction

Osteoporosis (OP) is a systemic skeletal disease characterized by a total bone mass reduction and by the microarchitectural deterioration of bone structure. These factors lead to a state of enhanced bone fragility and hence susceptibility to fracture [1]. OP diagnosis is still mainly based on T-score, computed from bone mineral density (BMD) measurements, obtained by Dual energy X-ray Absorptiometry (DXA). However, fracture incidence cannot be totally explained by this variable. On the other hand, the development of computational bone remodeling models provides valuable tools for the assessment of bone density as well as bone micro-architecture. In this sense, this work conjugates a hierarchical bone remodeling model with DXA as an approach towards patient-specific bone remodeling simulation in OP context. This analysis was preceded by the computational model validation [2].

Methods

The hierarchical computational model characterizes the relative bone density as well as the bone trabecular architecture [3], assuming bone tissue self-adapts in order to obtain the stiffest structure, with the amount of bone mass regulated by a metabolic cost factor (parameter k). A sample of 160 female Caucasian DXA femoral exams was used throughout this study. As a first approach towards patient-specific bone remodeling simulation, individual mathematical relations were established between this parameter and several biological variables: age, T-score and Bone Mass Index (BMI). For this end, linear and quadratic regression studies were performed using a weighted linear least-squares formulation. The mathematical relations obtained were analyzed through qualitative comparison, between DXA and computational model results, based on density distribution profiles. Finally, a multiple regression study was performed correlating simultaneously the biological variables considered with parameter k .

Results

A correlation coefficient of -0.8068 was obtained for the quadratic regression study between k and T-

score. From this study, one can obtain the following mathematical relation:

$$k = \frac{3 \times 10^{-3} - \sqrt{4,68 \times 10^{-6} + 1,6 \times 10^{-6} \times Tscore}}{8 \times 10^{-7}} \quad (1)$$

The qualitative comparison results based on (1) are presented in figure 1:

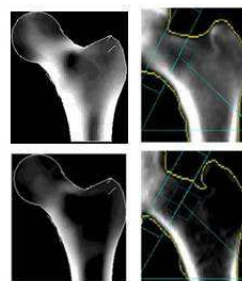


Figure 1: $k=550$ (top-left) compares with DXA of healthy bone (top-right) and $k=3100$ (bottom-left) with DXA of osteoporotic bone (bottom-right).

Discussion

The results suggest a strong correlation between the biological variables and k . The qualitative comparison results evidenced a fair agreement between DXA and computational model results. These results represent the first step towards patient-specific bone remodeling simulation, which may provide a novel understanding basis to OP fracture incidence.

Acknowledgements

This study was supported by the grants SFRH/BD/42115/2007 and SFRH/BD /25033/2005 from the Portuguese Foundation for Science and Technology.

References

- [1] S.R. Cummings, L.J. Melton III, "Epidemiology and outcomes of osteoporotic fractures". *Lancet*; 359, 1761-67, 2005
- [2] L.Santos et al "A Dual Energy X-ray Absorptiometry validation of a bone remodelling model for the assessment of osteoporotic bone quality", In Proc of The 6th Int Conf on Eng Comp Tech, ISBN 978-1-905088-22-5 (CD-ROM), (2008)
- [3] P.G. Coelho et al, "Numerical Modeling of Bone Tissue Adaptation – A Hierarchical Approach for Bone Apparent Density and Trabecular Structure", *Journal of Biomechanics*, 2009 (in print).

MULTI-CELL SIMULATIONS OF GASTRULATION AND SOMITOGENESIS USING COMPUCELL3D

James A. Glazier (1), Ariel Balter (1), Ying Zhang (1), Cornelis Weijer (2)

1. Indiana University, USA; 2. University of Dundee, U.K.

Introduction

Together, gastrulation and segmentation lay down the body plan of developing vertebrate embryos. However, despite their importance, many key biological aspects of these processes remain unclear, partly because experimental results involve multiple mechanisms acting simultaneously, and thus are difficult to disentangle. Computer simulations can clarify these mechanism.

Methods

In the GGH model [Swat, 2009], Objects are *Generalized Cells* or *Fields*. Generalized Cells are spatially-extended objects, residing on a 2D or 3D *Cell Lattice*, corresponding to biological cells, subcompartments of cells, or portions of non-cellular materials, e.g., ECM, fluids, solids, etc. *Fields* are continuously-variable concentrations, e.g. of chemicals, which reside on additional lattices with the same discretization. The GGH model describes cell capabilities and interactions through an *Effective Energy*, which mixes true energies, such as cell-cell adhesion; terms that mimic energies, e.g., the response of a cell to a chemotactic gradient of a *Field*; and *Constraints* describing other cell properties, e.g., membrane area. *Dynamics* employ a Monte-Carlo caricature of cytoskeletal fluctuations for cell motility, hard-coded algorithms for cell division and standard solvers for *Field* PDEs.

Results and Discussion

In the chick embryo, gastrulation starts with the elongation of the primitive streak from Koller's Sickle and rapidly develops into two large-scale vortical cell flows, while during somitogenesis, the initially homogeneous presomitic mesoderm created during gastrulation separates into a series of discrete somites. Mechanisms we consider in our simulations include cell adhesion and repulsion, which vary in time depending on cell history, contacts and concentrations of regulatory signals, cell motility and chemoattraction and repulsion to molecules secreted at various locations in the embryo.

Discussion

In gastrulation, only a combination of chemorepulsion of Hensen's Node cells by Koller's Sickle and planar-polarity alignment reproduces all experimental observations.

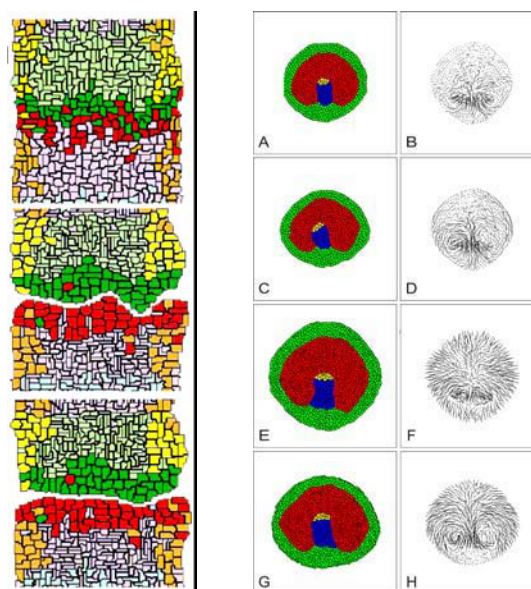


Figure 1: Left: Sequence of events during boundary-definition phase of somitogenesis. Right: Cell-flow patterns for different hypotheses concerning signaling in gastrulating chick.

In somitogenesis, an extension of the models of the somitic clock and determination front of Goldbeter, Pourquié and Lewis, with our hypotheses for the translation of Wnt and Lfrg levels into N-CAM, N-cadherin, EphA4 and ephrinB2, and the regulation of cell division in the tailbud, reproduces the dynamics of somitogenesis [Glazier, 2008].

Acknowledgements

This research was partially funded by NIH grants R01 GM76692-04 and 1R01 GM077138-01A1.

References

- Glazier et al, *Current Topics in Developmental Biology* 81: 205-247, 2008.
- Swat et al, *Methods in Molecular Biology* 500: 361-428, 2009.

REMODELLING RATE VARIATION CAN ACCOUNT FOR SUBJECT SPECIFIC BONE ADAPTATION

Tomasz Szwedowski (1), W.R. Taylor (1), M. Müller (2), M.O. Heller (1), G.N. Duda (1)

(1) Julius Wolff Institut and (2) CMSC, Charité – Universitätsmedizin Berlin, Germany

Introduction

Clinical studies that have tracked proximal femoral bone mineral density (BMD) after total hip arthroplasty (THA) have shown periprosthetic remodelling rate differences between patient groups, mainly based on gender [Sabo, 1998]. The prediction of periprosthetic bone remodelling after THA using computational based methods is becoming widely accepted. Since such computational schemes investigate the organ and tissue level biological and mechanical interactions, they provide one of the few methods to separate influencing factors and therefore enable insight into the relative contributions of patient-specific parameters on subsequent bone adaptation patterns. With the goal of better understanding the role that subject specific parameters may play in bone adaptation, the aim of this work was to assess the sensitivity of multiple patient-specific models to the rate of remodelling.

Methods

Computed tomography images were acquired for 5 THA patients, 1 day before and 7 days after a primary implantation of a Zweymüller total hip endoprosthesis (Zimmer Orthopaedics Inc.). Each intact and implanted femur was segmented (ZIBAmira 2008) and converted into a NURBS surface (Geomagic Inc.). Virtual implantation (femoral head resection, reaming) was performed using Boolean operations on the femur and implant solids (NX 4.0), guided by an orthopaedic surgeon. A ten-noded tetrahedral mesh was generated (Patran 2008) and muscle and joint contact forces applied that were derived from validated musculoskeletal models [Heller et al. 2001]. Bone remodelling was simulated (Abaqus v6.7) in response to a change in the equivalent von Mises strain signal, defined as the weighted average of the peak loads during walking (80%) and stair climbing (20%) activities. The benchmark dead zone region was defined for each element as $100 \mu\epsilon$ around the local intact reference signal. The benchmark remodelling rate varied linearly between $100 \mu\epsilon$ and $2000 \mu\epsilon$ (s), beyond which remodelling processes became saturated at 50 mg/cm^2 per iteration (resorption and deposition). To identify the range of the saturation parameter s , that is reasonable for tuning the algorithm for subject specific remodelling predictions, s (rate multiplier) was set as: 250 (13.3), 500 (5), 1000 (2.2) or 4000 (0.5) $\mu\epsilon$.

Results

All models qualitatively resulted in BMD trends that resemble those seen clinically with the Zweymüller design. Difference comparisons between the benchmark and parameter variations showed that the changes in remodelling rate non-uniformly influenced BMD predictions (Figure 1).

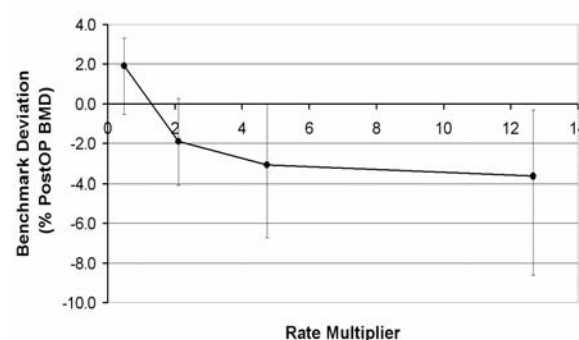


Figure 1: Mean and range (error bars) of the difference (%) pre- to post-operative BMD due to variations in the remodelling algorithm rate.

Discussion

This study has shown that for 5 patient specific models, variation in the rate of remodelling had a non-uniform effect on the subsequent BMD outcome. This range of saturation points could account for changes of up to 10% BMD, which is on the order of the gender differences detected in our own prospective study ($n=93$) and Sabo *et al.*. The role that such variation plays, and whether this process can facilitate improved prediction of local remodelling patterns remains to be seen and requires validation against the forthcoming 12 month postoperative BMD measurements. The changes in remodelling outcome due to subject specific parameters could, however, begin to explain the variation between patients that models have as of yet been unable to differentiate. Parametric tuning may help identify the relative contribution of biological or mechanical processes to longer term subject specific bone adaptation.

Acknowledgements

This study was partially funded by the SFB 760 and Zimmer Orthopaedics Inc.

References

- Sabo et al, Calcif Tissue Int, 62:177-182, 1998.
- Heller et al, J Biomech. 34:883-93, 2001.

Probabilistic and optimisation methods

MODELING ANATOMIC VARIABILITY FOR APPLICATION IN PROBABILISTIC SIMULATION OF LUMBAR SPINE BIOMECHANICS

Kelli S Huls (1), Amit Agarwala (2), Anthony J Petrella (1)

1. Computational Biomechanics Group, Colorado School of Mines, USA

2. Panorama Orthopedics & Spine Center, Golden, Colorado, USA

Introduction

Computational simulation is a promising option for evaluating the performance of new spinal implants and procedures before they are used in patients, but most models in the literature represent only a single subject [Grauer, 2006]. Probabilistic simulation methods make it possible to evaluate biomechanical function across an entire population of virtual patients before initiation of clinical trials in living subjects. The goal of our research is to use statistical shape modelling to develop a parametric representation of spine anatomy for use in probabilistic simulation. The present study focused on the L3 lumbar bone anatomy.

Methods

A statistical shape model (SSM) was developed for the L3 vertebra. Eight CT scans were used to form a training set. One specimen was arbitrarily chosen as a template, and a hexahedral mesh was created using Hypermesh (Altair Engineering, USA). The template mesh was morphed to fit the seven remaining specimens, ensuring identical topology among all eight meshes. Quadrilateral surface meshes were extracted for the SSM. Specimens were aligned [Spoor, 1980] with the template mesh to eliminate variations in rotation and translation, leaving only variations in size and shape. A principal component analysis (PCA) was performed on the system covariance matrix. In PCA, eigenvalues of the covariance matrix quantify variance of shape along each of the eigenvectors, which are the principal modes of shape variation. A leave-one-out validation was performed to assess the ability of the SSM to represent the shape of an unknown specimen. A randomly selected specimen was removed from the training data set and the SSM was recalculated with only seven specimens. A non-linear least squares optimization scheme was used to fit the SSM to the “left-out” specimen.

Results

The first five principal components (PC) of size and shape variation captured 95% of the variance in the data. PC₁ was a scaling mode (Fig. 1). PC₂ was associated with shape and angulation of the facet joints. PC₃ produced variations in the transverse processes. Higher modes were not visually obvious. Results of the leave-one-out validation revealed the

SSM was able to match the shape of an unknown specimen (Fig. 2) with a maximum Euclidian distance error of 5.6 mm and a mean error of 1.9 mm.

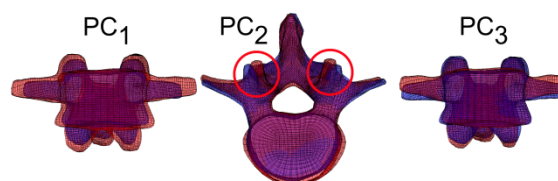


Figure 1: The first three principal components (PC). Red shows +1 std deviation, Blue shows -1 std deviation.

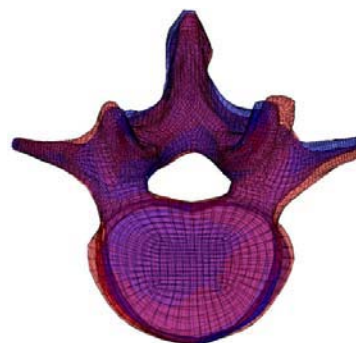


Figure 2: Leave-one-out specimen in Red. SSM fit to the “left-out” specimen in Blue.

Discussion

A key advantage of PCA is data reduction. In the present study five PC's captured 95% of the size and shape variance across eight specimens – not a significant reduction in this case, but it will become more important later as additional specimens are added to the training set. The leave-one-out validation exhibited a mean error similar to a previously reported pelvic SSM [Meller, 2004], but the max error was large around the facet joints (Fig. 2). Predictions of facet loads and contact distribution are known to be sensitive to facet geometry [Holzapfel, 2006], suggesting that a larger training set is needed to better represent anatomy and biomechanics for a realistic patient population. Future work in our lab will address this limitation and expand the model to parametrically represent the entire lumbar spine in a probabilistic simulation framework.

References

- Grauer et al, Spine J, 6:659-666, 2006.
- Holzapfel and Stadler, Eur Spine J 15:849-856, 2006.
- Meller et al, Int Congress Series 1268:561-566, 2004.
- Spoor and Veldpaus, J Biomech, 13:391-393, 1980.

OPTIMIZATION OF A BUOYANCY-DRIVEN MICRODEVICE THROUGH COMPUTATIONAL ANALYSES

Margherita Cioffi (1, 2), Katia Laganà (1), Elena Bianchi (1), Gabriele Dubini (1)

1. *Laboratory of Biological Structure Mechanics, Dept. of Structural Engineering, Politecnico di Milano, Milan, Italy*; 2. *IRCCS Istituto Ortopedico Galeazzi, Milan, Italy*

Introduction

Since 1983 the Polymerase Chain Reaction (PCR) has been playing a central role in the field of molecular biology. It is a powerful tool for creating large numbers of copies of specific DNA fragments for application like DNA fingerprinting, genomic cloning and genotyping for disease diagnosis. The common devices used for PCR consist of metal blocks that are repeatedly thermal cycled between various temperatures (~ 90 , 60 and 75 °C) required for the amplification process. Recently microfluidic PCR devices were developed, showing important advantages against standard bench-top thermal cyclers. Among these systems a typical PCR chip is the continuous flow type, which consists of microchannels continuously looped through different temperature zones [Park et al, 2003]. An alternative solution relies on temperature-induced density differences in the presence of a body force to induce a buoyancy-driven flow. This alternative method is easy to use and does not require expensive set-up, but, up to date, the thermo-fluid-dynamic field in the micro-channels still needs to be optimized. The main issue to be addressed is the thermal cycling process control.

The present study focuses on the design of microchannels, having innovative and optimized shape to obtain proper fluid actuation and DNA sample amplification within buoyancy driven flow PCR devices. The efficiency of such a configuration is compared to the standard continuous flow type by means of Computational Fluid Dynamics (CFD) modeling.

Materials and methods

Two CAD models were generated: a serpentine microchannel and a three-dimensional microchannel arranged in a 6 mm \times 5 mm closed loop. The dimensions of the former were chosen according to the literature [Li et al, 2006], while the microchannel cross-section of the latter was optimized by means of parametric study, including variation within the same loop. Transient simulations were carried out using the finite volume CFD package FLUENT (Ansys Inc., Canonsburg, PA, USA). Flow patterns within the cavities and loop structures were simulated in two dimensions

with water as a Boussinesq fluid. No slip conditions were imposed at the walls. For the serpentine microchannel, a flat velocity profile was imposed at the inlet, while zero pressure condition was applied at the outlet. Heater positioning was simulated by imposing constant-temperature boundary conditions, while the appropriate thermal resistance was applied at the other boundaries.

Results

The efficiency of the PCR device depends on the control of the thermal cycle to which the DNA samples are exposed. For each of the thermal phases this control must guarantee temperature uniformity and the required sample residence time. For instance, each thermal cycle lasts for ~ 12 s in the two-temperature cycling device shown in Fig.1, comparably to standard continuous flow devices.

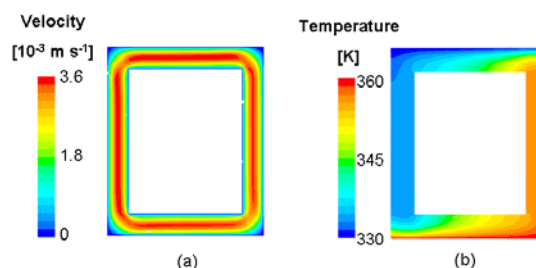


Figure 1: Example of a two-temperature, closed loop device. Velocity (a) and temperature (b) contour plots.

Discussion

The simulations showed that a closed loop configuration, effectively designed, is a promising alternative to the serpentine one. Although this kind of configuration presents significant advantages, such as absence of an external pumping system and no limitation of the number of executable thermal cycles, particular attention must be paid to the device material and its surface properties. Indeed the high recirculation enhances the risk of surface fouling by DNA and proteins adhesion.

References

Li et al, Journal of Microelectromechanical Systems, 15(1): 223-236, 2006.

Park et al, Anal Chem, 75: 6029-6033, 2003.

PROBABILISTIC FINITE ELEMENT SIMULATIONS OF ELASTOSONOGRAPHY FOR BREAST LESIONS DETECTION

Simona Celi, Francesca Di Puccio, Paola Forte

Dipartimento di Ingegneria Meccanica, Nucleare e della Produzione, Università di Pisa

Introduction

Breast cancer is one of the most common tumours in women in the western world and early diagnosis is essential for improved prognosis. Even if today the diagnosis involves several techniques, some tumours are not detectable by conventional imaging methods and, in the clinical practice, surgical biopsy is used to confirm the type of lesion. However, since the malignant/benign breast biopsy ratio averages only about 1:4, this implies a high number of unnecessary benign biopsies, with considerable financial cost. In the last decade, elastography by means of ultrasound technique has been proposed to identify lesions and their nature by imaging the strain field [Ophir et al., 1999]. This technique is based on the observation that the mechanical properties of tissues are generally correlated with pathological changes: in particular the breast lesions appear stiffer than the surroundings. However elastosonography is often considered not reliable because it is affected by the presence of many subjective factors (e.g. shape and dimension of the transducer or lesion diameter).

In order to improve the reliability of elastography, this work investigates the parameters that mostly influence the deformation contrast between the healthy and cancerous tissues by means of a probabilistic FE approach.

Methods

The FE analyses were performed on 2D and 3D models of phantoms in which a spherical inclusion was embedded in a homogeneous background. Both tumour and surrounding tissues were assumed to be incompressible, homogeneous and isotropic. Lesions were considered linear elastic or hyperelastic, implementing a strain energy function with material parameters taken from [Palomar et al.]. The different type of tumours were characterised as having different stiffness ratio with respect to the healthy tissue (up to 100 times for linear elastic material) and also changing the degree of bonding at the interface. It is known that malignant tumours present a stellate appearance while the benign ones have a smooth boundary and are loosely bonded to the surrounding tissue [Moon et al., 2002], therefore a zero friction value was used for benign lesions, while a firmly bonded form for the malignant ones. To simulate the action of

the transducer, the phantom was subjected to a compressive displacement. Probabilistic FE analyses were performed assuming as input parameters the diameter of the inclusion, its position with respect to the transducer, the stiffness ratio between the lesion and the surrounding tissue and the friction coefficient at the interface.

FE simulations were also used to quantify the strain field contrast (C_s) between the healthy tissue and the inclusion. Moreover different regions of interest (ROI), where the average strain is taken as representative of the strain field, have been selected and compared in order to magnify C_s and to better identify the lesion nature, fig. 1.a.

Results and discussion

The strain field for a 2D Neo-Hookean model representing an anatomical phantom is reported in fig. 1.b. The sensitivity analysis shows a directly proportional linear correlation between C_s and the phantom radius ($60 \leq R_{ph} \leq 100$), fig. 1.c, and also a linear correlation, with negative sign, with respect to the depth ($20 \leq H \leq 80$) of the inclusion, fig. 1.d.

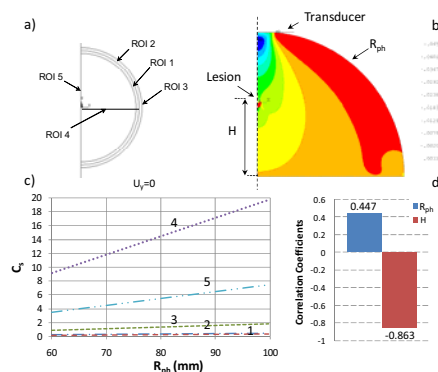


Figure 1: ROIs definition (a); ϵ_{yy} field (b); C_s with respect to R_{ph} for each ROI (c) and correlation coefficient for ROI 4 (d).

Results on the FE models show that ROI 4 and 5 emphasise the contrast coefficient and that C_s is not significantly correlated with the displacement of the transducer.

References

- Moon et al, J Biomech Eng, 20:100-107, 2002.
- Ophir et al, J Biomech, 37:1-10, 1999.
- Palomar et al, Med Eng Phys, 30:1089-1097, 2008.

Tissue adaptation

LOAD INDUCED BONE ADAPTATION MONITORED WITH *IN VIVO* MICRO-COMPUTED TOMOGRAPHY

Floor M Lambers, Gisela Kuhn, Friederike A Gerhard, Ralph Müller

Institute for Biomechanics, ETH Zurich, Zurich, Switzerland

Introduction

A better understanding of how mechanical forces regulate bone remodeling would provide opportunities to develop new treatment for bone diseases and disorders. *In vivo* micro-computed tomography (micro-CT) allows monitoring the 3D bone microstructure over time, enabling the visualization of subject-specific changes. The aim of our study was to evaluate load induced microstructural bone adaptation with *in vivo* micro-CT.

Methods

Microstructural bone adaptation was induced by cyclic loading of the 5th caudal vertebra through pins inserted in adjacent vertebrae. Loading was applied three times per week for four weeks at 0N (n=9), or 8N (n=9) in 15 week old female C57BL/6 mice. Weekly *in vivo* micro-CT scans were performed of the 5th caudal vertebra at a resolution of 10 μ m. To analyze specific changes in the bone structural parameters, the longitudinal data were registered (fig 1c). Automatic masks were used to select full, trabecular or cortical regions from which the bone structural parameters were calculated. To determine significant differences between the groups, ANOVA for repeated measurements and at the last time point were performed with a Bonferroni post-hoc test ($P < 0.05$).

Results

In the trabecular region there were significant differences between the 0N and the 8N group for most bone structural parameters as well as for the total change over the four weeks (table 1).

	0N	8N
%Bone volume ^{1, b}	108.2 \pm 7.9	118.4 \pm 6.0
%Bone surface	99.4 \pm 4.1	100.7 \pm 3.5
%Bone volume density ^{1, c}	108.1 \pm 8.1	121.6 \pm 5.3
%Trabecular thickness ^{1, a}	106.8 \pm 5.9	113.4 \pm 3.6
%Trabecular spacing ¹	102.1 \pm 4.2	99.1 \pm 5.3
%Trabecular number	99.0 \pm 3.0	100.7 \pm 4.9

Table 1: Parameters at day 28 in percent of baseline.¹ $P < 0.05$ for repeated measurements. ^a $P < 0.05$, ^b $P < 0.01$, ^c $P < 0.001$ for total change.

The increase in bone volume density (BVTV) in the trabecular region was mainly caused by an increase in trabecular thickness (fig 1a). In the cortex the increase in BV/TV was significantly greater for the

8N than for the 0N group, which was caused by significant thickening of the cortex for the 8N group (fig 1b). From the registered images it was evident that more bone formation occurred for the 8N group than for the 0N group (fig 1c).

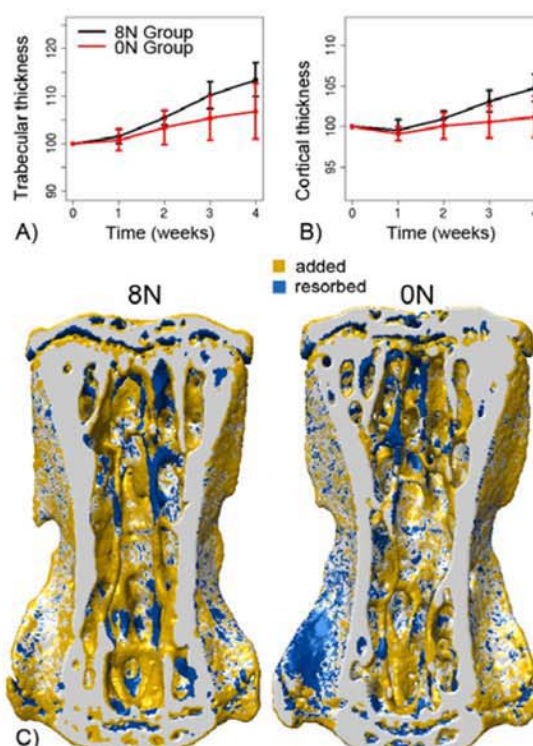


Figure 1: Parameters in percentage of baseline A) trabecular thickness B) Cortical thickness. Values are displayed as mean \pm standard deviation. C) Registered images of an 8N and 0N mouse.

Discussion

Load induced bone adaptation could be imaged and quantified accurately with *in vivo* micro-CT. Four weeks of loading resulted in a significant increase in BV/TV, which resulted mainly from thickening of the existing bone structures. *In vivo* micro-CT did not only allow monitoring differences in bone microstructure between the groups, but was sensitive enough to monitor local changes within single animals. These measurements would thus also allow validation of computer models predicting load induced changes in the bone microstructure.

Acknowledgements

The authors acknowledge funding from the European Union for the Osteoporotic Virtual Physiological Human project (VPHOP FP7-ICT2008-223865).

THE PREDICTION OF CORTICAL AND TRABECULAR BONE REMODELLING IN AN IN VIVO MODEL OF BONE ADAPTATION

Duncan Webster (1), Philip Morley (1), Harry van Lenthe (1), Ralph Müller (1)

1. Institute for Biomechanics ETH Zürich, Zürich Switzerland

INTRODUCTION

Bone remodelling is known to be a function of its mechanical environment. However the precise nature of the mechanical signal governing bone formation is poorly understood. As well as improving our understanding of bone formation and bone quality maintenance, a quantitative understanding may ultimately reveal novel approaches for the treatment or prevention of age related fractures and diseases such as osteoporosis. Several computational models have attempted to provide theoretical frameworks which explain load induced adaptations. Whilst these models are able to mimic bone adaptation qualitatively, they lack quantitative validation. Here, using an in vivo model for synchronous cortical and trabecular bone adaptation, we attempt to characterize more precisely the relationship between the mechanical environment and bone remodelling.

METHODS

In a previous study we demonstrated appreciable 25.9% and 11% increases in both trabecular and cortical bone volume density, respectively when subjecting the fifth caudal vertebrae (C5) of C57/BL6 mice (15 weeks of age) to an acute loading regime (Amplitude of 8N, 3000 cycles, 10 Hz, 3 times a week for 4 weeks) [1]. We have also established a validated finite element (FE) model of age matched C5 vertebra using micro-computed tomography (μ CT) [2]. To investigate the relationship between load-induced bone adaptation and mechanical strains, in vivo and in silico data sets were compared. We divided cortical and trabecular compartments into 15 sub-regions (figure 1) and determined, for each region, a bone formation parameter $\Delta BV/BS$ (a cross-sectional measure of the bone volume added to cortical and trabecular surfaces following the described loading regime). Linear regression was then used to correlate mean regional values of $\Delta BV/BS$ with mean regional values of strain energy density (SED), orthogonal strains and shear strains. All mechanical parameters were derived from the FE models, similarly compartmentalized.

CONCLUSIONS

These results show that SED is able to predict the addition of cortical bone mass following an acute loading regime. The absence of any correlation for

trabecular remodelling may be indicative of two distinct remodelling mechanisms. In this study we have established a combined experimental and computational approach which will provide further insight into bone remodelling mechanisms when implemented with in vivo imaging technologies.

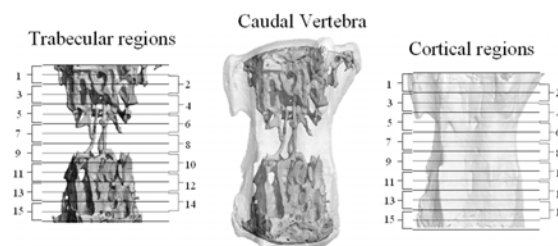


Figure 1: Digital image of a whole B6 vertebra (C5) showing cortical and trabecular compartments which are subdivided into 15 overlapping regions (1–15).

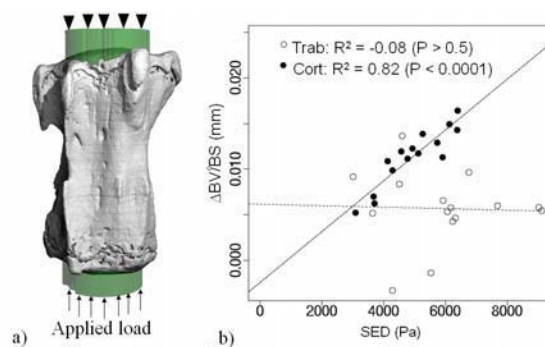


Figure 2: (a) Diagram showing the FE model. (b) Linear correlation of mean regional SED and mean regional $\Delta BV/BS$ for both trabecular and cortical bone.

Acknowledgements

The Swiss National Science Foundation (SEP 2-74153-02)

References

1. Webster et al, Abstracts 30th Annual meeting ASBMR, F527, 2008.
2. Webster et al, Computer Methods Biomech Biomed Engin. 2008 Oct;11(5):435.41

DEVELOPMENT OF MULTISCALE CAPABILITY FOR CELL BASED MODELLING OF EPITHELIAL TISSUE

Goodarz Khodabakhshi (1), Rod Smallwood (2), Rod Hose (3)

1 & 2. *The Department of Computer science, The University of Sheffield, United Kingdom*
; 3. *School of Medicine and Biomedical science, The University of Sheffield, United Kingdom*

Introduction

In the context of biology and physiology, various length scales are defined in terms of levels of biological organisation. A definition of multi-scale is suggested as being a model which includes components from two or more of these levels of organisation (multiple length scales) [Southern, 2008].

The main goal of the present research is to develop a multi-scale model to study the physical interaction of very large numbers of cells ($\sim 10^6$) during normal development, wound healing, and the development of malignancy, with links from cellular mechanical models to continuum mechanical models of tissue. Therefore, a finite element model of the forces acting on cells as a result of growth, division, and death of up to $\sim 10^6$ cells in three dimensions has been developed. This model is related to the continuum mechanical properties of collections of cells (i.e. tissues) in such a way that the constitutive properties at the tissue level can be derived from individual cell behaviour; that the effect of forces applied at a tissue level on individual cells can be ascertained; and that the signalling that results from forces applied to individual cells can be ascertained.

Method

Due to the non-homogeneity in material properties and multi-scale nature of the system (collection of cells), the conventional FEM would not be a proper choice for mathematical modelling; therefore an alternative approach has been chosen which is using the "Multiphase elements" [Lippmann, 1997]. The main idea of using Multiphase element is that the different material properties are assigned to individual integration points in the element. Thus, each Gauss point (not element), where the constitutive relationship is evaluated, will have different value for material properties. This effectively captures the variation in material property that occurs within a single element when its size is large. [Shim, 2007 and Fernandez, 2005]

Results and Discussion

The proposed model has the following advantages in comparison to the conventional FE modelling:

1-Higher flexibility of the models because one regular mesh can be used for the simulation.

2-Increased resolution of material gradients since different constitutive relations can be used in one element.

3-Increased numerical efficiency: if one would decompose one 8-node multiphase hexahedral element with eight Gaussian points into eight 8-node single-phase elements, the CPU-time for the calculation would be about 16-times higher in the single-phase simulation.

The proposed method shows a good agreement with the available data in the literature and used in conjunction with the biological model to construct a computational model of cell behaviour within the context of tissue architecture.

All simulation within this paper are carried out with the software package CMISS, which is developed at the bioengineering institute in Auckland. This modelling software package is designed for Finite element techniques for variety of complex bioengineering problems. It consists of a number of modules including an open source graphical front end (CMGUI) tool with advanced 3D display, and a computational backend (CM) that may be run remotely on powerful workstations or supercomputers.

Acknowledgment

We gratefully acknowledge financial support from EPSRC (UK) for this research.

References

- Southern J., et al., *Progress in biophysics and molecular biology*. 96 (2008) 60-89.
- Lippmann N. et al., *computational materials science*, 9 (1997) 28-35
- Shim V., et al., *Journal of biomechanics*, 40 (2007) 26-35.
- Fernandez, J. et al., *Biomechanics and Modelling in Mechanobiology*, 2(3) 2005, 139–155.
- CMISS, The Bioengineering Institute, University of Auckland. <http://www.cmiss.org>.

HIERARCHICAL BONE REMODELING MODEL WITH PERMEABLE MICROSTRUCTURES

Pedro G. Coelho (1), Paulo R. Fernandes (2), Hélder C. Rodrigues (2), José M. Guedes (2), João B. Cardoso (1)

1. FCT-UNL, Portugal; 2. IDMEC-IST, Portugal

Introduction

In this work a three-dimensional hierarchical bone remodelling model is presented. A global (macro) and local (micro) scales are identified with the whole bone and material (trabeculae), respectively. A global material distribution problem evolves concurrently with local material definition at each point of macroscale assuming that bone self-adapts to improve mechanical efficiency. However, pure mechanical criteria don't have been able to reproduce some features encountered in real bone such as permeability. In that way, the proposed global-local approach enables to introduce multiple local design constraints such as permeability.

Methods

At global scale bone is assumed as a continuum material characterized by equivalent (homogenized) mechanical properties. At local scale a periodic cellular material model approaches bone trabecular anisotropy in terms of mechanical properties. For each scale there is a material distribution problem governed by density based design variables, which at the global level can be identified with bone relative density [Coelho, 2008]. The macro-density ρ is coupled with micro-density μ through:

$$\rho(\mathbf{x}) = \int \mu(\mathbf{x}, \mathbf{y}) dY, \forall \mathbf{x} \in \Omega \quad (1)$$

where Ω correspond to the whole bone domain and Y is the micro-cell domain. The law of bone remodeling assumes that bone adapts to functional demands in order to satisfy a multi-criteria for structural stiffness (maximized) and metabolic cost k of bone formation (minimized) [Coelho, 2007]. A local requirement imposes that microstructure design must satisfy a proper relation between volume fraction and permeability according with [Kohles and Roberts, 2002], i.e., $K_{ii} \geq K_{min}$ e $K_{ij, i \neq j} \approx 0$, (\mathbf{K} is the homogenized permeability tensor).

Results

In figure 1 is shown the apparent density distribution for a proximal femur and respective microstructures obtained for the selected elements. The numerical model reproduces some anatomic features of real bone such as the external compact bone layer, medullar cavity, Ward's triangle and the

less dense spongy bone region. Microstructures exhibit a minimum permeability in all directions of the space. This is consistent with biological functions such as blood supply and cell migration.

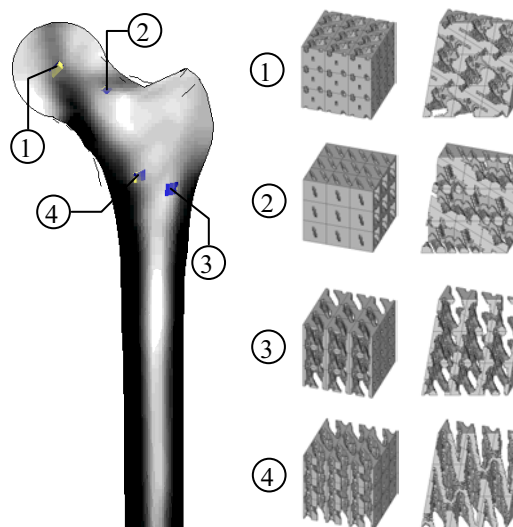


Figure 1: Apparent density distribution and representative microstructures for the selected elements (cut on microstructures shown at right).

Discussion

Simple stiffness maximization leads to microstructures with closed walls, which is not biologically consistent [Sigmund, 1999]. The actual model represents a new approach to computational prediction of bone adaptation taking into account specific features of trabecular architecture such as permeability. Thus, the two-scale model can be a valuable tool to medical diagnoses, to gain insight into the fine structure of bone as well as to support scaffolds design in the field of tissue engineering.

Acknowledgements

This work was supported by FCT through the project PTDC/EME-PME/71436/2006 and scholarship SFRH/BD/25033/2005. The results presented here were produced using the ISTcluster (IST/Portugal).

References

- Sigmund, ISBN0792356152, 221-234, 1999.
- Coelho et al, ISBN9789806939103, 221-227, 2007.
- Coelho et al, Struct Multisc Optim, 35:107-115, 2008.
- Kohles and Roberts, J Biomech Eng, 124:521-526, 2002

New numerical methods and tools #2

STRUCTURED TREE OUTFLOW BOUNDARY CONDITIONS FOR 3D LUNG SIMULATIONS

Andrew Comerford, Wolfgang A. Wall

Institute for Computational Mechanics, Technische Universität München, Germany

Introduction

Mechanical ventilation is an indispensable tool for the survival of critical care patients suffering from Acute Respiratory Distress syndrome (ARDS) or Acute Lung Injury (ALI). However the mortality rates of these diseases remains high, approximately 40%. In addition, it is widely known that the use of mechanical ventilation is itself the cause of a number of further associated complications, which are collectively termed ventilator induced lung injury (VILI) [Ware, 2000]. Understanding the reason why the lungs still become damaged or inflamed during mechanical ventilation, even with modern protective strategies, is a key question sought by the medical community. Here we present a model working towards understanding lung pressure air flow mechanics during mechanical ventilation.

Methods

The present model utilises a realistic 3D model of the lower airways with up to seven generations segmented. The airways beyond the 3D domain are modelled using a 1D approach where the impedance is calculated based on a 1D structured tree methodology, which has previously been used in 1D arterial simulation [Olufsen, 1999]. This model has been modified in order to represent the physiological environment in the pulmonary tree. The coupling of the 1D model to the 3D model is achieved utilising a Dirichlet to Neumann coupling similar to an approach previously used in artery blood flow simulations [Vignon-Clemental et al, 2006]. In this method the downstream 1D domain is applied as a pressure based condition on the outlets of the 3D domain. The coupled flow simulations were performed in an *in house* developed finite element multiphysics code.

Results

Simulations were performed using a realistic ventilator flow curve. A comparison of resulting pressure distribution between traction free and impedance based conditions is indicated in Figure 1. Evidently without the peripheral vessels the pressure is considerably lower (up to 27%). Furthermore from the results it was found that the transient flow pressure dynamics are different. The flow in the lung is *quasi-steady* (Womersley

numbers ~ 1), therefore flow rapidly responds to pressure changes. Both boundary conditions exhibit phase differences between flow and pressure during the deceleration phase, this indicates that the upper generations contribute more dominantly to the lung impedance than the peripheral vessels. However the peripheral vessels are important for correct pressure distribution/level in the lower generations.

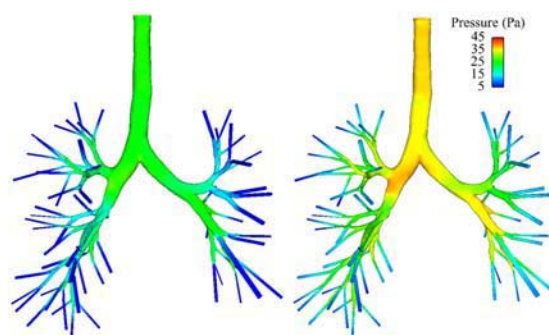


Figure 1. Comparison of pressure distribution between traction free (left) and impedance (right) boundary conditions, at max inspiration.

In addition the realistic geometry leads to elevations in pressure occurring in the higher generations, in particular pressure elevations and drops correspond respectively with widening and narrowing of the lumen.

Further to healthy lung simulations a *hypothetically* diseased lung was also investigated. The upper left lobe (superior) of the lung was blocked in order to simulate a lung of reduced functional capacity. This resulted in elevated pressure throughout the lung (up to 28% higher). This highlights a scenario which could potentially lead to *volutrauma*, due to an increase in lobular pressure.

Future work will involve coupling the present models to recently developed alveolar models [Wiechert, 2009]. This is in order to produce a full (airway and parenchyma) model of lung dynamics.

References

- Olufsen, M., American journal of physiology, 1999.
- Vignon-Clemental et al, CMAME, 2006.
- Ware et al, NEJM, 2000.
- Wiechert et al, J. Eng. Mech, 2009, accepted.

COMPUTATIONAL ANALYSIS OF SHOULDER ARTHROPLASTY: BONE REMODELLING AND JOINT WEAR

Carlos Quental(1), Nelson Ribeiro(1), João Folgado(1), Paulo Fernandes(1), Jacinto Monteiro(2)

1. IDMEC - IST, TU Lisbon, Portugal; 2. Medical School, University of Lisbon, Portugal

Introduction

Aseptic loosening is the most frequently long-term-complication in total shoulder arthroplasty (TSA) [Bohsali, 2006]. The harmful effect of polyethylene (PE) particles released during prosthesis wear has been pointed as one of the principal causes of loosening. The process of failure, as well as other complications, such as periprosthetic fracture, can also be associated with bone remodelling, which occurs in humerus after implant insertion. In this work computational models were developed to analyze the bone remodelling of the humerus and the wear of articular PE components, after a TSA.

Methods

The bone remodelling model is based on a global optimization criterion expressed as the minimization of a function which takes into account both structural stiffness and the metabolic cost related with bone maintenance [Fernandes, 1999]. The humerus was submitted to six loading conditions referring to six different movements. The action of ten distinct muscles was considered together with the glenohumeral reaction. Cemented and press-fit stems were modelled, considering different simulation conditions for cement-implant and bone-implant interfaces.

For wear determination, two models of prosthesis were built: anatomical and reversed. The modelled movement was unloaded abduction of the humerus from 5° to 180° [van der Helm, 1994]. The pressure distribution in PE was achieved using a finite element model of the shoulder obtained from computed tomography data. The contact problem, of rigid-flexible type, involved the articular surface of PE and the articular metal component (modelled as a rigid sphere). Wear was calculated in each contact node of PE [Fialho, 2007]. Finally, the influence of radial mismatch between articular components was analyzed in normal bone and bone degenerated by rheumatoid arthritis.

Results

Remodelling results for bonded models (implant fully bonded to bone or cement, regarding to the type of stem) presented some loss of bone mass in the proximal region of humerus. For the models that considered contact between implant and bone or implant and cement, which better reproduce *in vivo* conditions, no significant bone mass loss was

observed (Figure 1 (a-b)). The wear analysis evidenced that contact pressures and linear wear developed in the anatomical prosthesis were larger than the ones in the reversed prosthesis (Figure 1 (c-d)). However, the latter exhibited a worse volumetric wear performance. Relatively to the influence of radial mismatch, results indicated higher values of volumetric wear for higher congruent models, in both types of prostheses. At last, volumetric wear was higher in arthritic bone comparing with normal bone.

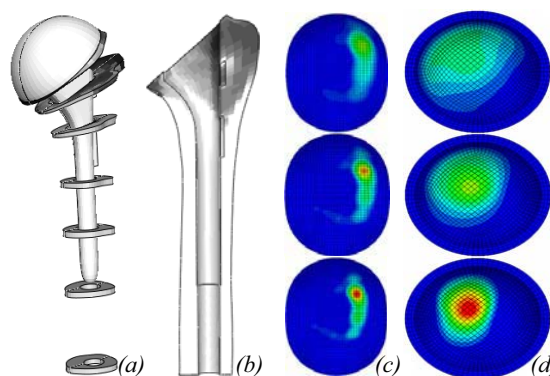


Figure 1: (a) Implanted geometric model; (b) Bone remodelling result for cemented stem; Linear wear results for (c) anatomical and (d) reversed model (results for several radial mismatch).

Discussion

Results of the remodelling analysis led to the conclusion that stress shielding and the resulting bone remodelling in humerus do not play a major role in failure of shoulder prosthesis.

Regarding wear analysis, it was observed that the constrained and congruent nature of reversed prosthesis promotes higher contact areas comparing with anatomical prosthesis (of unconstrained nature). In fact, this is the key factor for the highest values of volumetric wear registered in the reversed model, opposing the higher contact pressures and linear wear visualized in the anatomical implant. The same type of reasoning can be done to analyze the effect of radial mismatch in wear.

References

- Bohsali et al, J Bone Joint Surg Am, 88:2279-2292, 2006.
- Fernandes et al, Comput Meth Biomech Biomed Eng, 2:125-138, 1999.
- Fialho et al, J Biomech, 40:2358-2366, 2007.
- van der Helm, J Biomech, 27:527-550, 1994.

MORPHOLOGICAL STUDY OF OVINE SPINAL FACET JOINTS

Mohd Juzaila Abd Latif, Zhongmin Jin and Ruth K. Wilcox

School of Mechanical Engineering, University of Leeds, Leeds, LS2 9JT, UK

Introduction

The ovine spine is often used as a model for the human spine, although the anatomical comparisons of the spinal facet joints have yet to be established. The facet joints are important in governing the kinematics of the spine and a recent computational study has shown that the level of curvature of the facet surfaces has a significant effect on the segment load-displacement characteristics and the facet stress distribution [Holzapfel, 2006].

Although studies have been made to characterise the facet curvature [Van Schaik, 1999; McLain, 2002], newer imaging methodologies will now allow more accurate characterisation. The purpose of this study was to develop a new method to characterise the facet curvature from micro-computed tomography (μ CT) images and investigate the morphology of ovine spinal facet joints.

Methods

Two female Texel ovine spines (age, 4 to 5 years) were dissected into two-vertebra segments and imaged using μ CT. The scan plane was parallel to the upper endplate of the segmented vertebra. The facet orientation angles were evaluated using the transverse scan images as shown in Figure 1.

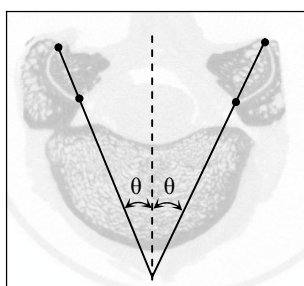


Figure 1: Facet orientation angle measurement.

Based on the active contour segmentation method [Chan, 2001], the facet joint images were segmented and the edge was detected using the Canny method in a MatLab (MathWorks Inc.) program. Boundaries were then created at the superior and inferior curvatures of the facet articular surface and the points along the boundaries were extracted. The points were used to create circles using a least-squares method to determine the superior and inferior facets radii as in Figure 2.

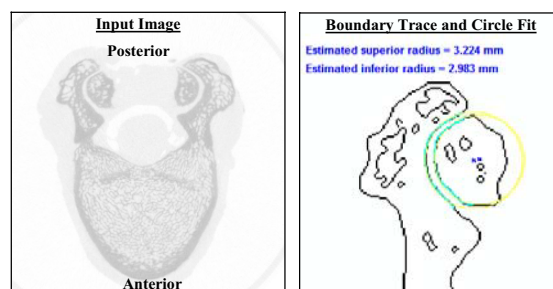


Figure 2: Transverse facet radius measurement.

Results

The measurements of the facet radii and angles from the lumbar region are illustrated in Figure 3. The facet joints of the thoracic vertebral segments from T2 to T11 were found to be virtually flat.

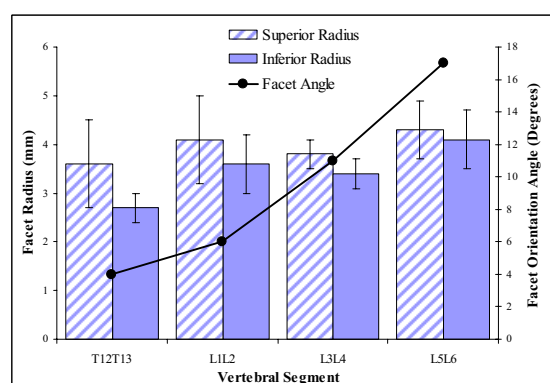


Figure 3: Results of facet radius and angle.

Discussion

This anatomical study described a new method to characterise the facet joint curvature using μ CT. The results provide a comprehensive morphologic database of the Texel ovine facet joints curvature. Although there were differences in the facet radius compared with the human, the lumbar region possesses similar curvature and might be used as a model for the human spine.

References

- Chan et al, IEEE Trans Image Proccs., 10:266-277, 2001.
- Holzapfel et al, Eur Spine J, 15:849-856, 2006.
- McLain et al, Spine, 27:E200-E206, 2002.
- Van Schaik et al, J Spinal Disorders, 12:341-347, 1999.

CLINICAL SOFTWARE DEVELOPMENT: WHY RESEARCH SYSTEMS FAIL TO TRANSLATE INTO CLINICAL SERVICE

Steven Wood

Sheffield Teaching Hospitals NHS Foundation Trust, UK

Abstract

This paper seeks to outline some of the major issues that relate to the clinical application of research software. Most of these issues are not particularly difficult to solve if they are considered during the design phase of the software. However, they can be very difficult, if not impossible, to solve effectively as an afterthought. For academic software development, it is common to realise the functional requirements first, before adding the management aspects once the software has demonstrated its clinical effectiveness. In the clinical environment, management and security requirements (outlined below) are often required before testing on any kind of scale can begin. This lack of engagement from developers early in the design process results in the software never undergoing proper, or even modest sized, clinical trials and therefore the software struggles to make the transition into routine service.

Five simple rules

Contained here is a short, but not exhaustive, list of common issues which can prevent research software being run in a healthcare environment.

Application Security: Having the ability to decide who is able to run an application is almost mandatory in clinical institutions today, with most commercial systems implementing some form of Role Based Access Control (RBAC). Therefore, integration with enterprise LDAP servers such as Microsoft Active Directory is vital to determine these access policies is vital.

Data Security: Sadly, the theft of PCs is a large problem in many open access institutions such as hospitals. Therefore, it is a requirement that no clinically identifiable data must be stored on the hard drives of machines. If you cannot provide the facility for your software to use UNC shares for such storage, other options such as bundling disk encryption applications such as TrueCrypt, may help with this requirement.

Deployment: Most enterprises use large-scale deployment tools such as Microsoft's SMS to remotely install packages on PCs. These tools generally require that there is a non-interactive

version of the installation process. The typical setup.exe process can often be called with the /s command line switch if the developers have thought to implement it. Having to manually click Next->Next->Next on three thousand PCs can be very costly.

Java!: In the experience of the author, some of the worst clinical software problems experienced have been due to the unpredictable nature of Java deployments and the applications that run on them. The fact that there is no enforcement of a link between which version of Java was used to build the software, and which version it is executed on, is a huge clinical risk and completely negates any quality testing that may have been carried out. At the very least, developers should embed checks into their application that ensure the code is running on a tested version of the JVM to avoid such issues.

Proxy servers: Many applications are based on web services or similar technology, but do not have the option of utilising a proxy server. Almost every large institution has a proxy server and in many of them, it is simply not possible gain access directly out of the firewall even if it is a "standard port". The assumption that clinical institutions, or indeed any large enterprise, have as flexible an approach to firewall configuration as academic institutions leads to software that will not even be considered by IT services, regardless of clinical functionality.

Design for the enterprise

The major considerations for use in a sector such as healthcare are scalability and security, and in fact these will often take precedence over functionality. In general, if an IT professional cannot deploy and begin testing within an hour, the software would be considered too immature for evaluation. Missing dependencies and obscure error messages are not acceptable, and whilst this will not be a shock to many developers, experience suggests researchers are still surprised at just how low the threshold is for professional IT service providers.

PULLOUT STRENGTH OF ORTHOPEDIC SCREWS CAN BE ACCURATELY ESTIMATED FROM A NOVEL *IN SILICO* TECHNIQUE

Andreas J. Wirth (1), Thomas L. Mueller (1), Wim Vereecken (2), Ralph Müller (1), G. Harry van Lenthe (1, 2)

1. Institute for Biomechanics, ETH Zurich, Zurich, Switzerland;

2. Division of Biomechanics and Engineering Design, K.U.Leuven, Leuven, Belgium

Introduction

Osteoporosis is a bone disease characterized by low bone mass and impaired bone strength, which leads to an increased risk of fracture. Due to pathological changes in bone's inner architecture, the treatment of osteoporotic fractures using orthopedic implants is complicated. Current methods to design better screws are hampered by the fact that the precise failure mechanisms of bone implants are still incompletely understood. Computational techniques to determine the pullout strength for screws in trabecular bone could potentially aid to further improve our understanding of the failure mechanisms. In particular, micro-computed tomography (μ CT) in combination with micro-finite element (μ FE) analysis appears to be a potent methodology to investigate these mechanisms. Therefore, the aim of this study was to test the feasibility of μ CT-based finite element analyses to quantify the stability of bone-implant constructs.

Methods

Orthopedic screws were inserted *ex vivo* in 10 sheep vertebral bodies. Pullout tests were performed in accordance to ASTM standard F 543, and pullout strength of the screws was measured. Before experimental testing, the samples were measured with μ CT. Subsequently, the μ CT images were converted into micro finite element (μ FE) models and solved using a large-scale linear FE-solver [Arbenz, 2008] on 720 dual-core processors of a Cray XT3 system. Strength was estimated, applying a criterion as developed for μ FE models of human distal radii [Pistoia, 2002]. For that purpose, analyses were performed on cylindrically shaped volumes of interest around the screws. Biomechanical measurements and results derived from μ FE analyses were correlated using the Pearson product-moment correlation coefficient.

Results

The μ FE models consisted of up to 17.9 million elements, and provided a detailed reconstruction of bone and implant geometry. All models were

solved for stresses and strains in less than 5 minutes. A visual representation of the Von Mises stress distribution of one representative specimen is given in Figure 1. Micro-FE calculated pullout strength correlated highly with the experimentally measured pullout strength ($r^2 = 0.87$) thereby statistically validating the μ FE approach (Figure 1).

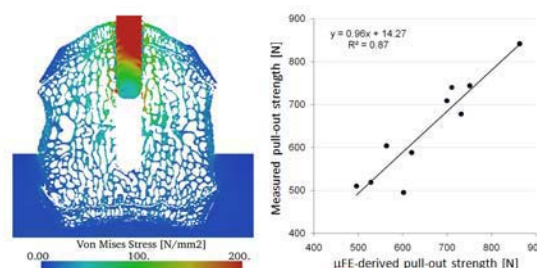


Figure 1: Von Mises stress distribution of one typical specimen. Linear correlation between μ FE estimated and mechanically measured pullout strength ($r^2 = 0.87$).

Discussion

Strong correlations were found between pullout strength as estimated from μ FE and the one measured experimentally, thereby validating μ FE analysis as a technique to determine the pullout strength of bone screws. This indicates that μ FE analyses can be used as a tool for the assessment of stability and strength of bone-implant constructs. Hence, μ FE analyses may lead to a mechanistic understanding of why low density bone offers less potential for screw fixation than normal bone, and may aid to systematically develop more appropriate screws to treat osteoporotic fractures.

Acknowledgements

This study was funded by the AO Foundation (network grant CPP1). Computing time was granted by the Swiss National Supercomputing Centre CSCS (Manno, Switzerland).

References

Arbenz et al, Int J Numer Meth Eng, 73(7):927, 2008.
Pistoia et al, Bone, 30(6):842, 2002.

Orthopaedic biomechanics

STRONGER IMPLANTS DO NOT CAUSE STRESS-SHIELDING IN THE FIXATION OF HIP FRACTURES – VALIDATED FINITE ELEMENT ANALYSIS AND CADAVER TESTS

Sebastian Eberle (1), Claus Gerber (2), Geert von Oldenburg (2), Peter Augat (1)

1. Trauma Center Murnau, Biomechanics Laboratory, Germany, 2. Stryker Osteosynthesis, Germany

Introduction

A stable fixation by osteosynthesis is essential to allow an early mobilization of patients with hip fractures. However, there are cases of implant failure. The reason for these failures can be amongst others pseudarthroses or high bodyweights of the patients.

When these patients are supplied with stronger implants to improve the fracture stability, it is feared that stress-shielding occurs. Stress-shielding is the effect when the load on the bone decreases and the load on the implant increases, because of the high stiffness of the implant. Especially reinforced intramedullary nails bear the risk of a shift of the failure mode from the nail to the lag screw in the case of overloading.

It was hypothesized that a reinforced intramedullary nail does not cause stress-shielding but results in lower strains and stresses within the implant during loading. The risk for fatigue failure would therefore be lower for a stronger implant than for a current nail design.

Methods

Two intramedullary nails were compared, a Gamma3 long and a reinforced prototype with a larger diameter of the proximal shaft.

Initially the von Mises stress distribution on the implants was calculated by finite element (FE) models. These models simulated the implant in the standardized femur [Viceconti, 1996] and were validated by strain measurements on the nail in a previous study [Eberle, 2009]. The implants were analyzed in two fractures (AO 31A3.1/A3.3) and two load cases. The two load cases simulated the maximum hip joint force with and without an additional muscle force, which acted on the lateral side of the femur. The forces were calculated based on the findings of Bergmann et al [Bergmann, 2001].

To check the results by the FE models, analog experiments in human cadaver bones were carried out. Six pairs of human femurs (age 67 ± 7) were osteomized and fixated with the two implants in a paired cross-over design. The specimens were tested in a servo electric testing machine to measure

the construct stiffness and the strains on the nail by two strain gauges during maximum load.

An unpaired t-test was used to determine statistical significant differences between the two implants ($p < 0.05$).

Results

The finite element simulations resulted in 11-28% lower stresses on the nail, 22-71% lower stresses on the lag screw and a similar construct stiffness (-7-12% difference) for the stronger implant in both fractures and load cases.

In the cadaver tests the stronger implant resulted in significant lower strains at the two strain gauges ($p < 0.001$; $p = 0.016$) and a comparable stiffness ($p = 0.446$) albeit the fracture type and the load case.

Discussion

The enhanced stability and stiffness of the implant by the reinforced proximal part of the nail shaft did not cause stress-shielding. The risk of fatigue failure was lower for the stronger implant because of the lower stresses and strains within the osteosynthesis. This was true for the nail shaft and the lag screw. Thus, obese patients or patients with expected delays of fracture healing may potentially benefit from the application of stronger implants.

References

- Bergmann G et al., J Biomech. 34(7):859-71, 2001.
- Eberle et al, Clin Orthop Relat Res, in review process with conditional acceptance, 2009.
- Viceconti M et al., J Biomech 29(9):1241, 1996.

INVESTIGATION OF INFLUENCE LOCATION OF MOBILE TYPE ARTIFICIAL DISC REPLACEMENT ON THE LOWER CERVICAL SPINE LOADING AND STABILITY

Lenka Jirkova (1), Zdenek Horak (1)

1. CTU in Prague, Fac. of Mechanical Eng., Laboratory of Biomechanics, Czech Republic

Introduction

The cervical spine instability is a common disease in clinical practice. Surgical treatments for degenerative disc disease can be grouped into two categories: fusion (arthrodesis) and total disc replacement (arthroplasty). Because fusion limits motion of the fused segments, it is believed that fusion may induce or accelerate degenerative change at adjacent levels. The objective of this study is to develop an experimentally validated three dimensional nonlinear finite element (FE) model of lower cervical spine using previously published data to provide useful information for artificial disc designers and examine the effects of surgical treatment on the structure for clinicians. The validated FE model was used to evaluate the mobil-type disc prosthesis on the range of motion in the multi-level C3-C6.

Method

A three-dimensional nonlinear model of a three-level ligamentous cervical segment (4 vertebrae and 3 discs) was built and implemented with the FEM software ABAQUS 6.6.3. Fig. 1. Two different configuration of the model were considered: a) a 'healthy model' was built and validated by comparing with previously published data b) a 'mobile model' had the middle level implanted with a artificial intervertebral disc replacement Prodisc-C made by Synthes.

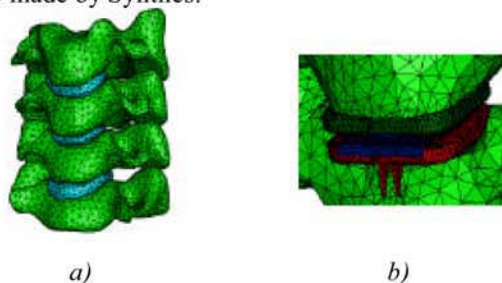


Figure 1: FE model of the cervical spine column C3-C6 a) healthy model by the motion in flexion, b) mobile model with the artificial disc implanted in C4-C5 in the flexion

Loading conditions: Both models were loaded by a) 1.0 Nm flexion/extension moment, b) 1.0 Nm axial

rotation moment, c) 1.0 Nm lateral bending moment. The loads were applied to the top surface of C3, while the bottom surface C6 was constrained the same way as in the in vitro experiments [Goel,1998], [Teo,2001].

Boundary conditions: The translational degree of freedom of the nodes from the underlying endplate of the lowermost vertebra have been restricted completely.

Results

The segment movement-ROM of intact spine was higher than the implanted spine at C4-C5 by all of movements with the exception rotation. These values ROM for the intact spinal segment are in very good accordance other measurements [Ha, 2005]. The ROM of the prosthesis implanted C4-C5 was reduced by about 50-70 % by (flexion, extension and right lateral bending). Under axial rotation moment, the ROM of the prosthesis implanted C4-C5 level is increases by about 18%.

Discussion

The FE analysis and experimental testing of cadaveric spine are the best method of investigating mechanical function and failure of the spine. Especially FE models can be used to explain experimental results of spine tissues. The movement of intact spine was validated with previously numerical and published results. In this project was carried out verification of modeling technique that is highly reproducible and objective. Nevertheless project is still in progress and the next step of this work is going to test next three mobile prosthesis, which has different mechanical properties and shapes as well.

Acknowledgements

The study was supported by a grant from Ministry of Education: Transdisciplinary research in Biomedical Engineering II, No. MSM 6840770012

References

- Goel V.K., Clausen J.D., Spine, 23: 684-691, 1998.
- Teo E.C., Ng H.W., Med Eng Phys, 23:155-164, 2001.
- Ha K.S., Mechanical Engineering and Physics, 28:534-541, 2005.

IN VIVO ARTICULAR CONTACT ANALYSIS IN A TKA – A FINITE ELEMENT STUDY

Bernardo Innocenti (1), Claudio Belvedere (2), Fabio Catani (2,3), Luc Labey (1), Andrea Ensini (2,3), Alberto Leardini (2)

1. European Centre for Knee Research, Smith&Nephew, Leuven, Belgium.
2. Movement Analysis Laboratory, Istituto Ortopedico Rizzoli, Bologna, Italy.
3. Department of Orthopedic Surgery, Istituto Ortopedico Rizzoli, Bologna, Italy.

Introduction

In this study the condylar and post-cam contact patterns in a total knee arthroplasty during in-vivo dynamic weight-bearing activities were evaluated using an innovative technique using finite element (FE) analysis. This technique utilises in-vivo 3D kinematics obtained from videofluoroscopy as input for the corresponding FE models.

Methods

Five patients implanted with a bi-cruciate posterior stabilized prosthesis (Journey® Bi-Cruciate Stabilized Knee System, Smith & Nephew, Memphis, TN) were analyzed with standard mono-planar three-dimensional fluoroscopic analysis during chair rising-sitting, stair climbing and step up-down [Banks, 1996]. These kinematics series were imported into original FE models of the femoral and tibial components to calculate tibio-femoral contact patterns, both at the condyles and at post-cam articulation. For each motor task and patient, the condylar contact points and the relevant contact line orientation were calculated at each collected frame by the model, and compared with corresponding estimations from traditional fluoroscopy-based only techniques [Banks, 2003]. Sensitivity of the FE analysis, and experimental tests were also performed to validate the technique.

Results

Both from fluoroscopy only and from additional FE analyses, and for all motor tasks, medial pivoting behavior was observed. The FE-based contact-line rotations were 15.3° for chair- rising/sitting, 14.8° for stair climbing and 14.5° for step-up/down as averaged over the 5 patients. The roll-back and screw-home mechanisms, typical of natural knee kinematics [Johal, 2005], were also found to be well replicated in all patients and motor tasks. The FE technique also showed, for all activities, that the post-cam mechanism is engaged during about 60% of the motor task time. In particular, in all three motor tasks, anterior contact at the post occurred at nearly full extension (for flexion angles smaller than 5° on average), posterior contact starts between 40 and 60°, no contact in between, as expected by the design. The experimental

validation revealed an error in the pressure centroid smaller than 2 mm.

Discussion

The FE technique derived from fluoroscopy reproduced well the contact points displacement, but with smoother, more reliable and consistent patterns (fig.1). The results suggest also that design features, such as anterior/posterior post cam guiding mechanism, can induce relatively normal kinematics during the investigated activities [Hill, 2000]. FE analysis confirmed that video-fluoroscopy is a suitable technique for evaluating in vivo knee kinematics but the addition of FE analysis is necessary for accurate contact point calculation and post-cam mechanism analyses.

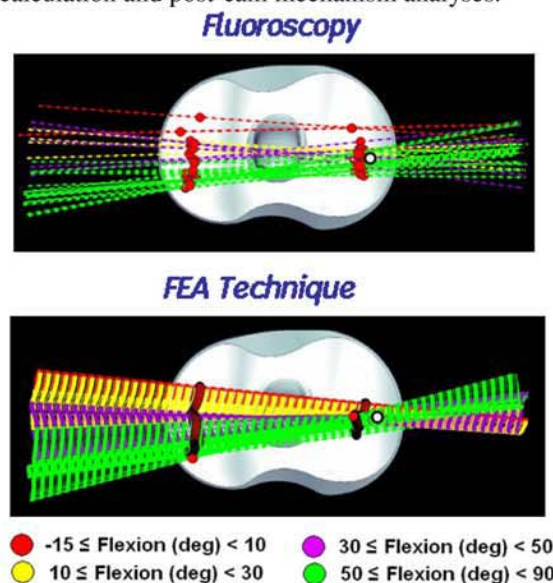


Figure 1: Comparison of the contact points location (red dots) and contact line rotation between those obtained using traditional fluoroscopy (on top) and those obtained using the FE model during chair rise-sitting motor task.

References

- Banks et al, IEEE Trans Biomed Eng, 413: 638-649, 1996
- Banks et al, Clin Orthop Relat Res, 410:131-138, 2003
- Hill et al, J Bone Joint Surg [Br], 82: 1196-1198, 2000
- Johal et al, J Biomech, 38:269-276, 2005

EVALUATION OF OSTEOSYNTHESIS OPTIONS AND FRACTURE HEALING PROGRESS FROM CT BASED FEA

Julia Koerber(1), Sebastian Eberle(1), Stephanie Panzer(1), Peter Augat(1)

1. Biomechanics Research Laboratory, BGU Murnau, Germany

Introduction

The bone healing process is primarily determined by the mechanical environment provided by osteosynthesis and the bone itself. The purpose of this study was to develop and validate patient-specific finite element analysis (FEA) generated from computed tomography (CT) data for the evaluation of fracture stability. These models have two primary purposes: To evaluate initial fracture gap movement with various osteosynthesis options and to assess changes in the stability during the fracture healing process.

Methods

In order to create patient-specific finite-element-models for various osteosynthesis options, trabecular bone and cortical bone were segmented according to their CT Hounsfield Units (HU) and the 3D geometries of these tissues were generated. Next fracture segments were aligned, potential implants were inserted and these volumes were meshed for FEA (Figure 1). Custom-written software was used to assign local bone mineral density (BMD) to elements in the model [Taddei et al, 2004], from which BMD-based material laws allow the stiffness of the bone to be predicted. Five material laws from the literature were tested in order to get the most accurate estimate of stiffness.

To validate the estimated mechanical properties, eight human femora were scanned and afterwards were loaded according to Bergmann et al to simulate the actual loads occurring in the femur. The overall stiffness was measured with a materials testing system (Zwick GmbH, Ulm, Germany) and the local displacement was measured by a 3D video measurement system (Pontos, GOM, Braunschweig, Germany). Mechanical tests of A3.1 and A3.3 fractures were also performed. The overall stiffness and local displacements were calculated with FEA and compared to the mechanical test results.

Results

It was found that the accuracy of these models was highly sensitive to the BMD-based material law used. Estimates of overall stiffness and deformation at specific points within 15 % were possible.

Finite element models of fracture callus are currently being validated with fractured ovine tibias at 6 weeks healing time. These models are being validated with axial compression, bending and torsion tests.

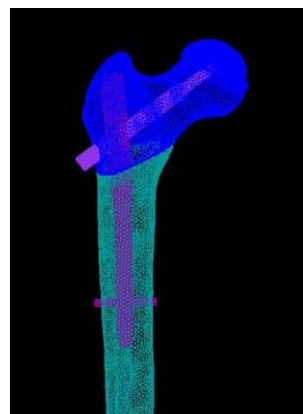


Figure 1: FEM of A3.1 fracture stabilized by an intertrochanteric nail

Discussion

In the future, patient-specific FEA from CT scans may be a useful tool to predict mechanical stiffness and local deformation of a bone-implant interface with a reasonable level of accuracy. In the future, this could be a useful tool to evaluate osteosynthesis options for a particular fracture scenario. Further, finite element models of fracture callus could be a potential tool to evaluate the healing progress of a fracture.

References

Taddei et al, Med Eng & Phys, 26: 61-69, 2004.

DESIGN OF TREATMENT STRATEGIES FOR AN ATROPHIC NONUNION CASE IN FRACTURE HEALING

Liesbet Geris, Jos Vander Sloten, Hans Van Oosterwyck

Division of Biomechanics and Engineering Design, K.U.Leuven, Belgium

Introduction

Over the last decade, many mathematical models on bone regeneration have been formulated that were able to simulate normal healing processes. However, the real interesting application of these models lies in simulating impaired healing cases and looking at potential therapies. In this study, a previously developed model (Geris et al., 2008) was applied to simulate an impaired healing case and design possible treatment strategies.

Materials & Methods

The mathematical model expresses the change of a number of continuum-type variables – growth factor concentrations, cell densities and matrix densities – as a function of time and space, resulting in a system of highly coupled and non linear partial differential equations. The model encompasses several key aspects of the bone regeneration process such as intramembranous and endochondral ossification and angiogenesis.

The impaired healing case modelled in this study is an atrophic non-union model (Reed et al., 2003) that represents fractures with massive soft tissue damage. Stripping of the periosteum and curetting of the intramedullary canal at fracture resulted in the formation of a vascularised fibrous callus. It was hypothesised that a shortage of precursor cells caused the healing process to fail.

Besides modelling the impaired healing process itself, several treatment strategies were investigated *in silico* such as the administration of mesenchymal stem cells (MSCs) or growth factors either at fracture induction or 3 weeks after fracture.

Results

The model was able to capture key aspects of the impaired healing process, i.e. the absence of cartilage and bone, the presence of a vascularised fibrous callus eight weeks after fracture.

Figure 1 shows the results for the various treatment strategies tested in silico. Administration of mesenchymal stem cells (Fig. 1a) at fracture induction led to a rather normal healing process with both intramembranous and endochondral ossification taking place. Administration of growth factors enhancing the proliferative capacity of the few mesenchymal stem cells that were present in

the callus (Fig. 1b, based on Makino et al., 2005) also resulted in a normal bone regeneration process. Administration of mesenchymal stem cells 3 weeks after fracture only led to ossification of the callus when the cells were administrated centrally (Fig. 1c) in the callus. Injection of a carrier with mesenchymal stem cells outside of the callus (Fig. 1d) 3 weeks after fracture led to the formation of a bony shell at the outside of the callus that prevented any further migration of stem cells into the callus which ultimately led to an insufficient recapitulation of the healing response.

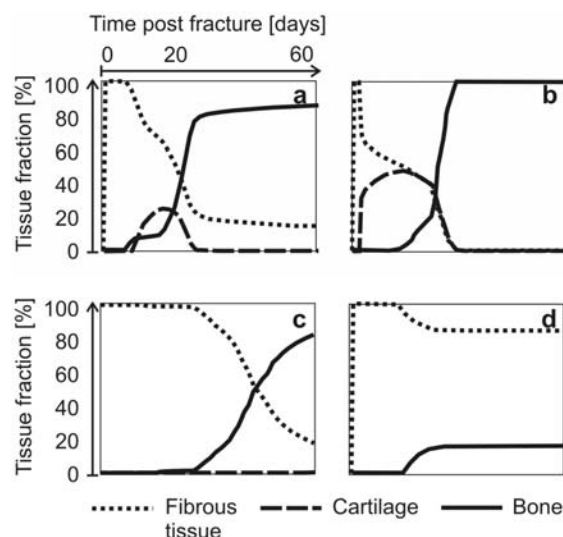


Figure 1: results of various treatment strategies. (a) addition of MSCs at fracture induction; (b) increasing MSC proliferation at fracture induction; (c) administration of MSCs at post fracture day (PFD) 20 in centre of callus (d) administration of MSCs at PFD 20 at outside of callus.

Conclusion

The model was able to reproduce essential aspects of the experimental atrophic nonunion model, demonstrating its potential for future applications.

Acknowledgements

L.G. is a postdoctoral research fellow of the Research Foundation Flanders (FWO).

References

- Geris et al, J Theor Biol, 251:137-158, 2008.
- Makino et al., J Orthop Res, 23:632-638, 2005.
- Reed et al., J Bone Joint Surg, 85:604-610, 2003.

THE ROLE OF BONE ARCHITECTURE ON IMPLANT ANCHORAGE

Davide Ruffoni (1), Ralph Müller (1), G. Harry van Lenthe (1, 2)

1. Institute for Biomechanics, ETH Zurich, Zurich, Switzerland

2. Biomechanics and Engineering Design, K.U. Leuven, Leuven, Belgium

Introduction

The determining factors for the mechanical fixation of implants in bone are the implant-bone interface and the peri-implant bone. Substantial efforts have been devoted to better understand how interface conditions affect implant anchorage and various methods have been proposed to enhance the bonding between bone and implant [Davies, 2007]. Less is known about the role of peri-implant bone. From a biomechanical view point, the amount and the arrangement of bone in the peri-implant region play important roles in the primary stability of implants but the precise effects are unknown. Nevertheless, this knowledge is crucial to better understand implant failure, especially in an osteoporotic bone [Goldhahn, 2007], which is characterized by a reduction of mass and a deterioration of architecture, leading to a higher probability of implant loosening. Therefore, the purpose of this work was to quantify the relative role of different architectural parameters on the mechanical stability of the bone-implant construct.

Methods

The foam-like architecture of trabecular bone was idealized as a three-dimensional cubic lattice (Figure 1a). Each trabecula was modelled with 4 Timoshenko beam elements that account for axial, bending and shear deformations. The microstructural features of the lattice such as trabecular thickness, trabecular number and trabecular separation were varied in a systematic and controlled way. Disorder was introduced in the trabecular network by a random displacement of the trabecular intersections. Bone material was modelled as elasto-plastic and the role of an infinitely rigid implant attached to the lattice was simulated with appropriate boundary conditions for the nodal displacements. The mechanical pull-out problem was solved numerically using the finite element method with ABAQUS (Rising Sun Mills, RI, USA).

Results

The stiffness and strength of the bone-implant construct were strongly dependent upon the relative density of the peri-implant bone region. A reduction in bone volume of 35% (to simulate a typical loss caused by osteoporosis) resulted in a decrease in the

ultimate force of 25% when the architectural deterioration was due to an increase in trabecular spacing (i.e. coarsening), in a decrease of 44% in case of trabecular thinning and in a decrease of 65% when the bone loss involved resorption of entire trabeculae (Figure 1b). Increasing the amount of disorder of the trabecular network had a negative effect on the stiffness of the bone-implant system but, conversely, increased the ultimate pull-out force.

Discussion

Although idealized, the current approach is helpful for a mechanical understanding of the role played by peri-implant bone in the implant failure mechanisms. The gained knowledge could also help tailoring osteoporosis treatment which should target the “weakest” architectural aspect. In addition, combining the present model with a more realistic representation of the trabecular network obtained through a skeletonization technique [van Lenthe et al, 2006], could give a fast specimen-based prediction of implant stability in osteoporotic bone.

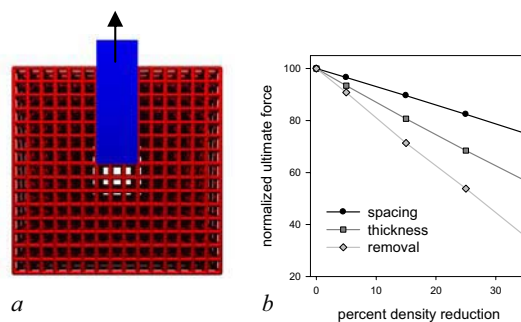


Figure 1: a) Idealized three dimensional beam model for the bone-implant system. b) Normalized ultimate force versus relative density for three different mechanisms of reducing bone mass.

Acknowledgments

This study was funded by the AO Foundation (network grant CPP1).

References

- Davies et al., *Biomaterials* 28: 5058-5067, 2007.
- Gabet et al., *Bone*, 39: 276-282, 2006.
- Goldhahn et al., *Osteoporos Int*, 37:1-10, 2006.
- van Lenthe et al., *Bone* 39:1182-1189, 2006.

Biomedical signals and instrumentation modelling

NUMERICAL SIMULATION OF THROMBUS ASPIRATION IN REALISTIC MODELS OF CATHETER TIPS

Giancarlo Pennati, Rossella Balossino, Francesco Migliavacca, Gabriele Dubini

Laboratory of Biological Structure Mechanics - LaBS, Dept. of Structural Engineering, Politecnico di Milano, Milan, Italy

Introduction

Thrombus aspiration catheters are devices used to remove a blood clot from a vessel, usually prior to angioplasty or stent implantation. These devices consist essentially of a catheter connected to a vacuum suction console or a syringe for manual aspiration. They are easier to use compared to other devices and limit the risk of releasing small particles in the microcirculation [Burzotta et al, 2007]. However, *in vitro* results [Hara et al, 2007] showed that the use of different commercial devices could produce very different thrombus removals, suggesting a primary dependence on the distal tip configuration of the catheter.

Methods

A computational methodology based on realistic catheter tip modelling was developed to investigate the factors affecting the thrombus suction. Two different catheter tip designs were considered, either with a single central lumen (model C) or a combination of central and side holes (model CH).

First, steady-state aspiration of distilled water from a reservoir was numerically simulated and compared with experimental tests. In particular, the pressure-volume flow rate relationship (ΔP -Q) was derived for the two catheter tips, according to the experimental set-up. In this set of simulations the fluid domain comprised also a portion of the basin where the fluid was aspirated.

Subsequently, the aspiration of a totally occlusive thrombus, modelled as a high viscous fluid, was simulated. For the sake of simplicity a totally occlusive thrombus was defined marking a number of cells in the fluid domain in order to model the blood clot as a cylinder with the same diameter of the blood vessel and 1.1 cm long (Fig.1). A two-phase flow analysis was performed, where blood and thrombus were modelled as two immiscible fluids having density of 1060 kg/m³ and 1300 kg/m³ and viscosity of 0.0035 kg/m·s and 0.035 kg/m·s, respectively. In particular, the benefit of additional openings was investigated.

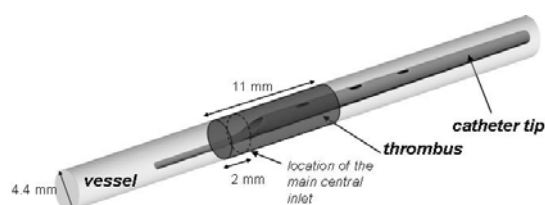


Figure 1: Fluid domains for the numerical simulations in the presence of the thrombus.

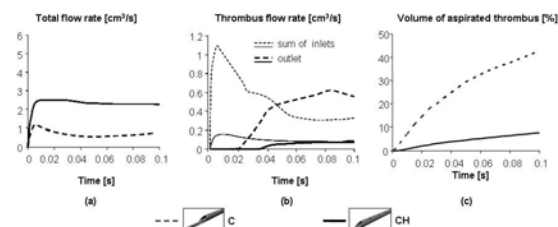


Figure 2: (a) total volume flow rate (thrombus and blood) at the catheter outlet; (b) thrombus volume flow rate at the catheter inlets and outlet and (c) thrombus percentage removed from the vessel.

Results and discussion

Good matching between the steady-state experimental and numerically simulated hydraulic behaviours allowed a validation of the numerical models. Numerical results of thrombus aspiration showed that the catheter with central and side holes had a worse performance if compared with the single central lumen catheter (Fig.2). Indeed, the inlets in contact with both blood and thrombus preferentially suck the former due to its much lower viscosity. This effect hindered the aspiration of thrombus. The amount of aspirated thrombus highly depends on the complex, two-phase, fluid dynamics occurring across the catheter tips.

Acknowledgements

The authors are indebted to Dr. Katia Laganà for her technical assistance in the *in vitro* experiments and to Invatec S.r.l (Roncadelle, BS, Italy) for supporting Rossella Balossino's PhD studentship.

References

- Burzotta F et al, J Invasive Cardiol, 19(8):317-323, 2007.
- Hara H et al, Euro Interv, 2:487-492, 2007.

IN SILICO BIOREACTOR FOR SIMULATING TISSUE ENGINEERING USING A MULTI AGENT MODEL. PRELIMINARY RESULTS

Laura Gaetano (1), Luis Antunes (2), Giacomo Di Benedetto (1), Gabriella Balestra (1)
Franco M Montecvecchi (1), Umberto Morbiducci (1)

1. Politecnico di Torino, Torino, Italy; 2. Universidade de Lisboa, Lisboa, Portugal.

Introduction

Cardiovascular disease (CVD) is the main cause of death and disability in the world, causing over 4.35 million deaths every year only in Europe. Tissue engineering is the new paradigm for the treatment of CVD: cells are cultured *in vitro* on scaffolds and tissue is matured in a bioreactor, in order to obtain functional implantable constructs. However, several problems arise *in vitro* culturing cells, due to the management of the complexity occurring in the whole system cell/scaffold/tissue. Aimed at supplement and extend the empirical techniques currently employed in tissue engineering, the *in silico* approach could play a fundamental role in analysing basic processes, integrating different experimental data, and predicting biological behaviours [Semple JL, 2005]. One promising tool in these terms is Multi Agent System (MAS): a network of intelligent agents, i.e., independent processing entities interacting with the external environment, and communicating with other agents and the environment to pursue their particular set of goals [Russel S, 1995]. In this study, the problem of simulating a tissue engineering experiment is addressed by creating a software framework based on MAS able to incorporate both a variety of phenomena that influence tissue growth and a model of cell population dynamics. In particular, we present a preliminary approach to the design of cardiomyocytes (CMs) adhesion, migration, proliferation.

Method

We designed adhesion, migration and proliferation of CMs, since these biological activities are the basis for many physiological and pathological processes. Simulations has the purpose to mimic the interaction of Cell Agents (CA): each CA represents a single cell with the specific main goals of proliferating and generating the new cardiac tissue. To pursue these aims, every agent acts in a manner that depends on process rules and on its inner state, that is represented essentially by cell position, cell size and some time parameters. In our model, the 2D space of observation represents a virtual scaffold, covered by sufficient culture medium, on which a finite number of cardiac cells is placed. Every single cell follows its "fate" (Figure 1): a sequence of events beaten by several time parameters (adhesion time T_0 , cell cycle G_1

phase time TG_1 , etc.) derived from literature data. We developed model's rules by considering data derived from *in vitro* experiments.

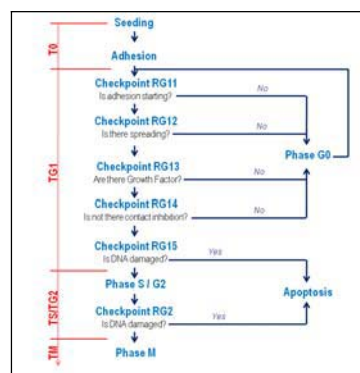


Figure 1: Cell "fate": sequence of events that every Cell Agent follows.

Results

The rule-set governs individual cells responses in the presence of some environmental changes: on the basis of this, we could simulate the proliferative activity of cultured CMs in presence of different concentration of calcium in the medium. The preliminary results we obtained showed accelerated proliferation of cells in low calcium concentration condition, in agreement with literature results.

Discussion

Our preliminary *in silico* bioreactor based on a MAS is able to simulate the basilar principles that lead to an *in vitro* tissue formation starting with single cells. We developed a network of CAs performing cell adhesion, migration and proliferation. In the near future, the model will include more complex intercellular signalling, mechanical stresses imposed on the construct cell/scaffold and dynamic micro-flow condition, in order to mimic all the aspects required for a generation of functional cardiac tissue. With these added features, MAS will become the tool not only for hypothesis testing, but also for hypothesis generation in regenerative medicine.

References

- Semple JL. et al, Tissue Eng, 11(3-4):341-356, 2005.
- Russel S. et al, Prentice-Hall, Saddle River, NJ, 1995.

AN OVERVIEW OF COMPUTATIONAL MODELLING IN NEONATOLOGY

Luiz C .Wrobel (1), Maciej K. Ginalski (2), Andrzej J. Nowak (3)

1. School of Engineering and Design, Brunel University, Uxbridge, UK; 2. FLUENT Europe, Sheffield Business Park, Sheffield, UK; 3. Institute of Thermal Technology, Silesian University of Technology, Gliwice, Poland

Introduction

The maintenance of an optimal thermal environment is regarded as a priority in neonatology. While healthy neonates are able to regulate their body temperature, premature and small infants may have difficulties adapting to temperature changes. For this reason, keeping an optimum environmental temperature is essential for their healthy development and even survival.

This paper reviews some of our recent applications of Computational Fluid Dynamics (CFD) to model heat and mass transfer processes in neonatology, and investigates the most relevant heat and mass transfer mechanisms taking place in medical devices such as incubators, open cots and oxygen hoods. This includes novel MATHEMATICAL developments giving rising to an Infant Heat Balance Module, which was fully integrated with the CFD solver and its graphical interfaces. The numerical simulations are validated through comparison tests with experimental results from the medical literature. It is shown that CFD simulations are very flexible tools that can take into account all modes of heat transfer in assisting neonatal care and the improved design of associated medical devices.

Methods

The governing equations of fluid and heat flow have been solved with the utilisation of the commercial CFD solver FLUENT. Heat exchange by conduction, convection and radiation between the neonate and the surrounding environment is determined through the solution of the mass, momentum and energy conservation equations. The airflow is considered to be turbulent and viscous. The Shear-Stress Transport (SST) turbulence model has been used in all simulations, with a correction for flows characterised by a low Reynolds number.

Most of the mathematical analysis carried out in bioheat transfer to date is based on Pennes' equation. Capabilities for solution of the bioheat equation are also available in the FLUENT solver. Metabolic contributions are included as distributed energy sources. Other effects also included as heat sources in the bioheat equation are the heat transferred with blood per unit volume of tissue, moisture evaporation from the infant's skin and

latent heat of evaporation from the infant's skin per unit volume of tissue.

Results

A series of validation tests has been performed based on extensive experimental studies of Hammarlund *et al.* (1977) and Sedin *et al.* (1983), who provided information on the weight, length, mass and gestation age for a group of 34 different infants. More information on the test cases analysed is given by Ginalski *et al.* (2007, 2008).

Typical results produced for the analysis of a double-walled incubator are shown in Figure 1.



Figure 1: CFD simulation of double-walled incubator. Flow path lines coloured by temperature.

Discussion

The results of the CFD simulations have been validated against experimental measurements and proved to be reasonably accurate in estimating the core and skin temperatures of infants nursed within incubators. The study also demonstrated the CFD capabilities of simulating transient processes occurring within oxygen hoods.

References

- Ginalski M K, Nowak A J and Wrobel L C, Medical Engineering and Physics 29:531-41, 2007.
- Ginalski M K, Nowak A J and Wrobel L C, Biomedical Materials 3: 034113, 2008.
- Hammarlund K, Nilsson G E, Oberg P A and Sedin G, Acta Paediatrica Scand. 66:553-62, 1977.
- Sedin G, Hammarlund K and Stromberg B, Acta Paediatrica Scand. (Supplement) 31:305-27, 1983.

A REAL-TIME HAEMODYNAMICS-BASED TEMPERATURE MODEL FOR HYPOTHERMIC PATIENTS

Martin W. Krueger (1), Michael Schwarz (2), Claudia Heilmann (3), Olaf Dössel (1)

1. Institute of Biomedical Engineering, Universität Karlsruhe (TH), Germany;
2. Institute of Industrial Information Technology, Universität Karlsruhe (TH), Germany;
3. Department of Cardiovascular Surgery, University Medical Center Freiburg, Germany

Introduction

Induced hypothermia is a common and effective method for tissue protection against ischemia during open-heart surgery. During such a procedure the patient is connected to a heart-lung machine, which pumps, oxygenises and cools the blood. However, the perfusionist obtains only little information on the various tissue temperatures. A real-time model of thermodynamics of the human body is presented to provide detailed temperature information.

Methods

In our model the body is represented by six elliptical cylinders (head, torso, arms, legs). Model individualisation is achieved by variable length and diameter of the cylinders to match the patient's body volume. Each cylinder is discretised according to its organ structure to minimise computational effort (e.g. a leg has less structural elements than the torso). 23 different organs and tissue types are distinguished within the model. Location and shape of the organs are based on a segmented Visible Human dataset (Sachse et al., 1996). Figure 1 illustrates the shape of the brain exemplarily. Non-organ volumes are set to composite tissues to achieve an overall body composition consistent with empirical data from literature.

Heat transfer in each of the 8464 elements is described based on Pennes' bioheat equation (Pennes, 1948). Each tissue is therefore characterised by its physiological and physical properties required for thermodynamic modelling: density ρ , thermal conductivity λ , specific heat capacity c , perfusion rate \dot{v} and metabolic rate \dot{w} .

Heat transfer also strongly depends on blood flow. Haemodynamics is modelled based on Avolio's transmission line model of the arterial system (Avolio, 1980; Schwarz et al., 2008). 61 terminal segments are identified and mapped to the 23 domains in the temperature model.

The coupled model is implemented on rapid-prototyping hardware for real-time simulation. The hardware is connected to the heart-lung machine via serial interface and supplies the model with

measurement signals (arterial and venous pressure and flow, blood and core temperatures).



Figure 1: Shape of the brain: Visible Human (left), cylinder model (right)

Results / Discussion

The inner energy U_i of the coupled model is constant for isolating boundary conditions stating its mathematical correctness. The model converges to normal steady state temperatures in a thermo-neutral environment (fig. 2, left), which proves its physiological accuracy. Simulations of procedures in hypothermia agree with several measurement datasets. Figure 2, right, depicts the signals of two simulated temperatures compared to the measured signals.

The model is capable of providing detailed and reliable information on the temperature of different organs to the perfusionist during cardiac procedures in hypothermia.

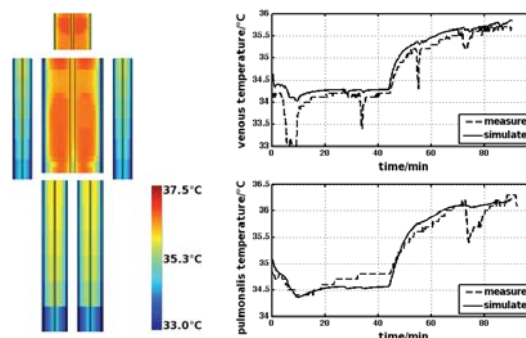


Figure 2: Left: Temperatures in the longitudinal plane of the temperature model in steady state. Right: Measured and simulated venous temperature (top) and in the pulmonary artery (bottom)

References

- Avolio, Med Biol Eng Comput, 18:709-718, 1980.
- Pennes, J Appl Physiol, 1(2):93-102, 1948.
- Sachse et al., Proc First Users Conference of the National Library of Medicine's Visible Human Project, 1996.
- Schwarz et al., Proc 6th IASTED Int Conf Biomed Eng, 193-198, 2008.

CFD ANALYSIS FOR VORTEX DESIGN IN MICROMIXERS

Francesco M. Mastrangelo¹, Francesco Pennella¹, Marco Rasponi (2), Alberto Redaelli (2), Franco M. Montevicchi¹, Umberto Morbiducci¹

1 Department of Mechanics, Politecnico di Torino, ITALY; 2. Politecnico di Milano, Italy

Introduction

Many sensor problems can be addressed in clinical medicine by applying new knowledge from the rapidly growing MEMS, BioMEMS, and microfluidics fields. For example mixing reduces longitudinal dispersion, which is important in determining performance in pressure-driven chromatography [Stroock, 2002]. In this sense μ -TAS involves many of the functions found in chemical analysis, including fluidic transport, mixing, reaction, and separation. Microfluidic systems are often compact in size, disposable, and admit analysis at higher speed using decreased sample volumes: mixing becomes crucial for most reaction performance. Many fundamental issues that are not observed in macro flows are prominent in microscale fluid dynamics. In the design of microfluidic systems engineers face the challenge to properly design duct geometry and fluid behaviour to induce mixing vortices. Object of this work is the simplification of passive mixer design by the use of CFD derived “rule of thumb”.

Methods

Dean studied the secondary flows induced by curvature [Dean, 1928], introducing stream curvature as source of instability. Dean criterion defines a lower limit for curvature k for induced Dean vortices in terms of

$$Dn = Re_D \sqrt{\frac{D}{R}} = Re_D \sqrt{kD} \quad (1)$$

where D and Re_D are respectively duct diameter and its relative Reynolds number. In the “Dean plane” [$\log(Re_D) // \log(kD)$] the fluid stability criterion is represented by a straight red line [Fig. 1.C], while the geometric constrain (pipe diameter cannot exceed the double of radius of curvature) limits the minimal Reynolds number (@ $Dn=36$, $Re_D=18\sqrt{2}$ [Dean, 1928]) at which instability should create vortices.

Clearly this is not the case for microfluidic flows: Re_D is strictly lower than critical. In a straight pipe pressure head decays linearly in the stream wise direction while the flow pattern maintains its parabolic profile (Poiseuille flow). Many researchers adopted the hypothesis that curvature has a marginal effect on the flow [Taylor, 1923] [Dean, 1928]. This hypothesis has been tested on a

transition geometry (clothoid//arc) using incompressible Navier–Stokes equations by means of the finite volume method. The transition geometry has a linearly increasing curvature with the curvilinear coordinate s ($k=\pi s$ Cèsaro eq. for the clothoid). The onset of vertical structures function of curvilinear position (duct curvature) will be resumed in empirical relation at subcritical Re_D similarly to (1).

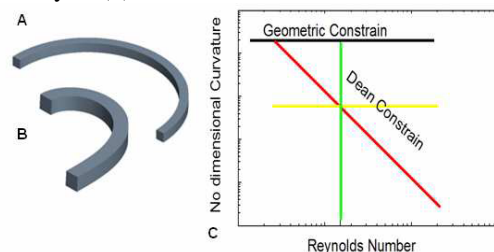


Figure 1: CFD of squared duct geometry duct $k=cost$ and $k=\pi s$ length (clothoid) (B). Bi-logarithmic Dean plane (C): the red line represents the Dean criterion. Horizontal line represents constant curvature (at different Re_D), vertical lines at const Re_D but varying curvature (clothoid duct).

Results

CFD analysis on the clothoid duct [Fig. 1.B] shows that pressure decays linearly streamwise at low Re_D ; the velocity varies only in radial direction in first approximation. These observations confirm the hypothesis that pressure loss is not significantly dependent on duct geometry at low Re_D . Numerical simulations inside the clothoid duct explore the Dean plane trough vertical lines until instability region is reached [Fig. 1.C].

Discussion

From our results on clothoid duct we speculate that the proposed model of microchannel might simplify mixing design task by controlling vortex onset. In this sense, CFD analysis is very helpful in deriving simple rules, for properly design microfluidic systems with increased effectiveness in mixing and, as a consequence, in chemical reactions.

References

- G. I. Taylor. Phil. Trans. A 223, 289 (1923)
- Dean WR. Philos. Mag. 5:673 (1928).
- Stroock et al., Science (2002).

A BOUNDARY ELEMENT MODEL OF VASCULAR MICROBUBBLE TRANSPORT IN GAS EMBOLOTHERAPY

Andres J. Calderon (1), Brijesh Eshpuniyani (2), J. Brian Fowlkes (1), Joseph L. Bull (1)

1. University of Michigan, USA; 2. IIT Kanpur, India

Introduction

This study is motivated by a novel developmental gas embolotherapy treatment for cancer that involves occluding blood flow to tumors using selectively formed microbubbles [Bull 2005]. In this approach, extremely small lipid- or protein-coated liquid droplets ($\sim 6 \mu\text{m}$ or smaller in diameter; small enough to pass through capillaries) of a perfluorocarbon (dodecafluoropentane, DDFP) are injected into the blood stream at a convenient location. Although these DDFP droplets are superheated at body temperature (boiling point 29°C at atmospheric pressure), the shell prevents the droplets from spontaneously vaporizing. At the desired location these droplets are selectively vaporized using high intensity ultrasound, termed acoustic droplet vaporization (ADV), to form gas bubbles that are approximately 150 times larger in volume than the initial droplets. These microbubbles eventually lodge in the microcirculation in or around the tumor to occlude its blood supply and thus induce tumor necrosis.

Each step in this sequence, e.g. (1) ADV, (2) microbubble transport, and (3) microbubble lodging, must be understood in order to design of intelligent treatment strategies for gas embolotherapy. Previous studies have examined ADV [Kripfgans, Fowlkes et al. 2000; Kripfgans, Fowlkes et al. 2002; Kripfgans, Fabiilli et al. 2004; Ye and Bull 2004; Ye and Bull 2006], bubble transport [Calderon, Fowlkes et al. 2005; Eshpuniyani, Fowlkes et al. 2005; Eshpuniyani, Fowlkes et al. 2008], the mechanics of lodging of bubbles that are large compared to the vessel diameter [Calderon, Heo et al. 2006], and the ability to occlude flow in vivo [Kripfgans, Orifici et al. 2005]. This study is focused on the transport of microbubbles through bifurcation, which affects the ultimate homogeneity of microbubble lodging and occlusion.

Methods

This model considers the time-dependent motion of a semi-infinite bubble through a geometrically symmetrical two dimensional bifurcating channel. The bubble contacts the channel walls and is driven by a constant bubble pressure. The surrounding liquid is assumed to be incompressible and Newtonian. Since the microcirculation is a low Reynolds number regime ($\text{Re} \ll 1$), we solve the

Stokes equation (conservation of momentum) and conservation of mass. These equations are solved using the boundary element method, which we have previously used for microscale and interfacial flows.

Results

Simulations conducted for a range of physiologically relevant non-dimensional parameter values for arterioles and capillaries. Some of these results are briefly described here. We define the splitting ratio as the ratio of the bubble lengths that enters each daughter branch of a bifurcation, such that it is between zero (bubble entirely enters one branch) and one (even splitting). Increasing driving pressure increases the splitting ratio.

Discussion

This study has shown that the splitting ratio increases with increasing driving bubble pressure while it decreases as the bifurcation angle is increased. Viscous losses at the bifurcation affect the bubble speed significantly. Achieving a uniform tumor occlusion will require high splitting ratios at bifurcations near the tumor.

Acknowledgements

This work is supported by NIH grant R01EB006476.

References

- Bull, J. L. Critical Reviews in Biomedical Engineering, 33: 299–346, 2005.
- Calderon, A. J., et al. J. Appl. Physiol., 99: 479–487, 2005.
- Calderon, A. J., et al. Applied Physics Letters, 89: Art. No. 244103, 2006.
- Eshpuniyani, B., et al. Int. J. Heat Fluid Flow, 26: 865–872, 2005.
- Eshpuniyani, B., et al. Int. J. Heat Mass Trans., 51: 5700–5711, 2008.
- Kripfgans, O. D., et al. J. Acoust. Soc. America, 116: 272–281, 2004.
- Kripfgans, O. D., et al. Ultrasound Med. & Biol., 26: 1177–1189, 2000.
- Kripfgans, O. D., et al. IEEE Trans. UFFC, 49: 726–738, 2002.
- Kripfgans, O. D., et al. IEEE Trans. UFFC, 52: 1101–1110, 2005.
- Ye, T. and J. L. Bull J. Biomech. Eng., 126: 745–759, 2004.
- Ye, T. and J. L. Bull J. Biomech. Eng., 128: 554–563, 2006.

Poster Presentations

Poster Session A

EXPOSURE OF CELL CULTURE TO LF ELECTRIC FIELDS. INDUCTION OF ALKALINE PHOSPHATASE ACTIVITY

**Bruno Bisceglia (1), Hylde Zirpoli (2), Mariella Caputo (2),
Francesco Chiadini (1), Antonio Scaglione (1), Mario Felice Tecce (2)**

1. Department of Information and Electrical Engineering,
University of Salerno, Fisciano (SA), Italy; bbisceglia@unisa.it

2. Dipartimento di Scienze Farmaceutiche, Univ. of Salerno, Fisciano (SA), Italy.

Introduction

LF (Low Frequency) electromagnetic fields are currently used for clinical therapies of several bone diseases. These treatments are given with the goal to increase bone regenerative processes, but their efficacy is based on clinical evidences. To identify possible molecular mechanisms accounting for LF fields ability to stimulate bone regenerative processes, we evaluated at a biochemical level the effect on cultured cell lines of the signal of currently used clinical apparatus (frequency 60 kHz, frequency of the modulating signal 12.5 Hz, peak-to-peak voltage 26 V).

Methods

Two different human cell lines, bone SAOS-2 and liver HepG2, were used for LF field stimulation, representing a considerable model of patient tissues, since they allow a strictly controlled experimental condition and a precise effect analysis.

The cultures were exposed to the signal whose characteristics are described in the introduction. Planar electrodes are placed on of the largest bottle walls (dimensions 4.7 x 5.4 cm, thickness 1 mm). An elementary electric model of the system can be represented by a parallel plate capacitor.

Results

LF fields significantly increased alkaline phosphatase enzymatic activity within both cell lines after 1 hour of stimulation. The increase was of about 35% in SAOS-2 and of 80% in HepG2 cells. No temperature variations were detected during LF fields exposure.

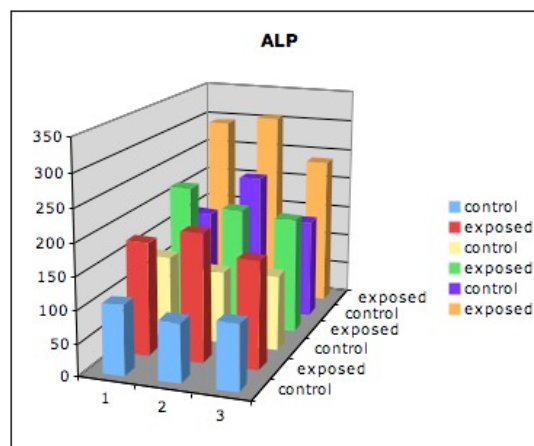


Figure 1: Increase of Alkaline Phosphatase for HepG2 culture.

Discussion

Since alkaline phosphatase expression is considered a typical marker of bone tissue regeneration, the reported results represent a valuable evidence of biological effects of LF field treatments in clinical therapies of bone diseases.

In addition, the finding of similar effects in cells derived from two different tissues is more likely indicating their existence in living organisms.

Acknowledgements

Thanks to Igea for the availability of the exposure system.

References

- Impagliazzo et al, J of Orth and Traumat, 2006.
- Lewin, Computing in Science & Engineering, 2002.
- Lohmann et al, J of Orth research, 2000.

CAPACITIVELY COUPLED ELECTRIC FIELDS TREATMENT OF SPINE. EVALUATION OF ELECTRIC FIELD IN TISSUES.

Bruno Bisceglia (1), Ruggero Cadossi (2), Nicola Cappetti (3), Assunta De Vita (4), Michele Pappalardo (3), Maurizio Sarti (5), Stefania Setti (2), Giovanni F. Solitro (3)

1. Department of Information and Electrical Engineering, University of Salerno, Via Ponte Don Melillo, 84084 Fisciano (SA), Italy, bbisceglia@unisa.it
2. IGEA, Via Parmenide, 41012 Carpi (MO), Italy,
3. Department of Mechanical Engineering, University of Salerno, Via Ponte Don Melillo, 84084 Fisciano (SA), Italy.
4. TWG, University of Sannio, C.so Garibaldi 107, 82100 Benevento (BN), Italy,
5. CNR-IREA, via Diocleziano 328, 80124 Napoli, Italy.

Introduction

A customized spinal column model is developed for evaluating the effect of *Capacitively Coupled Electric Fields* (CCEF) treatment employed to resolve some bone related disorders as an alternative procedure to conventional intervention of orthopaedic surgery [A. Impagliazzo]. An electric signal with CCEF technique is applied at the fracture site. The performed computations could be an useful tool for studying the processes of fracture and bone healing.

Methods

Starting from a 3D CAD model of part of a spinal column composed by three vertebrae, we developed a model made of a geometric wireframe skeleton, controlled by parameters, that holds the external surfaces of the vertebra [G. Amato, 2007]. Vertebrae models were obtained from TAC images by Reverse Engineering techniques, and assembled by contact of articular facets in order to represent a real lumbar tract. In particular, other than discs and vertebrae volumes, the spinal cord, meninges, capsular ligaments, muscles and skin volumes are present. A 60 kHz 20 V_{pp} signal was placed on a pair of external electrode in contact with the skin. As in the clinical practice, the electrodes were placed directly onto the skin at the sides of the spinal column, at 10 cm distance from each another. *Comsol Multiphysics* simulation code, based on the *Finite Element Method*, was used to solve the model described above.

On the upper part of the vertebral body of the mid vertebra, a thin clove was created, that represents a crack zone which doesn't divide completely the vertebral body. Cracked column models differ from healthy column model only for characterization of material properties of the clove so meshes and boundary conditions are identical, and differences of results depend only on electrical properties in the cracked zone [Fig 1].

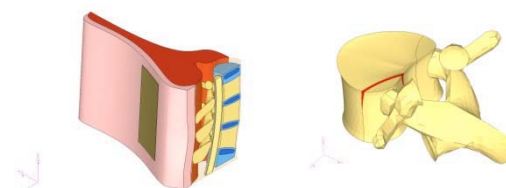


Fig. 1a: Spine model. Fig. 1b: Cracked vertebra

Results

The electric field and the current density were evaluated in the various tissues, providing a description of the evolution of the entire analyzed phenomenon. The obtained values confirm previous results present in literature [Table 1].

Tissue	E field [V/m]	Current density [A/m ²]
Bone	12.63/12.62	1.06/1.05
Muscle	6.64/6.64	2.36/2.36
Fracture	12.79/8.76	1.07/6.14

Table 1: Mean value of electric field and current density for spine healthy and fractured inside some tissue.

Discussion

The correlation between the exposition and the process of recovery is not an objective immediately achievable. The obtained results, the conformity of such results with the experimental data at the moment represent a good support for investigation of CCEF effects on biological processes.

References

- A. Impagliazzo et. al., "Treatment of nonunited fractures with capacitively coupled electric fields," J. of Orthop. Traum., pp: 16-22, vol. 7, 2006.
- G. Amato, N. Cappetti, A. Naddeo, and G.F. Solitro, A customizable spinal column CAD model, ICCB 2007, III International Congress on Computational Bioengineering, Caracas, Venezuela, September 17-19, 2007.

A PARAMETRIC FINITE ELEMENT EVALUATION OF PROPHYLACTIC VERTEBROPLASTY

Vithanage N Wijayathunga (1), Robert J Oakland (1), Richard M Hall (1), Ruth K Wilcox (1)

1. Institute of Medical & Biological Engineering, University of Leeds, Leeds, United Kingdom

Introduction

There are concerns that vertebroplasty may predispose patients to additional fractures in the adjacent vertebrae due to changes in the load distribution. To reduce this likelihood, augmentation of identified at-risk vertebrae prior to fracture (prophylactic vertebroplasty) has been proposed as a potential therapy. The aim of this study was to parametrically examine key patient and treatment variables on the effects of prophylactic vertebroplasty on the adjacent vertebrae.

Methods

A three-vertebra segment (T12-L2) was imaged using quantitative computer tomography and was prophylactically augmented with cement at the L1 level. It was tested in compression within the elastic limit, before and after augmentation. The pre-augmentation images were used to generate a finite element mesh, with the bony elements being assigned properties based on the image greyscale using a previously developed method [Wijayathunga, 2008]. The properties of the annulus (anisotropic) and nucleus (isotropic) were initially based on healthy tissue and were iteratively altered until the model behaviour matched that of the pre-augmentation experimental specimen, which had highly degenerated discs. Then, using data from the post-augmentation scans, a cement region was added in the L1 vertebra to simulate the prophylactic vertebroplasty. As a validation step, the augmented model behaviour was compared with that seen experimentally. In the subsequent parametric study, the properties of the disc and bone tissue as well as the cement region modulus and volume were varied. The effects were compared between each new model and the original based on the experimental specimen ('base state').

Results

The post-augmented predicted stiffness of the segment model (665 N/mm) closely matched the experimentally-measured (660 N/mm), indicating that the model is able to predict the gross behaviour of the segment following vertebroplasty. The segment stiffness was found to be higher with degenerated discs than with healthy discs and, to a lesser extent, also increased with increasing bone mineral density. The stresses in both the remaining

bone in the L1 vertebra and the bone in the L2 vertebra were higher in the degenerated disc model. The variation in segment stiffness with the cement region elastic modulus was found to be small (3.3% change in stiffness for 87.5% reduction in cement modulus). The stress in the adjacent T12 vertebra increased with increasing cement volume and led to high stresses when combined with degenerated discs (Figure 1). Compared to the base model, there was lower displacement across the disc and greater displacement across the adjacent vertebrae as the cement volume increased and the BMD decreased.

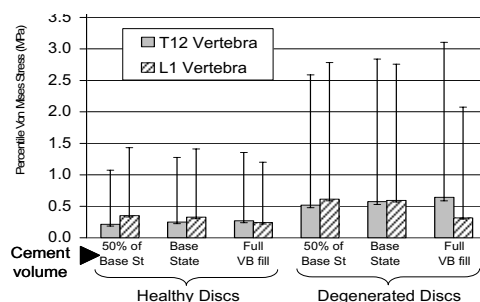


Figure 1. Median (range: 10th–90th percentiles) von Mises stress in the vertebral elements with varying cement volume.

Discussion

The finite element model was generated directly from images of an experimental specimen allowing one-to-one comparisons between the model predictions and the specimen behaviour. Good agreement was found in the post-augmentation behaviour but no comparisons were made with the internal stress fields and therefore model outputs were only used to compare between models.

Previously it has been indicated that post-procedural adjacent and peri-augmentation fractures may occur following prophylactic vertebroplasty [Oakland, 2008]. The outcomes of this study suggest that both the quality of the bone and adjacent disc tissue will affect the load transfer. The greatest risk of adjacent fracture is likely to occur if large volumes of cement are used in patients with low BMD and highly degenerated discs.

Acknowledgements

Funded by EPSRC and Action Medical Research.

References

- Oakland et al. J. Neurosurg. Spine, 8: 442-449, 2008.
- Wijayathunga et al. J. Eng. Med, 222: 221-228, 2008.

DEPTH AND TIME DEPENDENT POISSON RATIO OF CARTILAGE EXPLAINED BY A FIBER EMBEDDED BIPHASIC MODEL

Salman Chegini (1), Stephen J. Ferguson (1)

1. Institute for Surgical Technology and Biomechanics, University of Bern, Switzerland

Introduction

Achieving a cartilage model which is valid simultaneously for all experimental tests is a long standing challenge. Time and depth dependent Poisson ratio has been observed during unconfined compression experiments on articular cartilage, but existing cartilage models have not fully addressed or predicted these phenomena. We hypothesized that feeding detailed experimental data to the model would enable the model to capture this phenomena.

Methods

The axisymmetric geometry of the cartilage model was created based on the experiments of [Korhonen, 2002], in which cylindrical bovine cartilage plugs with a height of $h=1.15\text{ mm}$ and diameter of $d=3.7\text{ mm}$ were used for confined and unconfined compression tests. Depth dependent aggregate modulus and tensile modulus of the cartilage was extracted from experiments [Schinagl, 2004, Verteramo, 2004]. Also the depth dependent fluid fraction was taken into account [Shapiro, 2001]. The proteoglycan matrix and interstitial fluid were modelled as biphasic, with nonlinear strain dependent permeability [Lai, 1981]. Discrete orthotropic layers were embedded in this media, using the “embedded element” option within ABAQUS finite element software (ABAQUS 6.7-1, © Dassault systems), to account for the high tensile modulus of the cartilage. The step-wise displacement was applied to the model at $1\mu\text{m/s}$, followed by relaxation, to max. 20% nominal strain.

Results

To find the permeability material constants, the response of the model was fitted to the experimental data through a nonlinear optimization algorithm.

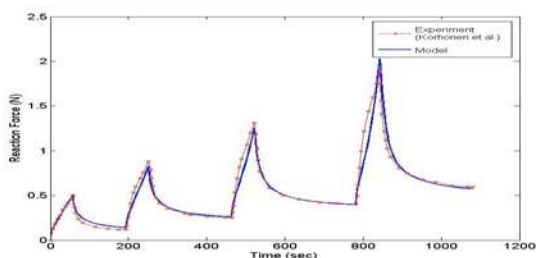


Fig 1. Reaction force from the model compared to confined compression experimental data.

Through this fitting, the initial permeability as well as the constant of nonlinear permeability were calculated as $k_0=5\times 10^{-15}\text{ m}^4/\text{N.s}$ and $M=2.3$ respectively. For validation the model prediction was compared with the unconfined compression data, for both reaction force and lateral displacement as shown in figure 2.

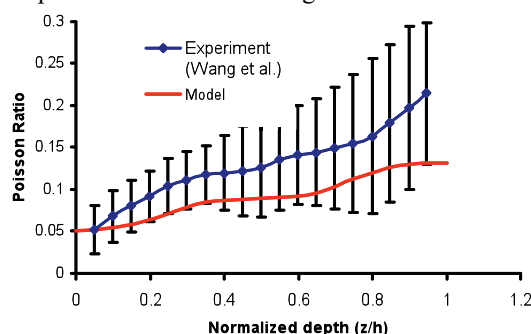


Fig 2. Poisson ratio as a function of depth during unconfined compression (10% strain).

Discussion

The complex behaviour of articular cartilage is due to composition and structure of these components. This study suggests that taking depth dependent aggregate and tensile moduli of the various layers of the cartilage into account helps to predict the overall time dependent reaction forces, as well as spatial and chronological distribution of lateral displacement. The presented model simultaneously fits experimental confined, unconfined and tensile testing results, using a single material property set. The model can be further improved by taking the viscoelasticity of the solid elements into account as well as considering the direction dependent permeability. Incorporating more experimental data on tensile tests on thinner, discrete layers rather than using just three main layers of the cartilage, would also increase the accuracy of the model.

Acknowledgements

Funding was provided by the Swiss National Science Foundation (NCCR CO-ME).

References

Korhonen et al, J Biomech, 35:903-909, 2002; Lai et al, J Biomech Eng, 103:61-66, 1981; Schinagl et al, J Biomech Eng, 126: 129-137, 2004; Shapiro et al, 9:533-538, 2001; Verteramo et al, Biorheology, 41:203-213, 2004

MODELING OF THE TRANSVERSE POST-YIELD BEHAVIOR OF BOVINE CORTICAL BONE

Fatma Oya Ayturk (1), Brandon G. Santoni (1), Daniel Woldtvedt (1), Christian M. Puttlitz (1)

1. Colorado State University, Fort Collins, CO, USA

Introduction

The anisotropic post-yield behaviour of cortical bone limits the prediction of its mechanical behavior and subsequent accuracy of computational models that use known material coefficients as input. A better understanding of this complex behavior can be achieved by obtaining extensive data sets and modeling the post-yield behavior using a variety of criteria. Previous studies have reported on the mechanical properties of bone in the longitudinal direction beyond yield [Bosisio, 2007], yet transverse properties have not been extensively studied. This study characterized the post-yield behaviour of bovine cortical bone loaded in the transverse direction and developed a FE model that more accurately predicts its mechanical properties.

Methods

Twenty-six (n=24) dog bone specimens oriented in the transverse plane were milled from one bovine tibia and two bovine femora. The long axis of each dog bone specimen was oriented in the transverse direction. Hydration was maintained throughout sample preparation via continuous irrigation. Each sample was subsequently loaded in a materials testing machine and tested to failure at an average strain rate of 0.00031 sec^{-1} . An extensometer was secured to the gage region of each sample during testing. To obtain an equation describing the post-yield behaviour of bovine cortical bone in the transverse direction, the Mean Coordinate Method was implemented. Mean values of stresses and strain for each characteristic point (Yield Point, Yield Offset Point, Maximum Stress Point and Fracture Point) were calculated and linear and polynomial equations were fit to these mean points. Three different offset yield values (0.05%, 0.1% and 0.2%) were evaluated. To model the post-yield behaviour, stress and strain values obtained in the Mean Coordinate Method with .05% offset yield value were introduced as plastic material properties into 3D FEA models [Womack, 2007] of bovine femoral and tibial sections ($E=8.4 \text{ GPa}$, $\nu=0.3$). Predicted stiffness and displacement experimental data at fracture were compared using ABAQUS.

Results

Mean values and standard deviations for stress and strain with regard to the yield, maximum and

fracture points were essentially equal when applying the 0.05% and 0.1% yield offset values

Yield Offset (%)		Stress (Mpa)	Strain (mm/mm)
0.5% (n=24)	Yield	Mean	16.500
		StDev	3.740
	Maximum	Mean	22.520
		StDev	4.623
	Fracture	Mean	21.560
		StDev	4.965
0.1% (n=24)	Yield	Mean	16.500
		StDev	3.742
	Maximum	Mean	22.520
		StDev	4.623
	Fracture	Mean	21.560
		StDev	4.965

Table 1: Mean stress and strain values with standard deviations using the mean points method.

For femoral models, non-significant differences were found with respect to the stiffness data between the experimental and finite element models with post-yield behaviour ($p = 0.319$). Predicted force at the fracture displacement was also not statistically different between the experimental and the post-yield finite element results for the femur ($p=0.87$).

		Experimental	FEM (Post-Yield)
Stiffness (Nmm)	Average Value	888.55	854.96
	StDev	142.81	139.13
	%StDev	16.07	16.27
Reaction Force (N)	Average Value	547.32	543.42
	StDev	71.38	74.57
	%StDev	13.04	1.72

Table 2: Average stiffness and predicted force at experimentally determined displacement at fracture.

Conclusion

The post-yield behaviour of bovine cortical bone in the transverse direction was successfully characterized using machined dog bone specimens and simple physical experiments. When incorporated into FEA models of bovine bone sections, the predicted outcomes matched those generated experimentally marking the development of a more accurate modelling tool to predict the true post yield material behaviour of cortical bone.

References

Bosisio et al, J Biomech, 2007, 40,9;2022-28
Womack et al, J Biomech, 2007, 41;194-99.

TEMPORAL PATTERNS OF DIFFERENT TISSUE TYPES DURING FRACTURE HEALING: EXPERIMENT VS. SIMULATION

A. Vetter (1), F. Witt (2), D.R. Epari (2), R. Seidel (2), P. Fratzl (1), G.N. Duda (2), R. Weinkamer (1)

1. Max Planck Institute of Colloids and Interfaces – Department of Biomaterials, Potsdam, Germany; 2. Julius Wolff Institute and Center for Musculoskeletal Surgery, Charité - Universitätsmedizin, Berlin, Germany

Introduction

During the process of bone healing different tissue types are formed within the newly formed callus around the fracture site. The spatial and temporal sequence of these tissue type patterns is thought to be crucially influenced by mechanical factors. To better understand the mechanical influence, animal experiments have been performed, where the fracture is stabilized by fixators of different rigidity. On the theoretical side starting with Pauwels [Pauwels, 1960] different mechano-biological rules have been proposed of how mechanical stimuli control differentiation of progenitor cells into either fibroblasts, chondrocytes or osteoblasts. Implementing these rules in computer models, different mechano-biological hypotheses can be tested [Lacroix, 2002]. Isaksson et al., for instance, compared how the choice of different mechanical stimuli influence the healing process in computer models [Isaksson, 2006]. A decisive advantage of *in silico* studies is that the potential influence of a single factor (corresponding to a single parameter in the model) can be investigated, an approach which is impracticable in *in vivo* studies.

The aim of our work is first to extract from histological sections of animal experiments a sequence of tissue type patterns, which describe the course of healing. These experimental patterns are then used for comparison with results of computer simulations to connect model parameters with different healing outcomes.

Methods

Experimental data was obtained in form of longitudinal histological sections of the fracture callus of 64 sheep at different post-operational time points after an osteotomy of the tibia [Schell, 2005]. To deal with the problem of individual differences between the sheep, the histological sections were classified into different healing stages according to the topology of the tissue type patterns. A novel averaging procedure was applied [Vetter, 2008] to obtain six different images corresponding to six stages in the healing process..

The design of our computational was aimed at a reduced number of model parameters. Parameters include only tissue maturation rates, thresholds for

mechanical induced cell differentiation and mobility of the progenitor cells. The formation of bone can occur either by endochondral and intramembranous ossification.

Tissue type patterns obtained by the simulation were compared with the averaged experimental images on a pixel by pixel basis.

Results

The averaging method was carried out for the lateral and medial side of the histological sections separately. No qualitative differences in the progression of healing were found between these two sides. As an example, Figure 1 shows images corresponding to three stages in the healing process for the lateral side. After initial intramembranous ossification, cartilage bridges the fracture gap periosteally and then cartilage is replaced by bone.

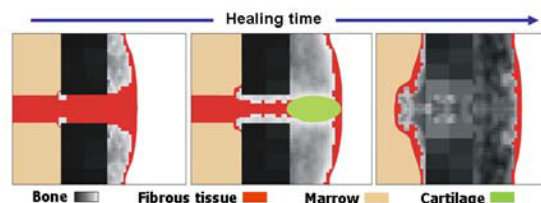


Figure 1: Tissue type patterns for three different healing stages (obtained by the novel averaging method)

Performing a parameter study of our computer model, parameters could be identified, which are responsible for a successful healing outcome. Comparison with the experimental images was crucial for the classification of the simulation results.

Discussion

The comparison between experimentally and computationally obtained tissue type patterns allowed a better identification of important parameters controlling the healing process in bone.

References

- Isaksson H. et al., J. Biomech., 39(8), 1507, 2006
- Lacroix D. et al., J. Biomech, 35, 1163, 2002
- Pauwels F., Z. Anat. Entwickl. Gesch. 121, 478, 1960
- Schell H. et al., J. Orthop. Res. 23(5): 1022, 2005
- Vetter A. et al., Calc. Tis. Int., 82 Sup.1: 79, 2008

POROUS VERSUS DETAILED MODELS FOR THE PREDICTION OF OXYGEN PROFILES IN A BONE ENGINEERING SCAFFOLD

Silvia Truscello (1), Jan Schrooten (2,3), Hans Van Oosterwyck(1,2)

1. Division of Biomechanics and Engineering Design, K.U.Leuven, Belgium; 2. Prometheus, Division of Skeletal Tissue Engineering, K.U.Leuven, Belgium; 3. Department of Metallurgy and Materials Engineering, K.U.Leuven, Belgium

Introduction

Oxygen concentration (pO_2) is an important factor for the in vitro culturing of cell-seeded tissue engineering (TE) constructs in perfusion bioreactors [1]. Computational Fluid Dynamics (CFD) models have been used to calculate pO_2 in porous scaffolds [2]. This study explores the use of porous versus detailed models for the prediction of pO_2 in cell-seeded bone TE scaffolds.

Methods

Oxygen profiles inside a regular titanium scaffold (6 mm width, 20 mm length, 0.5 mm height) were calculated either by modeling the detailed geometry of the scaffold or by using a porous medium approach. The ACIS-based solid modeller Gambit was used to build the 3D models and the mesh. The finite volumes code Fluent was used to set up and solve the steady state problem. In both models a flow rate of 0.2ml/min was imposed with a pO_2 of 160 mmHg corresponding to a mass fraction of $8.36e^{-06}$.

Detailed model: the real geometry of the scaffold was considered and Navier-Stokes equations were used for solving the problem. This model was built up to evaluate the influence of the local micro-structure on the oxygen distribution. Due to symmetry only one slice of the fluid domain was modelled. The mesh presented 1.137.780 tetrahedral elements and the element edge length was 25 μm . A monolayer of 10 μm thick was implemented on the walls of the structure with the aim of mimicking cell adhesion on the scaffold walls. A Michaelis Menten (MM) kinetics was considered for the oxygen consumption.

Porous model: the scaffold inside the chamber is considered as a porous continuous medium with a permeability of $1.84e^{-09}$ and porosity of 57%. The problem is solved by using Darcy's law. To compare it with the detailed model the same symmetric fluid domain was taken into account. The mesh presented 319.190 tetrahedral elements and the element edge length was 25 μm . The cells were supposed to be uniformly distributed in the porous medium and a MM kinetics weighted for the porosity of the structure was implemented.

Results

For both the porous and detailed models a decrease of oxygen concentration inside the scaffold was

predicted (Fig 1). The mean value of oxygen mass fraction at the outlet for the detailed model was equal to $8.27e^{-06}$ (decrease of $9e^{-08}$ with respect to inlet concentration), while a value of $8.07e^{-06}$ (decrease of $2.9e^{-07}$) was predicted using the porous approach. A local oxygen variation through the channel of the detailed model can be detected as well.

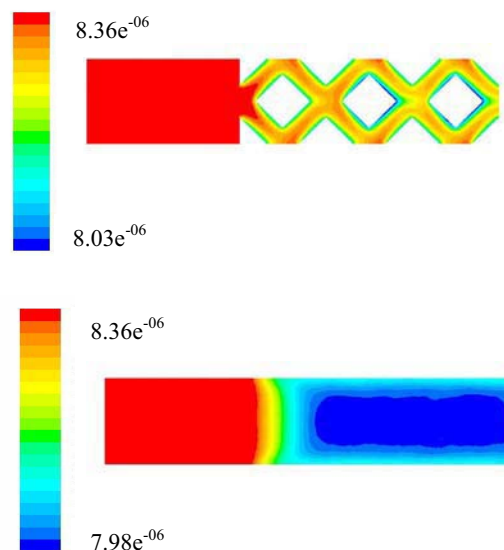


Figure1: Oxygen mass fraction plots of detailed (top) and porous (bottom) model

Discussion

The difference between oxygen inlet and outlet concentration was more than 3 times higher in the case of the porous model. Although for the selected example absolute differences were still very small, porous models may lead to substantial errors in case of much higher consumption rates (e.g. due to higher cell density or metabolic activity), or larger scaffold lengths.

Acknowledgements

This work is part of Prometheus, the Leuven Research & Development Division of Skeletal Tissue Engineering of K.U.Leuven.

References

- [1] G.D'Ippolito et al, Bone, 39: 513–522, 2006.
- [2] M. Cioffi et al, J Biomech, 41: 2918–2925, 2008.

3D REGISTRATION SCHEME OF MICROTOMOGRAPHIC VOLUMES FOR THE ASSESSMENT OF TRABECULAR BONE FRACTURE

Simone Tassani (1,2), Nikolaos Mouravliansky (3), Pantelis Asvestas (3), George K. Matsopoulos (3), Fabio Baruffaldi (1)

1. *Laboratorio di Tecnologia Medica, Istituti Ortopedici Rizzoli, Bologna, Italy;*
2. *Engineering Faculty, University of Bologna, Italy;* 3. *Bio-Medical Informatics Group, National Technical University of Athens, Greece*

Introduction

3D structures of human trabecular bone can be analyzed using microtomographic devices (micro-CT). Most of the published studies reported correlations between mechanical properties and morphometric parameters averaged on the whole specimen, without taking into account structural variations within the analyzed specimen. Identification of broken region is an important step for the understanding of fracture propagation. To the authors' knowledge, previous published studies related in the identifications of the acquired data to broken and non-broken regions were visually assessed [Perilli, 2008; Nazarian 2006] resulting in limitations to the tomographic plane (2D), while fractures are typically propagated in 3D, and high execution time. Automatic techniques should be applied for the identification of various regions within the acquired data. The aim of this paper is to introduce the application of a new methodology for the automatic identification of broken and non broken regions by registering the pre- and post-mechanical test micro-CT volumes and comparing them.

Materials and Methods

One trabecular specimen was extracted from a deceased donor without musculoskeletal disease and imaged using a micro-CT. The specimen was then mechanically compressed and imaged again using the same settings. Thus, two datasets were generated. Each dataset consisted of 1,000 consecutive slices each one having 1024 x 1024 pixels with voxel size 0.20 x 0.20 x 0.20 μm .

The proposed automatic registration scheme comprises of the following steps:

1. **Preprocessing:** The step involves sub-sampling at x-y orientation by a factor of two to speed up processing and morphological filtering (opening-closing operations) to reduce noise.
2. **Contour extraction:** The extraction is based on the enclosure of internal bone mass using a deformable contour model.
3. **Volume registration:** A 3D affine registration is applied on the two external bone mass surfaces of the two data sets [Matsopoulos, 2003]. Non broken regions should be matched while the

remaining regions should be recognized automatically as broken regions.

4. **VRML representation:** In order to visualize the data sets before and after registration, a surface rendering technique is used to create meshes of the external specimen surfaces in VRML format. Looking at the fused 3D model, the operator will be able to have a visual perception of the location and extension of broken and non broken regions and automatically locates both of them.

Results

Preliminary results on the application of the proposed methodology are presented in Fig. 1 showing fused surfaces before (a) and after registration (b). The broken regions could be then identified.

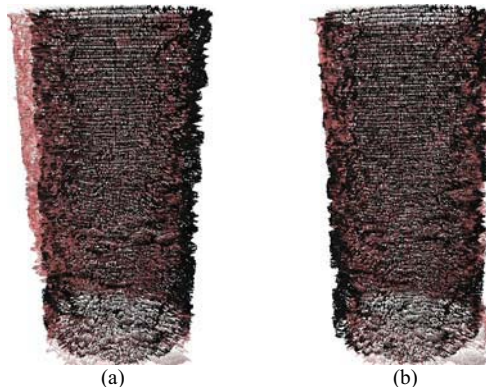


Figure 1: Fused surfaces before (a) and after 3D registration (b).

Conclusions

In this paper, a methodology for the automatic identification of broken and non broken regions by registering the pre- and post- mechanical test micro-CT volumes is presented. The methodology was applied on a pair of micro-CT datasets. The results, although preliminary, suggest the validity of the proposed method.

References

- E. Perilli et al, J Biomech, 41 (2):438-446, 2008.
 Nazarian, A et al, Bone 39(6): 1196-202G.K.
 Matsopoulos et al, Technology and Health Care, 11:19-232, 2003.

A MORPHOLOGICAL VALIDATION METHOD FOR MICRO FINITE ELEMENT MODELS OF BONE

Y Zhao (1), K A Robson Brown (2), Z M Jin (1), R K Wilcox (1)

1. *Institute of Medical and Biological Engineering, University of Leeds, Leeds, UK*

2. *Department of Archaeology and Anthropology, University of Bristol, Bristol, UK*

Introduction

Advances in medical imaging technology have improved the development of specimen-specific finite element (FE) studies of bone [Wilcox, 2007]. The aim of this study was to create an FE model of the compression of a bone-like material at the microscopic level, and develop methodologies to compare the FE-predicted trabecular deformation with corresponding experimental measurements.

Methods

A cylindrical specimen was cut from open cell polyurethane foam (Sawbone, Sweden) with diameter 6 mm and height 10 mm. The specimen was loaded in compression inside a micro-computed tomography scanner (SkyScan 1172, Belgium) and imaged at 25 μm isotropic resolution before and during the compression test.

The μCT images taken before compression were down-sampled to 50*50*50 μm voxel size to reduce the number of elements and a voxel-based FE model was created using commercial software (Simpleware, UK). The generated model consisted of approximately 1,600,000 elements. The sawbone ‘trabeculae’ were considered to be homogenous and linearly elastic. The FE model was set up and compressed 0.35 mm to mimic the experimental protocol using ABAQUS CAE 6.81 (Abaqus Inc, Providence, RI, USA)..Displacement at each end of the model in the horizontal plane was constrained.

Three vertical section slices were taken through the deformed FE model and the registered areas of each slice were compared with the same part of the μCT images taken at the same compression using an in-house Matlab code (Matlab 7.2, MathsWorks Inc, MA, USA). The differences between the sawbone trabeculae seen on the FE slices and the μCT images were calculated. The percentage errors over the whole area of trabeculae were also calculated. The FE model images were evenly divided into top, middle and bottom regions, each region was compared with the corresponding area on the μCT images, and the average error was calculated.

Results

The comparison between the FE predicted trabeculae deformation and that of the experiment

at selected positions is shown in Figure 1 and the differences between them are shown in Table 1. The variation in error between the top, middle and bottom regions are shown in Table 2.

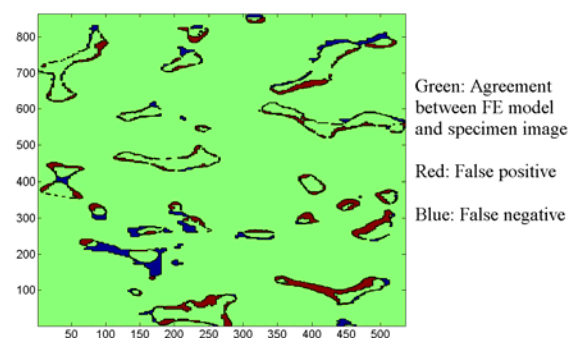


Figure 1: Comparison between FE slice & μCT image using Matlab

Image position	Left	Right	Middle
Error over trabecular area (%)	14.6	22.9	16.9

Table 1: Overall difference between FE predictions & experimental images

Region	top	middle	bottom
Average error over left, mid & right (%)	34.5	14.1	15.2

Table 2: Difference between FE predictions & experimental images at different regions

Discussion

This study developed a morphological comparison method to examine the accuracy of trabecular-level FE models. The result showed a reasonable FE model deformation prediction. The study also showed different errors at different regions, which indicates that slipping occurred during compression and more precise boundary conditions might improve the accuracy of the model.

Acknowledgements

This work was supported by EPSRC and DePuy International Ltd.

References

Wilcox, J. Biomech., 40(3), 669-73, 2007

THE EFFECT OF SPECIMEN GEOMETRY ON THE MECHANICAL BEHAVIOUR OF HUMAN CORTICAL BONE

Caroline Öhman (1,2), Massimiliano Baleani (1), Marco Viceconti (1)

1. *Laboratorio Tecnologia Medica, Istituto Ortopedico Rizzoli, Bologna, Italy;*
 2. *Engineering Faculty, University of Bologna, Bologna, Italy*

Introduction

To validate musculoskeletal numerical models there is a need of reliable experimental data about the material properties of bone tissue. However, in the literature, several different protocols (e.g. different specimen size and shape) have been used to perform compressive tests on cortical bone and consequently different results have been obtained [Dempster, 1952; Keller, 1994; Les, 2002]. The aim of this study was to define a reliable protocol for compressive testing of cortical bone. A previous work [Keaveny, 1997] suggested that the most reliable way to measure tissue deformation is measuring it directly on the tissue. To do this slender shaped specimens are preferable. Hence, a first study was done to determine the optimal diameter of a cylindrical specimen. Furthermore, it was verified whether cubic specimens, where no direct measure of tissue deformation is possible, would give the same results. A cubic specimen would have the advantage of allowing the determination of the anisotropic mechanical behaviour of cortical bone tissue.

Methods

From a first diaphysis five bone slices of about 22 mm were obtained. From each slice two 2-mm, two 3-mm and two 4-mm cylindrical specimens were extracted. Following the recommendations for cancellous bone [Keaveny, 1997], the specimen free lengths were set to 8, 12 and 16, respectively (six extra mm were added for fixation). Some of the 4-mm specimen extractions had to be repeated since the extracted specimen was not complete. Ten specimens were obtained for each diameter.

From a second diaphysis six bone slices of about 30 mm were obtained. From each slice four 5x5x5 cubes were cut out (the largest specimen size possible to obtain from the cortical wall). From the same slice, directly under each cube a 3-mm cylindrical specimen was extracted. The diameter was based on the results from the first part of the study. A total of 48 specimens were obtained.

All specimens were left in Ringer's solution for at least 24 hours before testing. The cylindrical specimens were cemented directly onto the testing machine. An extensometer was attached to the

central part of the specimen. The cubic specimens were placed between two polished parallel platens. An extensometer was attached to the platens.

All specimens were loaded to failure and from the data registered Young's modulus (E) and ultimate stress (US) were calculated.

Results

In five cases of the 2-mm diameter group, the strain data was lost because of extensometer slippage.

No significant difference in mechanical properties could be found among the three different diameters (ANOVA, E: $p=0.57$, US: $p=0.28$).

No statistically significant difference was found between cubes and cylinders in US (unpaired T-test $p=0.21$). However, the cubic specimens had a significantly lower E (unpaired T-test $p<0.0001$) of about 60% compared to the cylindrical ones.

Discussion

The results obtained for all cylindrical specimens were in agreement with several studies in the literature [Carter, 1978; Keller, 1994]. However, a diameter of 3-mm was chosen as the optimal one since no problems occurred during specimen extraction or testing.

A systematic underestimation of E was found testing cubic specimens, due to end-artifact errors. This kind of underestimation of E would drastically affect the results of numerical models, as discussed by [Helgason, 2008]. Therefore, model validations have to be performed using experimental data where specimen deformation has been measured directly on the tissue.

Acknowledgements

This work was supported by the EC (project n°: IST-2004-026932; acronym: LHDL and project n°: MRTN-CT-2006-035763; acronym: 3D Anatomical Human).

References

- Carter et al, Clin Orthop Relat Res, 135:192-217, 1978.
- Dempster et al, Am J Anat, 91:331-362, 2006.
- Helgason et al, Clin Biomech, 23:135-146, 2008.
- Keaveny et al, J Orthop Res, 15:101-110, 1997.
- Keller et al, J Biomech, 27:1159-1168, 1994.
- Les et al, J Orthop Res, 20:607-614, 2002.

COMPUTATIONAL MODELLING OF CONGENITAL HEART DEFECTS FOR CLINICAL AND SURGICAL INTERVENTION PLANNING

Adelaide de Vecchi (1), David Nordsletten (1), Matthew McCormick (1), Nicolas P. Smith (1)

1. Computing Laboratory, University of Oxford, Oxford, UK

Introduction

The increasing need to identify a time-frame for pharmacological and surgical intervention has highlighted the lack of mechanistic understanding into the fluid-mechanics of the congenital heart. This poses severe limitations to the development of customised care of congenital patients, preventing the optimisation of subject specific treatments and the reduction of national health service costs.

An overview of the current work for integrating the electrical, mechanical and biochemical functions into a multi-scale model of the heart can be found in [Smith, 2004]. The focus of the present contribution is on the fluid-structure interaction inside the left and right ventricles after surgical intervention such as the atrial switch procedure, whereby a tunnel is created between the atria to re-direct the oxygen-rich blood to the systemic right ventricle and the oxygen-poor blood to the left ventricle and pulmonary artery.

This work aims to identify the effects of congenital heart defects on cardiac function by developing a geometric model of the congenital heart based on patient data and MR images. Through the implementation of coupled fluid-structure numerical simulation on this geometry the objective is to provide useful information on the energy and stress distribution inside the chambers. Our aim is to use these data, along with computed velocity and pressure fields, to shed light on the patient pre- and post-intervention conditions and ultimately reassess the metrics which define clinical care.

Methods

The current work was divided into two phases: the building of a geometric model and the performing of numerical simulation on the geometry.

Image digitisation was performed manually using Zinc digitiser. In the fitting procedure, endo and epicardium were treated separately: a linear rectangular mesh was generated on a partial ellipse that covered approximately each surface. A non-linear fitting algorithm [Fernandez, 2003] was utilised to fit the endo and epicardial meshes to the data. Finally, linear interpolation between the corresponding nodes on the two surface meshes was performed to obtain the cubic hexahedral

volume mesh. The unstructured fluid mesh consisted of quadratic tetrahedral elements.

The numerical simulations were performed using a fluid-structure solver based on the Galerkin/Petrov-Galerkin finite element method and the ALE formulation [Nordsletten, 2007, 2008]. The geometrical models were obtained through segmentation of MR data from congenital patients and a healthy volunteer: the latter represents the benchmark case and has been used in a preliminary study for code validation purposes.

Results and discussion

Using normal and congenital heart models we have computed the velocity flow field and the wall stress distribution. Given the lack of information on the congenital heart dynamics, the validation of the results was performed step by step: first, assumptions were made on the movement of the ventricle walls and the flow field was approximated. The outcome of the simulation was then compared to the clinical data obtained via high resolution flow acquisition. Using the calculated flow profile, the validity of the assumptions on the structure movement was checked by analysing the contraction mechanism. These results were finally compared to the dynamic tagging MRI sequences.

Future work will use inotropic patients data to further validate our congenital heart model. From these results the correlation between clinical metrics and the simulation outcome will be used for evaluation of the correct time for surgical or pharmacological intervention.

Acknowledgements

This work is supported by the EuHeart project (WP7). The authors would like to thank the Oxford University e-research centre (OERC) for its support and for the computing facilities.

References

- Fernandez et al, Biomech Model Mechanobiol, 2:139-155, 2003.
- Nordsletten et al, Int. J. Num. Meth. Fluids, 56: 1457-1463, 2007.
- Nordsletten et al, submitted to SIAM J. Num. Anal., 2008.
- Smith et al, Acta Numerica, 371-431, 2004.

SIMULATION OF THE ANTERIOR LONGITUDINAL LIGAMENT WITHIN SPINAL SEGMENTS: A SENSITIVITY STUDY

Alison C Jones (1), Ruth K Wilcox (2)

1. University of Leeds, UK; 2. University of Leeds, UK;

Introduction

Short segment spinal finite element models are increasingly being trusted as tools to investigate surgical procedures. These segments, include soft tissues such as the ligaments, whose material properties are not well understood, with a wide range of values found in experimental tests. Consequently the ligaments are modelled using a wide variety of material properties and geometries. This study focuses on the sensitivity of range of motion (ROM) in extension to the properties of the anterior longitudinal ligament (ALL) in a lumbar spine model. The deformation of individual components during that motion is also analysed.

Methods

A generic finite element model of a functional spinal unit in the lumbar spine, from a previous study [Wilcox, 2006], was modified by removing the posterior elements and all ligaments except the ALL. The ALL is represented using truss elements. Firstly, the number of elements was varied, for a fixed ALL width and total cross-sectional area, to inform a mesh convergence analysis. Secondly, the Young's modulus of the elements was varied to observe its relationship with the range of motion in extension. Finally, the effect of pre-stress was observed. For each case motion in extension was measured for a moment of 10Nm.

Results

It was found that an increase in element numbers stiffens the ligament structure, increasing the effect of the ligament. Figure 1 shows the effect of Young's modulus and pre-stress change. With increased Young's modulus and pre-stress the degree of motion converges towards to a fixed number of degrees.

Discussion

In this study we show that the number of truss elements, the Young's modulus value, and the pre-stress all have potentially significant effects on the ROM, within in the range currently used [Jones, 2008].

It has been shown that the spinal ligaments are in tension at rest [Heuer, 2007], stabilizing the spine and putting the discs under a degree of pressure. It is shown in Figure 1 that the effect of the Young's modulus value is dependent on this pre-tension. The effect of pre-tension on the distribution of compression between the disc and the vertebrae can also be seen. Therefore ligament pre-tension should be carefully considered in studies where the bone stress or disc pressure are measured.

References

- Wilcox et al, J Eng. Med., 220:565-572, 2006.
- Jones et al, Med. Eng. Phy., 30:1287-1304, 2008.
- Heuer et al, J. Biomech., 40:271-280, 2007.

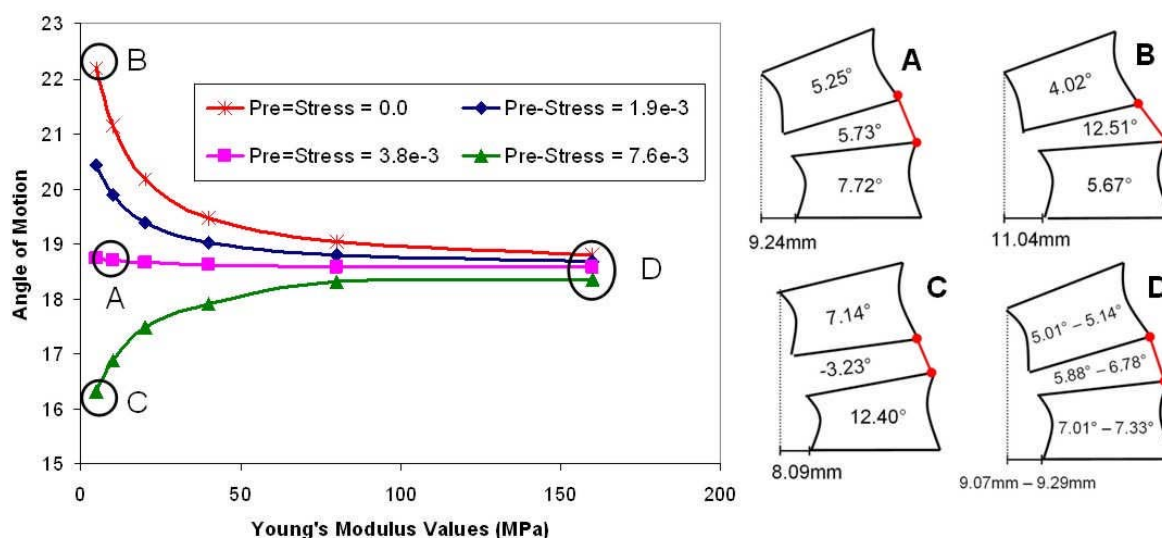


Figure 1: Angle of extension for various values of ALL elastic modulus and pre-stress. Each component breakdown (A, B, C, and D) gives the contribution to the overall motion angle from each spinal component.

EFFECT OF LUMBAR FUSION SURGERY ON THE MOMENT ARMS OF THE MULTIFIDUS: A BIOMECHANICAL MODELING STUDY

Ameet K Aiyangar, Darryl Thelen

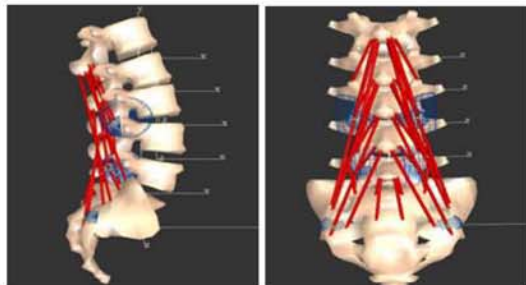
Department of Mechanical Engineering, University of Wisconsin, Madison USA

Introduction

Lumbar fusion surgery is often used to treat degenerative disc disease. While this procedure can alleviate symptoms in the short term, adjacent segment disease is a potential long-term complication which can arise from altered lumbar mechanics [Eck, 1999]. In particular, it has been shown that fusion at one level can induce greater mobility and loads at adjacent levels [Eck, 1999, Park, 2004]. The aim of this study was to investigate a potential causal relationship between changes in mobility and loading. Specifically, we used musculoskeletal models to analyze the effect of fusion on lumbar muscle moment arms, and discuss the implications for lumbar loading patterns.

Methods

A musculoskeletal model of the lumbar spine (Fig. 1) was generated in SIMM (Software for Interactive Musculoskeletal Modelling; Motion Analysis Inc.).



(a) (b)

Figure 1: Sagittal (a) and posterior (b) views of the lumbar model with fascicles of the multifidus.

The model consisted of the five lumbar vertebrae and sacrum. Adjacent segments were coupled by single degree of freedom joints at the disc centers, allowing for lumbar flexion in the sagittal plane. The overall lumbar flexion angle was initially distributed into inter-segmental flexion angles based on cadaveric measures [Panjabi, 1994]. Fascicles of the multifidus were represented as a series of line segments between origin and insertions [Bogduk, 1992]. Wrapping objects were included to allow the muscles to wrap around vertebral segments during flexion (Fig. 1). Fusion was simulated by restricting motion at the L5-S1 intersegmental level, and partitioning net lumbar flexion proportionately among the other four joints. Lumbar extension moment arms for each of the fascicles of the multifidus were computed both

before and after simulated fusion. We report the observations made at a net lumbar flexion angle of 40 degrees.

Results and Discussion

We found that fascicles that did not span the L5-S1 joint experienced an increase in their moment arms, with the increase ranging from 10-13%. However, the muscle fascicles that spanned the fused joint experienced a decrease in moment arms (Fig. 2). In particular, fascicles spanning joints closest to L5-S1 exhibited the largest changes, with decreases in moment arms of up to 38%.



Figure 2: Percent change in lumbar flexion moment arms for each fascicle of the multifidus after simulated fusion at L5-S1 joint.

The restoring moment developed at a joint is the product of the muscle force and the moment arm. If the moment arm is decreased, the muscle force must proportionally increase in order to generate an equivalent restoring moment. The results show that the largest decreases in the moment arm occurred at the segment closest to the fusion, i.e. at the adjacent segment. This implies that larger muscle forces are developed at the adjacent segment after fusion, resulting in larger reaction forces at the adjacent disc. These results suggest that surgery-induced changes to multifidus moment arms could lead to increased loads on adjacent segments, and thus may contribute to adjacent segment disease.

References

- Eck et al, American Journal of Orthopaedics, 28(6):336-340, 1999
- Park et al, Spine, 29(17):1938-1944, 2004
- Panjabi et al, JBJS, 76-A (3):413-424, 1994
- Bogduk et al, Spine, 17(8):897-913, 1992

VPH2_VIEWER: VISUALISATION AND FUSION OF BIOMEDICAL CARDIAC DATA

Debora Testi (1), Gordon Clapworthy (2), Nigel McFarlane (2), Hui Wei (2)

1. SuperComputing Solutions, Italy; 2. University of Bedfordshire, UK

Introduction

Computer aided medical instruments available for use in cardiac clinical practice are currently rather limited. Most are provided as post-processing tools integrated into the control deck of diagnostic imaging systems. It is generally difficult, if not impossible, for users simultaneously to employ data from multiple imaging sources in order to perform measurement, analysis or modelling. Medical professionals know that to produce the best diagnosis, they have to combine information from multiple sources, but at present the only tool available to integrate these data is their own mind.

One solution to this complex scenario is to develop an application specifically for the multimodal data fusion of cardiac data.

The application, VPH2_Viewer, is part of the VPH2 advanced framework currently under development and is a “work area” in which the clinician can manipulate the model to make a first evaluation of the specific patient ‘case’. The framework will use specific components to allow the clinician to check and to simulate a surgical intervention and traditional planning instruments to evaluate and plan all the activities that he/she has to forecast to assure the task.

The application

VPH2_Viewer is being developed within the VPH2 framework to address the visualisation and multimodal data fusion issues. The application employs principles developed in the Multimodal Application Framework, an open source framework for the rapid developed of computer-aided medical application (www.openmaf.org) and is compatible with it.

VPH2_Viewer allows the user to import many types of medical data (e.g. DICOM images, patient information, etc.). Then the data can be visualised using specialised visualisation techniques which allow the user to inspect the same data with different modalities (e.g. using an orthoslice and direct volume visualisation to see the same MRI volume) and/or to view different types of data (i.e. an MRI volume and left ventricle surface within the same orthoslice view or a static and a time-varying MRI together in a global slice view). The user can open as many views as he/she likes to better understand the patient’s anatomy and, when

interactively modifying them, the views will always remain synchronised (Figure 1).

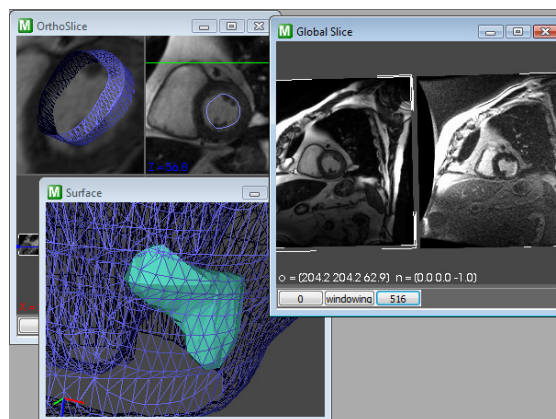


Figure 1: Visualisation with VPH2_Viewer

In this way, the user can extract new information from the data. Besides standard measuring tools, the user also has available advanced operations to interactively extract geometry information of the cardiac wall.

In particular, based on previous work on muscles [Krokos, 2005], a powerful operation is being implemented to support the rapid creation of a heart model from 4D imaging data. The initial form allows semi-automatic segmentation from the time-dependent imaging data and, in future releases, this will allow the surgeon to view the effects of the planned intervention on the full heart cycle.

Conclusions

VPH2_Viewer provides one of the most advanced tools for clinicians to fuse and visualise biomedical data of the heart within an interactive and coherent environment. Future releases will be further improved by integration with simulation tools and the fusion of medical images with simulation results, thus providing the final users with a unique software tool for surgical planning.

Acknowledgements

This research is partially funded by ICT for Health Unit of the European Commission within the FP7 project VPH2 (IST-2008-224635).

References

Krokos M et al, Proc. IEEE Medical Information Visualisation (MediVis 05), 3-8, 2005.

NEURAL BASES OF CROSSMODAL SPATIAL ATTENTION: A NEURAL NETWORK STUDY

Elisa Magosso (1), Andrea Serino (2), Giuseppe di Pellegrino (2), Mauro Ursino (1)

1. Dept. of Electronics, Computer Science and Systems, University of Bologna, Italy;

2. Dept. of Psychology, University of Bologna, Italy

Introduction

A central issue in cognitive neuroscience is how the brain integrates information from different senses (e.g., visual and tactile) to represent the unity of an external event and adaptive behaviour. This process may be favoured by mechanisms of attention in space [Driver, 1998]. Attending to a space location in a specific sensory modality (e.g. tactile), enhances also the processing of information of different modalities (e.g. visual) at the same site [Driver, 1998]. Exogenous attention (driven reflexively by an external cue) is traditionally distinguished from endogenous attention (driven voluntarily by expectancy) [Eimer, 2001]. Aim of the study is to investigate the neural bases of visual-tactile integration in exogenous and endogenous spatial attention, via a neural network model.

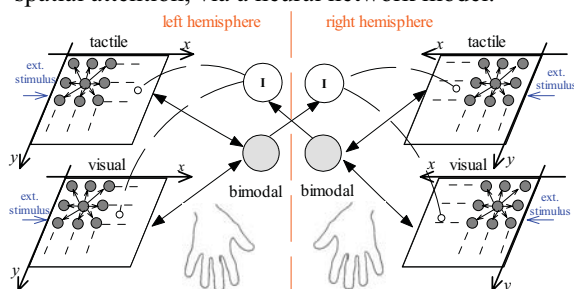


Figure 1: Network layout. Dashed/continuous lines: inhibitory/excitatory connections.

Methods

Since visuotactile attention is investigated *in-vivo* by applying stimuli on the hands [Spence, 2000; Kennett, 2001], the model embodies two networks, each referred to the contralateral hand (Fig. 1). The single network includes two unimodal areas of neurons, which respond to tactile and visual stimuli on the hand respectively, and communicate with a downstream bimodal area. The two networks are reciprocally interconnected via inhibitory interneurons (*I*), realizing a competitive mechanism. External stimuli have random amplitude. Response performance to a target stimulus on any side was assessed by computing the 98% settling time (T_s) of the corresponding bimodal neuron.

Results

We performed two different set of simulations. *A*) The network was stimulated by a 30 ms tactile cue

on one side, followed by a target stimulus of either modality on any sides. Ten simulations per side and target modality were performed. Responses were faster for targets (both modalities) on the same side as cue (Fig. 2, Table 1). *B*) A constant excitatory top-down input was delivered to the tactile neurons in one side (mimicking voluntary allocation of tactile attention towards one side). Ten simulations per side and target modality were performed. T_s was shorter for target stimuli (both modalities) on the attended side (Fig. 2, Table 1).

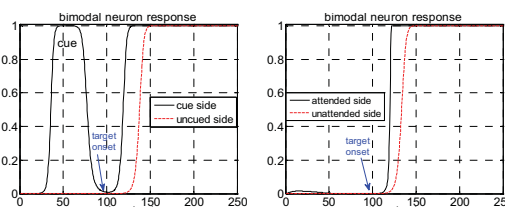


Figure 2: Exemplary response to a visual target on each side, in trials *A* (left) and *B* (right).

	same side	different side
<i>A</i>	$T_s=32.7\pm 1.7$ ms (<i>T</i>)	$T_s=52.3\pm 14.8$ ms (<i>T</i>)
	$T_s=35.1\pm 2.4$ ms (<i>V</i>)	$T_s=49\pm 8.1$ ms (<i>V</i>)
<i>B</i>	$T_s=10.9\pm 0.3$ ms (<i>T</i>)	$T_s=41.5\pm 4.7$ ms (<i>T</i>)
	$T_s=36.9\pm 4.9$ ms (<i>V</i>)	$T_s=46.3\pm 4.8$ ms (<i>V</i>)

Table 1: T_s (mean \pm std) to tactile (*T*) and visual (*V*) targets in the same/different side as tactile cue (*A*) or tactile top-down excitation (*B*).

Discussion

Results in Table 1 agree with *in-vivo* data of exogenous and endogenous attention [Spence, 2000; Kennett, 2001]. Hence, both forms of attention can be explained via the mechanisms included in the model. In particular, two mechanisms play a major role in producing the T_s differences between the two sides: the inhibitory competition among hemispheres (especially in trials *A*) and the shift of the working point of the bimodal neuron (due to the tactile cue or top-down excitation) which increases its responsiveness. Model predictions may help interpretation of behavioural results on spatial attention and crossmodal construction of space.

References

- Driver et al, Trends Cogn Sci, 2:254-262, 1998.
 Eimer et al, Neurosci Biobehav Rev, 25:497-511, 2001.
 Kennett et al, J Cogn Neurosci, 13:462-478, 2001.
 Spence et al, J Exp Psychol, 26:1298-1319, 2000.

A MASS MODEL OF INTERCONNECTED THALAMIC POPULATIONS INCLUDING BOTH TONIC AND BURST FIRING MECHANISM

Marco Pirini (1), Mauro Ursino (1)

1. Department of Electronic, Computer Science, and Systems, Università di Bologna, Italy

Introduction

Mutual excitatory and inhibitory interactions between Thalamo-Cortical Relay Nuclei (TCN) and the Thalamic Reticular Nucleus (TRN) generate patho-physiological oscillations that can be transmitted to the cortex and observed in EEG as δ , θ , and α rhythms. TCR and TRN neurons show both tonic and burst firing, related to different operational modes set by the modulatory inputs (MODs) from the brainstem [Steriade, 2005]. Burst firing is related to Ca^{2+} T-type membrane channels. In the classical Neural Mass Model (NMM) framework, the relationship between the mean membrane potential (V) and the mean firing rate (FR) of a population is a non-linear, instantaneous input – output curve (a sigmoid), thus modelling only tonic firing. Aims of this work are: a) to present a computational model of interacting TCN and TRN populations through a novel, modified NMM framework allowing for both tonic and burst firing, in order to investigate the generation of oscillatory patterns in a more physiological manner, and b) to study how MODs set the firing mode of the model.

Methods

The model includes a TCN and a TRN population. It considers the mutual interactions between TCN and TRN and the MODs to both populations. We modelled tonic firing as in classical NMMs and burst firing as (basically) in [Suffczynski, 2001]). We computed the global FR of the population as the sum of tonic and burst FRs. In summary:

$$\text{FR}(t) = (F_B(V, t) \cdot G_B) + ((1 - F_B(V, t)) \cdot f_\infty(V) \cdot G_T) \quad (1)$$

G_T and G_B : maximum tonic and burst pulse densities; f_∞ : sigmoidal function for tonic firing mode; and F_B : fraction of the population that is bursting. The latter is described by:

$$F_B(V, t) = (n_\infty(V) \cdot n(t)) \cdot m_\infty(V) \quad (2)$$

n_∞ , m_∞ : sigmoidal static functions representing the fractions of the population for which Ca^{2+} T-type channels are de-inactivated and activated, respectively; and $n(t)$: kinetic of de-inactivation. The latter is described by a second-order dynamics. Synaptic interactions between populations are dynamically described as in standard NMMs, while we modelled MODs (assumed as slowly varying) as constants directly summed up to the V of the populations. The effect of different MODs on the

oscillatory behaviour of V in TCN was investigated through simulation runs ($t = 100$ s). The output was depicted through the peak frequency in the Power Spectral Density (PSD) of the TCN V .

Results

Fig. 1 shows the results from an I-O analysis. Different oscillatory modes can be set by independently varying the MODs. The model can show α , higher θ (as an effect of α slowing due to sigmoidal nonlinearities) and δ (when slow GABA_B receptors on the TCN come into play, not shown) rhythms. Such rhythms arise from the coupling of tonic-tonic (Fig. 1, C), burst-tonic (Fig. 1, A2), and burst-burst (Fig. 1, A1 and B) firing of the TCN and TRN, respectively. Moreover, the oscillatory behaviour depends by the coupling parameters between TCN and TCR (the higher the synaptic strengths, the larger the regions in the input plane for which the model shows oscillations, not shown).

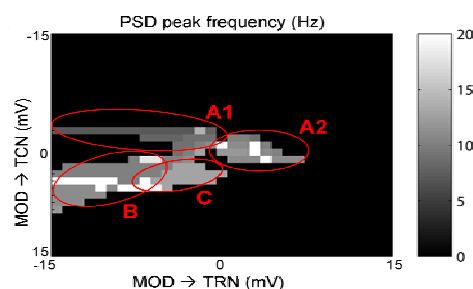


Fig. 1: input - output analysis

Discussion

The inclusion of both tonic and burst firing mechanisms in a thalamic NMM tremendously enhances the complexity of model behaviour, with oscillatory activities (resembling physiological ones) arising from limit-cycle dynamics without the needing for an external noisy input (in contrast with classical NMMs). Interestingly, strong rhythms emerge even when one or both populations lies hyperpolarized by MODs. Such a condition would not be allowed by using classical NMMs. In perspective, the model may be integrated with cortical NMMs to analyze the interaction between thalamic and cortical rhythms in several conditions of neurophysiological importance.

References

- Steriade, Trends Neurosci, 28(6):317-324, 2005
Suffczynski et al, Int J Psychophys, 43:25-40, 2001.

MODELLING THE MECHANICAL EFFECT OF MUSCLES: THE LOWER LIMB MECHANISM

S. Martelli (1), F. Taddei (1), G. Farinella (1), S. Van sint Jan (2), M. Viceconti (1)

1. *Laboratori di Tecnologia Medica, Istituto Ortopedico Rizzoli, Bologna (Italy)*
2. *Laboratory of Anatomy, Biomechanics and Organogenesis, Université Libre de Bruxelles, Belgium*

Introduction

A correct modelling of the mechanical muscle effect on bones and joints is probably a fundamental step to achieve reliable simulations of bone strains. A muscle consists of a large number of muscle fibres, which can be grouped into motor units able to independent contraction [Akima, 2000]. Most modelling techniques represent the muscle action on bones by a pre-defined scheme of force vectors, resulting in muscle models that mimic the muscle mechanical effect with an unknown accuracy. Aim of the present study was to determine a muscle schematisation for the lower muscles so as to ensure the model ability to predict the muscle mechanics. To achieve this aim an error threshold was defined and the minimum number of fibres to ensure the desired accuracy was defined following the guide-lines proposed by [Van der Helm, 1991].

Methods

Data were obtained from both legs of a cadaveric specimen in the frame of the EC-funded project LHDL: bone geometries were extracted from CT data while the muscular anatomy, including the muscle fibre path and the bone attachment locations, were derived from a dissection study. The muscles attachment sites were subdivided according to shape into points, straight lines, curved lines and surfaces [Van der Helm, 1991]. Each muscle was then schematised by a combination of attachment shapes. A mathematical description of the muscle attachment area was fitted to the data points using a least squares criterion. The digitised fibre paths were used to derive a map for the muscle bundles distribution from origin to insertion. This map was assumed to be sufficient to locate a large number of rectilinear elements (200) and to model the muscle mechanical effect (Y_{200}). The muscle force was assumed uniformly distributed between fibres. The generalised force vector contained the force and the resulting moment on the moving bone. The error was defined as:

$$e = 100 * \frac{\|Y_{200} - Y\|}{\|Y_{200}\|}$$

where Y is the generalised force vector computed for a reduced fibre number. The correct refinement of each muscle model was defined as the minimum fibre number that limit the error below a chosen threshold ($e < 5\%$) through the entire joint range of motion.

Results

Preliminary simulations showed that the mechanical effect of most muscles can be adequately modelled with 6 fibres or less. However a few muscles with large attachment areas (i.e. gluteus medius muscle, Fig. 1) required up to 20 fibres to ensure $e < 5\%$.

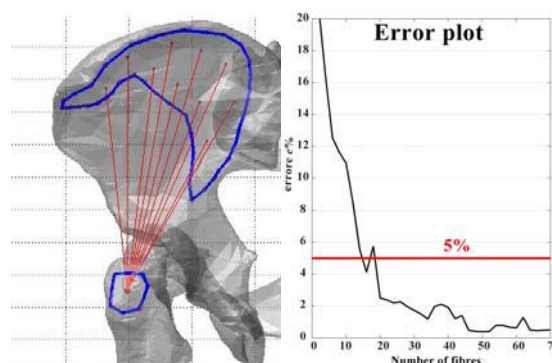


Figure 1: The left gluteus medius discretization (left) and the error-number of fibres plot(right).

Discussion

Preliminary results seem to agree with previous reports [Van der Helm, 1991] although, in few particular cases (i.e. the gluteals), the minimum number of fibres increased up to 20 fibres. Whether this muscle schematisation is sufficient to correctly predict bone strains or not will be the subject of further investigations.

Acknowledgments

This study was partially funded by the EC-funded projects LHDL (IST-2004-026932) and VPHOP (Grant #223865)

References

- Van der Helm, et al, J Biomech 24:1151-63, 1991.
Akima, et al, Eur J. Appl Physiol 83:475-80, 2000.

SENSITIVITY OF BIPEDAL DYNAMIC BEHAVIOURS TO CPG-OSCILLATOR GAINS

Betsy V. Hunter (1), Yasin Y. Dhafer (2)

1. Northwestern University, USA;

2. Northwestern University, Rehabilitation Institute of Chicago, USA

Introduction

With high incidence of locomotor dysfunction following neurological disorders, restoration of intra-limb coordination and kinematic symmetry is a primary goal of gait rehabilitation. Identifying the underlying neural mechanisms of common abnormalities is necessary to establish successful therapeutic paradigms. Recent investigations in our laboratory indicate that alternate joint torque coordination patterns in hemiparetic patients may contribute to the asymmetric gait behaviours observed post stroke [Cruz, 2008]. However, the quantitative affects of these torque patterns on gait kinematics is unclear. Our goal is to develop a computational framework of lower limb mechanics to assess how motor control changes, manifested in the form of joint torques, may affect gait performance.

Methods

Recent control approaches based on central pattern generators (CPGs) have been shown to successfully generate rhythmic movement patterns of both bipeds and quadrupeds [Kimura, 1999]. Due to its similarity to the central nervous system behaviour and its adaptive capability, a neural oscillator network based on the CPG concept was chosen for the present model [Taga, 1991]. Two mutually inhibitory neurons per joint simulate the behaviour of an antagonist muscle pair wherein each neuron contributes to an opposite function about a joint (Fig 1A). Unique inhibitory connection weightings alter the configuration and output of the network. The dynamics of the stance hip, swing hip and swing knee (a three degree-of-freedom model) were described using equations of motion of the form:

$$M(\theta)\ddot{\theta} + C(\theta, \dot{\theta})\dot{\theta} + N(\theta) = \tau \quad (1)$$

where M , C and N represent terms of inertia, coriolis and gravitational matrices, respectively, and τ is the joint torque vector applied by the controller. Conservation of angular momentum was used to calculate the impact dynamics at heel strike. The knee was free to rotate during swing, however locked through the stance phase at full extension. A homonymous feedback mechanism was used to provide information about the current mechanical state of the system to the neural oscillators.

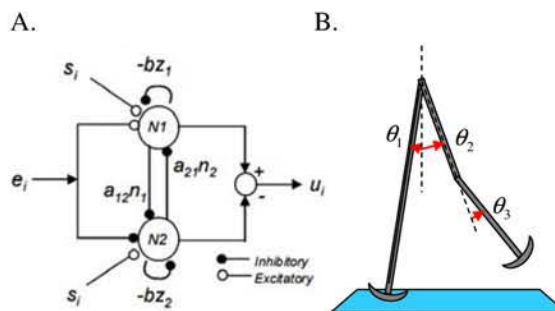


Figure 1: A.) Neuron Oscillator Pair. Each pair includes both cross (a) and self (b) inhibitory gains. B.) Three-link lower limb model with degrees-of-freedom at the hip and swing knee.

Results

Our initial simulation results show that the inclusion of the neural oscillator network provides sufficient control to maintain the stability and rhythmic movement of the model. The kinematics generated by the model correlated well with hip and knee joint angles of recorded healthy overground gait kinematics. Preliminary perturbation analyses of the different oscillator gains indicate varying sensitivity of each parameter to simulation results. For instance, the coordination and symmetry of the limbs seem to have high dependency on the self-inhibitory gain, b , a parameter that may have physiological relevance to the inhibitory Renshaw cells of the spinal cord [van Heijst, 1998].

Discussion

This preliminary study on a three-link lower limb model demonstrates the feasibility of using a physiologically based torque-driven model to investigate the effects of motor changes on gait. Further simulations incorporating three dimensional motions will be conducted in order to fully investigate observed gait abnormalities following neurological pathology.

References

- Cruz et al, Stroke, 39:139-47, 2008.
- Kimura et al., Autonomous Robot. 7: 247-258, 1999.
- Taga et al, Biol Cybern, 65:147-59, 1991.
- van Heijst et al., Neural Netw., 11:1305-16, 1998.

A NEW METHOD USING WARPED GAIT DATA TO CREATE SUBJECT SPECIFIC MUSCULOSKELETAL MODELS FOR CADAVERIC BONE SAMPLES

D E Lunn, (1) P J Watson (1), P O'Higgins (2), M J Fagan (1), C A Dobson (1)

1. Department of Engineering, University of Hull, UK; 2. Department of Anatomy, Hull York Medical School, University of York, UK

Introduction

Gait is a daily requirement involving interactions between the central nervous system and musculoskeletal system. Three dimensional (3D) analyses of gait patterns enable the clinical and biomechanical assessment of locomotive movement. Motion capture analyses of bi-pedal locomotion are routinely performed, allowing for patient-specific assessment [Lenaerts *et al*, 2008; Scheys *et al*, 2005] with the gait data being successfully applied to biomechanical analyses to assess musculoskeletal interactions [Heller *et al*, 2001]. Subject specific assessment can be performed through software such as, Qualisys (Qualisys, Sweden) and Vis3D (C-Motion, United States), which estimate bone geometries from marker positions. However, when constructing biomechanical analyses from cadaver bone specimens, motion capture data are not available on a patient specific level. Consequently, techniques are required that can adapt existing motion capture data to the geometry of cadaveric bone specimens. A technique is presented which utilises geometric morphometrics methods (GMM) to warp motion capture data to that of cadaver specimens, in order to perform biomechanical analyses.

Method

A 3D motion capture system (Qualisys) consisting of ten infrared sensitive cameras, was used to track the movement of sixteen 14mm reflective markers, which were attached the subject's lower body, at a rate of 100Hz. The markers were placed in accordance with the 6 degrees of freedom formation [Liu *et al*, 1997]. The kinematic data collected supplied information such as marker position, position changes and velocities for half body modelling. This model can calculate angular velocities and important positional data from the joint centre locations.

Initially the captured pelvis and femur are warped to the size of a cadaveric specimen, obtained from the Vakhum dataset (Univeristy of Brussels), using warping software [*morphologica*, O'Higgins and Jones, 1998].

The corresponding motion capture data is then warped to the geometry of the cadaveric specimen at each time frame.

This scaled motion capture data is incorporated into a biomechanical model of the cadaveric hip joint, performed within the musculoskeletal software AnyBody (AnyBody Technology, Denmark). The lower limb movement is driven via the warped hip joint angles, enabling kinematic movements which are representative of the original gait pattern. Validation of the biomechanical hip joint model is performed through analysing the kinematic data, to that of conventional gait patterns.

Results & Discussion

A biomechanical model of the adult hip joint during gait is produced, and driven using motion capture data from a different subject.

Successful application and validation of this modelling technique will enable construction of kinematic analyses of cadaveric bone specimens, providing useful information for input to musculoskeletal modelling software.

This technique is advantageous over conventional scaling methods [*e.g.* Kepple *et al*, 1997], because it allows the modelling of juvenile cadaveric bones which display non uniform growth.

Future studies aim to apply this technique to replicate juvenile locomotive movements, for use within musculoskeletal analyses. These models are subject specific to cadaveric juvenile remains, thus the application of the method to motion capture data from comparably aged subjects will enable realistic muscle forces to be output from the software and used for subsequent finite element analyses.

References

- Heller *et al*, *Journal of Biomechanics*, 38:115-1163, 2005.
- Kepple *et al*, *Journal of Biomechanics*, 31:77-80, 1997.
- Lenaerts *et al*, *Journal of Biomechanics*, 41:1243-1252, 2008.
- Liu *et al*, *Human Movement Science*, 16:283-298, 1997.
- O'Higgins *et al*, *Journal of Anatomy*, 193:251-272, 1998.
- Scheys *et al*, *International Congress Series*, 1281:62-67, 2005.

SUBJECT-SPECIFIC TIBIO-FEMORAL CONTACT ESTIMATION DURING STEP UP/DOWN MOTOR TASK

Luigi Bertozzi, Rita Stagni, Silvia Fantozzi, Angelo Cappello

ALMA MATER STUDIORUM – Università degli Studi di Bologna, Italy
Department of Electronics, Computer Sciences and Systems

Introduction

The knowledge of how the articular surfaces interact in physiological conditions is fundamental for the development of clinical, surgical, and rehabilitative procedures aimed at treating articular degeneration processes, such as arthritis and arthrosis. Due to the complexity of the problem and to the necessity to limit invasiveness, the only possible way to reach this knowledge in living subjects is a modelling approach. The aim of the present study was the estimation of the tibio-femoral interactions, in a living and healthy subject, during the execution of a daily living motor task.

Methods

Subject-specific 3D geometries were reconstructed from the NMR dataset, and 3D accurate quantification of bone kinematics was calculated by means of 3D fluoroscopy [Bertozzi, 2007]. A 3D Euclidean distance map with a resolution of 1 mm was defined around each tibial plateau [Bertozzi, 2008]. The proximity between femur and tibia was estimated for each frame keeping distance maps fixed in the space and moving the femoral condyles according to the acquired kinematics (Figure 1). This approach allowed to quickly evaluate the distance of femoral points using a tri-linear interpolation of the pre-calculated values stored at the 8 adjacent nodes. Lateral and medial contact points (LCP and MCP) were estimated as the mid-points between femoral and tibial closest points. Lateral and medial contact areas (LCA and MCA) were estimated as the convex hull of the cloud of points which were at a distance smaller than a contact threshold from NMR. Contact points and areas were estimated during 9 repetitions of the step up/down motor task.

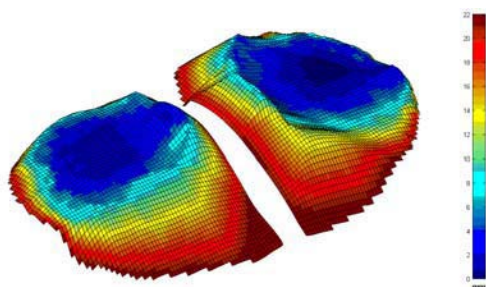


Figure 1: 3D proximity map between the femur and the tibia at the full extension position [mm].

Results

LCP moved posteriorly of about 8 mm from 0° to 40° of flexion, then it remained almost in the same position (Figure 2). MCP did not move along A/P direction, except for a posterior translation of about 10 mm from 0° to 15° of flexion. Translations along the M/L direction were very small, and almost negligible along the P/D direction. LCA and MCA were little dependent on the flexion angle with values from 100 mm² and 500 mm². LCA was slightly more repeatable than MCA. Similar behaviours and variability were obtained for extension and flexion movements.

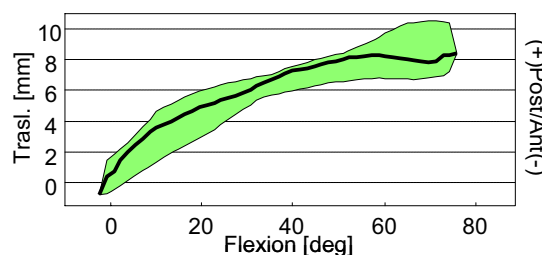


Figure 2: Antero-posterior translation of the lateral contact point during extension movements.

Discussion

The devised model, based only on imaging technologies, was suitably used to reach the aim of the study. The model produced physiologically meaningful results, and it showed that some biomechanical behaviours, typical of passive and simulated loading conditions, were also present during active motor tasks, such as the step up/down. On the lateral side, the physiological rolling and sliding movements were obtained for little and higher flexion angle respectively, whereas on the other side, the physiological medial pivot seemed to be obtained [Goodfellow, 1978]. Contact areas were in accordance with the data reported in the literature. In conclusion, the devised methodology can become an important tool for suggesting effective pre-operative, surgical and rehabilitative procedures for pathological subjects.

References

- Bertozzi et al, J Biomech, 40:S38-S44, 2007.
- Bertozzi, PhD Thesis, Università di Bologna, Italy, 2008.
- Goodfellow et al, J Bone Joint Surg, 60:358-369, 1978.

EXPLORING THE USE OF SOCIAL BULLETIN BOARDS IN ADAPTIVE AGENTS FOR FAST CHANGING ENVIRONMENTS

Mariam Kiran

Department of Computer Science, University of Sheffield, Sheffield UK

Introduction

Adaptation is an important factor for the survival of living organisms. Most communities like ants have shown to behave collusively to ensure the collective survival of their community. These systems can best be modelled using agent-based modelling techniques, where agents use techniques to continually adapt themselves. Although the advent of powerful parallel computers have allowed extensive research in different kinds of agent-based models with large agent concentrations, true forms of adaptation are still being ignored; as most of these models are written for static environments. These models are usually designed as predictive models for agents behaving in certain manner with ideal environmental conditions. Unfortunately in real systems, agents are subject to unknown conditions where environments are constantly changing and agents are continuously adapting their behaviour. How quickly agents adapt to these fast changing environment hold vitals to their personal survivals as well as of the community. This paper presents the use of central boards for the agents to use to adapt their behaviour and circulate good strategies to other agents.

Methods

Inspired by the memetic algorithms proposed by Dawkins [Ong et al. 2006], the working of the proposed algorithm has been summarised in Box 1. (SB- Social Board, A-Agent)

SB 1: Initialise random memes (strategies).
SB 2: Assign fitness equal to threshold level.
While(stopping conditions)
SB 3: Use Roulette Wheel selection to distribute a collection of memes to each agent.
A1: If strategies in my personal database are less than threshold level. Select one of received personal memes. Perform strategy.
A2: Optimise by crossover/mutation.
A3: Post (strategy, fitness) to social board.
SB 4: Collect and update database.
End

Box 1: Algorithm of Central Social Boards for Agent communication.

Every agent has a personal threshold level (biological fitness) to satisfy. These agents read off a certain number of strategies from the bulletin board, based on roulette wheel selection ensuring

the strategies of high fitness have higher chances to be chosen. Each agent then adopts one of these chosen strategies in their personal database, performs it and receives a certain payoff against it, which would be its fitness. This fitness would be similar to the biological fitness of the agent. The agent can also optimise the strategy using crossover/mutation techniques. All agents work independently, therefore some agents would do better than others in some conditions, showing heterogeneous behaviour. At the end of the iteration, the agents send their current tried strategies and the received payoffs to the social board. The board then collects the information from all agents and rearranges itself, copying the new fitness of the strategies, as well as adding new improved strategies. The *good* strategies with high fitness will have a higher probability to be chosen by the agents the next time round. The agents know when to request for new strategies when the payoffs of the current strategies are lower than the personal threshold level. Progressively, through collusion all agents would find the good strategies in the group and use them until certain conditions arise and the new payoffs returned are *not good* (lower than threshold). Thus old memes are seen deteriorating on the bulletin board and new memes emerge, which are more suited to the new conditions.

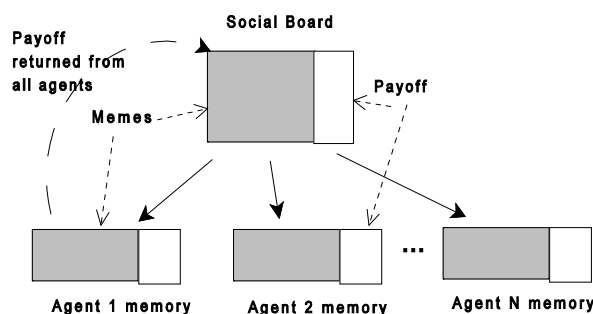


Figure 1: Pictorial representation of the social boards interacting with the agents

This is work in progress, and further analysis is being carried out on the speed of adaptation of agents with varying speeds of changing environment.

References

Ong Y. S. and Lim M. H. and Zhu N. and Wong K. W. (2006). "Classification of Adaptive Memetic Algorithms: A Comparative Study". *IEEE Transactions on Systems Man and Cybernetics -- Part B*. **36** (1): 141.

USING THE LEARNING WINDOW IN AGENT MEMORY TO REDUCE COMPLEXITY IN REACTIVE AGENTS

Mariam Kiran

Department of Computer Science, University of Sheffield, Sheffield UK

Adaptation is an important facet for the survival of living organisms to adapt to changing environments. In multi-agent systems, where agents are used to predict the performance of biological models, it is essential for the agents to possess this capability of knowing when to alter their structures to suit their new surroundings. Various disciplines in multi-agent research [Jennings et al 2000] have separated agents into one realm- *deliberative* or *reactive* – to provide agents with the mechanism of *thought* for how to behave and when. The theories have resulted in reactive agents being more complex and computational more expensive than processing deliberative agents. Unfortunately most models in biology are not deliberative; they usually behave in unknown ways, reacting to unpredictable surrounding conditions. This paper proposes the use of the learning window variable, as part of the agent memory to make it easy for agents to know when to change behaviour and not to compensate on computational resources.

Methods

We propose the use of FLAME (Flexible Agent-based Modelling Environment) for modelling biological systems, as it uses the principle for X-machines to represent individual agents with memory. The framework can allow simulations of millions of agents to run over parallel platforms and provide results in finite time [Kiran et al 2008].

Every X-machine agent possesses a set of memory variables, which accompanied by incoming messages change to different states allowing different behaviours to be incorporated. X machines have been described as reactive agents in the works of Kefalas [Kefalas 2002].

Inspired from the theories of behavioural psychology [Ferster et al. 1997], which explains how babies learn to respond to environments and how quickly they grow out of their habits, we propose the use of a learning window variable in the memory of every agent to allow it to use different times to work out new behaviour for itself.

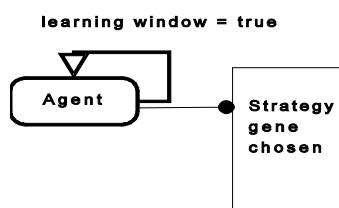


Figure 1: Agent architecture with learning window

When the simulation begins, the agent checks for the window value, if null, the agent knows it has to choose a strategy to perform.

At the end of every simulation, the agents check the performance of their strategies. If they performed well, they add a default addition of x time steps to the window length, else they set the window length to be null. Thus, at the next time step, if the window is null the agent knows it has to choose a different strategy. A graph plotted of window lengths would depict how successful the agent has been performing and following a certain strategy.

An experiment was performed to show the performance of the learning window on groups of agents for which the environment becomes unfavourable for Group 2 at time $t=150$.

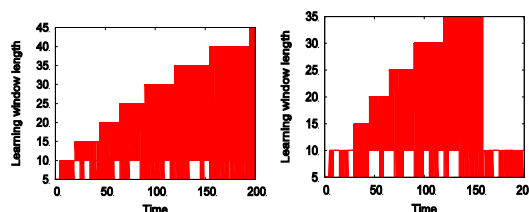


Figure 3: Window lengths for agents in Group 1,2.

Figure 3 is a graph of the different lengths of the learning windows of the agents in Groups 1 and 2. It is shown that the length of the learning window significantly decreases for all agents in Group 2. This is because the environmental conditions become unfavourable and the agents are struggling to find new good strategies, whereas Group 1 is unaffected. The different lengths of the window show heterogeneous behaviour within the group, with some agents performing well but others still choosing new strategies to survive.

References

- Nicholas R. Jennings and Michael Wooldridge, On agent-based software engineering, *Artificial Intelligence*, 117-277-296, 2000.
- Mariam Kiran, Simon Coakley, Neil Walkinshaw, Phil McMinn, Mike Holcombe: Validation and discovery from computational biology models. *Biosystems* 93(1-2): 141-150 (2008)
- P. Kefalas. Formal modelling of reactive agents as an aggregation of simple behaviours. In *SETN '02: Proceedings of the Second Hellenic Conference on AI*, pages 461–472, London, UK, 2002. Springer-Verlag.
- C. Ferster, B. F. Skinner, Carl D. Cheney, W. H. Morse and P. B. Dews, *Schedules of Reinforcement*, ISBN-978-0874118285, 1997

AN EFFICIENT AND ACCURATE PLOTTING TOOL FOR 3D CURVE ANALYSIS IN BIOLOGICAL SAMPLES

Duncan J.B. Payne (1), Sarah R. Fahle(2), Mike W. Holcombe (1), Rhonda R. Snook (2)

1. Computer Science, The University of Sheffield, UK; 2. Animal and Plant Sciences, The University of Sheffield, UK

Introduction

The ability to digitise data presented in 3D can be a difficult task. The nature of desktop computers limits any view of data to 2D approximations. We intend to show that such approximations can be used to quickly build up accurate representations of 3D data, without the need for highly expensive machinery or a great degree of expertise.

It has been suggested that sperm takes on a species-specific three-dimensional shape once inside a female egg [Karr, 1996]. This theory has, however, only ever been based on visual observations and not on any form of statistical analysis [Karr, 1991].

A number of techniques have been used in the past as a methods of digitising 3D structures, such as “Crumbs” in the CAVE (a 3D virtual reality environment) [Brady et al, 1995], but such tools are complicated and expensive. We present a simple, cheap and *portable* tool, capable of running on a standard desktop computer.

Method

Figure 1 shows a screenshot of the software application that has been developed. It shows a sample image, in the process of being plotted in 3D. The software application is made up of the main image and a slider, which allows the user to navigate “through” the 3D structure in $2\mu\text{m}$ layers. The user will place at least one point for every layer on which they can see a section of sperm curve. The two smaller windows to the right of the main image allow for a “zoomed in” representation of an area surrounding the mouse pointer in the main image, providing both a top-down view (the first of the two), and effectively a side-on view into the stack of images. This allows for a greater degree of accuracy when placing a point on the sperm curve, as well as an ability to effectively resolve areas of information which might otherwise not be seen.

Once plotted, it is possible to draw a cylindrical tube along the plotted points in a 3D window. This makes it possible to ensure the accuracy of the plots when combined with a 3D view of the original data set.

As a further test of accuracy, the lengths of plots can be calculated using this application and can be compared against those already known for

Drosophila sperm, from which the average lengths of sperm are known [Pitnik et al, 1995].

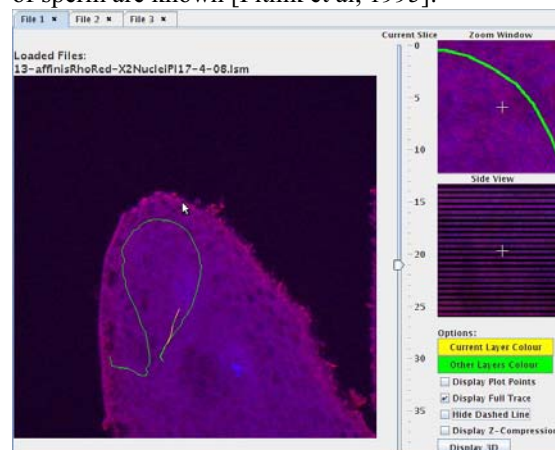


Figure 1: Screenshot of the application developed with a sample image.

Results

When comparing this application with those designed for use in virtual reality environments, the relative simplicity and ease of use has meant that no special training has been required to build up plots of the data for this project. The 3D environment requires the user to constantly rotate and view the 3D data at different angles, adding more time to the effort of plotting data.

Discussion

We have briefly introduced an application developed as a solution to the problem of digitally representing data in 3D, for the purpose of scientific analysis. We have shown that the digital representation can be tested for accuracy through the use of a number of techniques, to ensure that this data is of a great enough degree of accuracy to be used (in this context) in the characterisation and analysis of these 3D curves, as seen in the images captured through confocal microscopy.

References

- Brady et al, BIOMEDVIS, 18-25, 1995.
- Karr, Mech Dev, 34:101-112, 1991.
- Karr, Current Topics in Development Biology, 34:89-115, 1996.
- Pitnik et al, Proc Natl Acad Sci USA, 92(23): 10614-10618, 1995

Poster Session B

EXPERIMENTAL PROCEDURE FOR WEAR MODEL VALIDATION: FROM MACRO TO MICRO ANALYSIS

L. Mattei (1), E. Ciulli (2), F. Di Puccio (3), S. Affatato (4)

1,2,3. Dept. Mechanical, Nuclear and Production Engineering, University of Pisa, Pisa, Italy

4 Medical Technology Laboratory Rizzoli Orthopaedic Institute, Bologna, Italy

Introduction

It is recognized the main cause of hip prostheses failure is the wear of articular surfaces. Both theoretical and experimental wear studies are very important. Wear models allow simulating *in vivo* wear, avoiding time-consuming and costly tests, whereas experimental analysis [Affatato, 2008] are fundamental for model validation, often offering a more detailed information about wear. This work proposes a systematic experimental procedure for wear model validation and characterization, which correlates macroscopic and microscopic data.

Wear model

Theoretical wear studies on hip prostheses are based on computational models that, combined with a wear law, such as Archad's law, simulate wear trend. These models typically get prosthesis CAD model and physiologic load as inputs, calculates the pressure distribution and the displacements, returning a wear 3D map. Their validation is generally carried out by means of weight loss measurements of corresponding implants tested in simulators. In metal-on-metal and metal-on-plastic hip implants a wear trend of respectively 28.17 [Onisoru, 2006] and 0.15 mm³/mil. cycles [Liu, 2008] has been estimated.

Experimental wear analysis

Experimental tests executed in wear investigations can be divided in macroscopic and microscopic, as described in the following.

Macro analysis. Quantitative macro analysis includes: weight loss measurements by means of microbalances; 3D geometry reconstruction of unworn-worn surfaces for the valuation of volumetric material loss and 3D spatial wear distribution, using CMM machine or 3D scanner.

Micro analysis. Quantitative micro analysis consists in profilometer measurements, such as medium and total surface roughness and skewness, at different latitudes of head, using a contact SRM machine. Optical (OP) and Scanning Electron Microscope (SEM) images allow a qualitative micro analyses of cup-head; moreover, 3D defects reconstruction can be obtained from 2 SEM images, by means of MEX software [Bassani, 2006].

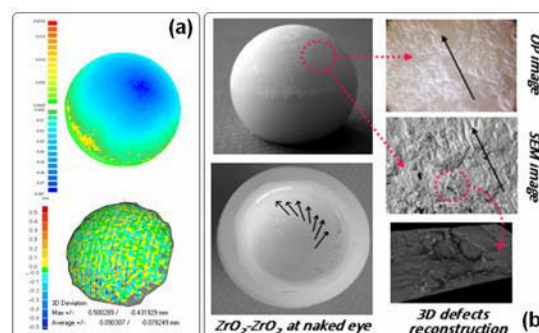


Figure 1: Wear analysis of ZrO₂/ZrO₂ pair. 3D reverse engineering process of head (a). Cup at OP and SEM, and example of 3D reconstruction of a defect. Orientation of texture damage is confirmed by macro observation of the cup (a).

Combined macro/micro analysis

The present study suggests a systematic approach for experimental wear investigations usable as reliable tool for wear model validation: it's based on a combined macro/microscopic analysis that gives a complete description of wear.

Three ceramic on ceramic (CoC) (head/cup: Al₂O₃/Al₂O₃; ZrO₂/Al₂O₃; ZrO₂/ZrO₂) pairs were run in hip simulator and analysed using aforementioned techniques [Mattei, 2008]. Weight measurements were conducted using a microbalance with an accuracy of 0.03 mg, while 3D head reconstruction using a 3D scanner based on stereoscopic vision, with 0.01 mm of accuracy. Experimental results (Fig. 1) were analysed for each pair and compared. Volumetric material loss from 3D reverse engineering verifies the measurement of weight loss, while 3D wear map points out the more stressed regions, corresponding to higher roughness zones and more damaged zones evidenced in OP and SEM images.

Even if only three CoC implants have been considered, the results match the literature ones and the procedure assessment is in progress on many hip implants of different typology.

References

- Affatato S. et al., *Med Eng & Phy*, 30: 1305-1317, 2008.
- Bassani R. et al., AIMETA Trib Conf, 415-422, 2006.
- Liu F., et al., *J Biomech*, 41: 686-694, 2008.
- Mattei L. et al., GNB2008, Pisa, 491-492, 2008.
- Onisoru J., et al., The Annals of Univ. Dunarea, 2006.
- Taddei P. et al, *J Mat Science*, 41: 5310-5316, 2006.

EXPERIMENTAL VALIDATION OF FINITE ELEMENT MODELS OF THORACOLUMBAR VERTEBRAE

Sami Tarsuslugil (1), Corinne Hanlon (1), Rochelle O'Hara (2), Nicholas Dunne (2), Fraser Buchanan (2), John Orr (2), David Barton (1), Ruth Wilcox (1)

1. University of Leeds, United Kingdom; 2. Queen's University Belfast, United Kingdom

Introduction

Computational modelling of the spine offers a particularly difficult challenge to analysts due to its complex structure and high level of functionality. Previous studies [Wijayathunga, 2008; Jones, 2007] have shown that finite element (FE) predictions of vertebral stiffness are highly sensitive to the applied boundary conditions and therefore validation requires careful matching between the experimental and simulated situations. The aim of this study was to develop and experimentally validate specimen specific FE models of porcine vertebrae in order to accurately predict the stiffness of single vertebra specimens.

Methods

Nine single vertebra specimens were excised from the thoracolumbar region of two porcine spines. The specimens were mounted between two parallel PMMA housings and each specimen was imaged using a micro computed tomography (μ CT) system (μ CT80; Scanco Medical, Switzerland). In order to accurately match the experimental conditions, a radio-opaque marker was positioned on the specimen housing at the point of load application.

The vertebrae were separated into two groups: a development set (set 1) consisting of three specimens and a validation set (set 2) of six specimens. Specimens from set 1 were used to establish the optimum method of conversion from image greyscale, to element material properties. The models in set 2 were used to assess the accuracy of the stiffness predictions for each model.

The vertebrae were tested in a materials testing machine (AGS-10kNG; Shimadzu Corp., Japan) under axial compression and the stiffness for each specimen was calculated. The μ CT data was imported into an image processing package (Scan IP, Simpleware, UK). The software enabled the images to be segmented and the vertebra, cement housings and position of load application to be identified. The segmented images were down-sampled to 1mm voxels, enabling a FE mesh to be generated (Scan FE; Simpleware, UK) based on direct voxel to element conversion. The Young's modulus of each bone element was assigned, based on the greyscale of the corresponding image voxel. The PMMA housing plates were assigned homogeneous material properties ($E = 2.45$ GPa).

Abaqus CAE 6.8 (Simula, Providence, Rhode Island, USA) was used for the processing and post-processing of all the models.

Results

The mean experimental stiffness was 4321 N/mm (standard deviation = 415 N/mm). The optimum conversion factor was calculated for set 1, which yielded a root mean squared (RMS) percentage error of 7.5% when compared with the experimental stiffness. Using this optimised scale factor, FE models of specimens from set 2 were created. The predicted stiffnesses for set 2 were compared to the corresponding experimental values and yielded an RMS error of 10.1%. The results are shown in Figure 1.

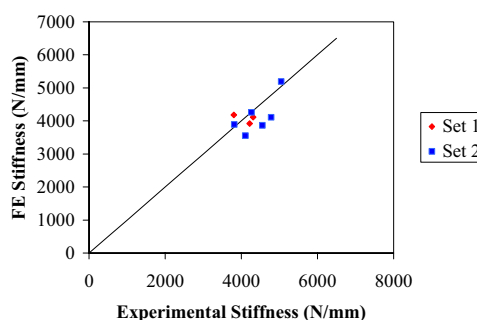


Figure 1: Predicted FE versus experimentally measured stiffness of all specimens

Discussion

The results indicate that specimen specific models can provide good agreement with the corresponding experimental specimen stiffness. In addition, the method employed in this study proved robust enough to be applied to vertebral tissue obtained from different animals of the same species. The level of error obtained in this study is comparable to that obtained in previous studies [Wijayathunga, 2008; Jones, 2007]. This method will now be developed to assess treatments for traumatic spinal injuries.

Acknowledgements

This work was funded by the EPSRC

References

- Jones et al, J Biomech Eng, 40:669-673, 2007.
- Wijayathunga et al, Proc. IMechE, Part H: J. Engineering in medicine, 222:221-228, 2008.

INVERSE ANALYSIS BASED DETERMINATION OF MATERIAL PARAMETERS FOR ALVEOLAR PARENCHYMA ON DIFFERENT SCALES

Sophie Rausch, Lena Wiechert, Wolfgang A. Wall

Institute for Computational Mechanics, Technische Universität München, Germany

Introduction

Mechanical ventilation of patients with Acute Respiratory Distress Syndrome (ARDS) and Acute Lung Injury (ALI) is a life saving treatment. However, due to insufficient understanding of lung mechanics can cause overstraining of the parenchymal tissue resulting in additional inflammatory injuries. Such ventilation induced lung injuries (VILI) occur mainly in the alveolar tissue. The goal of our research is to improve mechanical ventilation, and thus to reduce the frequency and severity of VILI.

This work is part of a wider project concerned with modelling the entire human lung utilising multiscale and multiphysics methods. The focus of this part is on the alveolar tissue where VILI initiates. Our aim is to determine a better material description of lung tissue in our complex simulations.

Methods

Precision-cut lung slices (PCLS) are prepared from isolated rat lungs as previously described [Martin, 1996]. These slices, viable for at least three days, are then used for uniaxial tension tests by means of the Bose ElectroForce 3100 (Bose Cooperation). The force transducer of the machine has a range of ± 0.5 N and a resolution of under 0.005 N and the displacement transducer has a range of ± 2.5 mm and a resolution of under 0.025mm.

Due to the viscoelastic material properties of the tissue the specimens are preconditioned before the actual experiment. The living lung slices are cyclically loaded and individual stress-strain curves are obtained.

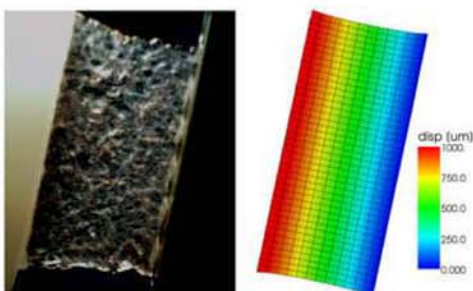


Figure 1: Comparison between experiment and homogenized simulation.

In our research code we have a number of different material models for soft biological tissue. The one

used here is based on the formulation of [Holzapfel, 2001] and [Ogden, 1974], see [Wiechert, 2009].

By using an inverse analysis we are able to estimate material parameters in order to achieve similar stress-strain curves in the simulation to the ones measured experimentally. In this method the FE simulation is repeatedly performed while adjusting the material parameters according to the Levenberg-Marquardt-Algorithm, see Figure 1. This is done until the parameters fit, within a given tolerance, to the experimentally obtained curve.

Results and Conclusion

With this work we are able to determine material parameters for homogenized lung parenchyma by performing an inverse analysis on experimentally tested PCLS. This established already a great enhancement of our computational lung model.

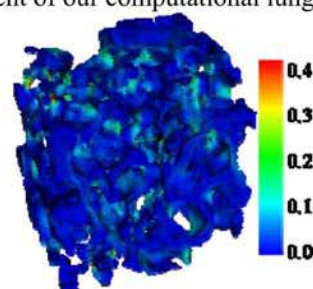


Figure 2: CT based real alveolar geometry under uniaxial tension, the colouring shows the 1st eigenvalue of principal strain. (Imaging by group of Prof. J. Schittny, see [Schittny, 2008])

However, for a better understanding of the initiation of VILI, we need to investigate the microscale, i.e. the individual alveolar walls. Hence we will extend our method to the lung microscale based on artificial and real alveolar geometries. Figure 2, shows the 1st eigenvalue of the principal strain of a real alveolar geometry simulated in our research code. Using this kind of geometry we are able to estimate material parameters for single alveolar walls. Future work will involve discretizing the full microscale of the PCLS in order to perform an inverse analysis on the actual geometry of the tested specimen.

References

- Holzapfel *et al*, J Biomech Eng, 126:264-275, 2004.
- Martin *et al*, Eur Respir J. 9:2479-87, 1996.
- Ogden, R., Mech. Phys. Solids, 22:547-553, 1974
- Schittny, J., Am J Physiol, 294: 246-254, 2008.
- Wiechert *et al*, J. Eng. Mech., accepted 2009

FREE-HAND SONOGRAPHIC SYSTEM FOR BONE CORRECTION PLANNING

Ewelina Świątek-Najwer (1), Paweł Krowicki (1),
Romuald Będziński (1), Krzysztof Krzysztoforski (1),

1. Wrocław University of Technology, Institute of Machines Design and Operation,
Biomedical Engineering and Experimental Mechanics Laboratory,
Łukasiewicza 7/9, 50-371 Wrocław, Poland

Introduction

The aim of the study was to create a software for the free-hand sonographic system for aiding bone correction. Algorithms of data analysis were created and implemented. The realized system is applied for designing of surgical scenario on real dataset registered by the probe and to support the surgeon intra-operatively.

Material and Methods

The computer system combines infrared optical tracking system (Polaris, NDI) and sonographic linear probe (with portable sonographic system EchoBlaster 128, Telemed). The acquired and analysed 3D digital dataset provides description of voxels in patient coordinate system defined by reference frame on the patient body. To determine the coordinates a calibrating matrix is required. It describes the tilt of scanning plane in relation to the coordinate system of sensor mounted on probe. Mathematical apparatus of matrix transform between coordinate systems is implemented in the system [Świątek-Najwer, 2008].

The system is applied to measure bone geometrical parameters on the basis of landmarks positions defined by a surgeon on ultrasound scans. Measured parameters are course of limb axes and anatomical angles. The course of limb mechanical axis is a factor determining loading conditions.

The bone surface reconstruction algorithm is divided into three phases: pre-processing (filtration of images), segmentation (delineation of bone contour) and bone reconstruction (calculation of mesh built of triangles with vertices defined by the points of bone contours). The filtration of sonographic scans is a very demanding procedure, because of various artefacts introduced by reverberations. Standard methods of filtration like mean and median filters were applied. Additionally two images were registered in the same location and subtracted to eliminate noises. To delineate the bone contour gradient mask was applied and the bone interface was determined from downwards. To reconstruct the shape, the Delaunay 2D algorithm was applied to determine the scheme of

vertices connection into a mesh of triangles. On obtained virtual model the surgeon designs bone correction and simultaneously controls resulting limb geometrical parameters. The osteotomy procedure can be performed using straight or dome osteotomy plane.

To apply the data registered pre-operatively and follow designed surgical scenario in the operational room the fusion procedure must be performed. The Best-Fit algorithm determines transform between two dataset of landmarks in two coordinate systems to bring them to cover with smallest distance.

Results

The accuracy of Tracking System was determined using calibrated measuring plate with palpable cones. The Fiducial Localisation Error equals 0.35mm. The accuracy of developed system, described by Target Registration Error (TRE) was tested on sawbones with mounted cones, which are perfectly imaged by probe and addressed by navigated instrument. The error means the distance between image point transformed by fusion matrix and real related point in the intra-operative coordinate system. Value of TRE reached 2.08mm.

Discussion

Developed system consisting of sonography and tracking system provides tool for bone surface imaging. The identified shape of bone is applicable for virtual planning of correction for complicated bone deformities. Obtained results revealed relatively high accuracy of the systems. To improve the accuracy advanced algorithms of image conditioning are required.

The research has been performed in cooperation with Wrocław Clinic of Orthopaedy.

Acknowledgements

This paper is supported by the Polish Ministry of Science and Higher Education in the framework of project with register number N R 13 0012 04.

References

Świątek-Najwer E. et al., Acta of Bioengineering and Biomechanics, Vol.10 (4), 2008.

NUMERICAL EVALUATION OF CHANGES IN RETINAL PERFUSION RATE DURING LASER IRRADIATION

Marek Jasiński

*Department for Strength of Materials and Computational Mechanics,
Silesian University of Technology, Poland*

Introduction

Transient heat transfer in human eye is described by Pennes equation in the form

$$x \in \Omega_e : c_e \dot{T}_e = \lambda_e T_{e,ii} + Q_e \quad (1)$$

where e identifies successive layers of model: cornea, aqueous humor, lens, vitreous humor and retina, c_e [$\text{Jm}^{-3}\text{K}^{-1}$] and λ_e [$\text{Wm}^{-1}\text{K}^{-1}$] are the volumetric specific heat and thermal conductivity, respectively, T_e denotes temperature, while Q_e [Wm^{-3}] corresponds to internal heat sources containing components connected with perfusion, metabolism and lasers [Welch, 1984].

In current work perfusion heat source is defined as

$$Q_{e,perf} = c_B G_{B0} w(\theta) [T_B - T_e] \quad (2)$$

where c_B [$\text{Jm}^{-3}\text{K}^{-1}$] is volumetric specific heat of blood, T_B is blood temperature and G_{B0} [$(\text{m}^3 \text{ blood s}^{-1})/(\text{m}^3 \text{ tissue})$] is initial blood perfusion rate, while $w(\theta)$ is polynomial function which argument denotes tissue injury integral

$$\theta(x) = \int_0^{t^F} A \exp[-\Delta E R^{-1} T_e^{-1}] dt \quad (3)$$

Parameter A [s^{-1}] in equation (3) is the pre-exponential factor, ΔE is the activation energy [J mole^{-1}] and R is universal gas constant [$\text{J mole}^{-1} \text{K}^{-1}$] [Abraham, 2007].

Laser heat source is given by formula

$$Q_{e,las} = \mu_{ea} \phi_e I_0 \exp[-\mu_{ea} x] \quad (4)$$

where μ_{ea} [m^{-1}] is the absorption coefficient, I_0 [Wm^{-2}] is the irradiance on the cornea anterior surface, ϕ_e denotes lens focalization rate while x is the spatial co-ordinate [Amara, 1995].

Equations (1) are supplemented by convection condition with emissivity on cornea surface, the Robin condition on the retina surface, while between sub-domains the ideal thermal contact is assumed. Initial parabolic distribution of temperature is also known.

Results

On the stage of numerical realization the 1st scheme of BEM has been applied.

The temperature distribution and the perfusion rate profiles in retina for different kinds of lasers (Nd:YAG and Ruby) has been calculated.

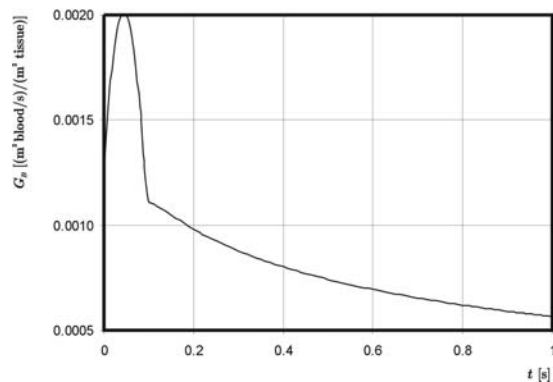


Figure 1: Maximal perfusion rate in retina during Ruby laser irradiation

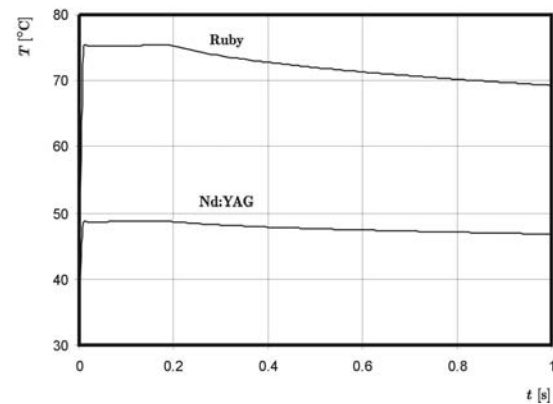


Figure 2: Maximal temperatures in retina during Nd:YAG and Ruby laser irradiation

The results of computations show that negative effects of laser irradiation have visible influence on perfusion rate.

Acknowledgements

This paper is part of grant N N501 3667 34

References

- Amara E.H., Int. J. Heat Mass Transfer, 38: 2479-2488, 1995.
- Abraham J.P. et al, Int. J. Heat Mass Transfer, 50: 2537-2544, 2007.
- Welch A.J., IEEE J. Quantum Electronics, 20: 1471-1481, 1984.

EVALUATION OF THERAPEUTIC RESPONSE TO RADIOTHERAPY BASED ON TUMOR GEOMETRY

Seishin Takao (1), Shigeru Tadano (1), Hiroshi Taguchi (2) and Hiroki Shirato (2)

1. Graduate School of Engineering, Hokkaido University, Japan;

2. Hokkaido University Graduate School of Medicine, Japan

Introduction

Precise assessment of therapeutic response to radiotherapy is important for accurate prognosis and evaluation of prescribed treatment. Tumor diameter is commonly used as an indicator to evaluate therapeutic response in cancer patients. Since the 1970s, the World Health Organization (WHO) had suggested to assess tumor response by measurement of maximum diameter and largest perpendicular diameter [WHO, 1979]. For more precise assessment, it would be useful to examine three-dimensional (3D) morphological features of tumors.

This study aims to propose a method to evaluate therapeutic response to radiotherapy quantitatively based on the 3D tumor geometry.

Analysis Method

To quantitatively evaluate 3D tumor geometry, distances from tumor center to its surface at every azimuthal angle φ and horizontal angle θ were used. The distance could be represented by radius R in spherical coordinate system $O-R\theta\varphi$, whose origin is at the center of gravity of the tumor. Moreover for visual understanding of feature of the 3D geometry, 2D surface geometry map was introduced. In this map, values of tumor radius $R(\theta, \varphi)$ were represented by color and plotted on θ - φ plane. Sizes of each map associate with tumor volumes.

Tumor volume V , surface area S and radius R were examined as geometric factors. Sphericity of tumors was evaluated by spherical shape factor (SSF). The value of SSF represents how much the tumor shape is close to a sphere. The SSF is defined as follows,

$$SSF = \frac{36\pi V^2}{S^3} \quad (1)$$

Three cases of regional lymph node enlargement in head and neck treated in Hokkaido University Hospital were analyzed in this study. Furthermore, changes of tumor geometries were calculated using our simulation method and compared with actual tumor geometries [Takao, 2007].

Results and Discussion

Figure 1 shows one of the changes of tumor geometries during the treatment period and calculation result using surface geometry maps.

These maps provide visual understandings of 3D tumor geometries. From these maps, it was found that tumor shrink keeping its original morphological features throughout the treatment period. Geometric factors enable to evaluate characteristics of 3D tumor shapes and to compare simulation results with actual tumor geometries quantitatively.

References

Takao S., Tadano S. et al., Computer Simulation of Malignant Tumor Reduction by Radiotherapy, *J. Biomech.*, 40, Suppl. 2:S416, 2007.
WHO, WHO handbook for reporting results of cancer treatment, 1979.

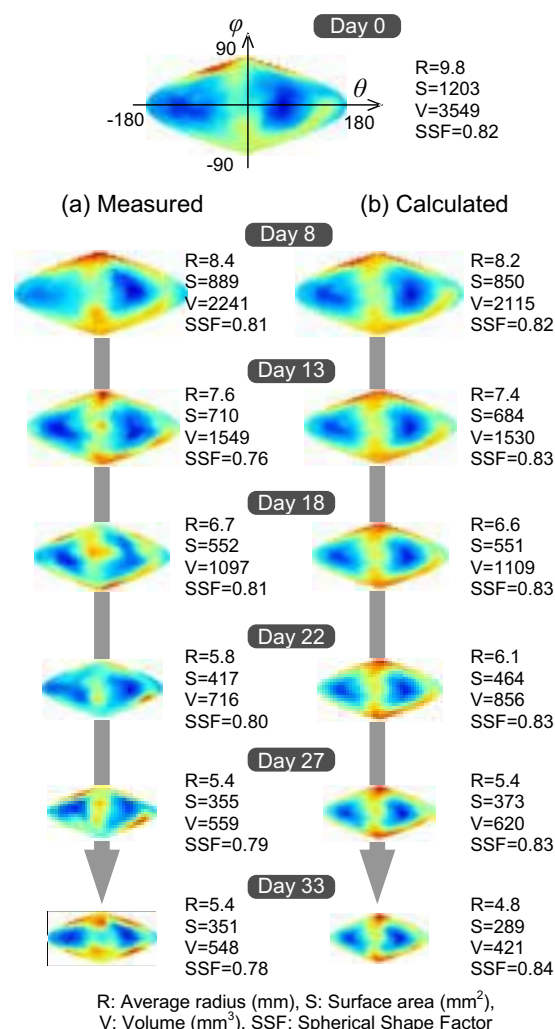


Figure 1: Tumor geometries represented in surface geometry maps and geometric factors.

INNOVATIONS IN MEDICAL IMAGE PROCESSING FOR THE DESIGN OF CUSTOM MEDICAL DEVICES AND IMPLANTS

Maarten de Vleeschouwer (1), Alessandro Motroni (2)

1. *Materialise NV, Leuven, Belgium*, 2. *CMF Marelli, Milano, Italy*

Introduction

There is a growing trend towards the personalization of medical care, as evidenced by the latest developments in multi-slice CT imaging [Mather, 2005] and ultra-fast MR imaging, personalized treatment planning in a variety of surgical disciplines [Poukens, 2003] and the development of more suitable implantable devices [Harrysson, 2007]. In this paper we will describe the use of 3D medical image information of individual patients as well as selected patient populations, combined with computer aided engineering (CAE) tools and processes, in the rapid product development of custom and standard implantable devices. We propose a method of ‘digital’ CAD for the development process of medical implants or devices. The term ‘digital’ refers to the method of describing 3D structures with discrete elements (triangles), contrary to the ‘analogous’ way of describing these structures in traditional CAD packages using continuous surfaces, ruled by mathematical equations (NURBS). Being able to use design tools directly on STL files eliminates the need for time consuming reverse engineering and preserves the accurate geometry. This allows for faster and more accurate design of medical implants or devices.

Methods

Medical imaging systems typically generate stacks of gray scale images. These images are saved in DICOM format, the standard in medical imaging. To correctly process these image stacks, Materialise medical imaging software Mimics® is used. Mimics® is a powerful, yet user friendly software that generates 3D models of the tissues of interest. For the design of patient-specific devices or implants, 3-matic® is used. This software allows the use of CAD-tools directly on STL files, the so called digital CAD. For finite element analysis, the surface mesh of the STL in Mimics® is first optimized before it is converted to a volumetric mesh, which is generated inwards from the surface mesh. To run a simulation of forces or fluids further requires assigning material properties and boundary conditions. In Mimics® it is possible to assign material properties to the volumetric mesh, based on the gray values from the original image dataset.

Results

Three different applications are presented. In the first one the patient data is prepared for FEA analysis through sequential steps used to produce image-based volumetric meshes. In the second application the image-based custom implant design process is analyzed, applied to the design of a patient-specific cranioplate, a procedure that has been largely automated in 3-matic®. The final study is focused on the pre-operative diagnosis and device evaluation using CAE methods, applied to a case of aneurysm.

Discussion

The approach to implant and device design, based on 3D medical image data proposed in this paper is different from the current design processes in the medical industry, which rely completely on traditional CAD methods. The digital CAD concept might not be commercially interesting for mass production of generic implants, but is undoubtedly beneficial when designing custom implants. Custom implants lead to more patient satisfaction, but come at a higher cost. However, since we noticed an increase in the personalization of medical care over the last years, custom implants and custom devices might one day become the standard in medical care. Virtual simulation techniques like FEA and CFD are not yet widely accepted in the medical field, mainly because at the moment the complexity of human tissues (and our limited understanding thereof) prevents us from choosing the appropriate boundary conditions, thus leading to many assumptions that in turn affect the accuracy of the simulation and its translation to reality. Still, the benefit of CAE simulations is that they have the potential to reduce the amount of in vitro tests with prototypes, animal tests, cadaveric tests, maybe even clinical trials.

References

- Harrysson et al, BMC Musculoskeletal Disorders, 8(91), 2007
- Mather et al, Radiology Management, 27(3): 46-48, 2005
- Poukens et al, Computer Aided Surgery, 8(3): 146-154, 2003

CFD ANALYSIS OF DETERMINANT FOR CAROTID BULB GEOMETRY

Masako Himeno (1), Shigeo Noda (1), Kazuaki Fukasaku (1), Ryutarō Himeno (1)

1. Advanced Science Institute, RIKEN, Japan

Introduction

The abnormal shapes of blood vessel such as stenosis and aneurysm causes in cerebrovascular diseases and heart diseases. In advance to study about these abnormal developments, we examined which factors lead to normal development of blood tube. It was supposed that artery shapes adapt to local blood flows. So, fluid dynamic and mechanical factors were examined by optimization of blood tubes using blood flow analysis. We studied which factors led to reproduce the actual artery shape. We take up carotid artery bifurcation from following two reasons. 1) It has carotid bulb that is specific expanded area from common carotid artery to internal carotid artery. The size and shape of carotid bulb of individual persons varies a lot. So, we can study the factors with various types of bifurcation shapes. 2) We can also examine what factors cause to stenosis because atherosclerosis often occurs in carotid bulb.

Method

We picked up typical 4 cases among 9 various sizes of carotid bulb form CT images of healthy volunteers. Blood flows were analyzed by using VOF and QUICK scheme developed by ourselves. We took two factors: wall shear stress (WSS) and surface area of artery. The endothelial cells of the inner side of the vessel wall produce angiectasis factors and cell growth factors and deform its shapes by sensing the degree of WSS. So, we presumed that blood vessel is created to keep away the region with high WSS. The other is surface area. We also presumed that blood vessel has the minimum amount of wall surface area from the saving material point of view. For multi-objective optimization analysis, we used the non-dominated sorting GA (NSGA-2), which is generally applied to solve multi-objected search problems.

Results

Fig.1 shows actual shapes. Shape A and B have large expansion of the carotid bulb, shape C has middle, and shape D has small. We performed multi-objective optimization using two factors in case A, B, C and D. Fig.2 is the result of case C, whose size of carotid bulb is middle among 4 cases. Fig.2-1 shows the shape of case C. The red dot displays the position of maximum value of WSS which was downstream of the area for optimization.

Fig.2-2 shows optimized solutions set. The red dot in Fig.2-1 shows the values of case C, which is on the pareto-front. This means shape C is one of the optimized shapes. In other 3 cases, the similar results were obtained. It was conformed that local WSS and total surface area play a significant role to determine the blood vessel shapes.

Discussion

It is difficult to suppose that blood vessel might have the mechanism sensing its total surface area. Blood vessels are exposed not only to WSS but also to the circumferential stress based on the blood pressure. It is reported that the endothelial cells sense the circumferential stress and the increase of circumferential stress leads to reduction of blood vessel radius. Therefore we confirm the factor for minimization of total surface area of blood tube to respond to the circumferential stress.

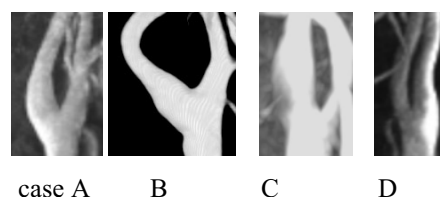


Figure 1: Actual shapes.

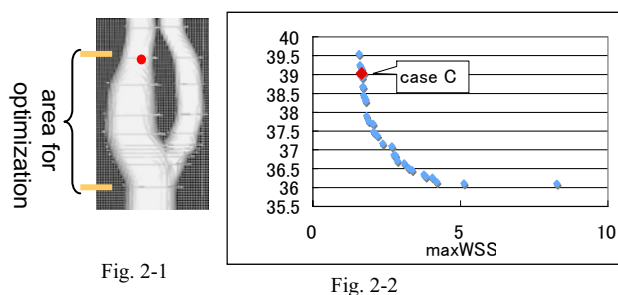


Figure 2: Result of case C.

References

- Deb et al. IEEE Transactions on Evolutionary Computation, 6-2; 182-197, 2002
- Masuda et al. Arteriosclerosis, 9: 812-823, 1989.
- Mecarthur et al. Biochem. Biophys. Res. Commun., 200: 395-400, 1994.
- Noda et al. World Congress on Medical Physics and Biomedical Engineering, 36-40, 2006.

SENSITIVITY OF WALL SHEAR STRESS TO TEMPORAL DISCRETISATION IN CAROTID BIFURCATION MODELS

Diana Massai (1), Raffaele Ponzini (2), Diego Gallo(1), Luca Antiga (3), Franco Maria Montecchi (1), Alberto Redaelli (4), Umberto Morbiducci (1)

1. Politecnico di Torino, Italy; 2. CILEA, Italy; 3. Mario Negri Institute, Italy; 4. Politecnico di Milano, Italy

Introduction

In computational fluid dynamics studies, finding a good compromise between accuracy and computational cost is crucial. In this study we present in silico investigations on two image-based, patient-specific models of carotid bifurcation, for investigating the sensitivity of two wall shear stress (WSS) derived vessel's wall indices (Time Averaged WSS, TAWSS, and Oscillating Shear Index, OSI) with respect to the time step of integration, and adopting two different rheological constitutive models. Our aim was to set the appropriate time step of integration for properly calculate TAWSS and OSI over the simulated cardiac cycle, verifying also whether the rheological properties of blood significantly influence the WSS based descriptors considered.

Methods

Starting from two image-based models of carotid bifurcations [Antiga, 2008], we performed unsteady flow simulations via a finite volume discretisation ($1.4 \cdot 10^6$ cells adopted, a mesh density sensibly greater than in literature). Walls were assumed to be rigid with no-slip conditions imposed. For minimizing the influence of the boundary conditions, straight flow extensions were added to common, internal and external carotid arteries. The sensitivity analysis with respect to the temporal discretisation was performed using time steps (dt) equal to 2, 4, 8, 10 and 20 ms per cardiac cycle $T=1$ s, and three cycles were implemented to damp initial transient. Blood rheology was simulated implementing two fluid constitutive relations: a Newtonian model (N) with constant viscosity equal to 3.3 cP, and the shear-thinning Carreau model (C) [Lee, 2007]. The blood-vessel interaction was evaluated computing TAWSS and OSI:

$$TAWSS = \frac{1}{T} \int_0^T |WSS| dt \quad OSI = 0.5 \left[1 - \frac{\int_0^T WSS dt}{\int_0^T |WSS| dt} \right] \quad (1)$$

The sensitivity analysis was carried out by computing the percentage differences of TAWSS and OSI values with respect to those calculated adopting the reference time step ($dt=2$ ms). For

each temporal discretisation, we evaluated the number of cells presenting percentage errors greater than 0.5%, 1% and 5%, respectively.

Results and Discussion

Considering TAWSS, the two rheological models present similar behaviour, and even using $dt=20$ ms all cells are characterised by percentage errors lower than 5%. Contrarily, we found OSI more sensitive both to rheology and time step of integration (Figure 1).

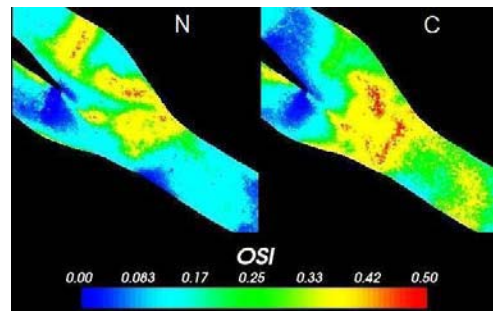


Figure 1: OSI colorimetric map calculated adopting $dt=2$ ms for N and C models.

In detail, for OSI the N model exhibits a greater sensitivity to the time step of integration than model C, as clearly shown in Figure 2.

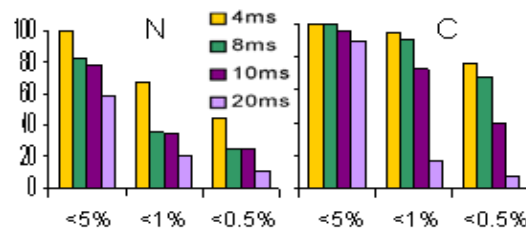


Figure 2: OSI percentage differences with respect to values calculated adopting $dt=2$ ms for N and C models.

Comparing the results obtained by using different time steps, we can conclude that a computational time step of 4 ms could be a good compromise between the computational accuracy and the computational cost both for Newtonian and Carreau rheological blood models.

References

- Antiga et al, MBEC, 46:1097-1112,2008.
- Lee et al, J Biomech Eng, 129:273-278, 2007.

A MULTISCALE MODEL OF CAROTID BIFURCATION HAEMODYNAMICS

Diego Gallo (1), Raffaele Ponzini (2), Filippo Consolo (1), Diana Massai (1), Luca Antiga (3), Franco M. Montecvecchi (1), Alberto Redaelli (4), Umberto Morbiducci (1)

1. Politecnico di Torino, Italy; 2. CILEA, Italy; 3. Mario Negri Institute, Italy; 4. Politecnico di Milano, Italy

Introduction

The initiation and progression of vessel wall pathologies have been linked to disturbances of local haemodynamics. Aiming at accounting for the influence of the global vascular net on the local haemodynamics in a specific vascular district, we coupled an image-based 3D model of carotid bifurcation with a lumped parameters (0D) model functionally mimicking the systemic behaviour at the boundaries of the 3D model. We aim at evaluating the effect of more physiological boundary conditions on wall shear stress (WSS) related vessel wall indexes and on bulk flow topology inside a carotid bifurcation. Two WSS based blood-vessel wall interaction descriptors were initially considered.

Materials and Methods

The finite volume method was used to solve the Navier-Stokes equations in an image-based 3D model of carotid bifurcation [Antiga, 2008]. A segregated solver was employed, the solution was determined with a second-order accuracy. A $9 \cdot 10^5$ cells discretization was used for the geometrical model. Sensitivity analysis was carried out to reach the proper grid refinement. Blood was assumed Newtonian. Unsteady flow conditions have been imposed in terms of inlet velocity profile (Fig. 1) [Marshall, 2004].

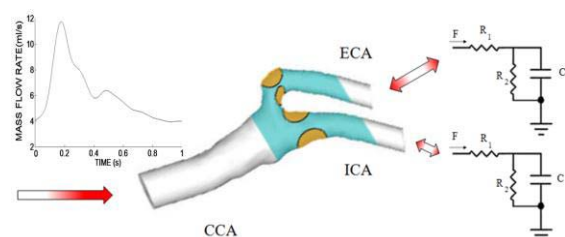


Figure 1: Overall scheme of the simulation set-up: 3D - 0D coupling is shown, together with BCs. Regions in which wall related indexes were calculated are shown.

Walls were assumed to be rigid. Two WSS-related indexes were calculated: TAWSS, defined as the magnitude of the cycle-averaged WSS vector, and OSI, which measures oscillation in WSS. Root-mean-square (RMS) values of TAWSS and OSI

were calculated over the region including the bifurcation, and over four patches (Fig. 1).

The two 0D models are coupled to the outlet sections of external carotid (ECA) and internal carotid (ICA) (Fig. 1) and provide the outlet pressure over the outlet sections of the 3D model, calculating it from the flow boundary conditions data that the 0D model receives from the 3D model. Four different simulations were carried out: the multiscale, and three without 0D network, imposing 50/50, 60/40 and 70/30 flow division ratio between ICA and ECA outlet section.

Results and Discussion

We found that the region characterized by the highest TAWSS is always the ECA internal wall. Low TAWSS were found for the extrados (Fig. 2A). The region characterized by highest oscillating shear stress is the external ICA; lowest OSI values were obtained at the intrados in ICA. (Fig. 2B). The results obtained suggest that the wall indexes are very sensitive to the presence of a coupled lumped model. In particular the OSI seems to be more sensitive than TAWSS.

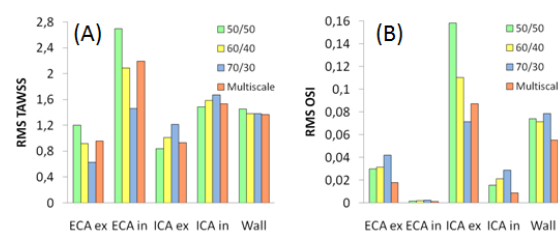


Figure 2: TAWSS (A) and OSI (B) computed RMS values.

With the use of a multiscale approach, it is possible to reproduce the mild physiological shift between systolic peaks of the flow rate waveforms among CCA, ICA and ECA as observed in vivo [Marshall, 2004], which cannot be modelled with the sole 3D CFD model. In the future, we aim at investigating the influence of the systolic shift on local fluid dynamics inside the carotid bifurcation.

References

- Antiga et al, Med Biol Eng Comput, 46:1097-112, 2008.
- Marshall et al, Physiol Meas, 25:691-697, 2004.

PREDICTION OF AEROSOL DEPOSITION WITHIN LUNGS: 3D CFD SIMULATION COUPLED WITH ANALYTICAL MODELLING

Marine Simoes-Pichelin (1), Ira Katz (1), Pierre-Antoine Muller (1), Georges Caillibotte (1)

1. Air Liquide CRCD Research Center, Medical Gases Group, France

Introduction

Aerosol therapy could be improved by targeting the delivery of inhaled drugs to appropriate sites within human lungs [Laube, 2005]. Therefore it is of great importance to clearly understand the factors affecting the behaviour and fate of inhaled particles. Useful tools in this approach are 3D Computational Fluid Dynamics (CFD) simulations and analytical modelling. In this study we used both techniques, in a coupled way, to predict aerosol deposition patterns within human lungs.

Methods

In a first step, medical imaging techniques were used to create a 3D realistic representation of the first generations of the tracheobronchial (TB) tree airways of a healthy human subject. However, due to limitations in imaging techniques, these realistic TB airways only represent the generations 0 through 6 of the lungs, generation 0 being the trachea.

In order to obtain a representation of the complete lungs, an idealized dichotomous symmetric description of the generations 7 to 23 was added to each of the outlet of the realistic TB (see Figure 1).

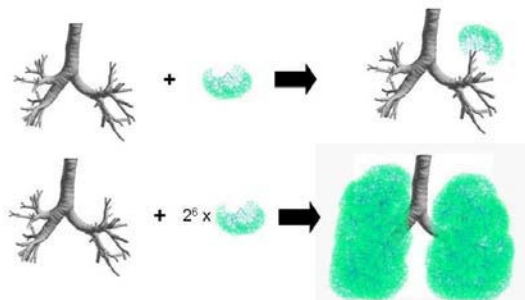


Figure 1: Hybrid representation of human lungs.

The first realistic generations issued from medical imaging techniques is called the Scanned TB (STB) whereas the following idealized generations are called the Analytical TB (ATB) from generations 7 to 16 and the Analytical Pulmonary (APU) region from 17 to 23. The analytical tree (ATB+APU) consists of $2^6=64$ identical trees, connected to each of the 64 outlets of the STB.

We used CFD (Fluent® code) to simulate airflows and particle trajectories and deposition during steady inspiration in the STB. The monodisperse inert particles were injected at the entrance of the trachea with a velocity equal to the air.

Deposition of inhaled aerosol coming into the ATB was calculated using an analytical model based on the three main particle deposition mechanisms (inertial impaction, sedimentation, and diffusion) [Isaacs, 2005]. This model, called Cyberlung®, used information from CFD simulation as input data, such as air flow rates at each outlet of the STB.

Results

3D CFD simulation provides detailed data on particles deposition sites and gives useful information on airflow rates and particle mass flow rates within the airway branches.

The analytical model computes the deposited mass fraction of particles in each generation of each tree. Figure 2 shows the large variability of deposition patterns among the ATB and APU segments for a given generation.

Global results of mass fraction of particles were also obtained in STB, ATB and APU regions. Analysis of particle deposition rates by lobes is also possible.

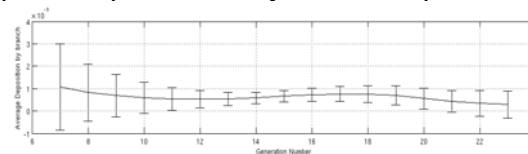


Figure 2: Mass fraction of particles deposited by generation of the analytical tree, average value and variability are represented.

Discussion

Improvement of our method is on-going, especially for simulating the exhalation phase. However, we believe that coupling CFD and analytical modelling is a promising way towards a better understanding of aerosol deposition and patient-specific treatment.

Acknowledgements

The authors gratefully acknowledge Dr A. Makarenko for his skilful assistance.

References

- Isaacs et al, Aerosols Handbook: Measurement, Dosimetry and Health Effects, Chap 6:75-100, 2005.
- Laube et al, Respir Care, 50:1161-1174, 2005.

BONE REMODELLING ON HIP RESURFACING PROSTHESIS WITH DIFFERENT CEMENT MANTLE THICKNESSES

M. A. Pérez (1), C. Desmarais-Trépanier (2), N. Nuño (2), P. A. Vendittoli (3), M. Lavigne (3), J. M. García-Aznar (1), M. Doblaré (1)

1. *Group of Structures and Materials Modelling. Aragón Institute of Engineering Research (I3A), University of Zaragoza, Spain;* 2. *Département de génie de la production automatisée, École de technologie supérieure, Université du Québec, Montréal, Canada ;* 3. *Hôpital Maisonneuve-Rosemont, Montréal, Canada*

Introduction

Metal-on-metal hip resurfacing prostheses were re-introduced and successfully applied in the last 10-15 years. These prostheses have the potential to better restore normal function because of more physiological distribution of the load in the femur. This technique is known to reduce bone loss due to stress shielding behaviour. Multiple factors may affect early and long-term prosthesis performance (femoral neck notching, improper implant position, poor cementing technique, etc.). In fact, the influence of femoral cement mantle thickness on the long-term results is still unknown. Therefore, the main goal of this study was to perform a 3D finite element analysis (FEA) of a resurfaced cemented prosthesis by varying cement mantle thickness to determine the long-term effect on the bone remodelling process.

Methods

Using the software Mimics, the medical images were segmented as a mean to get the personalized geometry of a 48 year-old male femur. Then, after a CAD reconstruction in Catia V5, finite element models were developed using ANSYS WorkBench. Arthroplasty simulation was oriented at 5° valgus with respect to the neutral axis line of the femoral neck [Amstutz et al, 2004]. To investigate the effect of cement mantle thickness, three different configurations were generated: 0.25, 1 and 3 mm maintaining the implant geometry. Bone was assumed anisotropic and heterogeneous with its mechanical properties estimated pointwise from the application of a bone remodelling model [Doblaré and García, 2001]. The stem and cement of the resurfaced femoral implant were considered linear and elastic with Young modulus of 200 GPa and 2.2 GPa, respectively and Poisson's ratio of 0.28 and 0.3, respectively. The tapered stem was modelled as debonded within bone (no friction), whereas the bone-cement and cement-implant interface were assumed to be rigidly bonded. Three loads cases corresponding to walking were applied. The FEA were performed using the commercial software Abaqus.

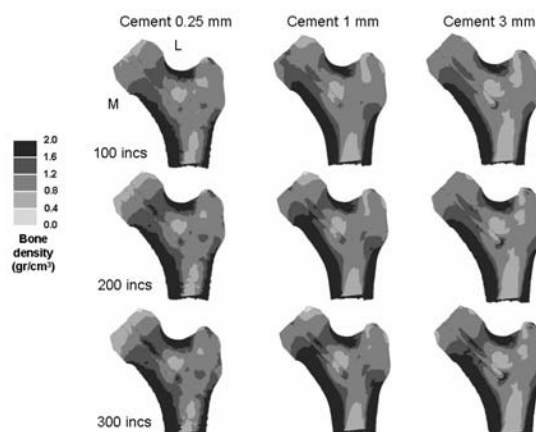


Figure 1: Bone density (gr/cm^3) distribution in the resurfaced femoral head at different time increments (incs) for the three cement mantle thicknesses (mid frontal view, M-medial, L-lateral).

Results

A very thin cement mantle (0.25 mm) increased bone resorption at the superior femoral head, while greater thickness (1 or 3 mm) had a lesser effect (Figure 1). In all cases, bone apposition was predicted around the stem and at the stem tip (Figure 1). Bone formation and resorption were observed clinically, and after performing a comparison, a good agreement with the predictions computed was obtained.

Discussion

Form the results predicted, 1-mm cement mantle thickness may be an appropriate cement configuration, being numerically closer to the clinical configuration [Amstutz et al, 2004]. Therefore, it has been demonstrated how bone remodelling models can be applied to study the long-term performance of resurfacing prostheses. It is a useful tool that may help to design this kind of medical components.

References

- Amstutz et al, *J Bone Joint Surg*, 86-A:1874-1877, 2004.
- Doblaré and García, *J Biomech*, 34:1157-1170, 2001.

LONG-TERM STABILITY ANALYSIS OF AUGMENTED KNEE ARTHROPLASTY USING BONE REMODELLING ALGORITHMS

Brendan Frehill (1), Andrew D. Crocombe (1), Serge Cirovic (1), Yash Agarwal (1)

1. Faculty of Engineering and Physical Sciences, University of Surrey, Guildford, UK

Introduction

Peripheral tibial defects in the proximal tibia are a common occurrence in patients undergoing total knee replacement (TKR) with methods to treat such defects having varying success. Clinical studies have shown that the use of cement to fill tibial defects has the highest rate of failure due to increases in the rate of loosening and fracture [Jeffery et al, 1994].

Bone loss in regions of interest (ROIs) adjacent to augmented features may play a vital role in the incidence of construct failure due to loosening or migration. The objective of this 2D finite element (FE) study was to determine if augmentation procedures have a significant effect on bone remodelling trends in the proximal tibia. Defects of 15° and 30° were examined with wedge, cement and block augments to fill the defects.

Methods

The algorithm implemented in the remodelling analysis was based on a uniform strain criterion initially proposed by Cowin and Hegedus [1976]:

$$\frac{dE}{dt} = \begin{cases} B(\varepsilon - \varepsilon_1)^{C1} & \varepsilon < \varepsilon_1 \\ 0 & \text{if } \varepsilon_1 < \varepsilon < \varepsilon_2 \\ B(\varepsilon - \varepsilon_2)^{C2} & \varepsilon > \varepsilon_2 \end{cases} \quad (1)$$

where E is the elastic modulus, B is the remodelling constant, ε_1 and ε_2 are target strains and C1 and C2 are the non-linear exponents of strain-adaptive remodelling. Maximum and minimum values of E were chosen as 0.01 MPa (total resorbed bone) and 13.5 GPa (cortical bone).

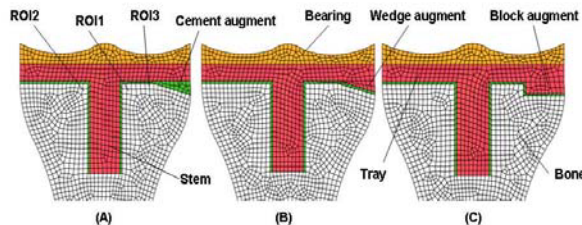


Figure 1: Diagram showing augments (A) Cement (B) Wedge and (C) Block and ROIs examined.

2D static plane strain FE models with appropriate loading and constraints were created of a TKR proximal tibia with augments (Figure 1) with eight-

noded quadratic reduced integration elements. The initial uniform modulus of bone was assumed as 6750 MPa (mid-value of total resorbed and cortical bone). Material properties used in the TKR models are shown in Table 1.

Material	E (GPa)	ν
PMMA	2.15	0.46
Ti4Al6V	110	0.36
UHMWPE	2.3	0.25

Table 1: TKR Materials [Nyman et al, 2004].

Results

The greatest bone loss occurred in the first six months of simulation with bone modulus changes becoming more gradual after this time similar to trends found in clinical studies [Li and Nilsson, 2000]. In all ROIs examined it was found that bone experienced the greatest resorption when repaired with a metal block augment. Greater bone loss was predicted in all ROIs when a 30° augment device was used (Figure 2).

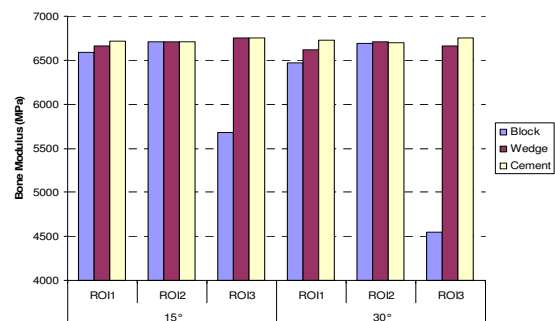


Figure 2: Predicted modulus values for 15° and 30° after 1000 days.

Discussion

The bone remodelling algorithm predicts that the higher rate of failure of cement wedges to fill defects is not due to the degree of bone resorption. Stress concentrations at the margin of the defect are suggested to be the most likely contributing factor to failure. 3D analysis in future work will be necessary to verify these predictions.

References

- Cowin and Hegedus, J Elasticity, 6:313-326, 1976.
- Jeffery et al, J Arthroplasty, 9:381-387, 1994.
- Li and Nilsson, J Ortho Res, 18:40-47, 2000.
- Nyman et al, J Ortho Res, 22:51-57, 2004.

MONITORING FRACTURE HEALING IN SHEEP: AN *IN VIVO* STUDY

J. Grasa (1), M. J. Gómez-Benito (1), D. Asiaín (2), J. Gómez-Arrúe (3), L. A. González-Torres (1), J. M. García-Aznar (1), F. Quero (2), M. Doblaré (1)

1. Grupo de Mecánica Estructural y Modelado de Materiales (GEMM), Instituto de Investigación en Ingeniería de Aragón (I3A), Zaragoza, Spain; 2. Escuela Universitaria Politécnica, La Almunia de Doña Godina, Zaragoza, Spain; 3. Unidad de Cirugía Mínimamente Invasiva Guiada por Imagen, Hospital Clínico Universitario Lozano Blesa, Zaragoza, Spain.

Introduction

Fracture healing is a very complex process (Einhorn, 1998), widely studied in literature, both in experimental (Wallace et al., 1994; Claes et al., 2002) and computational studies (Lacroix and Prendergast, 2002; Gómez-Benito et al., 2005). Despite the effort done to understand this process, many issues have not been completely understood yet, for example the effect of cyclical stimulation in the fracture healing process and the way to monitor fractures in humans.

This work presents an experimental study on fracture healing in which the load in the external fixator is monitored throughout the healing process in a sheep experiment.

Materials and Methods

A transverse osteotomy was performed in the posterior tibias of six adult sheep (mean age 3 ± 0.5 years and weight 63 ± 5 kg). The fractures were stabilized by unilateral external fixators (Fig. 1).



Fig 1: One of the sheep, with the external fixator (detail at right) and a backpack carrying the telemetric system.

The external fixators are instrumented by means of a set of strain gauges. Strains in the external surface of the fixator are monitored during the healing process. A wireless, remote monitoring of the system was performed thanks to a special designed external telemetric device.

The strain gauges are arranged in two different half-bridge Wheatstone configurations, which allow an easy post-processing of the signal. Thus, the axial and bending loads could be measured in the plane of the fixations pins.

Results

The load through the fixator during the healing process was calculated during the gait cycle. Full weight bearing of the injured leg was observed since the very first days. The tendency of the load in the fixator was quite similar in all operated tibias (see Fig. 2).

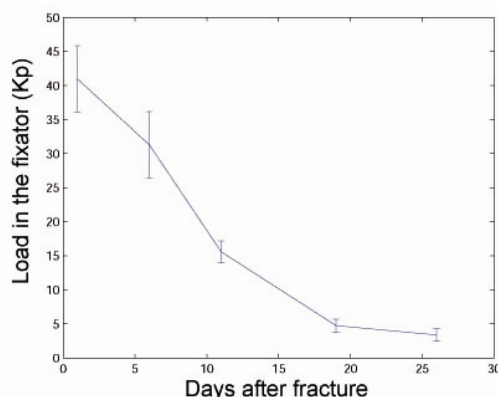


Figure 2: Evolution of the load amplitude in the fixator throughout the healing process.

Discussion

This work presents a successful, non-invasive system to monitor and record fracture healing in real time. Although this system has only been tested in an animal model, it could be used to monitor fracture healing in humans. This would allow a better assessment of the healing process.

Acknowledgements

This research was supported by the Spanish Ministry of Science and Technology (grant DPI2006-09692) and the Instituto de Salud Carlos III (CIBER initiative).

References

- Claes et al., J Orthop Res, 20:1099-1105, 2002
- Einhorn, Clin Orthop Rel Res, 355S:7-21, 1998
- Gómez-Benito et al., J Theor Biol, 235:105-119, 2005
- Lacroix and Prendergast, J Biomech, 35:1163-1171, 2002
- Wallace et al., Clin Orthop Rel Res, 301:281-290, 1994

MODELLING THE INFLUENCE OF TRANSMURAL CHANGES IN THE MECHANICAL ENVIRONMENT TO GROWTH

Holger Schmid (1), Paul Watton (2), Mikhail Itskov (1), Peter Hunter (3)

1. Department of Continuum Mechanics, RWTH Aachen University, Germany

2 Institute of Biomedical Engineering, University of Oxford, United Kingdom

3 Auckland Bioengineering Institute, University of Auckland, New Zealand

Introduction

Aneurysms are contingently pathological dilations of the arterial wall. Their rupture leads to subarachnoid haemorrhage which leads to severe impediments and in many cases death. It is therefore essential to determine the biochemical-mechanical interplay in the arterial wall to identify more precise rupture criteria.

Aneurysm formation itself is thought to be triggered by abnormal fluid mechanical stimuli at the arterial wall. Signalling cascades are activated and cause imbalances in the protein expression pathways. Thus the load bearing constituents of the arterial wall are being adapted. To understand the overall mechanism of aneurysm formation it is essential to develop 3-D finite element models that can incorporate the transmurally heterogeneous material properties [Kim, 2009] as well as the spatially dependent signalling cascades.

Methods

Previous models studied the formation of aneurysms with 2-D models by introducing various growth laws for the adaptive mechanism for e.g. the recruitment stretch of collagen [Watton, 2007], direction of collagen fibres, etc. Yet these models could not capture the transmural changes of the stress and strain state - in the finite element environment to allow for non-axisymmetric configurations - which will trigger the signal transduction pathways.

We thus developed a fully tricubic-Hermite element mesh of an artery to the study of long term evolution of the shape of the arterial wall into aneurysms. The model includes fibre families, heterogeneous material parameters and allows for remodelling of the recruitment stretch of collagen fibres as well as their local concentration to adapt to homeostatic values. The physiological values are taken from [Watton, 2007].

Results

The arterial segment was loaded to normotensive conditions with an axial prestretch. Subsequently the internal pressure was increased to hypertensive

values. Additionally a degradation of elastin was prescribed due to hypertension and the collagen was allowed to remodel. The results for a fusiform aneurysm can be seen in Figure 1.

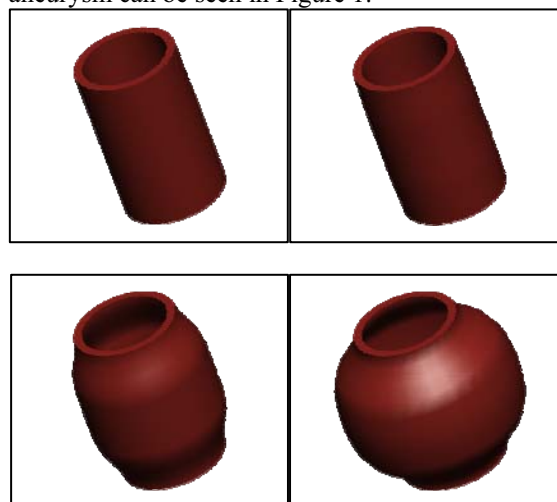


Figure 1: The evolution of a fusiform aneurysm. Top left: The cylindrical section in homeostasis. Top right: The beginning of hypertension, i.e. a step change in the internal pressure leads to an increased diameter. Bottom left: The cylindrical section inflates within a region in which elastin degrades and collagen adapts. Bottom right: The state of the aneurysm shortly before it becomes mechanically unstable.

Conclusion

We successfully implemented a fully 3-D FE model for the growth of a fusiform aneurysms.

This is a critical step towards a full framework that also includes fluid-structure interaction as well as the triggering of signalling pathways by complex flow patterns [Schmid, 2008].

References

- Kim, Y.S. et al., Journal of Biomechanical Engineering, 131, 1, 2009
- Schmid, H. et al., IFMBE Proceedings, J. Vander Sloten, P. Verdonck, M. Nyssen, J. Hauelsen, 22, 1894, 2008.
- Watton, P.N. et al., Biomechanics and Modelling in Mechanobiology, 3, 98, 2007.

WHAT CAUSES PARADOXICAL ANTERIOR TRANSLATION IN TOTAL KNEE REPLACEMENTS?

John L. Williams (1), Said T. Gomaa (2)

1. InMotion Musculoskeletal Institute & University of Memphis, Memphis, USA; 2. DePuy, a Johnson & Johnson Company, Warsaw, USA

Introduction

Paradoxical anterior translation has been reported to occur to varying degrees in total knee replacement devices. Although it has been observed in most fluoroscopic studies of posterior cruciate retaining devices, is not clear what design attributes might be contributing to this undesirable kinematic outcome. We compared simulations of a double leg squat of several total knee implant designs using measurements of the tibio-femoral ‘contact positions’ similar to those published in fluoroscopic studies, in order to examine the nature and extent of paradoxical anterior motion in relation to the sagittal curvature of the femoral components.

Materials and Methods

A virtual knee simulator (LifeMOD/KneeSIM, LifeModeler, Inc., San Clemente, CA), based on multibody dynamics, was used to simulate a double-leg deep knee bend. The model included tibio-femoral and patello-femoral contact, passive soft tissue (MCL, LCL and PCL, as well as the capsular tissues), and active muscle elements (quadriceps and hamstrings). Parasolid models of fixed-bearing cruciate-retaining total knee implant systems (Zimmer NexGen®, DePuy PFC® Sigma™ Curved, Biomet Vanguard™) were imported into the model. The systems were subjected to one 9-second cycle of knee bending up to 120 degrees of flexion (0 – 120 – 0 degrees). The anterior-posterior (AP) positions of the lowest points on the femoral lateral and medial condyles closest to the tibial tray (the same measure used in fluoroscopy studies) were recorded relative to the dwell points of the inserts.

Implant System	Medial	Lateral
PFC® Sigma™	35	35
Vanguard™	20	20
NexGen®	37	16

Table 1. Flexion angle (deg.) at which the para-sagittal radius of the femoral component decreased.

Results

The onset of paradoxical anterior motion occurred at angles that corresponded approximately with the flexion angles at which the femoral para-sagittal radius abruptly decreased (Table 1, Fig. 1).

Discussion

Despite differences in both the femoral and the tibial component para-sagittal plane curvatures between implants, the onset of paradoxical anterior motion was approximately related to the flexion angle at which the para-sagittal femoral radius of curvature at the contact points decreased abruptly relative to the radius at the contact points in extension. These findings suggest the principal cause of paradoxical anterior translation is a 30–50% discrete decrease in the femoral condyle para-sagittal radius at flexion angles between 20–40 deg.

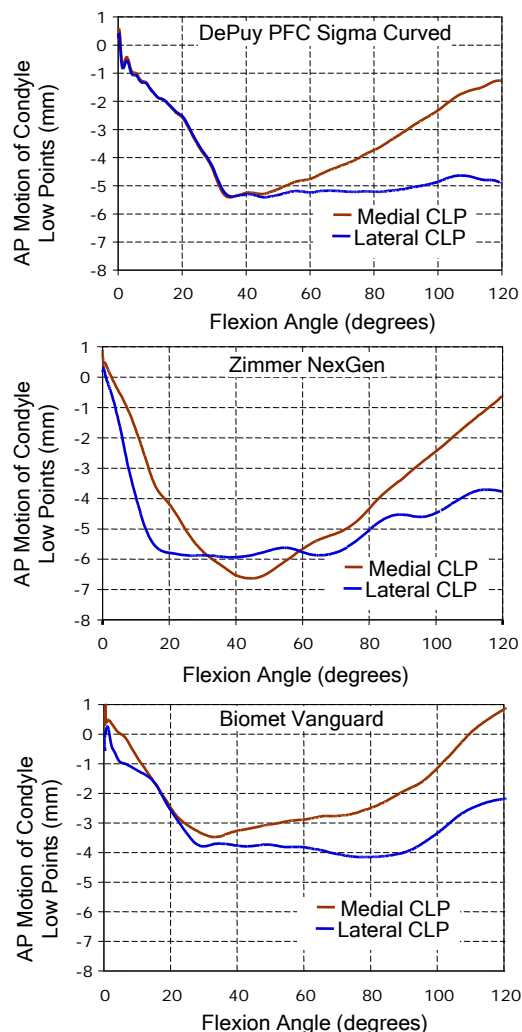


Fig. 1. Antero-posterior (+ANT) translation (mm) of the lowest condyle points (CLP).

THE INTERVAL AND FUZZY ANALYSIS OF THIGH BONE WITH ARTIFICIAL IMPLANT

Antoni John¹, Piotr Orantek¹ and Wojciech Świąszkowski²

1. Silesian University of Technology,
Department for Strength of Materials and Computational Mechanics, Poland

2. Warsaw University of Technology,
Faculty of Materials Science and Engineering, Poland

Introduction

Bioengineering concerns many significant problems applied to the human body. The thigh bone is one of the most important supporting elements in human pelvic joints but it is exposed to the injuries. Very often before and after surgical intervention the expertises about the stress, strain and displacement distributions in the thigh bone are needed. For the safety of the patient there are only two possibilities available to derive mentioned values: model testing and numerical calculations. The numerical model should be prepared before numerical calculations [John, 2001]. Numerical calculations require the characteristics of the material properties and the material parameters from the beginning. Usually the literature is the source of the material parameters, but sometimes this data is not suitable for the implementation. This is a reason for the experimental investigations to identify these parameters [Cowin, 2001]. It is well known that material properties of the living body depend on many factors: age, health, gender, environment and many others changing in time. As we are interested in results of analysis not only for a one patient but for a group of patients, we should assume an interval value of material parameters. In this paper the test of the interval and fuzzy analysis of the thigh bone is presented. The interval and fuzzy analysis concerns material properties. The finite elements method is applied [Zienkiewicz, 2000].

The uncertain analysis of the bone

The human thigh bone is restrained (Fig.1,2) and loaded on contact surface with pelvic bone. It is loaded with force F acting on artificial implant. Two cases of the linear elastic analysis were carried out. In the first case the force is assumed in one point, in the second case the force is considered as the continuous loading.

In the both cases the material parameters for each finite element are identified on basis of the CT system.

Additionally in the both cases the material parameters are modeled as the interval and fuzzy parameters. It is dependent of the health details of a group of patients. This approach allows to analysis health details of a group of patients.

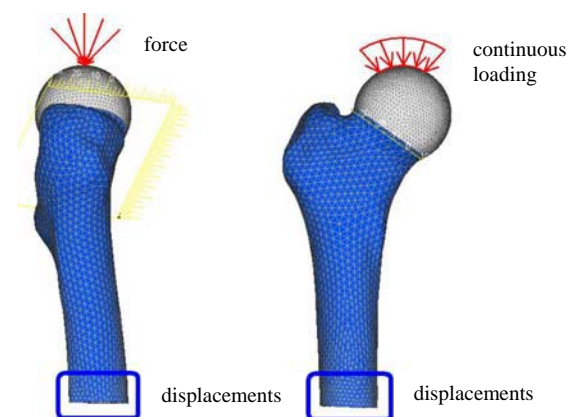


Figure 1: The model of bone with the boundary conditions.

Discussion

The paper is devoted to the analysis of the thigh bone with new type of artificial implant. Between bone and implant the layer of the cement is introduced. Two kinds of loading are considered.

The interval and fuzzy analysis allows to considere the group of patiences. The parameters of the bone depend of the many factors: age, health, gender, environment and many others changing in time, therefore can be modelled as the interval and fuzzy numbers. The interval and fuzzy finite element method are used.

Acknowledgements

The research is partially financed from the Polish science budget resources as a research project no. N51804732/3670.

References

- Cowin S.C. (Ed.), Bone mechanics handbook. CRC Press, 2001.
- John A., Numerical analysis of solid and shell models of human pelvic bone. Lecture Notes in Computer Science 1988, Eds.: L. Vulkov, J. Waśniewski, P. Yalamov, Numerical Analysis and Its Applications, Springer-Verlag, Berlin Heidelberg, pp. 764-771, 2001.
- Moore R.E. Interval Analysis, Prentice-Hall, EngleWood Cliffs, N.J., 1966.
- Zienkiewicz, O.C. and Taylor, R.L., The Finite Element Method, Vol. 1: The Basis, fifth ed., Butterworth-Heinemann, Oxford, 2000.

P-FE INVESTIGATION ON THE INFLUENCE OF ISOTROPIC OR ANISOTROPIC MATERIAL MODELS ON THE MECHANICAL RESPONSE OF THE PROXIMAL FEMUR

Nir Trabelsi and Zohar Yosibash

Dept. of Mechanical Engineering, Ben-Gurion Univ., Beer-Sheva 84105, Israel

Introduction

The quality and reliability of patient specific finite element (FE) analyses of the human femur depends mainly upon three modelling topics. Accurate geometrical description, the applied boundary conditions and the proper description of the material properties used in the model. This study presents a comparison of isotropic and orthotropic material models used for patient-specific FE analyses of the proximal femur based on computer tomography (CT) data. Novel subject-specific high-order FE models of the human femur were generated with two different methods for material properties determination: micromechanics (used to determine the orthotropic material constants) and empirically based, both being determined from CT scans. Two non-invasive and automatic methods to determine the anisotropic material principle directions were examined: (a) Based on structural consideration, (b) According to the stress and strain magnitudes as well as their principal directions. FE results were validated through displacements and strain measurements on two fresh frozen human femurs. The p-FE models with the orthotropic micromechanics-based material properties yield results which closely match the experimental observations and are in accordance with the empirically based FE models.

Methods

Two fresh-frozen femurs were defrosted, CT-scanned, and thereafter exposed to in vitro experiments while displacements, loads, and strains were measured. Structural p-FE models mimicking the experiments were created from the CT-scans (see [Yosibash 2007] for details). Four different types of material properties were assigned to the p-FE model (a) Empirically based isotropic inhomogeneous Young modulus [Keyak 2003] with a constant Poisson's ratio of 0.3: $E_{Cort} = 10200\rho_{ash}^{2.01}$, $E_{Trab} = 5307\rho_{ash}^{2.01} + 469$ [MPa] (b-d) Micromechanically based inhomogeneous material properties: isotropic, orthotropic and orthotropic with regards to the material directions (details are given in [Yosibash 2009]).

The methods for material directions determination were guided by the following concepts: (1) the principal directions follow the bone geometry, (2)

Wolff's law and (3) trabeculae orientation depend on the loading applied on it.

Results

To verify the accuracy of ours CT-based p-FE models, a comparison between the experimental observations (strains and displacements) and the FE results was conducted. Linear regression demonstrates the general assessment of the analysis quality for four types of material models are presented in Figure 1.

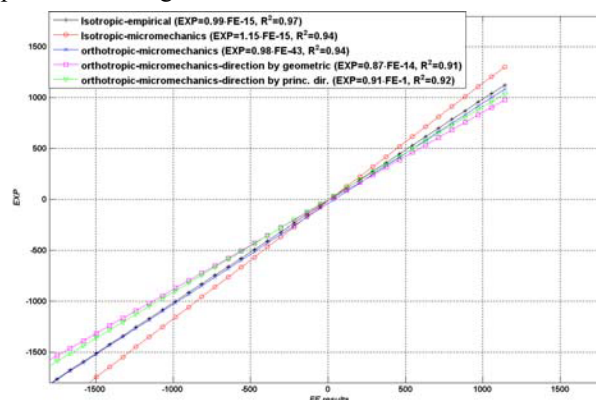


Figure 1: FE results vs experimental observations. Isotropic and anisotropic properties assigned by empirically and micromechanics-based

Discussion

Anisotropic material properties based on micromechanics with regards to the material directions was examine in this study. The isotropic FE model with micromechanics-based material properties provide results with poorer agreement compared to the empirically based case (however the difference was small). The orthotropic model improved the analysis result (making the model less stiff) with better correlation to experimental observations. The orthotropic models with regards to the material direction using local coordinate systems result of inferior quality compared to the one that uses a global system. This study demonstrates the ability to use anisotropic material properties by micromechanics-based model from CT scans in conjunction with p-FEs.

References

- Yosibash, Z et al. J. Biomech. 40:3688–3699, 2007.
- Keyak, J.H. et al, J. Med. Eng. Phys 25:781–787N, 2003.
- Yosibash, Z. et al, Int. J. Multiscale Comp. Eng.6:483-498, 2009.

PROGRESSIVE COARSENING & REFINING TECHNIQUES FOR INTEGRATIVE BIOMEDICAL COMPUTING

Chandrajit L. Bajaj (1), Antonio DiCarlo (2), Alberto Paoluzzi (2)

1. University of Texas at Austin, USA; 2. Università Roma Tre, Italy

Introduction

Biomedical images are becoming more and more important. Such (mostly 3D) images originate from a growing range of technologies available to the clinician. The need for integration and accessibility of images for diagnosis and care is trending upward as high bandwidth systems for medical imaging applications are becoming widely installed in hospitals. Moreover, moving from film to digital format, healthcare providers are facing an explosion of imaging content not only from radiology, but also from cardiology, pathology, operating rooms, etcetera. Data-intensive clinical applications would largely benefit from fast, secure and ubiquitous accessibility provided by specialized data grids. In addition, advanced and composable 3D processing services should be supplied, including image enhancement, fast volume visualization, automatic organ and feature extraction and indexing, meta-data-based search, progressive and adaptive mesh generation for predictive simulations.

Methods

Biomedical computing can greatly benefit from a progressive and adaptive approach to modelling, combined with novel adaptive methods for multiphysics and multiscale simulation, working on parallel and distributed supercomputers. Both symbolic and hierarchical characterizations of the various components should be allowed for, as well as shape reconstruction from high-resolution imaging techniques. Our proposal [Bajaj et al, 2008a] is based on a novel algebraic topological approach to field modelling [DiCarlo et al, 2007; DiCarlo et al, 2008]. We use a twin representation of geometry and topology, combining binary space partition trees, which store no topological information, with a complete representation of the stepwise-generated mesh topology [Bajaj et al, 1996] associated with the Hasse diagram of the polytopal complex. Our design choice allows the model generation to be split into fragments to be distributed to computational nodes for progressive detailing [Paoluzzi et al, 2005, Scorzelli et al, 2008].

Managing finer and finer details is often important. However, it is also essential to be able to coarse-grain complicated shapes and patterns, in order to identify their salient features. We seek to identify these features using a topological method based on the Morse theory [Goswami et al, 2006].

Results



Figure 1: Spatially realistic finite-element reconstruction of human heart from patient-specific imaging data [Bajaj et al, 2008].

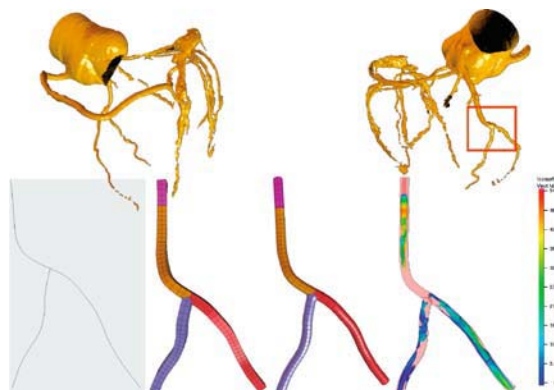


Figure 2: (top) Coronary arteries; (bottom, from left to right) 1D skeleton of a bifurcation district, control mesh, solid NURBS, and simulation results.

Discussion

An up-to-date approach to integrative biomedical computing has to embrace both data-grid techniques and grid-enabled computational farms providing first-class imaging services. We aim to add value to medical images, providing full support of 3D enhancement, segmentation, visualization and on-request extraction of computational models for, say, simulation of surgery operations or drug delivery systems.

References

- Bajaj et al, Proc SCG '96, 88–97, 1996.
- Bajaj et al, Proc ACM SPM 2008, 193–202, 2008.
- Bajaj et al, Phil Trans R Soc A, 366:3045–3065, 2008a.
- DiCarlo et al, Proc ACM SPM 2007, 73–84, 2007.
- DiCarlo et al, arXiv:0812.3249v1 [cs.CG], 2008.
- Goswami et al, Proc ACM SPM 2006, 27–37, 2006.
- Paoluzzi et al, Proc ACM SPM 2005, 203–212, 2005.
- Scorzelli et al, Int J Comput Geom Appl, 18:441–467, 2008.

PREDICTION OF PLAQUE DEVELOPMENT IN CORONARY ARTERIES USING COUPLING FE AND DPD METHOD

Nenad Filipovic (1-2), Milos Kojic (2), Vasilis Tsakanakis (3), Dimitris Fotiadis (3)

1. University of Kragujevac, Serbia; 2. Harvard University, USA; 3. University of Ioannina, Greece

Introduction

Coronary artery disease are caused by plaque rupture and, consequently, by an occlusion of the lumen by coronary thrombi. A major role in process of thrombosis is played by platelet activation and aggregation [Caro, 1971].

The purpose of this study is to simulate process of plaque formation in coronary arteries by implemented multiscale finite element calculation with the Dissipative Particle Dynamics (DPD) method. The coronary artery geometries are segmented from computed tomography angiography images of a few patients to generate an authentic 3-dimensional finite element mesh. A global hemodynamics analysis is determined with conventional finite element calculation, and DPD method is applied on the small zones where initial thrombosis is already started.

In a simplified model of these zones, where the presence of RBCs is neglected, blood is discretized into mesoscale particles representing plasma and platelets. Each platelet is modeled by one DPD particle. Besides the interaction repulsive, viscous and random forces among DPD particles, the attractive forces among activated platelets and with the wall, are included.

Methods

A complex 3D geometric model of the coronary artery is created from 1 mm DICOM images of a CT angiography (CTA) study acquired with a multi-detector-row CT scanner.

The three-dimensional flow of a viscous incompressible fluid is governed by the Navier-Stokes equations and continuity equation.

The basic equations of the DPD model of a fluid for a particle 'i' can be written as

$$m_i \dot{\mathbf{v}}_i = \sum_j (\mathbf{f}_{ij}^C + \mathbf{f}_{ij}^D + \mathbf{f}_{ij}^R + \mathbf{f}_{ij}^A) + \mathbf{f}_i^{ext} \quad (1)$$

where m_i is the particle mass; $\dot{\mathbf{v}}_i$ is particle acceleration as the time derivative of velocity; \mathbf{f}_{ij}^C , \mathbf{f}_{ij}^D , \mathbf{f}_{ij}^R and \mathbf{f}_{ij}^A are the conservative (repulsive), dissipative, random, and attractive interaction forces (see Fig.1).

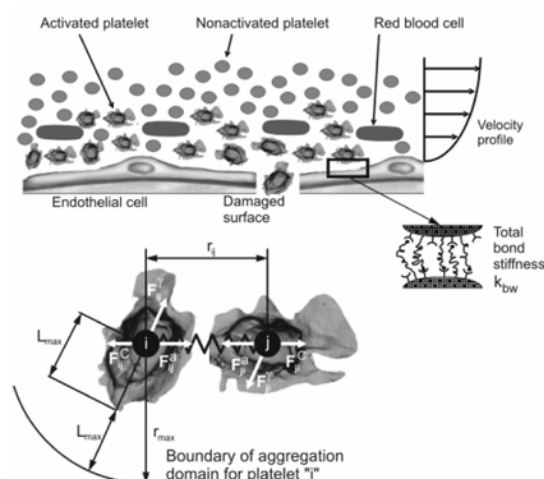


Figure 1: Schematics of platelet aggregation and adhesion. Activated platelets in the vicinity of an injured wall epithelium and binding of platelets at the walls using springs. Interaction forces for two aggregated platelets [Filipovic, 2008], [Kojic, 2008]. The domain of the interaction between platelets is denoted by r_{max} .

Results and Conclusions

The flow patterns show that washout effects are dominant even on the very complex geometry. A small vortices has been observed at a few sites indicated the possible zones of arteriosclerosis developing. The DPD method is implemented on these zones with the assumption about the wall attractive force, and activated platelets in blood. A progression of plaque development is simulated and follow up clinical study are necessary to validate this simulation methodology.

Acknowledgements

This work is partly supported by EU project FP7-224297 and Ministry of Science in Serbia with projects O1144028, TR12007.

References

- Caro, C.G. et al, Proc. R. Soc. London, Ser. B 177: 109–159, 1971.
- Filipovic, N. et al, Microvascular Research, 75: 279-284, 2008.
- Kojic, M. et al, J. Wiley & Sons, 2008.

EFFICIENT VOLUME PRESERVATION FOR A MODIFIED MASS-SPRING SYSTEM IN MYOCARDIUM MECHANICAL MODELLING

Oussama Jarrousse (1), Thomas Fritz (1), Olaf Dössel(1)

1. Institute of Biomedical Engineering, Universität Karlsruhe, Germany

Introduction

In a previous work a modified mass-spring system for simulating the passive and active mechanical properties of the myocardial tissue was presented [Jarrousse, 2008].

The strain-stress relations representing the passive mechanical properties of the myocardial tissue were approximated using several cubic functions for the fiber, sheet and sheet-normal directions. The functions' parameters were obtained by fitting the functions to strain-stress curves of energy density function proposed by Hunter *et al.* [Hunter 1997]. Using the methods of continuum mechanics, Fritz *et al.* showed how to directly calculate forces in a mass-spring system derived from an energy density function [Fritz, 2008].

In this work both concepts presented in the mentioned papers are combined to simulate the passive properties of myocardial tissue using a mass-spring system that eliminates the need of parameterization, and provides the system with higher accuracy.

A major drawback for mass-spring systems is that volume conservation is not accomplished easily. This makes mass-spring systems unfavourable for physical simulation of biological tissues. Retaining a constant volume under deformation is an essential property of the myocardium. And therefore using the well-established FEM to solve the continuum mechanics equations of non-linear elasticity, despite its high computational coasts, is preferable.

Previously a soft constraint approach proposed by [Bourguignon 2000] was used, but the method did not return convincing results.

Again, a method borrowed from the books of continuum mechanics, allows the relative change of volume to remain under 1% in our mass-spring simulations.

Methods

We refer to the energy density function proposed by Hunter *et al.* with the symbol ' W '.

Equation (1) shows an additional term we used to introduce incompressibility: this term is the volume pressure work.

$$W_v = W + p(\det(\mathbf{F}) - 1)^2 \quad (1)$$

' W_v ' is the energy density function from which the system's passive forces are derived. ' p ' is a parameter, \mathbf{F} is the deformation Tensor. The term $(\det(\mathbf{F}) - 1)$ represent the deviation from a constant volume. It has the value zero when the volume is unchanged in comparison with the volume at time $t=0$. If the volume changes, work is added to the energy density function, what will eventually generate penalty forces that try to keep the change in volume around zero.

The contraction of a truncated ellipsoid with myocardial tissue properties was simulated to validate the volume preservation method. Different values of the constant p were compared.

Results

The relative volume change against time is determined. The contracting force was increased linearly with time. The simulations showed that $p=10^6$ is a suitable value. Higher values are likely to drive the system to instability therefore they are not preferable. The results are displayed in Figure 1 and Table 1.

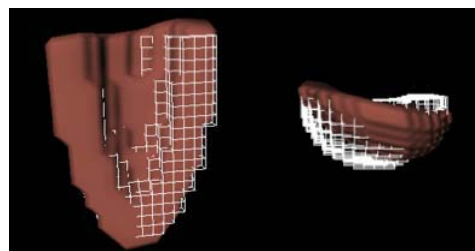


Figure 1: Truncated ellipsoid with realistic fiber twist, preserving volume under contraction.

P	$(\Delta V/V_0)_{max}$
10^2	11.30%
10^4	0.11%
10^6	0.0011%

Table 1: The maximal relative change of volume of the contracting model for different values of ' p '.

References

- Bourguignon D. et al, Comp. Sim. & Ani.:113-123, 2000.
- Fritz T. et al, IFMBE, 22: 2003-2006, 2008.
- Hunter P. et al, Comp. Bio. of the Heart: 345-408,1997
- Jarrousse O. et al, IFMBE, 22: 1943-1946, 2008

A COMPUTATIONAL STUDY OF THE MECHANICAL BEHAVIOUR OF DISCRETE TISSUE MODELS

Pras Pathmanathan (1), S. Jonathan Chapman (2)

1. University of Oxford Computing Laboratory, UK; 2. University of Oxford Mathematical Institute, UK

Introduction

So-called 'cell-centre' discrete models of tissue, such as [Meineke, 2001], are regularly used to investigate tissue function. These models often have two main mechanical components: (i) a definition of *cell connectivity*; and (ii) a *cell-cell interaction law*, a force law describing how two connected cells interact. Typical models of cell connectivity are a spheres-based approach (e.g. [Drasdo, 2001]) and a triangulation-based approach (e.g. [Meineke, 2001]), and there is a very large range of interaction law that have been proposed in the literature. In this work we study the mechanical behaviour of discrete tissue models by performing a series of computational experiments, where we reproduce standard laboratory compression, tension and shear experiments.

Methods

The compression experiment is as follows: we start with 2D monolayer model of a discrete tissue of 20 by 20 cells. We virtually compress the tissue between two 'plates', by displacing the top row of cells a small amount before allowing the tissue to deform to equilibrium whilst constrained between the two plates. We do however allow cells to slip in the compression experiment. Once equilibrium has been reached, we measure the total force on the top surface, and repeat the process. The tension and shear experiments are defined similarly.

Results

It was found that discrete tissues modelled in this way exhibit elastic-plastic behaviour, as shown in Figure 1. Initially, the tissue behaves near-linearly elastically. However, as the strains become large enough, the cells form new connections and can then deform plastically (i.e. irreversibly) and reduce the stress. It was also found that: in tension, the tissue behaves as a linear elastic solid until it tears; the triangulation-based definition of connectivity can be considered superior; and that the large-deformation form of the cell-cell interaction law has little bearing on the gross material behaviour of

the tissue. Also, certain parameters which have a large effect on the material behaviour were identified.

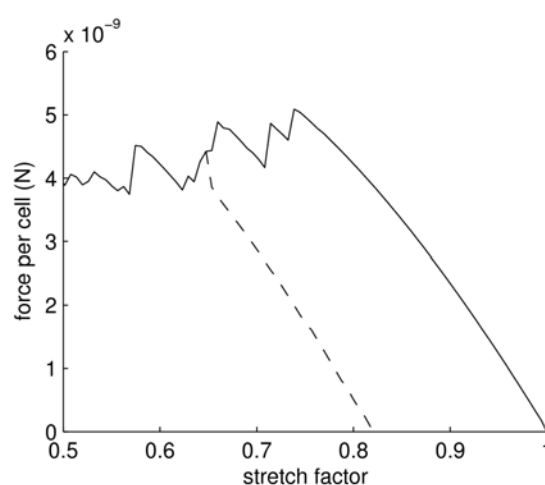


Figure 1: Force per cell (effectively stress) versus stretch factor in a compression experiment. As the stretch factor decreases from 1, the stress (solid line) increases until a plastic phase is reached, where the stress remains approximately constant. If the stretch factor is then increased (dotted line), the material returns to a linear elastic solid.

Discussion

We have performed a computational study of discrete tissue models and identified general elastic-plastic material behaviour, and compared some of the various types of model that have been used in the literature. This work is a first step towards calibrating models using experimental results on tissue material behaviour.

Acknowledgements

PP is pleased to acknowledge the support of the EPSRC through grant EP/D048400/1, *New frontiers in the mathematics of solids*.

References

- Drado et al, *Nonlinear Analysis*, 47(1):245-256, 2001.
- Meineke et al, *Cell Proliferation*, 34(4):253-266, 2001.

A MICROMECHANICAL MODEL TO PREDICT DAMAGE IN SOFT BIOLOGICAL TISSUES. APPLICATION TO ARTERIAL MODELLING.

V. Alastrué, E. Peña, M. A. Martínez and M. Doblaré

*Group of Structural Mechanics and Materials modelling.
Aragón Institute of Engineering Research. University of Zaragoza.
CIBER-BBN. Centro de Investigación Biomédica en Red en Bioingeniería, Biomateriales y Nanomedicina*

Introduction

The mechanical response of biological materials is determined by its micro-structural composition. Vascular tissue is composite-type material made of a wide variety of materials. Among other non-mechanically relevant ones, the most important components are elastin and collagen fibres, which are embedded in a ground substance with high water content [Fung, 1990]. The contribution to the overall mechanical response of the micro-fibres is crucial, since they provide most of the mechanical resistance exhibited by these tissues. Thus, the incorporation of the mechanical response of fibres at the micro-structural level is of vital importance in order to mimic the mechanical response of the vascular tissue [Alastrué et al., 2009].

The role of the micro-constituents is also of major importance in the modelling of inelastic phenomena such as tissue damage, which appear when some non-physiological load, or rather overload, is applied on the tissue. Then, the micro-fibres are deformed or broken, which is appreciated at the macro-structural level as a drop in the macroscopic stress-stretch curve. Hence, the incorporation to models of damage phenomena at the micro-structural level is of crucial importance to develop constitutive laws that accurately reproduce the experimental curves.

Methods

Within the framework of hyperelasticity, the vascular tissue is modelled as an anisotropic material. In order to account for incompressibility, an additive decomposition into volumetric and isochoric contributions is performed. Likewise, a further decomposition of the latter into isotropic and anisotropic contributions is applied, so that the strain energy density function may be written

$$\Psi = \Psi_{\text{vol}} + \Psi_{\text{iso}} + \Psi_{\text{ani}}. \quad (1)$$

The volumetric term is assumed to be a function of the local volume ratio $J = \det(\mathbf{F})$, whereas simple neo-Hookean term is used to model the isochoric isotropic contribution [Holzapfel et al., 2000]. Concerning the anisotropic contribution, a micro-

structurally-based approach is adopted. Thereby, Ψ_{ani} reads

$$\Psi_{\text{ani}} = \int_{U^2} n \rho \varphi dA \quad (2)$$

where U^2 represents the unit sphere, n the network chain density, ρ an orientation density function weight the contribution of micro-fibres in all directions of space [Gasser et al., 2006] and dA a differential surface element. Likewise, φ represents the mechanical response associated to the micro-constituents.

Damage is incorporated in the formulation by means of a scalar parameter, namely D , weighting the contribution of the intact fibre, i.e.

$$\varphi = [1-D] \varphi_0 \quad (3)$$

with $0 \leq D \leq 1$ [Simo, 1987]. By means of this parameter, total damage is reached when $D=1$, which means that the micro-fibre is broken, whereas $D=0$ means no damage.

This model was numerically implemented in order to check its suitability for the modelling of damage in arteries under different deformation cases. In the first place, a simple shear example was computed in order to check the validity of the proposed approach to an homogeneous deformation example. Secondly, a simplified cylindrical geometry with human coronary artery dimensions was simulated. Special emphasis was put in the computational efficiency of the implemented algorithms [Alastrué et al., 2009b].

Acknowledgements

Financial support from the Spanish Ministry of Education and Science through project DPI 2007-63254 is gratefully acknowledged.

References

- Alastrué et al., J Mech Phys Solid, 57:178-203, 2009
- Alastrué et al., Int J Numer Meth Eng, In press, 2009b
- Fung, Biomechanics: *Mechanical Properties of Living Tissues*, Springer, 1990.
- Gasser et al., J Roy Soc Interface, 3:15-35, 2006.
- Holzapfel et al. J Elasticity, V61:1-48, 2000.
- Simo, Comput Method Appl M, 60:153-173, 1987.

A SELF ADAPTATIVE PROSTHESIS USING TECHNIQUES OF BIOCAD MODELING

Daniel T Kemmoku, Jorge V L Silva, Pedro Y Noritomi

CTI (Renato Archer Information Technology Center), Brazil

Introduction

This work shows the development of a multidisciplinary solution as a growth compliant prosthetic device applied to an infant patient with a large cranial defect subjected to cranioplasty [Lee *et al.*, 2008].

Commercial solutions do not comply with the bone growth. This way, a new concept, capable of self adaptation and to provide mandatory mechanical protection was developed and produced as a new prosthetic device.

Methods

The development of a new prosthesis was made using BioCAD [Sun *et al.*, 2005] concepts, providing more intelligence to the biological 3D computational biomodels by using anatomical landmarks. This approach can specially use CAD entities to improve control over the complex geometries of anatomical structures. Besides, 3D BioCAD model brings the possibility to develop FEM (Finite Elements Method) analysis in order to estimate the mechanical behavior.

The prosthesis BioCAD was developed using the InVesalius as medical image processing for 3D biomodel and the Rhinoceros 3.0 as the software to convert it to a BioCAD model and to develop the prosthesis geometry itself.

The solutions employed in this development include the use of a four parts device (Fig. 1), selectively fixed to individual bones on the skull, in order to enable the bone growth compliance, by taking care of sutures as regions of bone growth.

The main part, central one, fixed on the remaining temporal bone and supported on opposite side passes over the lesion. This part is designed to resist to the most of the mechanical loads, working as a double curved arch that supports the other two side parts of the device.

All the four parts had their geometries conceived based on BioCAD copy of the natural bilateral symmetry of the skull, in order to recover the anatomical curvature, and their mechanical resistance were considered. Thickness and curvature were optimized for the central part as the shared resistance of the other parts with it.

The internal side of the parts follows the contour of the fracture, providing a better anchoring and facilitating positioning during surgery.

Results

The FEM analysis showed well mechanical resistance to some loads reproducing a fell down from stand position of the patient and the surgeon has approved the design. The prosthesis was easily implanted with a rapid recovery from surgery. The patient is still under medical supervision for monitoring the movement of the parts.

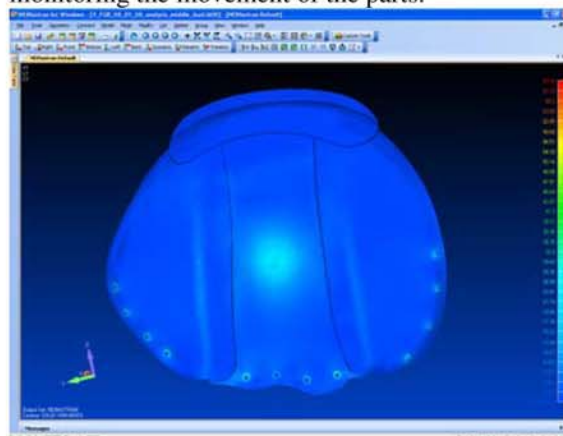


Figure 1: FEM analysis of the prosthesis

Discussion

The use of BioCAD concepts featured to anatomic landmarks showed highly efficiency to improve prosthesis aesthetic and mechanical quality.

The union of multidisciplinary knowledge is mandatory to reach innovative solutions for complex bioengineering problems.

FEM is a powerful tool to improve reliability of solution in multidisciplinary groups, despite the lack of precision due to uncertain of mechanical properties in biologic tissues.

Acknowledgements

The authors would like to thanks to Brazilian CNPq (National Counsel of Technological and Scientific Development) and to CTI (Renato Archer Information Technology Center) in Brazil.

References

- Sai-Cheung Lee, Chieh-Tsai Wu, Shih-Tseng Lee, Po-Jen Chen. Cranioplasty using polymethyl-methacrylate prostheses, 2008.
- W. Sun, B. Starly, J. Nam, A. Darling. Bio-CAD modeling and its applications in computer-aided tissue engineering, 2005.

Author index

Adachi, T.	120	Bonneau, D.	36
Adra, S.	123	Bonhoeffer, P.	100, 112
Affatato, S.	189	Bouda, T.	92
Agarwal, Y.	201	Boyd, S.	47
Agarwala, A.	135	Boyle, C.J.	102
Agostini, V.	76	Brasseur, J.G.	17
Aiyangar, A.	177	Brook, B.	41
Alastrué, V.	67, 98, 211	Buchanan, F.	190
Aliani, A.C.	17	Buchanan, T.S.	78
Antiga, L.	197, 198	Buck, A.	97
Antunes, L.	158	Bull. J.L.	162
Arbenz, P.	32		
Asiaín, D.	202	Cadossi, R.	166
Assi, A.	36	Caillibotte, G.	111, 199
Astolfi, L.	35	Calderon, A.J.	162
Asvestas, P.	172	Capelli, C.	99, 100, 112
Augat, P.	150, 153	Cappello, A.	37, 77, 184
Ayturk, F.O.	169	Cappetti, N.	166
		Caputo, M.	165
Babiloni, F.	35	Cardono, J.B.	142
Bækgaard, M.	13	Cardoso, L.	59
Bajaj, C.L.	207	Caselli, F.	51
Bakiri, S.	116	Catani, F.	152
Baleani, M.	60, 61, 174	Celi, S.	101, 137
Balestra, G.	158	Chapam, S.J.	210
Balossino, R.	157	Chandhry, B.	87
Balter, A.	132	Checa, S.	121
Banco, G.G.	17	Chegini, S.	58, 168
Barton, D.	190	Chiadini, F.	165
Bartoziej, J.	130	Chiapparini, I.	81
Baruffaldi, F.	60, 81, 172	Christen, D.	47
Bates, D.G.	113	Christen P.	58
Bazin, J.	116	Chung, S.	20
Będziński, R.	192	Cimrman, R.	80
Belvedere, C.	152	Cioffi, M.	81, 136
Benalla, M.	14	Cirovic, S.	201
Benegiamo, P.	108	Ciulli, E.	189
Beraudi, A.	61	Clapworthy, G.	30, 178
Bergmann, G.	38	Coelho, P.G.	131, 142
Berti, S.	101	Coley, S.C.	66, 68
Bertozzi, L.	184	Comeford, A.	144
Bianchi, E.	81, 136	Cona, F.	35
Bijnens, B.	41	Consolo, F.	198
Bisceglia, B.	165, 166	Cooper, J.	43
Bisegna, P.	51	Cope, J.	119
Bisi, M.C.	75	Corgiat Mansin, L.	76
Bluestein, D.	88	Cowin, S.C.	14, 59

Cremonini, S.	61	Franco, D.	81
Crisco, J.J.	39	Frangi, A.	15, 65
Cristofolini, L.	73, 107, 108	Fratzl, P.	56, 170
Crocombe, A.D.	201	Frehill, B.	201
		Fritz, T.	209
Das, A.	113	Fukasaku, K.	196
De Luca, R.	76		
Deriu, M.A.	82	Gaetano, L.	158
Desmarais-Trépanier, C.	200	Gailani, G.B.	14, 59
De Vecchi, A.	175	Gallo, D.	197, 198
De Vita, A.	166	Garcia, A.	98
De Vleeschouwer, M.	195	Garcia-Aznar, J.M.	128, 200, 202
Diaz, V.	41	Gastaldi, D.	99
Di Benedetto, G.	158	Gavaghan, D.J.	90
Di Carlo, A.	207	Geers, A.	15
Dideriksen, J.L.	13	Georgopoulos, N.	49
Di Pellegrino, G.	179	Gerber, C.	150
Di Puccio, F.	101, 137, 189	Gerhard, F.A.	129, 139
Doblaré, M.	67, 85, 98, 128, 200, 202, 211	Geris, L.	154
Doboeverie, F.	87	Giannessi,	63
Dobson, C.A.	24, 72, 183	Ginalski, M.K.	159
Doi, K.	124	Glazier, J.A.	132
Dössel, O.	160, 209	Gnudi, G.	75
Draher, Y.Y:	182	Gomaa, S.T.	204
Dubini, G.	136, 157	Gómez-Arrúe, J.	202
Duda, G.N.	95, 133, 170	Gómez-Benito, M.J.	202
Dunne, N.	190	González-Torres, L.A.	202
		Grasa, J.	202
Eberle, S.	150, 153	Grassi, L.	73, 108
Ehrig, R.M.	95	Grosse, T.	116
El Helou, A.	36	Grotto, O.	105
Enoka, R.M.	13	Guedes, J.M.	142
Ensini, A.	152		
Epari, D.R.	170	Haga, T.	124
Eshpuniyani, B.	162	Hall, R.M.	167
		Hanlon, C.	190
Fagan, M.J.	24, 72, 183	Hardman, J.G.	113
Fahle, S.R.	187	Hausselle, J.	36
Fantozzi, S.	77, 184	Heller, M.O.	95, 133
Farina, D.	13	Hellmich, C.	70
Farinella, G.	181	Heilmann, C.	160
Favre, P.	34	Himeno, M.	196
Ferguson, S.J.	58, 83, 168	Himeno, R.	196
Fernandes, P.R.	131, 142, 145	Ho, H.	64
Flore, E.	15, 65	Hoffman, M.	104
Filipovic, N.	208	Hojo, M.	120
Fletcher, K.	41	Holcombe, M.	123, 187
Fonseca, J.E.	131	Holtzapfel, G.A.	54
Fornells, P.	128	Horak, Z.	92, 151
Forte, P.	101, 137	Hose, R.	53, 66, 68, 119, 141
Fotiadis, D.I.	208	Hraiech, N.	27
Fowlkes, J.B.	162	Huls, K.S.	135

Hunter, B.V.	182	Larrabide, I.	15, 65
Hunter, P.J.	19, 64, 203	Latif, M.J.A.	146
		Lavigne, M.	200
Imai, Y.	84	Lawford, P.	41, 66, 68
Innocenti, B.	152	Leardini, A.	37, 152
Ishikawa, T.	84	Lee, J.C.	31
Ito, K.	45	Leventhal, E.	39
Itskov, M.	203	Liu, E.	30
		Lloyd, S.	43
Jarrousse, O.	209	Loosli, Y.	52
Jasiński, M.	193	Lukas, C.	56
Jenny, P.	97	Lukeš, V.	80
Jin, Z. M.	94, 146, 173	Lunn, D.E.	72, 183
Jirkova, L.	151	Lurz, P.	100
Jirman, R.	92		
John, A.	205	Maceri, F.	51
Jolivet, E.	36	Maes, F.	87
Jones, A.C.	94, 176	Magosso, E.	179
Juszczuk, M.	73, 107, 108	Malandrino, A.	93
		Malve, M.	85
Kameo, Y.	120	Majchrzak, E.	115
Kamm, R.D.	20	Manal, K.	78
Katz, I.	111, 199	Marai, G.E.	39
Kautzky-Willer, A.	126	Mariani, M.	101
Kawano, S.	124	Martelli, S.	26, 37, 107, 181
Kay, D.	89	Martinez, M.A.	67, 98, 211
Kemmoku, D.	212	Marzo, A.	66, 68
Khayyeri, H.	121	Massai, D.	88, 197, 198
Khodabakhshi, G.	141	Mastrangelo, F.M.	161
Kim, M.	15	Matsopoulos, G.K.	172
Kiran, M.	185, 186	Matsumoto, T.	109
Klaushofer, K.	56	Mattei, L.	189
Knaflitz, M.	76	McCormick, M.	175
Koerber, J.	153	McFarlane, N.	178
Kojic, M.	208	Migliavacca, F.	99, 100, 112, 157
Kondo, H.	84	Milan, J.L.	118
Kornaropoulos, E.I.	95	Mithraratne, K.	64
Kroon, M.	54	Monteiro, J.	145
Krowicki, P.	192	Montevecchi, F.M.	82, 88, 158, 161, 197, 198
Krueger, M.W.	160	Moore, D.	39
Kryzstoforski, K.	192	Morales, H.	15
Kuhn, G.	129, 139	Morbiducci, U.	88, 158, 161, 197, 198
Kumar, D.	78	Morley, J.W.	104
Kurachi, Y.	18	Morly, P.	140
Kutzner, I.	38	Motroni, A.	195
		Mouravliansky, N.	172
Labey, L.	152	Mueller, T.L.	148
Lacroix, D.	46, 93, 118	Mulder, L.	45
Laganà, K.	136	Muller, P.A.	111, 199
Laidlaw, D.	39	Müller, M.	133
Lalli, C.	102	Müller, R.	47, 129, 139, 140, 148, 155
Lambers, F.M.	129, 139	Murtada, S.	54

Naito, H.	109	Quental, C.	145
Narracott, A.	41	Quero, F.	202
Neuberger, T.	17	Rainbow, M.	39
Niderer, S.	89	Rasponi, M.	161
Nobili, M.	88	Rausch, S.	114, 191
Noda, S.	196	Readelli, R.	82, 88, 106, 161, 197, 198
Noordhoek, N.	45	Rehman, S.	57
Nordmeyer, J.	100	Ribeiro, N.	145
Nordsletten, D.	89, 175	Rizzo, G.	106
Noritomi, P.Y.	212	Robson Brown, K.A.	173
Nowak, A.J.	159	Rochette, M.	27
Nuño, N.	200	Rodrigues, H.C.	131, 142
		Rodriguez, B.	16
Oakland, R.J.	167	Rodriguez, M.A.	98
Obrist, D.	97	Rohan, E.	80
O'Hara, R.	190	Roshger, P.	56
O'Higgins, P.	24, 183	Rudolph, K.	78
Öhman, C.	60, 174	Ruffoni, D.	71, 155
Orantek, P.	205	Ryan, D.	125
Orr, J.	190		
		Sandino, C.	46
Pacini, G.	126	Santoni, B.G.	169
Panzer, S.	153	Santos, L.	131
Paoluzzi, A.	207	Sarti, M.	166
Pappalardo, M.	166	Saxon, L.	71
Paranjape, S.	32	Sbrignadello, S.	126
Parodi, O.	106	Scaglione, A.	165
Paruch, M.	115	Schievano, S.	100, 112
Patel, U.J.	66, 68	Schileo, E.	26, 37, 73, 107, 108
Pathmanathan, P.	90, 210	Schmid, H.	203
Payne, D.J.B.	187	Schrooten, J.	171
Peña, E.	98, 211	Schwarz, M.	160
Pendergast, P.J.	102, 121	Ścigala, K.	130
Pennella, F.	161	Seidel, R.	170
Pennati, G.	65, 81, 157	Serino, A.	179
Pérez, M.A.	128, 200	Setti, S.	166
Perez del Palomar, A.	85	Shabir, S.	50
Petrella, A.J.	135	Shintaku, H.	124
Petrini, L.	65, 99	Shitaro, H.	194
Petrone, N.	105	Silvia, J.V.L.	212
Pichelin, M.	111, 199	Simmons, A.	104
Pirini, M.	180	Sims, A.M.	104
Planell, J.A.	46, 93, 118	Singh, N.B.	38
Ponzini, R.	88, 106, 197, 198	Singh, P.K.	66, 68
Postek, E.	53	Skalli, W.	36
Pozo, J.M.	15	Smaill, B.H.	31
Price, W.S.	104	Smallwood, R.	49, 53, 119, 123, 125, 141
Puttitz, C.M.	169	Smith, N.	89
		Smith, N.B.	17
Quadrani, P.	29	Smith, N.P.	31, 175
Quarteroni, A.	21	Snedeker, J.G.	34, 52

Snook, R.R.	187	Veneziani, A.	106
Solitto, G.F.	166	Verdnock, P.	87
Soncini, M.	82	Vereecken, W.	148
Southgate, J.	50	Vergara, C.	106
Speranza, A.	105	Vetter, A.	170
Stagni, R.	75, 77, 184	Viceconti, M.	25, 26, 27, 29, 37, 60, 61, 73, 107, 108, 174, 181
Stait-Gardner, T.	104	Vickerman, V.	20
Stea, S.	61	Villa, M.C.	15
Stoico, R.	81	Villà i Freixa, J.	41
Stroetmann, K.A.	25	Villalobos, J.L.	85
Stroetmann, V.N.	25	Voide, R.	47
Sudo, R.	20	Von Oldenburg, G.	150
Świątek-Najwer, E.	192	Walker, D.	50, 119
Świążkowski, W.	205	Wall, W.A.	114, 144, 191
Szwedowski, T.	133	Wang, Y.	17
Tadano, S.	194	Watson, P.J.	24, 183
Taddei, F.	26, 27, 37, 73, 107, 108, 181	Watton, P.	203
Tagil, M.	121	Webb, A.G.	17
Taguchi, H.	194	Weber, B.	97
Tahir, H.	68	Webster, D.J.	129, 140
Takao, S.	194	Weeratunge, T.F.	68
Tanaka, H.	109	Wei, H.	178
Tanaka, M.	109	Weinkamer, R.	56, 170
Tarsuslugil, S.	190	Weijer, C.	132
Tassani, S.	60, 81, 172	Whiteley, J.P.	90
Taylor, A.M.	100, 112	Wiechert, L.	114, 191
Taylor, W.R.	38, 95, 133	Widmer, R.P.	83
Tecce, M.F.	165	Wijayathunga, V.N.	57, 94, 167
Tersi, L.	77	Wilcox, R.K.	57, 94, 146, 167, 173, 176, 190
Testi, D.	29, 30, 178	Williams, J.L.	204
Thelen, D.	177	Winhofer, Y.	126
Thiel, R.	25	Wirth, A.J.	148
Thomas, S.R.	42, 116	Witt, F.	170
Torcasio, A.	71	Woldtvedt, D.	169
Toyokita, Y.	124	Wolfe, S.	39
Trabelsi, N.	70, 85, 206	Wood, S.	147
Truscello, S.	171	Wrobel, L.C.	159
Tsakanakis, V.	208	Yamaguchi, T.	84
Tura, A.	126	Yosibash, Z.	70, 206
Ursino, M.	35, 63, 179, 180	Zachariou, M.	41
Vander Sloten, J.	154	Zavaglia, M.	35
Van Lenthe, G.H.	71, 47, 140, 148, 155	Zhang, C.	15
Van Oosterwyck, H.	154, 171	Zhang, Y.	132
Van Ransbeeck, P.	87	Zhao, X.	30
Van Rietbergen, B.	45	Zhao, Y.	94, 173
Van Sint Jan, S.	37, 181	Zirpoli, H.	165
Vanzulli, A.	106		
Vendittoli, P.A.	200		

ICCB 2009

www.iccb2009.org

info@iccb2009.org

www.centrocongressibertinoro.it/index_en.cfm



Published on behalf of the Scientific and Organizing Committee by:
Rita Stagni, DEIS, University of Bologna